Universidad de Valladolid

ESCUELA DE INGENIERÍAS INDUSTRIALES

DEPARTAMENTO DE INGENIERÍA ENERGÉTICA Y FLUIDOMECÁNICA

PhD THESIS:

Thermodynamic characterization of gas mixtures to introduce alternative gas fuels in the natural gas grids

Submitted by
ROBERTO HERNÁNDEZ GÓMEZ

for the partial fulfillment of a Doctorate in Philosophy by the University of Valladolid

Directed by:
CÉSAR R. CHAMORRO CAMAZÓN
MARÍA E. MONDÉJAR MONTAGUD

Valladolid, January 2016

PREFACE

“I never wanted to be an astronaut”

I admit it. I was very impressionable (and probably still remain so). Moreover, everything I don’t understand attracts me. The consequence of both things is that I have been obsessively passionate about many things. In the scientific field, when I was a child, the latest “scientific” acquisitions guided my steps. Firstly were the dinosaurs, then marine life, insects, archeology, geology… until one day it was the turn of the universe. Who hasn’t felt fascinated by the deep space sometime in life? Like many people, I was extremely fascinated. To imagine the meaning of words like “light-year”, “vacuum”, “Big Bang” or “black hole” has a lot of possibilities for a child’s mind. So far this is nothing unusual. However, for some reason, when I think about the motivation of this thesis, my mind has returned to this moment of my life to remember that, although the intricacies of the universe awakened in me an infinite interest, unlike the vast majority of children in this situation I never wanted to be an astronaut.

I have never thought about it until today (there was no reason to do that) but I like following my intuition and it tells me that I should wonder about why I didn’t want to be an astronaut. Initially, I thought this was out of place and I fought against this idea. However, I meditated on that and I think that going back to the moment when the bases which have concluded in a PhD thesis in thermodynamics were established makes a lot of sense. After all, this kind of projects needs more conviction than motivation and conviction isn’t achieved from one day to another. So, I will digress.

I don’t know how old I was when I came across the words mentioned above. However, I remember another more word: relativity. Therefore, without passing through Copernicus, Galileo, Kepler and Newton I stumbled upon the theory of the great German physicist. Suddenly, it wasn’t talking anymore about planets, stars and galaxies. It was talking about

atoms, particles and waves. I passed from the immense to the minuscule in a blink of an eye. Once again time I got carried away, attracted by incomprehension, and I inquired with devotion in the atomic world to conclude that I actually didn't understand anything. Some years later, this gave me the motivation to study and orient my choices to the scientific field to clarify the questions I raised.

That was all. I wanted to know more about the universe and I ended up staring at everyday objects and imagining how it was possible that things were made of atoms. The point is that I didn't meet any astronauts during my "space journey". This makes sense. I just know that in order to explain the origin of the universe, particle accelerators are more useful than telescopes. So, why would I go up there if the key to the universe is right under our noses? Inevitably, I preferred the work and miracles of Albert Einstein to those of Neil Armstrong. But, don't imagine that I studied quantum physics in my free time I was still a child and Wikipedia didn't exist. I was only inspired by the feats of the scientists who revolutionized physics in the early twentieth century. The different educational material that was within my grasp and some TV documentaries showed me something that years have demonstrated clearly to be the key to the development of modern physics: the importance of imagination in science. Not in vain, did Einstein say "*(…) imagination is more important than knowledge*". I know, this quote is preceded by "*in times of crisis…*", however, don't you know that this part is superfluous? Knowledge isn't useful without the inventiveness needed to make the most of it and regarding the times of crisis, we have talked too much about that in the recent years. I do not agree to limit the importance of imagination only to turbulent times. However, as I don't want to contradict a Nobel Prize winner and the end of the crisis is still far away, I totally agree with the quote. Today, it is usual to hear that we live in the Age of Knowledge. We can generate millions of scientific results every day and share them all over the world in a few seconds. This is absolutely great. However, I look forward the next step: the Age of Imagination. I don't want to be only a beholder. Do you know why? Because, although I never wanted to take my feet from the ground and sail outer space, I was made to imagine.

Imagining is how I got the conviction to dedicate my career to science and carry out this thesis. One day I realised that the *elementary particles* (whatever they may be) that the universe is made of (*matter*) are now exactly the same particles produced an instant after the *Big Bang*. Isn't that amazing? These elementary particles were made up of *subatomic particles* (for short, neutrons, protons and electrons) due to some physical forces. These

were then organized in *atoms* and a number of elements with different properties appeared. The forces causing these changes are governed by complex game rules and when they were suitable, some atoms reacted chemically together generating *molecules*. Thus, the elementary particles have been organizing themselves for billions of years, generating molecules and elements ever more complex in the different states of matter to make celestial bodies. In at least one of these celestial bodies, the optimum conditions to make an even more complex set of *matter* were produced. We know it as the *cell*. This cell had "special needs" and had to incorporate other molecules and elements into its structure. Life was created and also a new way to reorganize the elementary particles. In other words, *matter* could reorganize itself. Furthermore, *matter* could reproduce… and evolve. Thus, multicellular *matter* sets appeared, which also could reproduce and evolve, generating different kinds of complex *matter* sets grouped under the name of *living things*. Therefore, we could well be described as "stardust". The reorganization of *matter* continued, this time at a higher scale until, at some moment, *matter* turned self-conscious. This is, in my opinion, the most spectacular event of all. The consequences were (and are) overwhelming. Regarding my dissertation (or digression), the development of two languages was a consequence of that: one language to ask questions and another language to answer them. Now is when my imagination goes into action, when I try to answer some questions by using the same language in which they were formulated, because this makes me believe that the *matter*, which only exists as elementary particles after the *Big Bang*, has been reorganizing itself for billions of years and evolving to explain itself. I know. It seems like science fiction. However, can you show this is not true? Moreover, in the vastness of the universe, could there be other places where *matter* is organizing itself in other kinds of self-conscious *matter* which seeks the same objective. Physics and philosophy share much more than a few syllables. Physicists such as Born or Heisenberg attest to this in their latest works. Unfortunately, I don't have the ability to satisfy the deepest longings of *matter* by using the appropriate language (and I doubt anyone in the next centuries will have it), all the same, I think I can contribute to this with some insignificant answers.

Here is the origin of my conviction. My motivation is simple and is related to thermodynamics at last. Of course, imagination once again plays the leading role. If human beings are the most advanced self-conscious *matter* set in the known universe, the fact that we reorganize the rest of *matter* (alive or inert) according to our needs is something usual. This is what we do. We reorganize *matter* at the atomic and molecular levels and

also at a macroscopic level, which we called society. We live organized according to some rules which (in theory) promote our continued existence. Each person generates value for society, for the rest of the *matter*. Thus, life purposes are achieved by mutual cooperation and the *matter* advances to achieve its long-awaited answers. However, self-conscious has problems. Frequently, there are some distractions (to put it mildly) and individual desires or the desires of a small set of *matter* are placed before the desires of the whole *matter* set. There are several examples throughout history which still occur today, causing *matter* to deviate from its main objective. These distractions are abundant, complex and boundless, but, in my opinion, there is one that I consider highly responsible for the current conflicts: the production of energy.

Society has evolved and grown a lot during recent decades. These changes have caused a high demand in the production of food and other resources and facilities and, of course, an exponential increment in the demand for energy. The current model of energy production is mainly based on fossil fuels. Oil reserves have clearly diminished and the emissions of carbon dioxide (CO_2) and other greenhouse gases are leading to an unusual rise in the average temperature of the planet. Moreover, oil has been the excuse for the bloodiest armed conflicts of the last two decades and has caused serious environmental damage in several parts of the world. Due to this, new sustainable sources of energy have started to be investigated by scientists. I believe that the key to sustainability is the diversification of energy production, taking into account both the source and the place of production. Here is where the necessary motivation to carry out this thesis arises. A thesis in which new knowledge aimed at promoting the introduction of alternative fuels in the global energy mix are given. Consciously, I haven't given statistics, rules, forecasts, political commitments on energy consumption or CO_2 emissions data in this preface. I think they aren't needed. My imagination (and the imagination of many people) envisages a world where the production and use of energy are sustainable, where there are no emissions or waste which damage the environment, where nobody kills to keep the control of energy, and where energy is profitable, abundant and available to everybody. Definitely, it is a world where energy isn't a distraction for the inherent purpose of *matter*. I think this is the world which we must build, independently of statistics, rules, forecasts, and political or business commitments. The role of scientists, once moral conflicts have been overcome, is to make available to society everything technically possible to facilitate that *matter* keeps on reorganizing and evolving to find the answers that it seeks.

And if all I have said is nonsense, there won't be environmental disasters, death or poverty associated with energy production, at least. Now is when you tell me that I have too much imagination. If so, let me say two more things. Firstly, thank you for appreciating my inventiveness and finally, after everything some inert *elementary particles* have achieved, don't you think that the most difficult thing has already been done?

"See you in utopia".

Rober H.

“In this house we obey the laws of thermodynamics.”

Homer J. Simpson

ACKNOWLEDGMENTS

Living is facing one challenge after another. Some of them are looked for, other ones find us, some are achieved and we stumble in other ones. The good thing is that we learn from everyone. This thesis is a combination of all these things: I looked for it, but it found me; and to achieve it I have stumbled several times. Luckily, I have walked the path with wonderful people who offered me his hand in each misstep. Without their help, this challenge this challenge would have been more painful and less profitable.

Therefore, I wish to thank Dr. César Chamorro, director of this thesis, for his help, his support, his advices, his dedication, his patience, his passion and especially for his trust in me during this time.

I also wish to thank Dr. María E. Mondéjar, codirector of the thesis, for her dedication and support, especially in the first months of work, when she revealed the operation of the equipment. Thanks also for revising the English version of this work.

I also thank the rest of professors and colleagues of TERMOCAL for the affection, friendship and the good mood in the laboratory. I know I can always count on you.

I would like to thank Prof. Roland Span and Dr. Markus Ritcher for the hospitality and the help during my stay at Rühr Universität Bochum. *Danke schön!*

I also wish to thank Mark Hartley for helping me to express my deepest convictions in the English version of the preface.

Thanks to music, my friends and my family for giving me inspiration, fun and affection for giving me the force to approach this work.

And I wish to thank, of course, Vir, my parents and my brother for absolutely everything.

Finally, I would like to thank the project “Metrology for Biogas”, funded by the European Association of National Metrology Institutes (EURAMET) and the EU, and the Grants for Brief Stays in the Development of Doctoral Thesis of the Universidad de Valladolid, for providing me the funding to develop part of this work.

ABSTRACT

The research developed in this PhD thesis aims at contributing to the development and introduction of new gaseous fuels from renewable sources in the European energetic mix through the thermodynamic characterization of mixtures containing the main components of these alternative fuels.

The work provides high accurate experimental (*p, ρ, T*) data of three (CH_4 + He) binary mixtures with concentrations of (5, 10 y 50 mol-% He), a synthetic non-conventional gas mixture type CMM (*coal mine methane*) composed by ten components and containing 64 mol-% of methane and a synthetic biogas-like mixture composed by four components and containing 50 mol-% of methane. Nine isotherms between (240 y 400) K and up to 20 MPa of pressure were carried out for the (CH_4 + He) binary mixtures, seven isotherms between (250 y 400) K and up to 15 MPa for the CMM mixture and six isotherms between (275 y 400) K and up to 20 MPa for the biogas-like mixture. The second and the third interaction virial coefficients for the (CH_4 + He) binary mixtures were also estimated.

The experimental density results were compared with the values estimated from the GERG-2008 and the AGA8-DC92 equations of state, which are the reference equations for natural gases.

These results will contribute to the evaluation and improvement of equations of state which will allow the accurate estimation of the key properties of the new alternative fuels.

TABLE OF CONTENTS

Nomenclature ..... **XIX**

1. Introduction and objectives **1**

1.1. Introduction 3

1.2. Objectives of the thesis 5

1.3. Structure of the thesis 10

1.4. References 12

2. Sustainable alternatives to traditional fossil fuels. Biogas and non-conventional energy gases **15**

2.1. Introduction 17

2.2. Non-conventional energy gases 18

Extraction processes of non-conventional energy gases 20

Utilization and potential of non-conventional energy gases 22

2.3. Biogas 23

Uses and applications of biogas 25

Biogas and biomethane production in the EU 27

Biomethane integration into the actual natural gas grid 30

2.4. Thermodynamics and alternative fuels 31

Density and equations of state 37

Virial equation of state 38

2.5. Technical needs for introducing alternative gas fuels 40

2.6. References 42

3. The single-sinker densimeter with magnetic suspension coupling **45**

3.1. High accuracy methods for density measurements. State-of-the-art 47

Densimeters based on vibrating bodies 47

Piezometers 48

Bellow volumetry 48

Isochoric methods 50

Sinker densimeters 50

3.2. The single-sinker densimeter with magnetic suspension coupling 53
3.3. Description of the UVA densimeter 55
Measuring cell 57
Analytical balance 57
Weight changing device 58
Magnetic suspension coupling system 61
System for the measurement and control of the temperature 63
System for filling, evacuation and pressure measurement 66
Vacuum system 69
3.4. Measurement process 70
Filling and pressurization of the measuring cell 70
Pressure control in the measuring cell 71
Force transmission error 72
Apparent mass measuring process 74
Sinker volume calculation 76
3.5. Control and data acquisition software 80
3.6. Results of the measurements with nitrogen 85
3.7. Improvements on the equipment 86
3.8. References 89

4. Uncertainty analysis of the density measurements 93
4.1. Introduction 95
4.2. Uncertainty estimation method 95
4.3. Temperature uncertainty analysis 99
4.4. Pressure uncertainty analysis 100
4.5. Sinker mass uncertainty analysis 101
4.6. Density uncertainty analysis 102
4.7. Overall uncertainty of experimental density measurements 104
Molar mass uncertainty analysis 105
4.8. References 107

5. Preparation of gas mixtures for density measurements 109
5.1. Introduction 111
5.2. The gravimetric method for mixtures preparation 111

Mixture preparation 112
Uncertainty calculation 115
Verification of the mixture composition 116
5.3. Prepared mixtures for this work 118
5.4. References 119

6. Thermodynamic characterization of binary mixtures of methane and helium .. 121
6.1. Introduction 123
6.2. Mixture preparation 124
6.3. Experimental process 127
6.4. Experimental results 128
Force transmission error 129
Sorption effects in the measuring cell 129
6.5. Virial coefficients determination 130
Virial composition of the mixtures 133
Determination of interaction virial coefficients 134
6.6. Uncertainty analysis of the measurements 136
Molar mass uncertainty 138
Overall uncertainty of the measurements 139
6.7. Discussion 140
Relative deviation of experimental data from the reference equations of state 140
Virial fitting of experimental data 146
Analysis of the interaction virial coefficients 149
Stability of the studied (CH_4 + He) mixtures 151
6.8. Table of results 152
6.9. References 167

7. Thermodynamic characterization of a synthetic mixture of coal mine methane (CMM) 169
7.1. Introduction 171
7.2. Mixture preparation 173
7.3. Experimental process 178
7.4. Experimental results 179

Force transmission error 180
Sorption effects in the measuring cell 180
7.5. Virial coefficients determination 181
7.6. Uncertainty analysis of the measurements 182
Molar mass uncertainty 183
Overall uncertainty of the measurements 185
7.7. Discussion 185
Virial fitting of experimental data 185
Relative deviation of experimental data from the reference equations of state 187
Comparison with literature data 190
7.8. Table of results 193
7.9. References 196

8. Thermodynamic characterization of a synthetic biogas-like mixture (50 mol-% methane) 199
8.1. Introduction 201
8.2. Mixture preparation 202
8.3. Experimental process 204
8.4. Experimental results 205
Force transmission error 206
Sorption effects in the measuring cell 206
8.5. Virial coefficients determination 207
8.6. Uncertainty analysis of the measurements 208
Molar mass uncertainty 209
Overall uncertainty of the measurements 210
8.7. Discussion 211
Virial fitting of experimental data 211
Relative deviation of experimental data from the reference equations of state 212
Comparison with literature data 215
8.8. Table of results 218
8.9. References 222

9. Conclusions and future work **225**

9.1. Scientific contribution of the thesis..... 227

9.2. Future challenges 230

Appendix..... **235**

A.1. List of tables..... 237

A.2. List of figures 243

A.3. Publications related with the thesis 249

Resumen en castellano **259**

NOMENCLATURE

Symbols

a	Parameter for lineal expansion coefficient calculation, K^{-1}
A	Parameter for lineal expansion coefficient calculation, K^{-1}
b	Parameter for lineal expansion coefficient calculation
B	Buoyancy force, N Second virial coefficient, $cm^3 \cdot mol^{-1}$ Parameter for lineal expansion coefficient calculation, K^{-1}
C	Second elastic constant Third virial coefficient, $cm^6 \cdot mol^{-2}$
E	Young modulus, Pa^{-1}
f	Model function for the law of propagation of uncertainties
g	Gravity acceleration, $m \cdot s^{-2}$
H	Anisotropy factor
k	Coverage factor
m	Mass, kg
N	Number of components of a mixture
p	Pressure, MPa
r	Correlation coefficient
R	Resistance, Ω
s	Standard deviation
T	Temperature, K
u	Standard uncertainty
U	Expanded uncertainty
V	Volume, m^3
W	Resistance ratio Balance reading, g
x	Input quantity estimate
X	Input quantity
y	Output quantity estimate
Y	Output quantity
Z	Compressibility factor

Greek symbols

α	Reduced Helmholtz free energy Lineal expansion coefficient, K^{-1}
δ	Reduced density
ε_p	Apparatus specific constant
ϕ_0	Coupling factor
Φ	Parameter for lineal expansion coefficient calculation, K
ν	Degrees of freedom Poisson coefficient, K
ρ	Density, $kg \cdot m^{-3}$
Θ	Parameter for lineal expansion coefficient calculation, K
τ	Reduced temperature
χ	Magnetic susceptibility, $m^3 \cdot kg^{-1}$

Subscripts

0	Reference state or vacuum measurement
1	Titanium sinker Component 1 of a binary mixture (methane)
2	Silicon sinker Component 2 of a binary mixture (helium)
c	Critical parameter
atomic	Related to atomic weights of the components of a mixture.
eff	Effective degrees of freedom
exp	Experimental data
EoS	Calculated from a equation of state
grav	Gravimetric value
i, j, k	Input quantity numbers
MP	Measuring point
n	Number of independent repeated observations
N	Total number of input quantities
S	Sinker
S0	Sinker under vacuum
Sf	Sinker immersed in fluid
sorp	Related with sorption effects

T1	Overall uncertainty from gravimetric composition
T2	Overall uncertainty from virial fitting composition
Ta	Tantalum calibrated weight
Ti	Titanium calibrated weight
virial	Calculated from the virial fitting of experimental data
ZP	Zero point

Superscripts

0	Ideal gas behavior
r	Residual behavior

Abbreviations

AAD	Average absolute deviation
AGA	American Gas Association
BAM	Federal Institute for Material research and Testing (*Bundesanstalt für Materialforschung und –prüfung*)
Bias	Average deviation
CBM	Coalbed methane
CCS	Carbon capture storage
CEM	Spanish Center of Metrology
CF	Calibration factor
CMM	Coal mine methane
DKD	German Calibration Service (*Deutscher Kalibrierdienst*)
EBA	European Biogas Association
EC	European Commission
EIA	U.S. Energy Information Administration
EMRP	European Metrology Research Programme
ENAC	Spanish Institution of Accreditation (*Entidad Nacional de Acreditación*)
EoS	Equation of state
EU	European Union
EURAMET	European Association of National Metrology Institutes
FTE	Force transmission error
GERG	European Gas Research Group (*Groupe Européen de Recherches Gazières*)
GUM	Guide to the Expression of Uncertainty in Measurement

IEA	International Energy Agency
IUPAC	International Union of Pure and Applied Chemistry
JRP	Joint Research Programme
$MaxD$	Maximum relative deviation
MP	Measuring point Measuring position of the densimeter
NP	Null position of the densimeter
PRT	Platinum resistance thermometer
RMS	Root mean square
UVA	University of Valladolid
ZP	Zero point of the densimeter

Chemical symbols

Ar	Argon
CH_4	Methane
C_2H_6	Ethane
C_3H_8	Propane
i-C_4H_{10}	Isobutane
n-C_4H_{10}	Butane
i-C_5H_{12}	Isopentane
n-C_5H_{12}	Pentane
CO	Carbon monoxide
CO_2	Carbon dioxide
H_2	Hydrogen
H_2O	Water
He	Helium
N_2	Nitrogen
O_2	Oxygen
Si	Silicon
Ta	Tantalum
Ti	Titanium

CHAPTER 1

Introduction and objectives

1.1. Introduction 3
1.2. Objectives of the thesis..... 5
1.3. Structure of the thesis 10
1.4. References 12

1.1. INTRODUCTION

The Energy Roadmap of the European Commission for the year 2050 [1] stablishes a reduction of at least 80 % in the greenhouse gases emissions, to reach levels below than those registered in 1990. All of this should be achieved while keeping or improving the actual levels of reliability of electricity supply, energy security, economic growth and prosperity. The Renewable Energy Directive 2009/28/CE [2] specifies that 20 % of the consumption of energy should be from renewable sources by 2020. In this sense, diversification in the energetic provision is a clear commitment to European Union (EU) for the next years. One of the incipient initiatives aims at increasing significantly the amount of alternative energy gases injected into the natural gas grid. Moreover, The Energy Roadmap of the European Commission for the year 2050 identifies natural gas as a replacement of coal for the transformation of the energy system in the short-medium term.

According to data from 2012, the European Union 28 only produces 35 % of the consumed natural gas, so the EU must import almost 66 % [3]. Table 1.1 shows the evolution of the natural gas demand in the main economies from 1990 to 2010, and previsions to year 2035 [4].

Table 1.1. *Natural gas demand per area (10^{12} m^3)* [4].

	1990	2010	2015	2020	2030	2035	2010 - 2035 Annual growth rate / %
EU	368	536	509	540	592	618	0.6
USA	533	680	712	728	749	766	0.5
Japan	57	104	120	115	122	123	0.7
Russia	447	466	488	492	530	549	0.7
China	15	110	195	304	469	544	6.6
Africa	35	103	118	139	166	176	2.2
South America	60	146	163	182	227	249	2.2
World	2039	3307	3616	3943	4610	4955	1.6

The strongly dependence of the EU from imported gas makes the diversification of the provision of this fuel a key goal for the next years. Due to the diversity of sources, materials

and waste from which alternative gas fuels come, energy gases like biogas and shale gas present high possibilities to reach the desirable European stage by 2050.

Biogas is a renewable energy source produced from anaerobic fermentation of organic waste. It is mainly composed by methane (CH_4) and carbon dioxide (CO_2). The overall production of biogas in the EU in 2013 was 13.4 Mtoe. This figure represents an increment of 10.2 % with respect to the previous year. Furthermore, 52.3 TWh of the electricity was produced by biogas combustion in cogeneration engines [5]. Following this trend, it is estimated that the volume of biogas production within the EU member states will be approximately 280 Mtoe by 2020 [6].

Regarding non-conventional energy gases, like shale gas, the EIA (U.S Energy Information Administration) estimates that the technically recoverable world reserves are $7299 \cdot 10^{12}$ m^3. China, Argentina, Algeria, USA and Canada are the countries with higher estimated reserves [7]. These data have forced Europe and other countries to start studies and surveys to analyze the sustainability and profitability of such projects on their territories. Shale gas is considered the non-conventional gas with most development potential compared to other unconventional fossil fuels. In this sense, the technically recoverable resources of shale gas in Europe are estimated to be $16 \cdot 10^{12}$ m^3, approximately.

However, due to the different origin of these alternative fuels and the diverse organic waste from which biogas comes, there are technical challenges related to the storage and transport that must be solved before the practical introduction of these fuels in the existing natural gas network. In addition to the diverse origin of these fuels, their different final applications provoke the presence of various components and in different concentrations. For this reason, it is necessary to develop new tools that can estimate the thermophysical properties of these fuels over wide ranges of composition and working conditions in the homogeneous gas and liquid phases, supercritical regions, and in states of liquid-vapor equilibrium. The current measuring equipment and mathematical models were developed and evaluated for compositions closed to that of natural gas, so they do not satisfy the accuracy needs for the correct estimation of thermophysical properties of the new fuels. This means that more parameters are needed to simulate the behavior of alternative gas fuels and to estimate their thermophysical properties with the same reliability as in the case of natural gases. The knowledge of these parameters is essential to the whole integration of alternative gas fuels.

Further information about sustainable alternatives to traditional fossil fuels and data about the current uses of energy gases and future previsions are given in chapter 2 in order to justify the realization of this doctoral thesis.

1.2. OBJECTIVES OF THE THESIS

The research developed in this PhD thesis aims at contributing to the development and introduction of new gaseous fuels from renewable sources in the European energetic mix through the thermodynamic characterization of mixtures containing the main components of these alternative fuels. This will contribute to the evaluation and improvement of equations of state which will allow the accurate estimation of the key properties of these new fuels.

This work is supported by several national and European research projects. At the national level:

- *Gases energéticos: biogás y gas natural enriquecido con hidrógeno* (ENE2013-47812-R). Funded by Ministerio de Economía y Competitividad of Spain, under the module of R&D projects in the call of 2013 of 'Programa Estatal de Investigación, Desarrollo e Innovación Orientada a los Retos de la Sociedad'.
- *Biogás renovable y procesos de captura del CO_2 de combustión asociados como base a la sostenibilidad energética ambiental: Investigación termodinámica experimental* (VA391A12-1). Funded by Consejería de Educación of the Junta de Castilla y León within 'Programa de Apoyo a Proyectos de Investigación'.

At the European level this thesis is supported by two European research projects funded by the European Association of National Metrology Institutes (EURAMET) and the EU:

- EMRP ENG01 – *Characterization of non-conventional energy gases* [8].
- JRP ENG54 – *Metrology for Biogas* [9].

The project entitled "*Characterization of non-conventional energy gases*" was carried out from June 2010 to May 2013. It consisted in analyzing the interchangeability of gaseous fuels from traditional fossil fuels with non-conventional energy gases in the gas networks of the European Union, by studying their impact on the equipment and facilities designed for the operation with relatively uniform flow of natural gas with high concentration of methane. Measurement bases were established through the thermodynamic

characterization of these new non-conventional gas fuels. Retailers and gas suppliers were provided with traceability methods to analyze the composition, calorific value and moisture levels of these non-conventional fuels. The participation of the University of Valladolid (UVA) in this project was carried out indirectly, through the Spanish Center of Metrology (*Centro Español de Metrología*, CEM). Within this project M.E. Mondéjar carried out density measurements of different binary mixtures related to the new fuels [10][11][12][13].

The project "*Metrology for Biogas*" aims at developing measurement methods of different thermochemical parameters to promote the introduction of biogas and biomethane in the existing natural gas networks. Thus, the thermodynamic characterization of synthetic gas mixtures containing components typically present in biogas is one of the tasks of the project. UVA is one of the partners of the project whose execution period is from June 2014 to May 2017.

The main objectives of this PhD thesis are detailed as follows.

To make a review of current technologies for the experimental determination of gas densities in wide ranges of temperature and pressure

In order to estimate the density of gases over wide temperature and pressure ranges with high accuracy it is essential to develop reference equations of state for them. However, not all the methods for density determination of fluids are adequate to this goal. Thus, the available methodologies for density measurement will be briefly reviewed, identifying the most adequate techniques to obtain high accuracy density data in order to develop and validate new equations of state.

To tune up the single-sinker densimeter with magnetic suspension coupling and carry out calibration measurements with reference gases, identifying opportunities for improvement in the equipment or the process

The equipment used during the development of this thesis was acquired by the group TERMOCAL in 1996. Different researches were carried out with it within the framework of national and international projects. The result of the present and previous works consists

of nine publications in ISI-indexed international journals, and a doctoral thesis in which changes to improve the measurement uncertainty of the densimeter were evaluated and implemented [10].

In order to continue with the contribution to the knowledge of the thermophysical properties of fluids and the development of new technologies, a fine-tuning of the densimeter will be made in first instance. Nitrogen will be used as the measuring fluid and the correct operation of all components and auxiliary equipment of the densimeter in the apparatus working range will be validated. In order to evaluate the accuracy of the measurements, these results and their deviations will be compared with previous nitrogen measurements. Nitrogen measurements will be performance before and after every new fluid measurement.

To estimate the overall uncertainty of the density measurements, including uncertainties associated with temperature, pressure and fluid composition

The result of an experimental measurement is always an approximation of the real value of this magnitude. In this sense, a measurement is only completed when it is reported together with an uncertainty statement of the estimate. The uncertainty of a measurement characterizes the dispersion of the values which could be attributed to the experimental result. It gives also an idea of the quality of the measurements.

The experimental determination of the density of gas mixtures by using a single-sinker densimeter needs to account for the temperature and pressure values in each measured point. These magnitudes must be provided with their uncertainty values, which are estimated through the *uncertainty propagation law* described in the Guide to the Expression of Uncertainty in Measurement (GUM) [14].

The overall uncertainty of the measurements will be calculated from the uncertainties associated with all magnitudes involved in the experimental process (temperature, pressure and density) and the uncertainty of the fluid composition.

Thermodynamic characterization of binary mixtures of methane (CH_4) and helium (He) at different compositions and estimation of the cross virial coefficients from the experimental data

The description of the GERG-2008 equation of state [15] reveals weak points in the data sets used for the development of the equation, especially concerning data related to mixtures of methane and secondary natural gas components, like *n*-butane, *n*-pentane, isopentane and *n*-hexane, and also mixtures with oxygen, argon and helium. With these considerations, studying the behavior of mixtures of methane and helium at different compositions by the analysis of highly accurate (p, ρ, T) data was decided. The gas mixtures used in this work were prepared by the Federal Institute for Materials Research and Testing (BAM), Germany.

The thermodynamic characterization of the selected mixtures will be carried out by using a single-sinker densimeter with magnetic suspension coupling. High accuracy (p, ρ, T) data over a temperature range from (250 to 400) K and pressures up to 20 MPa will be obtained. Data will be recorded and stored by using specific software. The second and third virial coefficients of the selected binary mixtures and interaction virial coefficients will be estimated from experimental data.

Thermodynamic characterization of a synthetic mixture simulating the composition of a non-conventional energy gas of CMM type (coal mine methane)

Within the project "*Characterization of non-conventional energy gases*" the thermodynamic characterization of a multicomponent synthetic mixture emulating a non-conventional gas known as CMM (coal mine methane) will be carried out. The mixture was prepared by the Federal Institute for Materials Research and Testing (*Bundesanstalt für Materialforschung und –prüfung*, BAM) in Berlin, Germany. The mixture was composed by ten components, with 64 mol-% of methane. High accuracy (p, ρ, T) data in a wide range of pressure and temperature will be obtained in a temperature range from (250 to 400) K and pressures up to 15 MPa. The second and third virial coefficients of the CMM mixture will be estimated from the experimental data. In addition to this work, F.J. Pérez-Sanz obtained speed of sound data for a sample of a mixture of CMM with very similar composition [16].

Thermodynamic characterization of a synthetic mixture simulating the composition of biogas

On the first period of the project "*Metrology for Biogas*" the thermodynamic characterization of a synthetic biogas-like mixture will be carried out. The mixture was prepared by the Spanish Metrology Center (CEM) with four components, and 50 mol-% of methane. High accuracy (p, ρ, T) data in a wide range of pressure and temperature will be obtained in a temperature range from (275 to 400) K and pressures up to 20 MPa. The second and third virial coefficients of the biogas-like mixture will be estimated from the experimental data.

To analyze the suitability of the reference equation of state for natural gases AGA8-DC92 and GERG-2008 to represent the experimental behavior of the studied mixtures

The current reference equation of state used for natural gases is the GERG-2008 [15]. The previous one was the AGA8-DC92 equation of state [17]. The density data obtained in this work will be compared with the estimates from these two equations of state at the same pressure and temperature conditions. Deviations will be evaluated.

To contribute to the development of new reference equations of state suitable for alternative gas fuels and their mixtures with natural gas by providing accurate (p, ρ, T) experimental data

The development of equations of state is a continuous process. New accurate experimental data contribute to the improvement of the estimation of the thermophysical properties from these equations of state. In the case of multicomponent mixtures simulating biogas or other non-conventional energy gases, identifying and quantifying deviations of the experimental data from the values estimated by current equations of state is an important step to promote the introduction of these alternative fuels in the natural gas network. Therefore, experimental results obtained in this thesis will contribute to the development of new versions of equations of state customized to mixtures with lower methane content than natural gases.

1.3. STRUCTURE OF THE THESIS

The outline of this thesis is described as follows:

In **chapter 1** the main challenge of the European gas industry for the next years has been briefly presented, and the thesis objectives are exposed under this context. Equipment, materials and resources needed for the development of this thesis are also described.

Chapter 2 introduces the current situation of the production and consumption of natural gas, and the alternatives to reduce the energetic dependence on the fossil fuels. Technical challenges for the introduction of the alternative gas fuels and the role of thermodynamics in that process are analyzed in this chapter. Finally, the importance of the accurate density data to develop equations of state is also explained.

Chapter 3 contains a brief review of fluid density determination techniques. The measurement principle of the single-sinker densimeter with magnetic suspension coupling is also explained. The measurement process and all the equipment and control devices related to the acquisition of temperature, pressure and density data are described in detailed. All the equations and mathematical model needed to determine density of the studied mixtures are also detailed in this section. Finally, the results of nitrogen measurements to validate the correct work of the densimeter are shown.

In **chapter 4** the uncertainty analysis of the measured magnitudes for the thermodynamic characterization of the mixtures by the single-sinker densimeter with magnetic suspension coupling is explained. The involved magnitudes are temperature, pressure and density. In addition, two alternative methods are presented to estimate the overall uncertainty of density measurements.

Chapter 5 describes the gas mixtures preparation by the gravimetric method.

Chapter 6 presents the (p, ρ, T) data obtained from three binary mixtures of methane and helium at different compositions: (5, 10 and 50) mol-% of helium. The density data are compared with the estimates from the GERG-2008 and the AGA-DC92 equations of state. The second and third virial coefficients of the binary mixtures and interaction virial coefficients are calculated from the experimental data and are also presented.

Chapter 7 presents the (p, ρ, T) data obtained from a synthetic mixture of ten components simulating the behavior of a non-conventional energy gas of CMM type (coal mine methane). The mixture was composed of methane (64 mol-%), carbon dioxide (17 mol-%), nitrogen (17 mol-%), oxygen and light hydrocarbons. Density data are compared with the

estimates from the GERG-2008 and the AGA-DC92 equations of state and experimental data published by other authors from synthetic natural gases mixtures with similar compositions.

Chapter 8 presents the thermodynamic characterization of a synthetic biogas-like mixture containing methane (50 mol-%), carbon dioxide (10 mol-%), nitrogen (35 mol-%) and carbon monoxide (5 mol-%). Density deviations of the experimental data from the estimated values calculated by the GERG-2008 and the AGA-DC92 equations of state are shown. Finally, the experimental results are compared with density data from two binary mixtures (methane + carbon dioxide and methane + nitrogen) measured by TERMOCAL with the same equipment in previous works.

In **chapter 9** conclusions and scientific contribution of this work are summarized. Moreover, future research following the trend of this work is proposed.

Finally, the **appendix** collects a list of tables and figures of the thesis, and publications and conference contributions derived from this thesis.

1.4. REFERENCES

[1] European Climate Foundation, “Roadmap 2050,” 2010. [Online]. Available: http://www.roadmap2050.eu/. [Accessed: 04-Mar-2015].

[2] “DIRECTIVE 2009/28/EC OF THE EUROPEAN PARLIAMENT AND OF THE COUNCIL of 23 April 2009 on the promotion of the use of energy from renewable sources and amending and subsequently repealing Directives 2001/77/EC and 2003/30/EC.” [Online].
Available: http://eur-lex.europa.eu/legal-content/EN/ALL/?uri=CELEX:32009L0028. [Accessed: 04-Mar-2015].

[3] European Comission, “EU Energy. Statistical Pocketbook,” 2014.

[4] IEA - International Energy Agency, “World Energy Outlook 2012,” 2012.

[5] EurObserv’ER, “Biogas Barometer 2013,” 2013.

[6] Ministerio de Industria Turismo y Comercio. Gobierno de España, “Plan de acción nacional de energías renovables de españa (paner) 2011 - 2020,” pp. 2011–2020, 2011.

[7] U.S. Energy Information Administration (EIA), “Shale gas and tight oil are commercially produced in just four countries,” 2015. [Online]. Available: http://www.eia.gov/todayinenergy/detail.cfm?id=19991. [Accessed: 05-Mar-2015].

[8] “Characterization of energy gases: EMRP ENG01 N 912/2009/EC (2010-2013),” European Metrology Research Programme.

[9] “JRP Summary Report for ENG54 Biogas ‘Metrology for biogas.’” [Online]. Available: http://www.euramet.org/fileadmin/docs/EMRP/JRP/JRP_Summaries_2013/Energy_JRPs/ENG54_Publishable_JRP_Summary.pdf. [Accessed: 05-May-2014].

[10] M. E. Mondéjar, C. R. Chamorro, and R. Span, “Contribution to the development and introduction of renewable gaseous fuels through the thermodynamic characterization of mixtures of their components by using an optimized single sinker densimeter whit magnetic suspension coupling (Phd thesis),” Valladolid, 2012.

[11] M. E. Mondéjar, M. A. Villamañán, R. Span, and C. R. Chamorro, “(p, ρ, T) behavior of two mixtures of carbon monoxide with nitrogen in the temperature range from (250 to 400) K and pressures up to 20 MPa,” *J. Chem. Eng. Data*, vol. 56, no. 10, pp. 3933–3939, 2011.

[12] M. E. Mondéjar, R. M. Villamañán, R. Span, and C. R. Chamorro, “Accurate (p, ρ, T) data for two new (carbon dioxide nitrogen) mixtures from (250 to 400) K at pressures up to 20MPa,” *J. Chem. Thermodyn.*, vol. 48, pp. 254–269, 2012.

[13] M. E. Mondéjar, T. E. Fernández-Vicente, F. Haloua, and C. R. Chamorro, “Experimental Determination of (p , ρ, T) Data for Three Mixtures of Carbon Dioxide with Methane for the Thermodynamic Characterization of Nonconventional Energy Gases,” *J. Chem. Eng. Data*, vol. 57, no. 9, pp. 2581–2588, Sep. 2012.

[14] I. E. C. BIPM IFCC, ISO, IUPAC, IUPAP and OIML, “Guide to the Expression of Uncertainty in Measurement,” *Guid. to Expr. Uncertain. Meas.*, 1995.

[15] O. Kunz and W. Wagner, “The GERG-2008 Wide-Range Equation of State for Natural Gases and Other Mixtures: An Expansion of GERG-2004,” *J. Chem. Eng. Data*, 2012.

[16] F. J. Pérez-Sanz, “Development of an advanced technique based on acoustic resonance in gases for determining relevant thermodynamic constants and properties,” Universidad de Valladolid, 2014.

[17] K. E. Starling and J. L. Savidge, “Compressibility factors of natural gas and other related hydrocarbon gases - AGA Transmission Measurement Committee Report 8,” 1992.

CHAPTER 2

Sustainable alternatives to traditional fossil fuels. Biogas and non-conventional energy gases

2.1. Introduction 17
2.2. Non-conventional energy gases 18
2.3. Biogas 23
2.4. Thermodynamics and alternative fuels 31
2.5. Technical needs for introducing alternative gas fuels 40
2.6. References 42

2.1. INTRODUCTION

Natural gas is currently the third most consumed energy resource in the world and second in the European Union (EU). It contributes to almost 25% of the total energy consumed, as shown in Figure 2.1 [1].

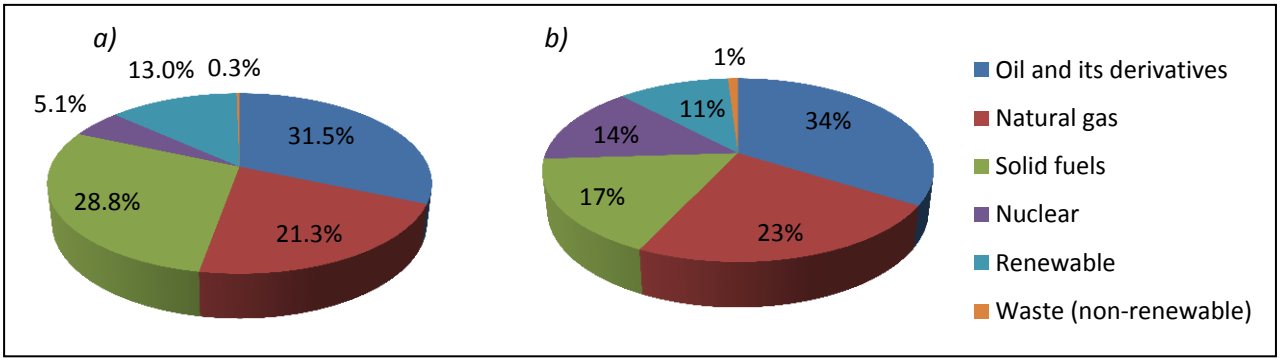

Figure 2.1. *Consumption of primary energy products: a) worldwide; b) in the EU-28* [1].

The natural gas consumption in 2012 in the EU was 392.8 Mtoe (millions tons of oil equivalent)[1], which corresponds to 23.3 % of the total energy consumption. In 1995, around 56 % of the natural gas consumed in the EU was produced in the EU. Great Britain, Netherlands, Germany, Italy and Denmark were the main producers of this fuel. However, according to data from 2012, less than 35 % of the consumed natural gas is now produced in the EU-28. Therefore, 66 % of the consumed natural gas must be imported. The main external sources of natural gas for the EU are Norway, Russia and Algeria. Table 2.1 shows the evolution and external dependence of the EU according to the kind of fuel from 1995 to 2012.

Table 2.1. *Percentage of fuel imports in the EU-28 in the period (1995 – 2012)* [1].

	1995	2000	2005	2010	2011	2012
Total	43.0	46.7	52.2	52.7	53.9	53.4
Solid fuels	21.5	30.6	39.4	39.4	41.7	42.2
Oil and its derivatives	74.0	75.7	82.1	84.4	85.1	86.4
Natural gas	43.4	48.9	57.1	62.1	67.1	65.8

[1] IEA/OECD (*International Energy Agency/ Organisation for Economic Co-operation and Development*) defines the toe (*tone of oil equivalent*) as 11.63 MWh.

The dependence on imported natural gas in the EU continues increasing. For this reason, the diversification of the provision of this fuel is a clear commitment for the EU. The Renewable Energies Directive 2009/28/CE [2] establishes a framework for the promotion of energy from non-fossil renewable resources in order to reduce CO_2 emissions and ensure energy supplies in the EU. In the field of energy gases, non-fossil renewable gases are understood as: landfill gas, sewage treatment plant gas and biogas.

The Energy Roadmap of the European Commission for the year 2050 [3] has the goal to achieve a low-carbon economy in Europe in 2050. The document identifies natural gas as a fuel substitute for coal. In this sense, in order to further improve security of supply, the European Council proposed in February of 2011 that the extraction and use of non-conventional fossil fuels should be assessed. However, the exploitation of these resources is not exempt of controversy, given the negative environmental impact involved in the production in many cases. Nevertheless, as will be explained in section 2.2, there are several non-conventional sources with very different extraction procedures that they can be an important source of energy. Moreover, the use of these resources can avoid the emission of greenhouse gases. Therefore, the thermodynamic characterization of a specific type of unconventional fuel gas was considered in this work.

2.2. NON-CONVENTIONAL ENERGY GASES

Non-conventional energy gases are the natural gas from rock reservoirs with low permeability (less than 1 milidarcy) where the accumulations of gas can be distributed along higher areas than conventional gas. The extraction of non-conventional gases cannot be done through the usual methods, so these sites require stimulation processes to make them productive. Recovery rates of non-conventional gases are much lower than those in the case of conventional gases. Approximately it is estimated that between (15 and 30) % of the present gas is able to be drawn.

There are three main types of non-conventional gases [4]:

- **Tight gas** is found in rock reservoirs with low porosity and permeability, such as limestone and sandstone. It appears in many cases in geological formations very similar to those of conventional gas, but with much lower concentrations.

- **Shale gas** comes from fine-grained sedimentary rock formations like shale or slate. These sedimentary rocks are made of consolidated clays and silt particles. Thin layers laminated with limited permeability are formed because of the compaction of clay particles by the accumulation of additional materials. The gas generated is adsorbed in traces of organic matter or exists like free gas in the natural fractures and microporosities of the rocks.

- **Coalbed methane** (CBM) is present in coal seams. CBM is mainly adsorbed in organic matter, in contrast to shale gas, although coal reservoirs have orthogonal fractures oriented perpendicularly to the coal seams that provide a primary channel for gas flow. The gas content can vary widely (from 1 to more than 25 m^3/ton), depending on the composition, depth and history of the reservoir. Production rates are influenced mainly by the permeability of the coal, which can be of the order of tens of millidarcies or a few millidarcies.

The growing interest of the EU in non-conventional gases comes mainly from the rapid increase in the production of these fuels recorded in North America, especially in shale gas, whose extraction in Europe through techniques such as fracking generates great controversy today. Table 2.2 shows the estimated recoverable amounts of conventional and non-conventional gases in Europe and other regions of the world.

Table 2.2. *Estimation of technically recoverable reserves of conventional and non-conventional gases (10^{12} m^3)* [4].

Area	Conventional	Tight	CBM	Shale (estimate average value)
Europe	11.6	1.4	1.4	8.9
USA	27.2	12.7	3.7	23.5
Canada	8.8	6.7	2.0	11.1
China	12.5	9.9	2.8	19.2
Rest of the world	364.9	14.6	15.6	34.7

Extraction processes of non-conventional energy gases

The extraction of tight and shale gas is currently performed by the combination of two methods: horizontal drilling and hydraulic fracturing. The thickness of the shale layers is usually small, so directional drilling techniques are usually employed to deepen horizontal layers by down-hole motors or directional rotary systems, which start to drill vertically from the surface. The shale layer is between 100 or 200 m from the surface. In that point, the drilling path varies between 10^o and 20^o per 30 meters until drilling horizontally. The length of these horizontal perforations is up to 2000 m. The hydraulic fracture is made in the horizontal section of the well. This rock stimulation is a process used for generating a long number of fractures in the shale layer so that the natural gas trapped in the rocks can flow to the well. This method increases the production rate and the total amount of gas that can be recovered. The pressurized water used for breaking the rocks transports sand to keep open the hydraulic fracture, allowing a continuous flow of gas. Other chemical additives (i.e. antibacterial agents and corrosion inhibitors) are also presented in small amounts to promote dissolution of minerals.

There are different groups of CBM depending on the type of field, composition and extraction process. In order, from highest to lowest concentration of methane, the following types can be identified[5]:

- Virgin coalbed methane (VCBM): extracted from surface surveys before the underground mining of coal.
- Enhanced coalbed methane (ECBM): Injecting N_2 or CO_2 is possible to stimulate the VCBM recover in the surveys of coal deposits. This method can be combined with carbon capture storage (CCS) processes.
- Abandoned mine methane (AMM) is obtained from abandoned coal mines.
- Coal mine methane (CMM) is obtained from coal extraction processes in working mines.
- Ventilation air methane (VAM) is also obtained during the coal extraction processes.

Table 2.3 shows the usual methane concentration obtained by each method and typical gas flow rates for each case.

Table 2.3. Usual methane concentration in CMB and flow rates [5].

CBM source	Methane concentration/ mol-%	Gas flow $x10^3$ m^3/día
VCBM	>95	1 - 18
AMM	35 - 90	11 - 86
CMM	35 - 75	6 - 195
VAM	0.05 – 0.08	4 - 140

Methane is one of the largest contributors to the greenhouse effect. The uncontrolled emission of this gas into the atmosphere contributes to global warming in a greater proportion than CO_2. As a matter of fact, the global warming potential (GWP) of methane is 25 times higher than that of carbon dioxide [6]. Therefore, the use of CMM and AMM as byproducts in coal and abandoned mines generates immediate benefits for the environment, reducing the emissions of these gases into the atmosphere. Moreover, the controlled extraction of these gases reduces the operating risks in mines.

The VCBM extraction is performed by perforations in conjunction with hydraulic fracturing techniques or pressurization and evacuation of coal seams with compressed air, in similarity to techniques described above for shale gas.

CMM is obtained from active coal mines by drainage techniques developed to ensure a safe coal extraction. The gas is channeled through wells or pipelines, avoiding flows at high concentrations inside the mine tunnels. Drainage techniques depend on whether the extracted gas is from an advanced point of the same seam where the coal production is carrying out or whether the gas is removed from the upper or lower seams where works are taking place.

AMM recovery processes are performed in coal seams which are unexploited but previously disturbed by mining work, usually in abandoned mines. The techniques for extracting AMM are similar to those described for VCBM, and they can provide higher flows compared to other types of CBM. The gas quality is encouraged by isolating the gas from the surface, which prevents the entry of air.

Utilization and potential of non-conventional energy gases

According to the US Energy Information Administration (EIA), USA, Canada, China and Argentina are the only producers of shale gas in the world at a significant volume according to market. In fact, the greatest amount of gas produced currently in the USA is shale gas ($3.5 \cdot 10^9$ m^3 in 2013). According to the EIA, the current worldwide technically recoverable identified reserves amounted to $7299 \cdot 10^{12}$ m^3. China, Argentina, Algeria, USA and Canada are the countries with higher reserves estimated [7]. These data have forced Europe and other countries to start studies and surveys to analyze the sustainability and profitability of such projects on their territories. Shale gas is considered the non-conventional gas with the greatest potential for development, compared to other unconventional fossil fuels. The technically recoverable resources of shale gas in Europe are estimated to be $16 \cdot 10^{12}$ m^3, approximately. This quantity is much higher than the estimated for low permeability gas ($3 \cdot 10^{12}$ m^3) or CBM ($2 \cdot 10^{12}$ m^3) [4]. Nevertheless, the economically recoverable percentage of these resources has still a high uncertainty and more exploration projects are required.

Figure 2.2 shows the worldwide basins with confirmed reservations of shale gas in May 2013.

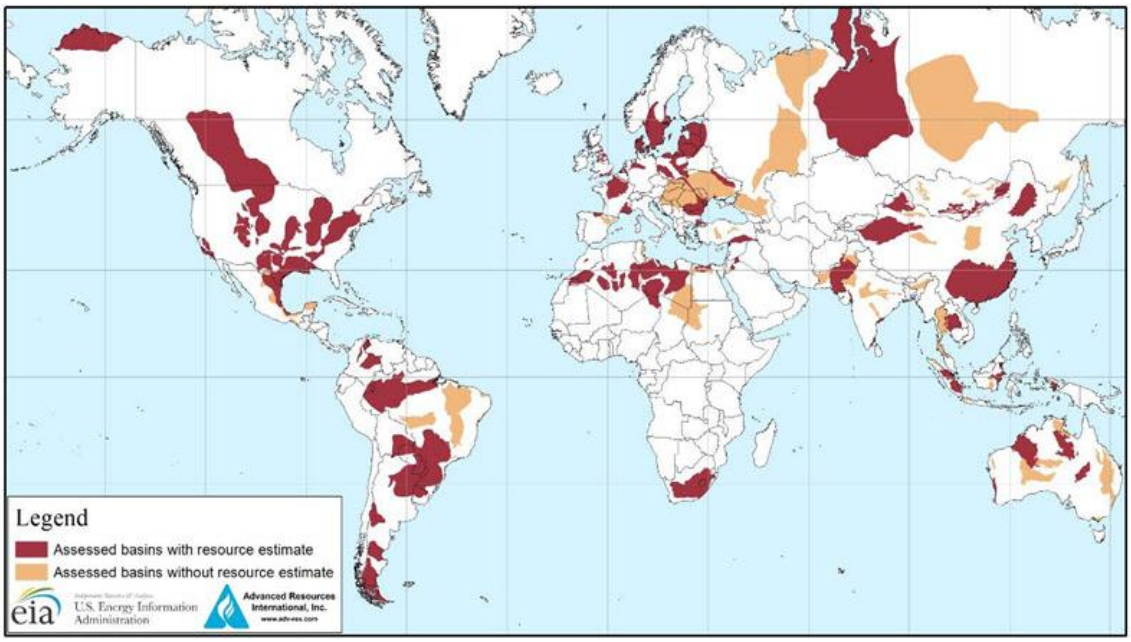

Figure 2.2. *Map of basins with proven reserves of shale gas in May 2013. The red colored basins have been quantified on an estimated basis. Source EIA* [7].

However, the exploitation of shale gas raises serious concerns about the risk of groundwater pollution. To achieve safety and environmental-friendly extractions of this

resource, the European Commission (EC) has published a recommendation for the development or adaptation of laws related to the hydraulic fracking [8]. There has been no commercial production of shale gas in the EU up to date. currently, the EU countries have different policies adapted to shale gas. For example, hydraulic fracking is forbidden in France and Bulgaria, while Poland and United Kingdom (UK) have permanent programs of exploratory drilling and hydraulic fracking tests. The member states with more advanced researches could start the commercial production of shale gas before 2017.

Regarding coalbed methane, the type of CBM currently produced varies from country to country. For example, in USA, 96% of the production of CBM is of the type VCBM, about 3.5% CMM and the rest of AMM. UK is the largest CBM producer in Europe, with about 23% of CMM and 77% of AMM. These countries have abundant supplies of natural gas, so the main use of CBM is as a low cost fuel for electricity generation at small scale. On the other hand, in developing countries, CMM recovery is seen as a good opportunity to reduce their emissions of greenhouse gases. Therefore, the production of CMM has been encouraged significantly along the last decade by governments and international aid agencies, mainly in China and India. The applications of CMM in these countries include the generation of electricity and local use in boilers and heaters.

With these data, although the EU will not be self-sufficient in regards to natural gas, the production of non-conventional gas fuel could balance its dependence on imported gas. Thus, in the best scenario, the extraction of non-conventional gases will be equivalent to $77 \cdot 10^9$ m^3 in 2035, 27 % of the estimated natural gas production in the EU ($285 \cdot 10^9$ m^3). In the same year, Europe will consume $692 \cdot 10^9$ m^3 of gas. Therefore, the European production of non-conventional gases could be around 11 % of the gas consumption. According to the International Agency of Energy (IEA), the prevision of the gas consumption among the total energy consumed in the EU in 2030 will be 30 %, so that the non-conventional gases will represent around 3 % of the total energetic mix [9].

2.3. BIOGAS

Biogas, also called *green gas*, is an energy source produced from the anaerobic fermentation of organic matter. Therefore, it is a renewable energy source. Its composition can vary significantly depending on the origin of the organic substrate from which it comes. Biogas is mainly composed of methane (CH_4) and carbon dioxide (CO_2), mixed with other

gases in lower concentration. Depending on its origin, biogas can be classified in three different groups:

- **Landfill biogas** is produced from municipal solid waste (MSW) landfills after they are sealed.
- **Biogas from urban sewage plant** is produced from the anaerobic digestion of primary sludge in sewage treatment plants.
- **OFMSW biogas** comes from the digestion of the organic fraction of municipal solid waste.
- **Agro-biogas** comes from waste and by-products of agricultural and livestock sectors. It is the kind of biogas which presents fewer impurities.

Table 2.4 shows the concentration of main components and impurities in biogas. The methane concentration varies substantially depending on the origin of the organic matter it comes from.

Table 2.4. Components and usual composition ranges of methane in biogas [10].

Substances	Concentration /mol- %
Methane	[50 - 75]
Carbon dioxide	[25 - 45]
Water	[1 - 2]
Nitrogen	[1 - 5]
Hydrogen	[0 - 3]
Carbon monoxide	[0 - 0.3]
Oxygen	[0.1 - 1]
Hydrogen sulfide	[0.1 - 0.5]
Siloxanes	-

Biogas comes from the anaerobic digestion of the organic matter. It is a microbiological process in which the organic matter becomes methane in the absence of oxygen. Anaerobic digestion can be summarized in two main stages: the hydrolytic fermentative stage and the methanogenic stage. In the first stage, the organic polymers are metabolized by hydrolysis and microbian fermentation in a mixture of volatile fatty acids. The products obtained in this first stage are transformed into methane and carbon dioxide by

methanogenic bacteria in the absence of oxygen. The methanogenic stage requires an external digestate that will be the starter of the process (except in the case in which manure or slurry are the organic substrate).

Use and applications of biogas

The amount of methane present in biogas gives ideal characteristics for the energy use of biogas. It is also remarkable the environmental and economic importance of this renewable source of energy, as it implies reduction of CO_2 emissions in the generation of electricity processes (in comparison with fossil fuels) and reduces costs of emission rights in compliance with the commitments to the Kyoto Protocol. On the other hand, the digestates used in biogas generation are usually valued as fertilizers. The substitution of mineral fertilizers by digestates can save up to 13 kg of CO_2 equivalent per ton of fertilizer. Finally, methane, nitrous oxide and other emissions from organic waste can be avoided by producing biogas from them.

Biogas must be purified before its use as fuel. Refining requirements are different depending on the energy application, as it is shown in Figure 2.3.

The purifying methods of biogas are described below:

- *Desulfurization*: Hydrogen sulfide (H_2S) is present in all types of biogas and it is not recommended in any of the applications of biogas. There are three kinds of desulfurization: microaerophilic desulfurization, external biological desulfurization, or by the addition of iron salts. Livestock waste has higher amounts of H_2S than other types of organic waste.
- *Dehumidification*: Water is removed of biogas by condensation, flowing the gas through refrigerant pipelines.
- *CO_2 elimination*: The elimination of carbon dioxide is necessary for all biogas application except for its use in cogeneration. There are several removal methods: washing with water or organic solvents, activated carbon filtration, separation by membrane, or cryogenic separation (which is currently under development).
- *Activated carbon adsorption of siloxanes*: Siloxanes are organic compounds formed by silicones, oxygen and methyl groups with structural unit $–(CH_3)_2SiO$ from production of shampoos, deodorants, cosmetics, detergents, medicines, lubricants and adhesives. During combustion, siloxane molecules are broken releasing oxygen and silicon,

forming silicates, silica and other compounds that settle on different internal parts of engines, causing abrasive wear. The permissible content of silicones according to the gas quality specifications from unconventional sources introduced in the gas system must not exceed 10 mg/m^3. A suitable method for removing siloxanes from biogas to acceptable levels for its use in power generation or heat production is the combination of cooling (down to values close to 2 °C) with activated carbon adsorption [11].

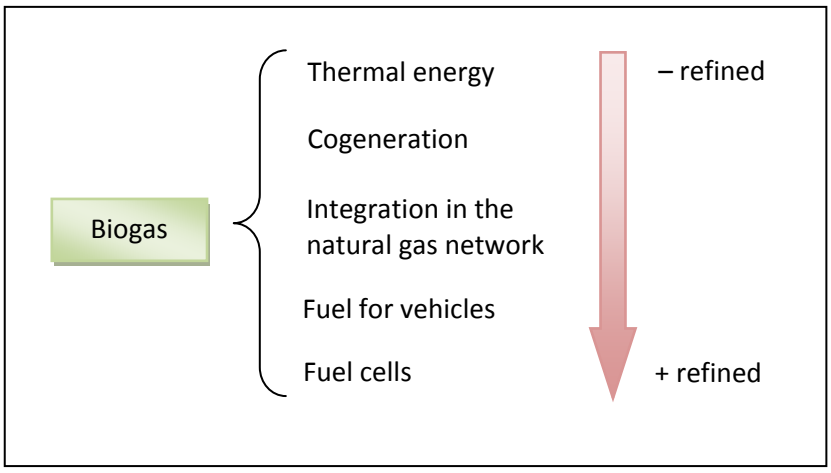

Figure 2.3. *Use of biogas depending on the level of purification* [10].

The content of methane in biogas for its use in *cogeneration engines* to produce both electric and heat power must be higher than 40 % and it is essential that H_2S is not present in the biogas, because it could produce corrosion. *Microturbines* are cogeneration systems that work at low capacities (between 30 and 200 kW). The use of biogas in microturbines is more extended than conventional turbines (from 0.5 to 30 MW). In that case, the methane content can be around 35 % and microturbines have higher tolerance to H_2S presence.

On the other hand, the use of biogas as *vehicle fuel* is an application which is becoming more extended and it requires an exhaustive purifying. The concentration of methane must be around 96 % and the presence of CO_2, O_2, H_2S and H_2O must be significantly reduced. According to NGVA Europe (Natural & bioGas Vehicle Association), there are 1.9 million of vehicles powered by biogas in Europe and 4501 filling stations [12]. The estimations of NGVA Europe said that if between (3.5 - 5.4) % of biogas was purified to fuel quality, about 10 % of renewable energy for transport proposed for 2020 in Renewable Energies Directive 2009/28/CE would be achieved [2].

Fuel-cells produce electricity by chemical energy conversion. In comparison with conventional batteries, fuel-cells do not need to be recharged; they operate continuously while fuel and oxidant are supplied. The operating principle of fuel-cells is the inverse of the chemical reaction of water electrolysis ($H_2 + ½O_2 \rightarrow H_2O$ + electricity). Biogas used as fuel for fuel-cells should be exhaustively purified and afterwards it should be converted to hydrogen by steam reforming or partial oxidation.

Finally, injection of biogas in the natural gas network is an interesting application to reduce the dependence of the imported gas in the EU and achieve the environmental objectives imposed by the EC. In order to distinguish natural gas from purified biogas, the refined biogas ready for its integration in the natural gas grids is usually called *biomethane*.

Biogas and biomethane production in the EU

The European Biogas Association (EBA) reports that there are 14563 biogas plants in Europe, according 2014 data. This corresponds to an installed power of 7857 MW [13]. The greatest biogas producers are Germany, with 9035 plants (most of them are small plants with an average of 400 kW of installed power) and Italy, with 1391 plants, as it can see in Figure 2.4. In Spain, there are currently 31 biogas plants.

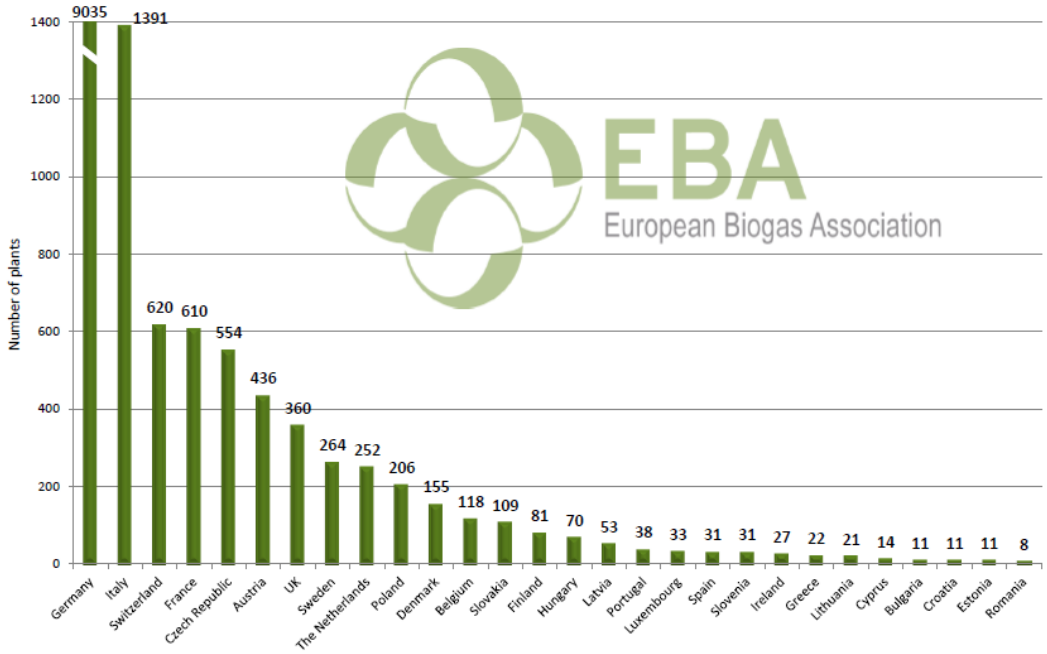

Figure 2.4. *Biogas plants in the EU* [13].

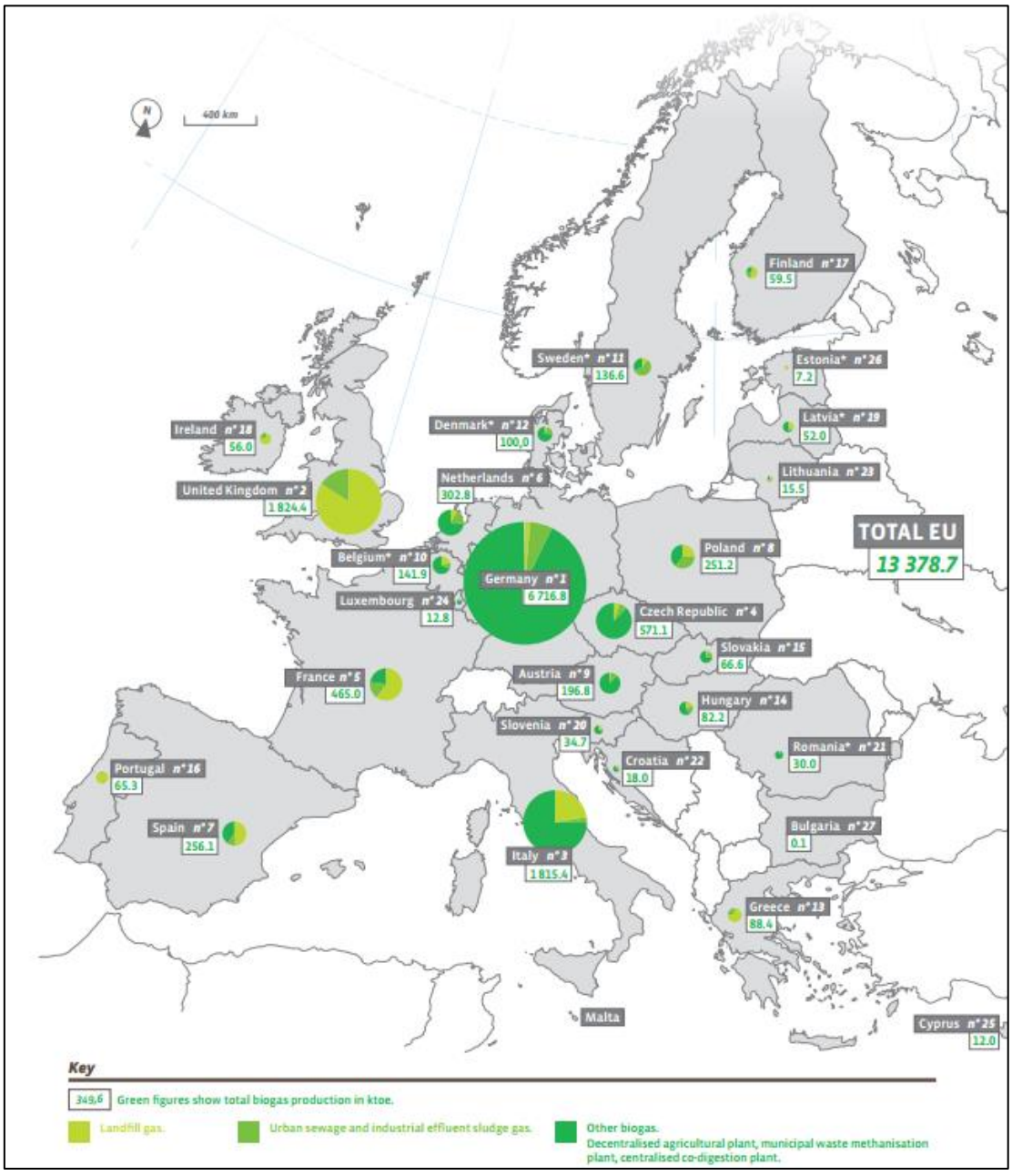

Figure 2.5. Overall production of biogas in the EU in 2013 (ktoe) according to the origin of the organic substrate. *Eurobserv'ER 2014* [14].

The overall production of biogas in the EU in 2013 was 13.4 Mtoe. This represents an increment of 10.2 % with respect to the previous year. Furthermore, 52.3 TWh of electricity were produced by biogas combustion in cogeneration engines [14]. Figure 2.5 shows the biogas production in the EU-28 according to its origin: landfill gas, urban sewage and industrial sludge gas and other biogas (decentralised agricultural plant, municipal waste methanisation plant and centralised co-digestion plant).

The industrial digestion of energetic crops and MSW is the method by which most of the biogas is produced (69 %). Germany, Italy, Czech Republic and Austria are the countries with highest production of this type of biogas. Landfill wastes (21.6 %) are the main source of biogas in UK, France, Spain, Portugal and Ireland. Finally, biogas production from urban sewage and industrial sludge (9.4 %) has the highest production in Sweden and Poland.

Regarding biomethane, there are 282 plants of biomethane production in the EU-28. The greatest amount of the gas generated in these plants is injected in the natural gas network. According to EBA, $1303 \cdot 10^9$ m^3 of biomethane were produced in 2013. Germany is the country with the highest production of biomethane, as it can be seen in Figure 2.6. As a matter of fact, biomethane represents currently 7.2 % of the biogas energy production in Germany. The Federal Agency of Gas Networks (*Bundesnetzagentur*) reports that 484 ktoe of biomethane were injected in the German network in 2013.

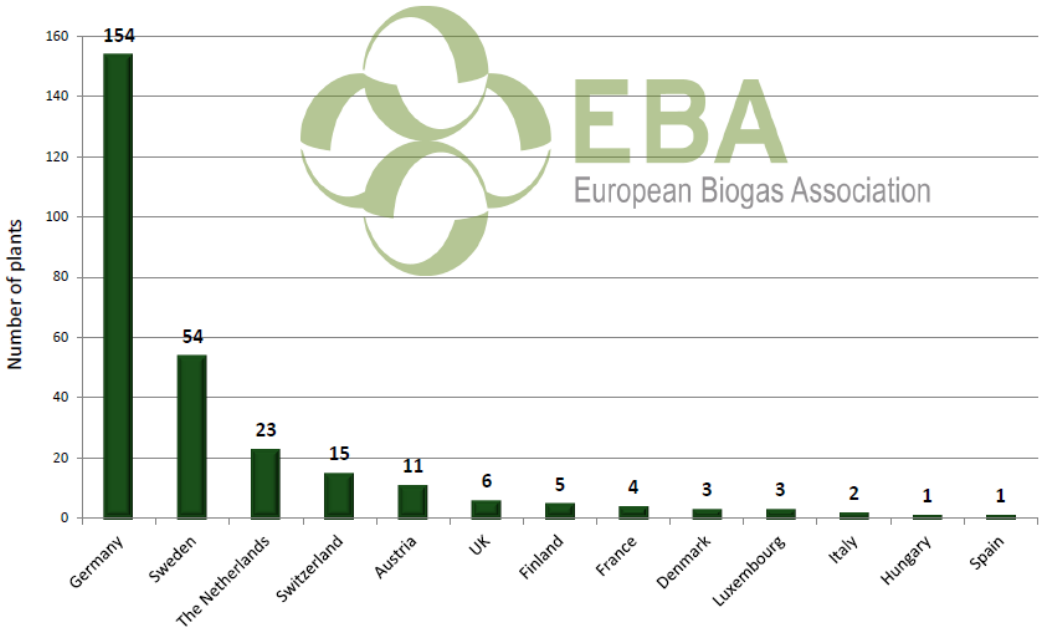

Figure 2.6. *Biomethane plants in the UE-28* [13].

Biomethane integration into the existing natural gas grid

The Renewable Energies Directive 2009/28/CE [2] establishes that 20 % of energy consumption should come from renewable sources by 2020, and biofuels should represent at least 10 % of the fuel used in transport. In order to achieve these objectives and take into account the prevision of the Energy Roadmap of the EC for the year 2050 [3], based on a carbon-free economy, there is an urgent need to increase the amount of biogas/biomethane injected in the natural gas grids. However, there are technical and administrative challenges to carry out this activity efficiently and develop the large-scale integration of biomethane into the natural gas network. According to EBA the next actions that have to be achieved are:

- **Tax incentives**: Currently, national support schemes for renewable energies are limited to *green electricity* while green gas production is often left out. Tax systems in Europe should offer similar incentives for biomethane, as the ones existing currently for liquid fuels. The future Taxation of Energy Directive, as well as aid schemes should recognize the important role of biomethane in the decarbonization of the energy sector in Europe.
- **Cross-border cooperation**: Technical standards, certification systems and the unwillingness of member states to take advantage of cooperation mechanisms of the EU (set in the Renewable Energy Directive) obstruct the development of cross-border trade.
- **Common European rules on the quality of gas for injection into the gas grid**: Countries that inject biomethane in the natural gas network have developed national quality standards that differ considerably from country to country.
- **Political recognition**: Very few Member States have set specific targets for biomethane and even EU rarely mentioned it explicitly in official documents.

In order to contribute to the introduction of biogas in the EU, following the requirements of the Directive 2009/73/CE [15] on common rules for the internal market in natural gas, the EC issued the Mandate M/475 to the European Committee for Standarization (CEN, *Comité Européen de Normalisation*) relative to specifications of biogas and biomethane for its injection into the natural gas network and its use as a transportation fuel, defining as a first step the development of an European standard to specify the quality of biogas [16].

Due to the diversity of organic matter used for biogas production, the composition of biogas may vary substantially. Biogas requires a larger number of equation parameters

than natural gases to predict its thermophysical behavior. The knowledge of these parameters is very important for the adequate use of pipelines and measurement equipment with biogas. The traditional approaches used for natural gas are not always compatible with biogas, for example, measuring the humidity range or estimating thermophysical properties (like density or calorific value).

For this reason, CEN has established the Technical Committee TC 408 to create specifications for the injection of biomethane into networks and its use as vehicle fuel. These specifications require metrologically traceable methods and reference materials to ensure that the measurements of the relevant properties of biogas are robust and reliable. For a considerable number of magnitudes there are not reference methods, so it is necessary to obtain reliable and accurate experimental measurements, with their respective uncertainties. This conformity assessment is a previous requisite for using biogas.

In Spain, the Action Plan for Renewable Energies (PANER) 2011-2020 [17] was published on June 30th of 2010. In this plan, the integration of biogas in the natural network is reported, among other issues.

2.4. THERMODYNAMICS OF ALTERNATIVE FUELS

The knowledge of the thermodynamic behavior of fuels is an essential requirement to develop, design and optimize processes of extraction, storage, transport and use of these fuels. The estimation of the thermophysical properties of fluids at specific physical conditions is done by using equations of state. There are different equations of state developed for diverse substances and applications, according to the accuracy requirements and the availability of experimental data.

The variety of sources and final applications of these alternative fuels influence the composition and concentration of these fuels. For this reason, developing tools for the calculation of the thermodynamic properties over wide ranges of pressure, temperature and composition in homogeneous gas and liquid phases, supercritical regions and in states of liquid-vapor equilibrium is an essential step.

The thermodynamic behavior of natural gas is well known with enough accuracy. Most of the applications of natural gas, like transport and storage, are carried out in gas phase at temperatures between (250 and 350) K and pressures up to 30 MPa. This operation range

is known as the “classical region” of natural gas and there are two main equations of state to estimate its thermophysical properties: AGA8-DC92 and GERG-2008 equations of state.

The first one was developed in 1992 by Starling and Savidge, with the support of the American Gas Association (AGA), as a thermal equation of state explicit in the compressibility factor [18].

The AGA8-DC92 allows the calculus of the thermodynamic properties of different natural gases and related mixtures of up to 21 components. The validity range is limited to gas phase at temperatures from (143 to 673) K and pressures up to 280 MPa. Due to the limited amount of experimental data used in its development, uncertainty estimation is only feasible at temperatures between (250 and 350) K and pressures up to 30 MPa. The uncertainty in density of AGA8-DC 92 in this operation range for density measurements of a standard natural gas is of 0.1 %. Likewise, at temperatures below 270 K deviations up to ±0.3 %, ±1 % and ±2 % from the experimental data have been reported for density, speed of sound and enthalpy difference at constant pressure, respectively. Furthermore, higher uncertainties have been identified for natural gases with high content of nitrogen, carbon dioxide, ethane or heavy hydrocarbons. The AGA-DC92 equation of state has been for many years the international standard to calculate thermodynamic properties in the “classic region” of natural gas, according to the ISO 20765-1 [19].

The development of the GERG-2008 equation of state started in the 90s thanks to the partnership of the European gas companies (GERG, *Groupe Européen de Recherches Gazières*) formed by the partners *Enagas, Gastransport Services, Gaz de France, Snam Rete Gas, Ruhrgas* y *Statoil*. The consortium hired *Ruhr-Universität Bochum* to develop an equation of reference for natural gases valid in a wide range and with more accuracy than the previous equations of state. The GERG02 equation of state was developed from this work. It was based on a multi-fluid approximation by the fundamental equations of the pure components and correlation equations developed from experimental data of binary mixtures of these components [20]. Starting from this work, Kunz, Klimeck, Wagner and Jaeschke developed the GERG-2004 equation of state for the estimation of the thermodynamic properties of natural gases and related mixtures up to 18 components [21]. This equation of state is adequate to almost all applications of natural gas and satisfies accurately the estimation of thermodynamic properties of both liquid and gaseous phase, as well as vapor-liquid equilibria. GERG-2004 is based on a multi-fluid approximation, like its predecessor.

The GERG-2008 equation of state is an expanded version of the GERG-2004. It allows calculating thermophysical properties of 21 pure components and mixtures of themselves [22]. Table 2.5 shows the 21 components included in the GERG-2008 equation of state.

***Table 2.5**. List of the 21 main and secondary natural gas components and their equations of state used for the GERG-2008 equation of state* [22].

Substance	Reference equation of state	Validity range		No. terms
		T/K	*p*/MPa	
		Main components		
Methane	Klimeck [23]	(90 – 623)	300	24
Nitrogen	Klimeck [23]	(63 – 700)	300	24
Carbon dioxide	Klimeck [23]	(216 – 900)	300	24
Ethane	Klimeck [23]	(90 – 623)	300	24
		Secondary components		
Propane	Span & Wagner [24]	(85 – 623)	100	12
n-butane	Span & Wagner [24]	(134 – 693)	70	12
Isobutane	Span & Wagner [24]	(113 – 573)	35	12
n-pentane	Span & Wagner [24]	(143 – 573)	70	12
Isopentane	Lemmon & Span [25]	(112 – 500)	35	12
n-hexane	Span & Wagner [24]	(177 – 548)	100	12
n-heptane	Span & Wagner [24]	(182 – 523)	100	12
n-octane	Span & Wagner [24]	(216 – 548)	100	12
n-nonane	Lemmon & Span [25]	(219 – 600)	800	12
n-decane	Lemmon & Span [25]	(243 – 675)	800	12
		Other components		
Hydrogen	Kunz et al. [21]	(14 – 700)	300	14
Oxygen	Span & Wagner [24]	(54 – 303)	100	12
Carbon monoxide	Lemmon & Span [25]	(68 – 400)	100	12
Water	Kunz et al. [21]	(273 – 1273)	100	16
Hydrogen sulfide	Lemmon & Span [25]	(187 – 760)	170	12
Helium	Kunz et al. [21]	(2.2 – 573)	100	12
Argon	Span & Wagner [24]	(83 – 520)	100	12

The normal range of validity of the GERG-2008 covers temperatures from (90 to 450) K and pressures up to 35 MPa. It corresponds to the usual operation range of most of the applications carried out for natural gas. The uncertainty in density in the temperature range from (250 to 450) K and pressures up to 35 MPa is 0.1 %. This uncertainty is valid for different types of natural gases, including enriched natural gases in nitrogen, carbon dioxide, ethane, hydrogen, etc.

The GERG-2008 equation of state is the current reference equation of state for calculating properties of natural gases and related mixtures, according to the international standard ISO 20765-2 [26].

The mixture models developed to design the GERG-2008 equation of state and its previous versions are based on multi-fluid approximations and are explicit in the Helmholtz free energy $a(\rho,T,x)$, state function with density ρ, temperature T and the vector of the molar composition as independent mixture variables. Mixture models use equations of state as fundamental equations for each component of the mixture along with additional correlation equations taking into account the residual mixture behavior. These models allow obtaining a complete description of the thermophysical properties of the fluid in wide ranges of pressure, temperature and composition. The Helmholtz free energy of a mixture is expressed usually in its dimensionless form $(\alpha = a/RT)$ by adding a residual term α^r to the ideal behavior α^0, according to eq. 2.1 [27].

$$\alpha(\delta,\tau,x) = \alpha^0(\rho,T,x) + \alpha^r(\delta,\tau,x) \qquad \textbf{Ec. 2.1.}$$

where δ is the reduced density of the mixture $(\delta = \rho/\rho_r)$ and τ the inverse reduced temperature of the mixture $(\tau = T_r/T)$, with ρ_r and T_r being the reducing functions dependant on composition, density and temperature, respectively.

The Helmholtz free energy is not an accessible magnitude by experimental measurements, so it must be calculated through mathematical and thermodynamic correlations. In the case of mixtures, the reduced Helmholtz free energy term for ideal gas and residual behavior are showed in eq. 2.2 and 2.3.

$$\alpha^0(\rho,T,x) = \sum_{i=1}^{N} x_i\left[\alpha_{oi}^0(\rho,T) + \ln x_i\right] \qquad \textbf{Eq. 2.2.}$$

$$\alpha^r(\delta,\tau,x) = \sum_{i=1}^{N} x_i \cdot \alpha_{oi}^r(\delta,\tau) + \Delta\alpha^r(\delta,\tau,x) \qquad \textbf{Eq. 2.3.}$$

where N is the number of mixture components; α_{oi}^{0} and α_{oi}^{r} are the reduced Helmholtz free energy for ideal gas state and the residual part of component i, respectively, and x_i is the molar fraction of the component i of the mixture. The residual part is divided in two terms. The first one is the linear contribution of all pure components presents in the mixture. The second term is the so-called departure function $\Delta\alpha^{r}$, which is the sum of all specific or generalized departure functions developed for the respective binary mixtures of all components of the mixture. The departure function depends on the variables δ, τ and, additionally, of the composition x. In general, the contribution of the departure function to the reduced residual Helmholtz free energy of the mixture is less than the contribution of the equations for the pure components and it depends on the empirical representation of experimental data.

Therefore, the development of mixture models based on a multi-fluid approximation requires the following elements:

- Equations of state of all pure components considered in the mixture.
- Composition-dependent reducing functions for density $\rho_r(x)$ and temperature $T_r(x)$ of the mixture.
- A departure function $\Delta\alpha^{r}$.

The mixture model of the GERG-2008 equation of state was developed from experimental data of the 21 pure components shown in Table 2.5 and 210 binary combinations of these components. Binary specific departure functions or generalized departure functions were developed for mixtures with enough high accuracy experimental data. However, due to the lack of accurate experimental data of some binary mixtures and the complexity of the process, only adjusted reducing functions were used for most of the binary systems. Therefore, the accuracy of the thermophysical properties estimated from GERG-2008 depends on the kind of correlation developed for the binary mixtures involved in the multicomponent mixture. Only 15 of the 210 binary mixtures considered in the GERG-2008 equation of state have associated binary specific or generalized departure functions.

Table 2.6 shows the binary mixtures for which binary specific or generalized departure functions were developed. Figure 2.7 shows different types of functions used for the description of the 210 binary mixtures considered in GERG-2008 equation of state.

***Table 2.6**. List of the binary mixtures for which binary specific or generalized departure functions were developed* [22].

Binary mixture	Departure function
methane – nitrogen	Specific
methane – carbon dioxide	Specific
methane – ethane	Specific
methane – propane	Specific
methane – *n*-butane	Generalized
methane – isobutane	Generalized
methane – hydrogen	Specific
nitrogen – carbon dioxide	Specific
nitrogen – ethane	Specific
ethane – propane	Generalized
ethane – *n*-butane	Generalized
ethane – isobutane	Generalized
propane – *n*-butane	Generalized
propane – isobutane	Generalized
n-butane – isobutane	Generalized

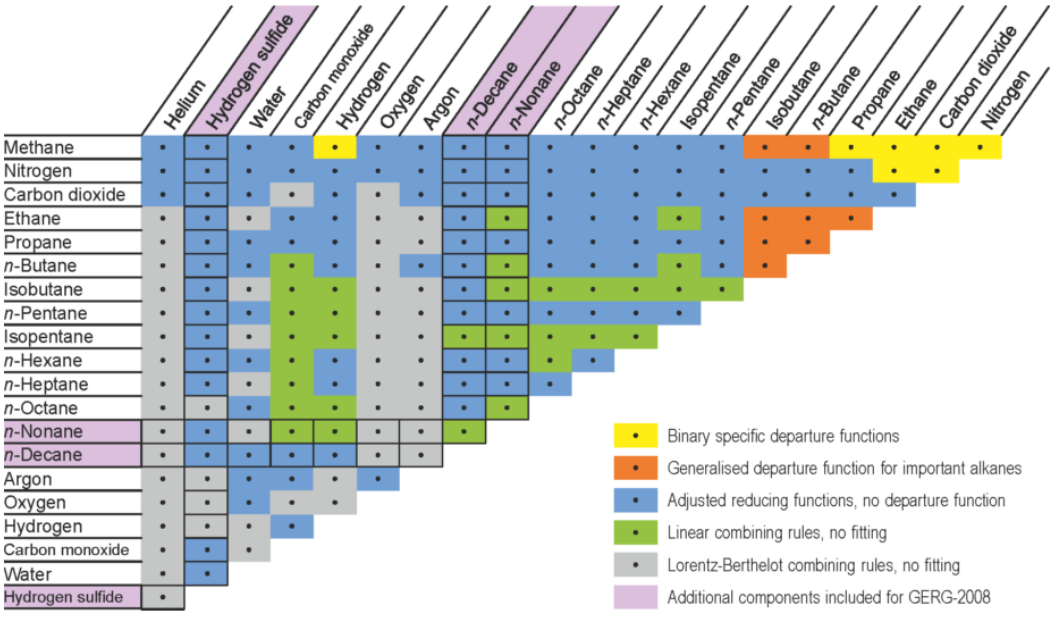

***Figure 2.7**. General description of the 210 binary combinations from the 21 natural gas components considered in the development of the GERG-2008 equation of state. Diagram illustrates the different types of functions used for the description of the binary mixtures* [22].

Density and equations of state

The basis for the development and validation of empirical equations of state, like the GERG-2008, is the measurement of accurate experimental data of thermodynamic properties of pure substances and also binary mixtures. These data are used to develop the structures, coefficients and parameters of the correlations and also to validate the behavior of the equations in different fluid regions. The quality and availability of the experimental data limits the accuracy of the equations of state in the estimation of thermophysical properties. In order to develop the equations of state GERG-2004 and GERG-2008 a continuously expanded data base was generated. More than 125000 experimental data of binary and multicomponent mixtures are recorded from more than 650 different sources. Data cover the gas and liquid homogeneous phases, supercritical region and vapor−liquid equilibrium (VLE) states in a temperature range from (16 to 2500) K and pressures up to 2000 MPa. The included thermodynamic properties are:

- Pressure, density and temperature (p, ρ, T)
- Isochoric heat capacity c_v
- Speed of sound w
- Isobaric heat capacity c_p
- Enthalpy differences Δh
- Saturated-liquid density ρ'
- VLE data (mainly (p, T, x, y) data).

In this sense, the measurement of density is an especially important step to develop, improve and validate equations of state. In fact, 70 % of the recorded data for developing the GERG-2008 EoS are (p, ρ, T) relations of pure fluids and binary mixtures (21 % VLE data and 9 % calorific properties). This is because the experimental accessibility of density measurements is higher, as described in chapter 3. On the other hand, fitting equation of state parameters is performed by minimizing the weighted residual deviations between experimental and estimated results. (p, ρ, T) data show a “quasi-linear behavior”, so by using functions of these variables, for example pressure as function of density and temperature $p(\rho, T)$, minimization tasks are easier to solve.

In conclusion, density measurements are essential to develop and validate equations of state for estimating the thermophysical properties involved in the usual applications of

natural gases. The key temperature range in these operations is from (250 to 350) K and corresponds to the homogeneous gas phase.

On the other hand, the transmission of speed of sound within the fluid is of great importance because these data are used to obtain other relevant thermodynamic properties, like heat capacities.

Therefore, by determining density and speed of sound for any fluid, thermal and other energy properties can be estimated and the thermodynamic behavior of the fluid can be characterized completely.

Virial equation of state

There are many equations of state for fluids, but virial equations are the only ones who have a firm theoretical basis based on statistical mechanics. This field of thermodynamics establishes that thermophysical properties of any fluid can be estimated from the knowledge of the interaction forces between molecules [28].

$$Z = \frac{p}{RT\tilde{\rho}} = 1 + \sum_{k=2}^{\infty} B_k \cdot \tilde{\rho}^{k-1} \qquad \textbf{Eq. 2.4.}$$

where Z is the compressibility factor, which gives the ideality ratio of the fluid, p is the pressure, R is the ideal gas constant, T is the temperature, $\tilde{\rho}$ is the molar density and B_k the virial coefficients, which have a physical meaning related to the interaction between groups of molecules. Thus, B_2 accounts for the interaction between a pair of molecules, B_3 takes into account the interaction between three molecules, and so on. The interaction between two molecules contributes to a larger extent than the interaction between three or more molecules. The contribution of the higher order terms to Z decreases quickly, so virial equation 2.4 is often truncated at the third term and even expressed in mass density as given in equation 2.5.

$$Z = \frac{pM}{RT\rho} = 1 + B \cdot \frac{\rho}{M} + C \cdot \frac{\rho^2}{M^2} \qquad \textbf{Eq. 2.5.}$$

where M is the molar mass of the fluid, B is the second virial coefficient (corresponding to the interaction between a pair of molecules B_2) and C is the third virial coefficient

(interaction between three molecules B_3). These virial coefficients depend on the fluid and temperature in a pure substance and there are experimental values for several gases.

For binary and multicomponent mixtures, the virial coefficients of equation 2.4 depend on the temperature and concentration of each component of the gas mixture. In a mixture with n components, the second virial coefficient B is given by equation 2.6.

$$B(T,x)=\sum_{i=1}^{n}\sum_{j=1}^{n}x_i x_j B_{ij}(T) \qquad \textbf{Eq. 2.6.}$$

where x_i y x_j are the molar fractions of the components i and j and $B_{ij}(T)$ is the second interaction virial coefficient, which represents the interaction between molecules of different substances and is function of the temperature. When $i=j$ it is corresponds to the second virial coefficient of a pure substance. In binary mixtures $(n=2)$, the second interaction virial coefficient can be calculated by equation 2.7.

$$B_{12}(T)=\frac{B(T,x)-x_1^2\cdot B_{11}(T)-x_2^2\cdot B_{22}(T)}{2\cdot x_1\cdot x_2} \qquad \textbf{Eq. 2.7.}$$

The third virial coefficient in a mixture with n components is given by equation 2.8.

$$C(T,x)=\sum_{i=1}^{n}\sum_{j=1}^{n}\sum_{k=1}^{n}x_i x_j x_k C_{ijk}(T) \qquad \textbf{Ec. 2.8.}$$

where $C_{ijk}(T)$ is the third interaction virial coefficient and it is also temperature dependent. In binary mixtures $(n=2)$ the third virial coefficient of the mixture can be expressed as shown in equation 2.9.

$$C(T,x)=x_1^3\cdot C_{111}(T)+x_1^2\cdot x_2\cdot C_{112}(T)+x_1\cdot x_2^2\cdot C_{122}(T)+x_2^3\cdot C_{222}(T) \qquad \textbf{Eq. 2.9.}$$

Starting from (p,ρ,T) experimental data it is possible to fit equation 2.5 and to estimate the value of the virial coefficients $B(T,x)$ and $C(T,x)$. From these values it is possible to calculate the second, $B_{12}(T)$, and the third interaction virial coefficients, $C_{112}(T)$ and $C_{122}(T)$, by using equations 2.7 and 2.9, respectively. The knowledge of these interaction virial coefficients has application in molecular simulation, especially the interaction virial coefficients between to substances $B_{12}(T)$. Molecular simulations are used to determine

the parameters of the correlations which describe the behavior of the binary combinations used in the development of equation of state like GERG-2008.

2.5. TECHNICAL CHALLENGES FOR THE INTRODUCTION OF ALTERNATIVE GAS FUELS.

In order to promote the use and production of non-conventional energy gases, like biogas and biomethane, some technical and administrative challenges need still to be assessed, before their complete introduction in the energy mix. The establishment of tax incentives, cooperation between countries and political recognition of this type of sustainable alternatives are some examples. In this sense, the establishment of standards specifying the quality of alternatives fuels is an essential previous step as a nexus between technical and administrative challenges that must be overcome. As it is detailed in chapter 2.3, there is a need to develop reference materials and adequate analytic methods to evaluate these new fuels. This also includes the establishment of metrological traceability networks, the development of methods for determining both chemical and thermodynamic properties, and even the content of biogenic methane in the network to characterize the fuel injected, regardless of its origin.

There are several international projects oriented to achieve these challenges, like the European project “Metrology for Biogas”, in which University of Valladolid (UVA) is a partner and which supports part of this thesis. “Metrology for Biogas” is funded by the European Metrology Research Programme (EMRP) and it has the following objectives [29]:

- Development of methods and measurement standards for determining the contents of key organic and inorganic impurities.
- Development of methods needed in determining the water dew point and particulate content of biogas and biomethane.
- Development of sampling techniques for determining the concentration of biomethane in biomethane and natural gas mixtures.
- Development of methods for calculating density, heat capacities and calorific values of biogas.
- Development of methods for field sampling and industrial methods of measurement.

Within this project the thermodynamic characterization of a synthetic mixture of biogas was carried out. The results for that mixture are described in chapter 8.

Other European project in which UVA participated was "*Characterization of non-conventional energy gases*". It lasted from June 2010 to May 2013. The project consisted in analyzing the "interchangeability" of gaseous fuels from traditional fossil fuels by non-conventional energy gases in the gas networks of the European Union, studying their impact on the equipment and facilities designed for operation with relatively uniform flow of natural gas high in methane. Measurement bases were established through the thermodynamic characterization of these new non-conventional gas fuels. Retailers and gas suppliers were provided with traceability methods to analyze composition, calorific value and moisture levels of these non-conventional fuels. The participation of the UVA in this project was indirectly through the Spanish Center of Metrology (*Centro Español de Metrología*, CEM). Thermodinamic characterization of the synthetic CMM mixture (*coal mine methane*) described in chapter 7 was supported by this project. Previously, M.E. Mondéjar carried out density measurements of different binary mixtures for this project [30][31][32][33].

In conclusion, the real-time determination of physical parameters, as calorific value or Wobbe index, is performed by equipment and equations developed specifically for natural gases. Knowing the thermodynamic behavior of natural gases mixed with alternative gas fuels by accurate estimation of their properties could be a great advance for the integration of alternative fuels into natural gas grids. In order to achieve this goal, it is first necessary to identify and quantify deviations of the experimental data from estimated values from reference equations of state. This is the main objective of this thesis. Later, new correlations to improve the equations of state will be developed from these experimental results.

2.6. REFERENCES

[1] European Comission, “EU Energy. Statistical Pocketbook,” 2014.

[2] “DIRECTIVE 2009/28/EC OF THE EUROPEAN PARLIAMENT AND OF THE COUNCIL of 23 April 2009 on the promotion of the use of energy from renewable sources and amending and subsequently repealing Directives 2001/77/EC and 2003/30/EC.” [Online].
Available: http://eur-lex.europa.eu/legal-content/EN/ALL/?uri=CELEX:32009L0028. [Accessed: 04-Mar-2015].

[3] European Climate Foundation, “Roadmap 2050,” 2010. [Online]. Available: http://www.roadmap2050.eu/. [Accessed: 04-Mar-2015].

[4] I. Pearson, P. Zeniewsk, F. Gracceva, P. Zastera, C. McGlade, S. Sorrell, J. Speirs, and G. Thonhauser, “Unconventional Gas: Potential Energy Market Impacts in the European Union,” 2012.

[5] D. Creedy and H. Tilley, “Coalbed methane extraction and utilization,” *Proc. Inst. Mech. Eng. Part A J. Power Energy*, vol. 217, no. 1, pp. 19–25, Jan. 2003.

[6] O. Boucher, P. Friedlingstein, B. Collins, and K. P. Shine, “The indirect global warming potential and global temperature change potential due to methane oxidation,” *Environ. Res. Lett.*, vol. 4, no. 4, 2009.

[7] U.S. Energy Information Administration (EIA), “Shale gas and tight oil are commercially produced in just four countries,” 2015. [Online]. Available: http://www.eia.gov/todayinenergy/detail.cfm?id=19991. [Accessed: 05-Mar-2015].

[8] European Commission, “Environmental Aspects on Unconventional Fossil Fuels (shale gas),” 2014.

[9] IEA - International Energy Agency, “World Energy Outlook 2012,” 2012.

[10] Dirección General de Recursos Agrícolas y Ganaderos, “El sector del biogás agroindustrial en España,” 2010.

[11] J. Reina Hernandez, “Humedad y siloxanos en el biogás generado en vertederos y depuradoras,” *Enery waste Technol.*, pp. 99–110, 2006.

[12] Natural & bioGas Vehicle Association, “European NGV Statistics,” 2014. [Online]. Available: http://www.ngvaeurope.eu/european-ngv-statistics. [Accessed: 10-Mar-2015].

[13] European Biogas Association, “EBA Biogas Report 2014,” 2014.

[14] EurObserv’ER, “Biogas Barometer 2013,” 2013.

[15] “DIRECTIVE 2009/73/EC OF THE EUROPEAN PARLIAMENT AND OF THE COUNCIL of 13 July 2009 concerning common rules for the internal market in natural gas and repealing Directive 2003/55/EC,” 2009.

[16] "M/475 Mandate to CEN for standards for biomethane for use in transport and injection in natural gas piplines," 2010. [Online]. Available: http://ec.europa.eu/enterprise/standards_policy/mandates/database/index.cfm?fuseaction=search.detail&id=459. [Accessed: 10-Mar-2015].

[17] IDAE - Instituto para la Diversificación y el Ahorro de Energía, "Plan de Energías Renovables 2011-2020," 2011.

[18] K. E. Starling and J. L. Savidge, "Compressibility factors of natural gas and other related hydrocarbon gases - AGA Transmission Measurement Committee Report 8," 1992.

[19] "ISO 20765-1. Natural gas -Calculation of thermodynamic properties- Part 1: Gas phase properties for transmission and distribution applications," Geneva, 2005.

[20] M. Jaeschke, A. Benito, A. Fredheim, J.-M. Henault, M. Sangalli, P. V Wesenbeeck, R. Klimeck, O. Kunz, R. Span, and W. Wagner, "GERG project: Wide-range reference equation of state for natural gases," in *International Gas Research Conference Proceedings*, 2001, p. 11.

[21] O. Kunz, R. Klimeck, W. Wagner, and M. Jaeschke, "The GERG-2004 Wide-Range Reference Equation of State for Natural Gases and Other Mixtures," *GERG Tech. Monogr. Fortschritt-Berichte VDI*, 2007.

[22] O. Kunz and W. Wagner, "The GERG-2008 Wide-Range Equation of State for Natural Gases and Other Mixtures: An Expansion of GERG-2004," *J. Chem. Eng. Data*, 2012.

[23] R. Klimeck, "Entwicklung einer Fundamentalgleichung für Erdgase für das Gas- und Flüssigkeitsgebiet sowie das Phasengleichgewicht.," Fakultätfür Maschinenbau, Ruhr-Universität Bochum. Bochum, Germany, 2000.

[24] R. Span and W. Wagner, "Equations of state for technical applications. I. Simultaneously optimized functional forms for nonpolar and polar fluids," *Int. J. Thermophys.*, vol. 24, no. 1, pp. 1–39, 2003.

[25] E. W. Lemmon and R. Span, "Short fundamental equations of state for 20 industrial fluids," *J. Chem. Eng. Data*, vol. 51, no. 3, pp. 785–850, 2006.

[26] "ISO 20765-2 Natural gas -Calculation of thermodynamic properties -Part 2: Single-phase properties (gas, liquid, and dense fluid) for extended ranges of application," Geneva, 2015.

[27] R. Span, *Multiparameter Equations of state - An accurate Source of Thermodynamic Property Data*. Berlin: Springer, 2000.

[28] J. H. Dymond and E. B. Smith, *The Virial Coefficients of Pure Gases and Mixtures. A Critical Compilation*. 1980.

[29] "JRP Summary Report for ENG54 Biogas 'Metrology for biogas.'" [Online]. Available: http://www.euramet.org/fileadmin/docs/EMRP/JRP/JRP_Summaries_2013/Energy_JRPs/ENG54_Publishable_JRP_Summary.pdf. [Accessed: 05-May-2014].

[30] M. E. Mondéjar, C. R. Chamorro, and R. Span, “Contribution to the development and introduction of renewable gaseous fuels through the thermodynamic characterization of mixtures of their components by using an optimized single sinker densimeter whit magnetic suspension coupling (Phd thesis),” Valladolid, 2012.

[31] M. E. Mondéjar, M. A. Villamañán, R. Span, and C. R. Chamorro, “(p, ρ, T) behavior of two mixtures of carbon monoxide with nitrogen in the temperature range from (250 to 400) K and pressures up to 20 MPa,” *J. Chem. Eng. Data*, vol. 56, no. 10, pp. 3933–3939, 2011.

[32] M. E. Mondéjar, R. M. Villamañán, R. Span, and C. R. Chamorro, “Accurate (p, ρ, T) data for two new (carbon dioxide nitrogen) mixtures from (250 to 400) K at pressures up to 20MPa,” *J. Chem. Thermodyn.*, vol. 48, pp. 254–269, 2012.

[33] M. E. Mondéjar, T. E. Fernández-Vicente, F. Haloua, and C. R. Chamorro, “Experimental Determination of (p , ρ, T) Data for Three Mixtures of Carbon Dioxide with Methane for the Thermodynamic Characterization of Nonconventional Energy Gases,” *J. Chem. Eng. Data*, vol. 57, no. 9, pp. 2581–2588, Sep. 2012.

CHAPTER 3

The single-sinker densimeter with magnetic suspension coupling

3.1. High accuracy methods for density measurements. State-of-the-art 47
3.2. The single-sinker densimeter with magnetic suspension coupling 53
3.3. Description of the UVA densimeter 55
3.4. Measurement process 70
3.5. Control and data acquisition software 80
3.6. Results of the measurements with nitrogen 86
3.7. Improvements on the equipment 86
3.8. References 89

3.1. HIGH ACCURACY METHODS FOR DENSITY MEASUREMENTS. STATE-OF-THE-ART

Density ρ is a physical magnitude referred to the amount of mass m in a determined volume V of any substance. Generally, density is expressed by equation 3.1 and its units in the International System of Units (SI) are kilograms per cubic meter ($kg \cdot m^{-3}$).

$$\rho = \frac{m}{V} \qquad \textbf{Eq. 3.1.}$$

The knowledge of the thermophysical properties of fluid substances is essential in design and implementation of industrial processes. These properties are calculated from equations of state, for whose development a great amount of experimental data are needed. In this sense, density is one of the most important properties for the development of reference equations of state. Therefore, density measurements in wide ranges of temperature and pressure are indispensable. However, not all density determination methods are adequate to this goal. The suitable densimeters to obtain experimental data to the development of equations of state must have the following characteristics [1]:

- The overall uncertainty of the apparatus in density terms (including temperature and pressure uncertainties) must be of the order of 10^4.
- The densimeters must work over wide ranges of temperature and pressure.

Only some sinker-densimeters keep strictly these conditions, however there are other techniques for density measurement of fluids. Density measurements methods can be grouped according to the scheme in Figure 3.1. There are five groups [2]: vibrating bodies, piezometer, bellows volumetry, isochoric methods and buoyancy densimeters.

Densimeters based on vibrating bodies

These kinds of densimeters are based in a mass-spring system. The resonance frequency of a body is measured and related with the density of the fluid around or inside the vibrating body. These densimeters are classified in:

Densimeters with vibrating hollow cylinders and vibrating forks: They is commercial equipment used to measure gas densities in natural gas supply pipelines. They work in moderate ranges of temperature (-10 and 80) ^{o}C and up to 15 MPa. Their standard uncertainty in density is around 0.5 % for natural gases and up to 3 % for pure fluids.

However there are corrections that reduce these values to 0.1 % for pure gases and 0.005 % for natural gases.

Vibrating-tube densimeters: This kind of densimeter is the most used apparatus for the experimental determination of density. They are commercial equipment with a resolution up to 10^{-3} kg·m^{-3} that allow fast and accurate density measurements of liquids in wide ranges of pressure and temperature. However, these densimeters require calibrations with reference fluids (water and nitrogen, usually) and the measurement accuracy is limited by the calibration process. Uncertainties are around of 0.1 %.

Vibrating-wire densimeters: The measuring principle in this kind of densimenters relates the viscosity or the buoyancy force with the frequency of the transverse oscillations of a wire immersed in the fluid. Their main application is in viscosity and density measurements of liquids, because the effect in gases is too small to be recorded reliably. They can cover wide ranges of temperature and pressures up to 1 GPa. Their uncertainty in density is approximately 0.1 %.

Piezometer

Methods for density determination based on this technique are divided in three categories:

Constant volume piezometer: Density is calculated by the gravimetric method from the mass of the fluid inside the cell.

Variable volume piezometer: The change of volume experimented in the cell is recorded and related to the fluid pressure.

Expansion piezometer: The sample is expanded and the ratio between the initial and the final volume is related to the density before and after the expansion.

Bellows volumetry

These densimeters are a kind of piezometer where the fluid is compressed inside a cell by a flex bellow. The lineal displacement of the bellow due to the pressure change is recorded and related to the fluid compression. There are different kinds of desimeters suitable for different temperature and pressure ranges, but all of them are oriented to be used with liquids.

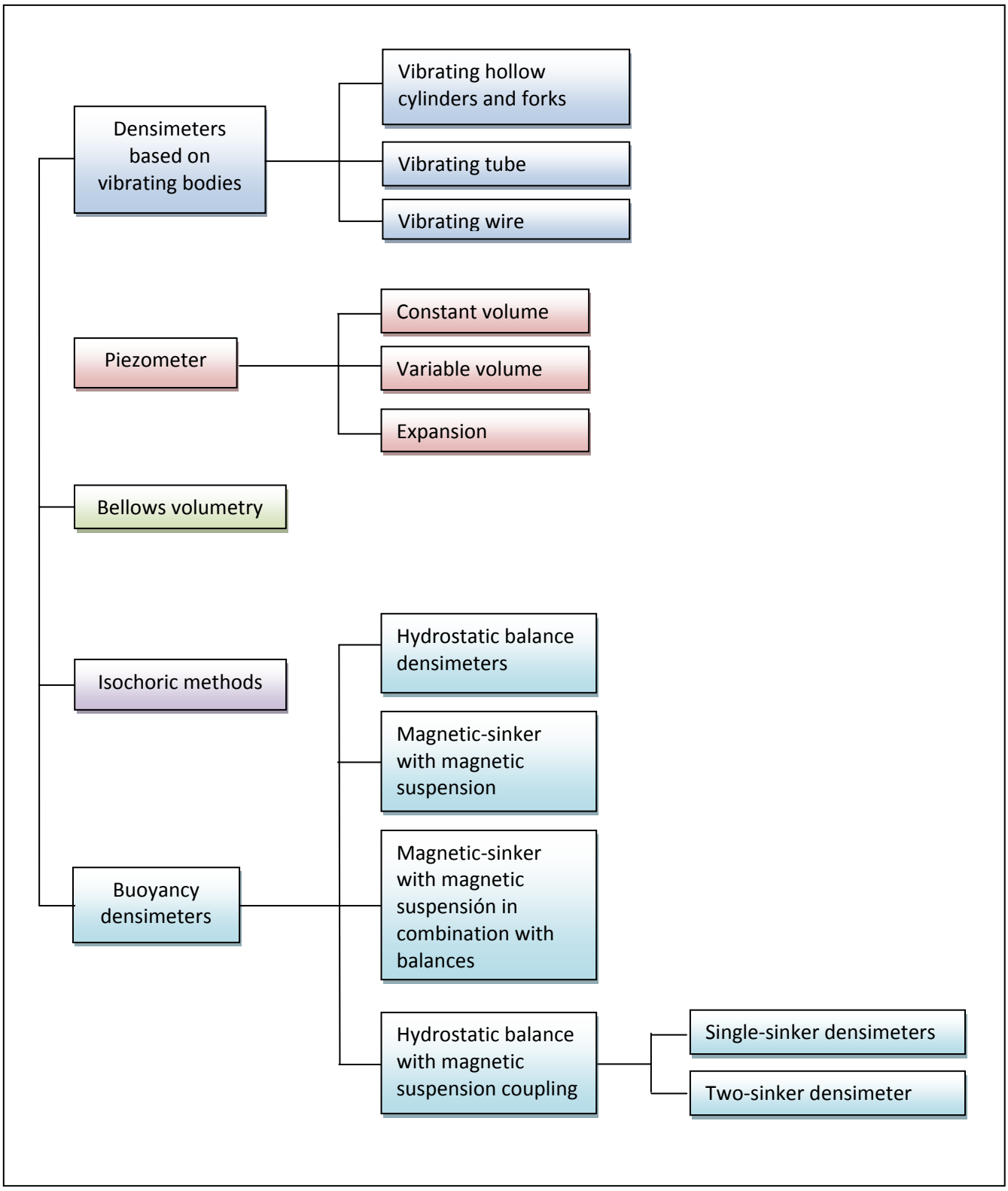

Figure 3.1. *Scheme of methods for density determination in fluids.*

Isochoric methods

In this kind of densimeters, an amount of fluid is compressed by using a compressor inside a small vessel of known volume immersed in a thermostatic bath. Density is determined by relating the volume of the vessel and the amount of fluid. Thanks to the simplicity to automate the process and the absense of contact with the fluid, isochoric methods have application with toxic fluids. Uncertainty is around 0.1 %.

Buoyancy densimeters

This kind of densimeters are based in the Archimedes' principle, which relates the buoyancy force experimented by a sinker immersed in the fluid with its density. Buoyancy densimeters are divided in four groups with different measuring systems, uncertainties and work ranges.

Hydrostatic balance densimeters: These densimeters are usually used in density measurements of liquids at ambient pressure and moderate temperature ranges. The overall uncertainty in density is close to 0.1 %. The measuring system consists of a sphere of glass or metal (sinker) suspended from an analytical commercial balance from a thin platinum wire. The liquid whose density will be determined is inside a thermostatized cell and the sinker is completely immersed in the fluid.

Magnetic float and magnetic suspension densimeters: These apparatus are used to measure liquid densities, mainly low densities at pressures up to 5 MPa (although there are some modifications that allow measuring up to 120 MPa) and temperatures between (90 and 300) K. The sinker remains in a stable position thanks to a solenoid located below the measuring cell. An optical device keep the sinker in a fixed position and the density is determined from the mass and the volume of the sinker (previously calibrated) and the magnetic force to keep the sinker in the fixed position.

Magnetic float and magnetic suspension densimeters in combination with balances: In this case the buoyancy force is directly weighed by a balance connected to the sinker with a thin wired. The liquid is inside a thermostatized cell and the sinker can be magnetically suspended by a solenoid with air core located on the cell. Density is determined measuring the weigh change of the sinker when the cell is evacuated and pressurized. There are different modifications reported, but in general the uncertainty is closed to 0.1 %. The cells are made of glass, so the pressure is limited to 5 MPa.

Hydrostatic densimeters with magnetic suspension coupling: Densimeters with magnetic suspension coupling calculates the apparent mass change of a non-magnetic sinker immersed in a fluid contained in a thermosttated cell by a balance without contact between the sinker and the balance. This methodology provides the most accuracy of all density determination methods described. It has application for liquids and gases in wide temperature, pressure and density ranges. Therefore, according to the considerations defined at the beginning of this section, these kinds of densimeters are the most adequate devices to obtain suitable experimental density data to analysins and development of equations of state.

Hydrostatic balance densimeters with magnetic suspension coupling are separated in two types in function of the number of sinker used:

- Two-sinker densimeter.
- Single-sinker densimeter.

The two-sinker densimeter was developed by Kleinrahm y Wagner [3][4] in the early eighties. The measuring method is based on the Archimedes principle but in a new way. The equipment has two sinkers with the same mass and the same surface but different volume. These sinkers are placed alternatively in a support connected to a commercial analytical balance through a magnetic suspension coupling system. Thus, the difference of the apparent mass of the two sinkers Δm^* can be determined accurately.

The magnetic suspension coupling was developed by Gast [5] and improved by Lösch et al. [6] to its application in the two-sinker densimeter. It consists of an electromagnet hanging from the weighing hook beneath the balance and a permanent magnet connected to the support where the sinkers are located by a thin bar. The electromagnet is in a casing independent of the measuring cell that keeps the magnets separated from each other. The distance between the magnets is adjusted by the power supplied to the electromagnet and controlled by the signal of a position sensor. Fluid density is calculated by equation 3.2.

$$\rho = \frac{\Delta m^* - \Delta m_{VAC}}{V_S - V_D} \qquad \textbf{Eq. 3.2}$$

where $\Delta m^* = \left(m^*_D - m^*_S\right)$ is the difference of the apparent masses of the two sinkers when the cell is pressurized, $\Delta m_{VAC} = \left(m_D - m_S\right)$ corresponds to the small difference of

apparent masses of the two sinkers when the cell is evacuated and V_S y V_D are the volumes of two sinkers.

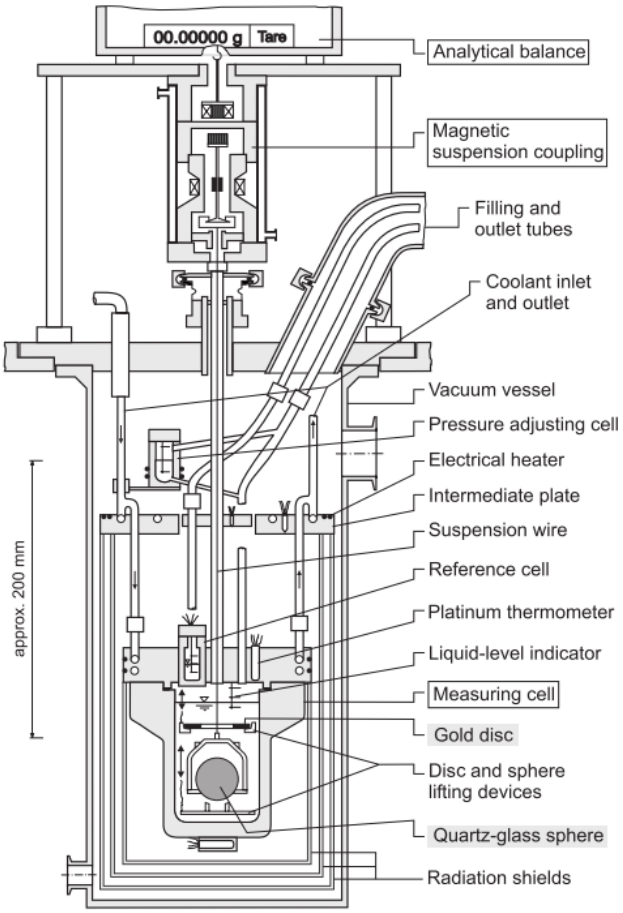

Figure 3.2. *Basic design of the two-sinker densimeter* [1].

This two-sinker system compensates secondary effects, like surface tension, adsorption effects, etc. Moreover it can operate in wide temperature and pressure ranges with very low uncertainties (a few parts in 10^5).

The sinker changing system is a very sophisticated device whose design is complex. Its main characteristic is that it gives a high accuracy in a wide range of density, including low gas densities. This is not always of significant importance, so a single-sinker densimeter with magnetic suspension coupling was developed in the beginning of the 90s, to simplify the measurement process of high and moderate densities. This equipment has been used to develop this doctoral thesis, so it is described in detail in the following section.

3.2. THE SINGLE-SINKER DENSIMETER WITH MAGNETIC SUSPENSION COUPLING

In the early 90s, Brachthäuser et al. [7] developed the first single-sinker, described in 1995 by Wagner et al. [8]. Since it has not a sinker changing device, the design and the measuring process are less complex than thoseof the two-sinker densimeter. However, secondary effects cannnot be offset, so the uncertainty in density is higher. The original design of the sinker-single densimeter was improved by Klimerck et al. [9] in order to reduce uncertainties in temperature, pressure and density. These improvements included a two-step thermostatic device that increased the stability and uniformity inside the measuring cell.

The measuring method is, as mentioned before, based on the Archimedes' principle. The buoyancy force experimented by a body (sinker) immersed in a fluid is proportional to the density of the fluid and the volume of the sinker. Thus, knowing the sinker volume, density can be determined by equation 3.3.

$$\rho(T,p)=\frac{B}{g\cdot V_S(T,p)}=\frac{m_{S0}-m_{Sf}}{V_S(T,p)} \qquad \textbf{Eq. 3.3}$$

where $\rho(T,p)$ is the fluid density in kg·m^{-3} as function of pressure and temperature; B is the buoyancy force expressed in N; g is the acceleration of gravity constant in m·s^{-2}; $V_S(T,p)$ is the volume of the sinker in m^3 as function of temperature and pressure of the fluid. The buoyancy force is determined by measuring the difference between the sinker mass when the cell is evacuated m_{S0} and the apparent mass when the sinker is immersed in the pressurized fluid m_{Sf}, both of them expressed in kg.

The single-sinker densimeter is currently used in research centers and industries for high accuracy density measurements. In the gas industry it is used to calibrate density transducers, as an example. In the research field, different laboratories have single-sinker densimeter in their installations [2]. At *Ruhr-Universität Bochum* in Germany, there are two single-sinker densimeters with different working ranges. The first one works in a temperature range from (233 to 523) K and up to 30 MPa. The other one is used to carry out density measurements in liquefied natural gas (LNG) samples at temperatures from (90 to 290) K and pressures up to 12 MPa. The uncertainty in density is less than 0.015 %. The *Physikalisch-Tesnische Bundesanstalt (PTB)*, in Germany, performs research related with

vapor-liquid equilibrium of pure fluids and mixtures by using two single-sinker densimeters. The reported uncertainty is 0.10 % for saturated vapor, and 0.02 % for saturated liquid. The densimeter of the *Texas A&M University* is designed to reach pressures up to 200 MPa at temperatures between (200 and 530) K. It is used to measure density of the components of natural gases and their mixtures. The uncertainty in density is between (0.05 and 0.10) %. The single-sinker densimeter of the *Keio University* in Yokohama, Japan, works in the temperature range from (223 to 423) K, pressure up to 15 MPa and densities up to 2000 kg·m^{-3}. Its uncertainty in density is 0.03 %.

Table 3.1. *Single-sinker densimeters used for researching.*

Research center	City, Country	Working range		$10^2\ U(\rho)$
		T/K	*p*/MPa	(*k* = 2)
Ruhr-Universität Bochum [8]	Bochum, Germany	233 - 523	30	$2\cdot10^{-4}\cdot\rho$
Ruhr-Universität Bochum [10]	Bochum, Germany	90 - 290	12	0.015
Physikalisch-Tesnische Bundesanstalt (PTB) [11]	Braunschweig, Germany	233 - 523	30	0.02 - 0.10
Texas A&M University [12]	College Station, EEUU	200 - 530	200	0.05 - 0.10
Keio University [13]	Yokohama, Japan	223 - 423	15	0.03
National Metrology Institute of Japan (NMIJ) [14]	Tsukuba, Japan	253 - 473	20	0.001
Chinese Academy of Sciences [15]	Beijing, China	210 - 300	6	0.01 - 0.08
Tsinghua University [16]	Beijing, China	273 - 423	35	0.033
National Engineering Laboratory (NEL) [17]	Glasgow, Scothland	233 - 423	30	0.015
Universität für Bodenkultur [1]	Vienna, Austria	-	-	-
Universidad de Valladolid [18]	Valladolid, Spain	233 - 523	20	0.025

The *National Metrology Institute of Japan* carries out density measurements of reference liquids (nonane, tridecane, water, tetrachlorethylene, etc.) used as density standards for subsequent calibrations of other densimeters. The working range of the densimeter is from (253 to 473) K and up to 20 MPa with uncertainties of a few parts per million. The *Chinese Academy of Sciences* of Beijing, China, has recently reported works with a single-sinker densimeter in the temperature range from (210 to 300) K and pressures up to 6 MPa. The single-sinker densimeter of the *Tsinghua University* in Beijing, China, is used to carry out

density measurements of binary mixtures in the temperature range from (273 to 423) K and pressures up to 35 MPa with uncertainties of 0.033 % (k = 2). The *National Engineering Laboratory (NEL)* of Glasgow has one densimeter especially designed for liquid density measurements in the temperature range from (233 to 423) K and pressures up to 30 MPa. The reported uncertainty in density is 0.015 %. Researchers at the *Universität für Bodenkultur* of Vienna, Austria, use their densimeter to study refrigerants and mixtures of the components of natural gases. Finally, the Universidad de Valladolid, Spain, has a single-sinker densimeter whose characteristics are descibed in detail in the following section.

3.3. DESCRIPTION OF THE UVA DENSIMETER

The single-sinker densimeter used in this work is located in the laboratory TERMOCAL, in the basement of the *Escuela de Ingenierías Industriales de la Universidad de Valladolid*, in an 18 m^2 room separated of the rest of the laboratory. The room is at atmospheric pressure and the temperature is controlled to (23 ± 2) ^oC thanks to an air-conditioning system, to avoid the influence of room temperature in the pressure transducers. Due to this, the room temperature is recorded during the measuring process. All the densimeter devices and auxiliary equipment are also located in this room. Finally, there is an extraction air system working continuously to avoid dangerous concentrations of toxic or flammable gases that may occur due to leaks or failures.

The main part of this single-sinker densimeter was made by *Rubotherm Präzisionsmesstechnik GmbH* and was bought by UVA in 1996. This is a compact version of the original single-sinker densimeter and it is used to determinate densities of pure fluids and binary and multicomponent mixtures in the gas phase. According to the manufacturer specifications, the densimeter works in the temperature range from (233 to 533) K and pressures up to 20 MPa. The implementation of the densimeter was carried out by Chamorro et al. [18] and later, Mondéjar [19] carried out important modifications to improve the uncertainties of the magnitudes involved in the measuring process: temperature, pressure and density.

The densimeter is formed by the measuring cell, an analytical microbalance, the weights changing device, the magnetic suspension coupling system, a system for the measurement and control of the temperature, a system for filling, evacuating and measuring the pressure, and a vacuum system. Special heat transfer oil is used as thermostatic fluid. The

fluid is previously thermostatized outside the measuring cell by a commercial thermostatic bath.

Figure 3.3 shows a scheme of the single-sinker densimeter used in this work and the main elements of the equipment which are described in the following sections.

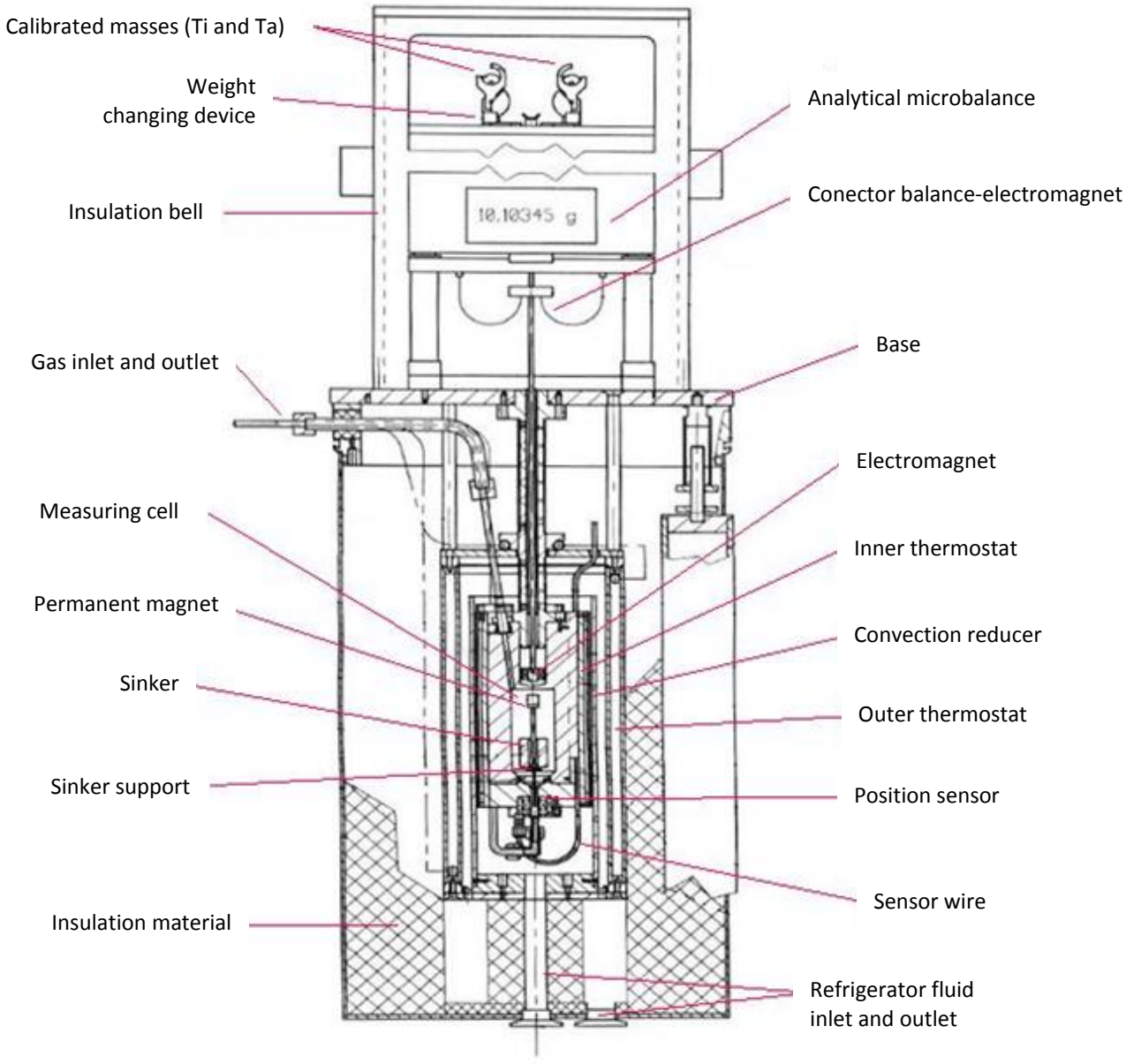

Figure 3.3. *Scheme of the single-sinker densimeter.*

Measuring cell

The measuring cell is divided in two hollows isolated from each other: the coupling housing (upper) and the measuring cell itself (lower). The electromagnet is located in the coupling housing and it is physically connected to the balance hook by a thin wire. The measuring cell is below the coupling house and contents the sinker and the permanent magnet, which is connected to the sinker support. Since the measuring cell is made in a copper, chrome and zirconium alloy (CuCrZr) its magnetic behavior is negligible and it has a high thermal resistance. The measuring cell is insulated by a silicone foam with density 250 $kg \cdot m^{-3}$ for a working range of (213 a 473) K and a casing made of polyethylene (Armaflex) for the temperature range (203 - 383) K. The measuring fluid is introduced and evacuated from the cell by two tubes.

Analytical microbalance

The sinker apparent mass measurements are performed by using an accurate analytical microbalance (Mettler Toledo AT261 DeltaRange). The technical specifications reported by the manufacturer are summarized in Table 3.2. The microbalance is inside an insulation bell above the measuring cell and located on a height-adjustable aluminum structure, to cancel vibrations produced in other parts of the equipment and ensure the horizontality of the balance. Figure 3.4 shows the microbalance and its support.

Table 3.2. *Technical specifications of the microbalance Mettler Toledo AT261 DeltaRange.*

Characteristic	Value
Resolution	0.01 mg
Maximal capacity	205 g
Repeatability	0.015 mg
Linearity	±0.08 mg
Linearity below 10 g	±0.03 mg
Stabilization time	8 - 12 seconds
Drift with temperature	±1.5 ppm/^{o}C

The measurement of the apparent sinker mass with the microbalance is carried out through the magnetic suspension coupling system between the lower balance hook and the sinker inside the measuring cell, so that there is not physical contact between them. This system allows operating in a wide range of pressures and temperatures with high accuracy. Since the microbalance is connected to a computer by mean of a data bus the measuring process is totally automatic. The magnetic suspension coupling system and the data acquisition software will be described in detail along this chapter.

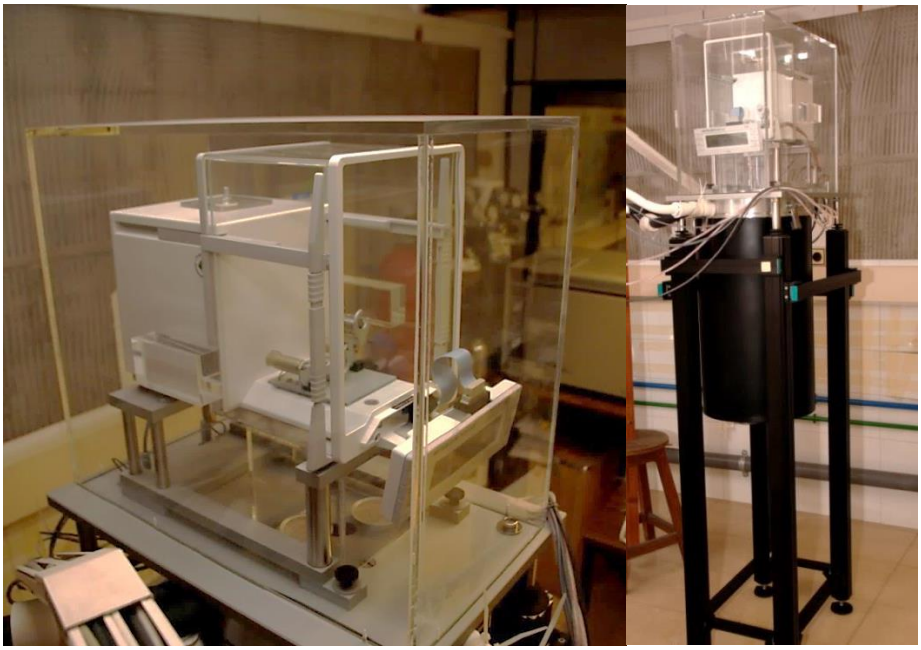

Figure 3.4. *Microbalance Mettler Toledo AT261 DeltaRange inside the insulation bell and adjustable support.*

Weight changing device

Balance calibration is carried out automatically by a weight changing device previously calibrated following the guidelines on the calibration of non-automatic weighing instruments of Euramet [20]. However, instead of the internal masses of the balance, external calibrated masses of tantalum and titanium are used.

These weights are made of tantalum ($\rho \approx 16670$ kg·m^{-3}) and titanium ($\rho \approx 4507$ kg·m^{-3}) with an approximate volume of 4.9 cm^3 ($V_{Ta} \approx V_{Ti} \approx 4.9$ cm^3). The balance is tared with both masses, so that the difference between them is close to the sinker mass ($m_S \approx 60$ g) thus reducing the "non-linearity effect" of the balance. Both weights were supplied by Rubotherm and were calibrated in the Mass Laboratory of the Spanish Centre of Metrology (CEM). The calibration of the weights was carried out by using a mass comparator with

mass standards Type MP5, under controlled room temperature, pressure and humidity. The volume was calibrated with a volume comparator with volume standards Type MP14 and MP12. The calibration results are detailed in Table 3.3.

Table 3.3. *Results from the mass and volume calibration of the weights of tantalum and titanium used in the changing device.*

Magnitude	Tantalum weight	Titanium weight
Real mass	82 g + 88.343 mg ± 0.100 mg	22 g + 399.677 mg ± 0.070 mg
Conventional mass	82 g + 94.748 mg ± 0.100 mg	22 g + 397.072 mg ± 0.070 mg
Volume (cm^3)	4.9240 ± 0.0007	4.9706 ± 0.0007
Density ($kg{\cdot}m^{-3}$)	16670.9 ± 2.5	4506.5 ± 0.6

The weight changing device can be operated manually by means of the controller provided by Rubotherm and shown in Figure 3.5, or automatically from the computer.

Figure 3.5. *Weight changing device controller.*

The weight changing device allows calibrating the balance without deviations due to the air buoyancy force on the calibrated masses. During the measurement process the calibration factor (CF) is also calculated to determine a meaningful value of the sinker apparent mass from the reading of the balance. The calibration factor is determined comparing the difference of the weight of the calibrated masses measured by the balance $(W_{Ta} - W_{Ti})$ with the weight difference from the calibration certifications of the both weights $(m_{Ta} - m_{Ti})$. The calibration factor can be calculated by equation 3.4.

$$CF = \frac{m_{Ta} - m_{Ti}}{W_{Ta} - W_{Ti}} \qquad \textbf{Eq. 3.4.}$$

The final value of the sinker apparent mass is calculated by multipliying the calibration factor CF and the reading value of the mass sinker in the balance m_{read}.

$$m = CF \cdot m_{read} \qquad \textbf{Eq. 3.5.}$$

The weight changing device is used because of the non-ideal character that any electronic balance presents, independently of its quality. This is the so called “non-linearity effect”. This effect is represented in Figure 3.6 and shows that there is a deviation between the real weight loaded in the balance and the reading of the weight, even if the balance has been calibrated in several points of the operation range.

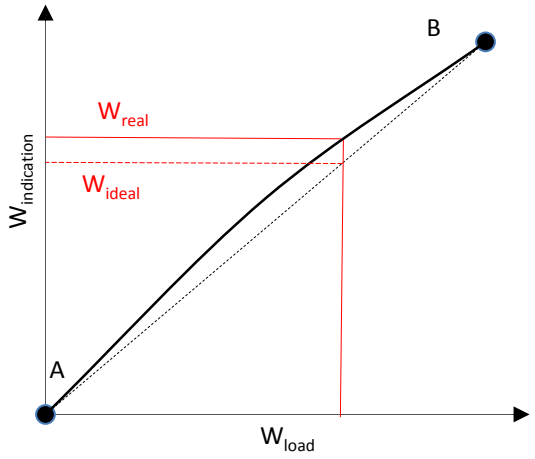

Figure 3.6. *“Non-linearity effect” of the real curve of a balance between two calibrated points (A and B).* W_{load} *refers to loaded weight and* $W_{indication}$ *indicates the balance reading.*

If a balance has been calibrated in the points A and B, the reading of any measurement between these calibrated points can differ from the real weigth of the load. However, if the weight of the load is close to one of the calibrated points, the difference between the real value and the balance indication will be negligible. The weights used to calibrate the balance always have an associated uncertainty. Thus, the most recommended working range to obtain high accuracy measurements avoiding the “non-linearity effect” is as close as possible to zero. This is the point where the weight changing device has application.

The weight changing device allows the balance to operate in a very small weight range. Thus, the effects due to the non-linearity of the measurements and the induced deviations due to the air buoyancy force are decreased to make them negligible. Moreover, as it can be seen in the specifications table, the non-linearity below 10 g is much lower than the

total non-linearity of the balance, so measurements will be more accurate working below this value.

The real mass of the sinker is approximately 60 g and the weight variations due to the buoyancy force produced by the fluid can be up to 10 g at densities near to 400 kg·m^{-3}. So, if the balance is tared with a calibrated mass whose mass is similar to that of the sinker (60 g), the measurements of the sinker mass will always be between zero and the variation due to the buoyancy force of the fluid (that will not be higher than 10 g). In this way, the "non-linearity effect" will be lower than if the balance recorded mass between (60 and 70) g. However, with the introduction of this calibrated mass with similar weight to the sinker, the air buoyancy force when the mass is placed in the balance has to be taken into account. The best alternative to cancel this effect is to use an additional calibrated mass with the same volume that the first one, so that the air buoyancy force is the same for both weights and it can be negligible. The weight changing device is above the balance, so the masses can be placed alternatively on the balance by two electronic motors, as is shown in Figure 3.7.

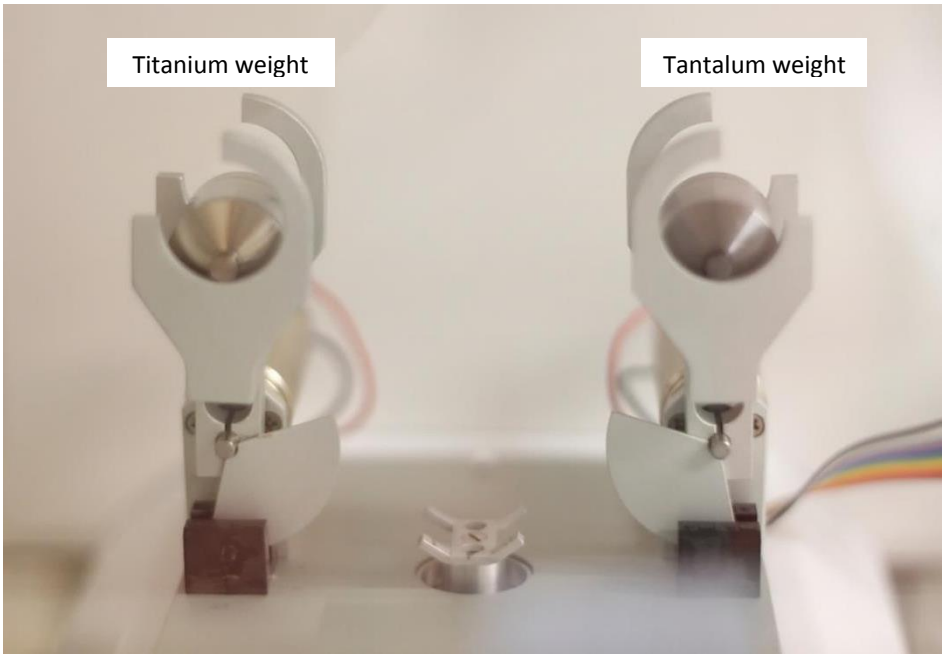

Figure 3.7. *Calibrated weight changing device.*

Magnetic suspension coupling system

The main component of the single-sinker densimeter is the magnetic suspension coupling device developed by Lösch et al. [6]. The device transmits the buoyancy force of the fluid

on the sinker to the accurate balance at atmospheric pressure without any contact between them.

The magnetic coupling is performed by two devices: the electromagnet hanging from the hook located below the balance and the permanent magnet assembled to the sinker support inside the measuring cell. Thanks to this system there is not physical contact between the sinker immersed in the fluid and the balance, allowing determining densities in wide ranges of temperature and high pressures.

The magnetic suspension coupling system can be controlled manually by the controller supplied by *Rubotherm* shown, in Figure 3.8, or automatically.

Figure 3.8. *Magnetic suspension coupling controller.*

This system allows controling the distance between the permanent magnet and the electromagnet, determining the position of the sinker support and, therefore the sinker position. There are two stable positions, in addition to the position when the system is off (OFF): *null position* (NP) and *measuring position* (MP). Each of the positions is explained below and all of them are represented in Figure 3.9.

- **Off position (OFF)**: When the magnetic coupling is switched off, both the sinker support and the sinker rest at the bottom of the measuring cell. The balance load in this case is the sum of the electromagnet weight and the balance hook weight.
- **Null position (NP)**: When the system is switched on, the permanent magnet is attracted by the electromagnet and the sinker support levitates without lifting the sinker. The balance load is the sum of the weights of the electromagnet, the balance hook and the sinker support.
- **Measuring position (MP)**: In this position both the sinker support and the sinker levitate together inside the measuring cell without any contact with the top of the cell. The balance load in the measuring position is the sum of the weights of the

electromagnet, the balance hook, the sinker support, and the sinker (independently if it is affected by the buoyancy force of the fluid).

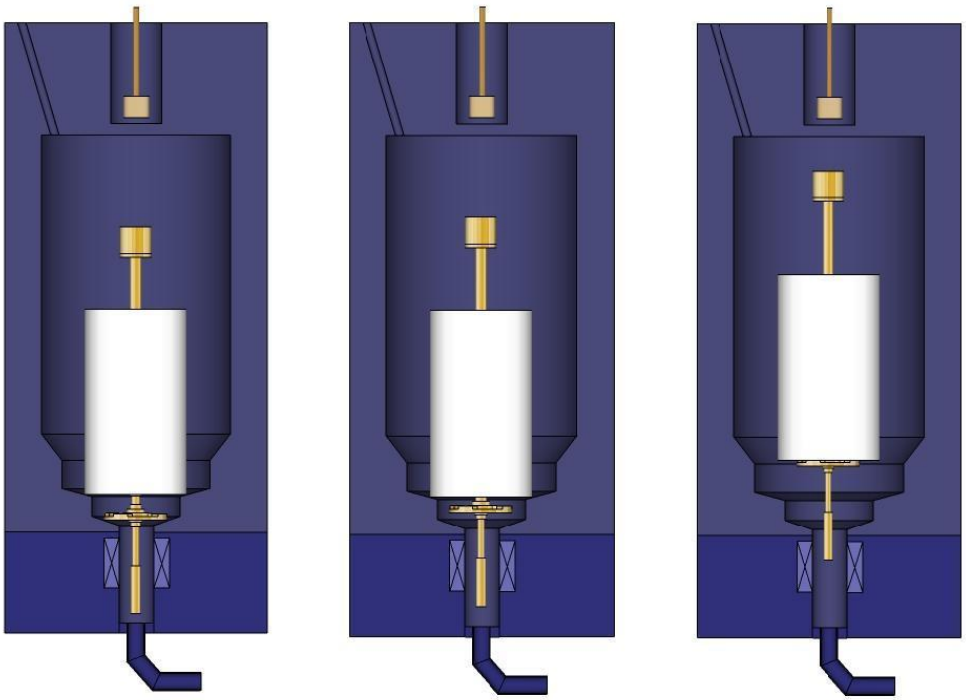

Figure 3.9. *Magnetic suspension coupling positions.*

The combination of the magnetic suspension coupling and the automatic calibration of the microbalance by the weight changing device determine the process of measurement of the apparent mass of the sinker.

System for measurement and control of the temperature

The measuring cell is thermostatized by two independent thermostatic systems: the outer thermostat system by which a "gross setting" of the temperature is made, and the inner thermostat system, directly in contact with the measuring cell, by which the "fine setting" of the temperature is made. The combination of both systems allows reaching the target temperature inside the measuring cell with high accuracy.

The outer thermostatic system consists in a double-walled stainless steel cylinder through which special heat transfer oil (*silicon oil Dow Corning 200 Fluid, viscosity 10 cst*) is passed. The temperature of the thermostatic fluid is controlled by a refrigerating-heating circulator

(Julabo FP50-HE) which acts on a thermostatic bath (Julabo FP50). According to the manufacturer specifications, the working range is from (–50 to 200) ^{o}C. Although the lines and the double-walled cylinder are covered with insulating material, the ambient temperature influences in the yield of the thermostatic bath and the temperature of the fluid. Therefore the setting temperature of the bath for each isotherm is lower than the target temperature inside the measuring cell (depends on if the required temperature is higher or lower than ambient temperature). The bath temperature values for each isotherm were established based on previous experiences along the years. A convection reducer cylinder made of copper is installed between the double-walled cylinder and the inner thermostatic system to ensure a homogeneous heat transmission to the cell. Figure 3.10 shows the outer thermostatic elements.

Figure 3.10 *Double-walled stainless steel cylinder and refrigerated-heating circulator Julabo FP50-HE.*

The inner thermostatic system consists of an electrical heating cylinder which is directly in contact with the measuring cell. The required temperature is set by an electronic controller (Julabo MC-E). This device works based on the temperatures registered by three temperature probes PRT-100 (A1, A2 and S). Probe “A2” is used for temperature control, “S” is a safety temperature probe and probe “A1” is used for secondary temperature control, which is not used in this configuration. Figure 3.11 shows the disposition of the temperature control probes in the inner thermostatic system, the electrical heating cylinder and the electronic controller.

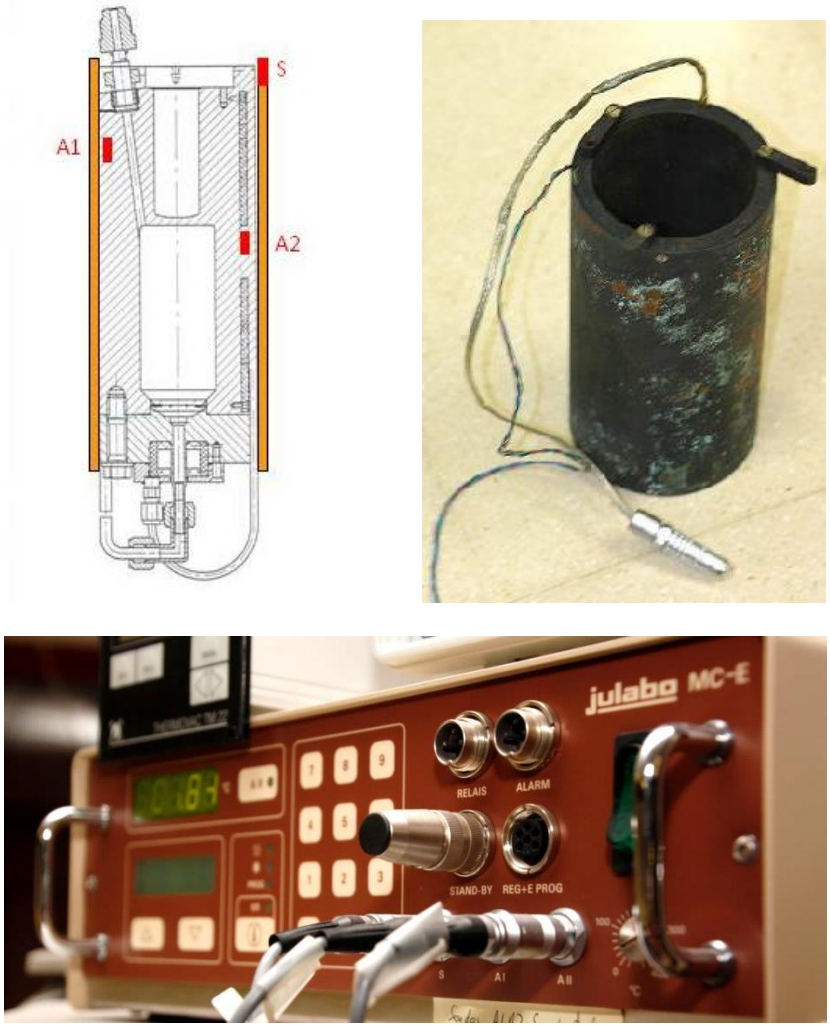

Figure 3.11. *Scheme of the inner thermostatic system with the location of the temperature controlled probes in the measuring cells, the electrical heating cylinder and the Julabo MC-E controller.*

Temperature inside the measuring cell is determined through two PRT-25 Minco S1059PJ5X6 probes (Minco 712 y Minco 713) located opposite to each other in the middle of the measuring cell, as shown in Figure 3.6. Another PRT-25 Rosemount probe is near to the coupling house to determine if there is vertical gradient of temperatures inside the cell. The three probes are connected to the AC comparator resistance bridge (Automatic Systems Laboratory F700) through a multichannel switchbox (Automatic Systems Laboratory SB 148/01). The bridge measures the resistance ratio between the PRT-25 probe and an external standard resistor calibrated and thermostatized to 36 ^{o}C (Tinsley 5685, 25Ω).

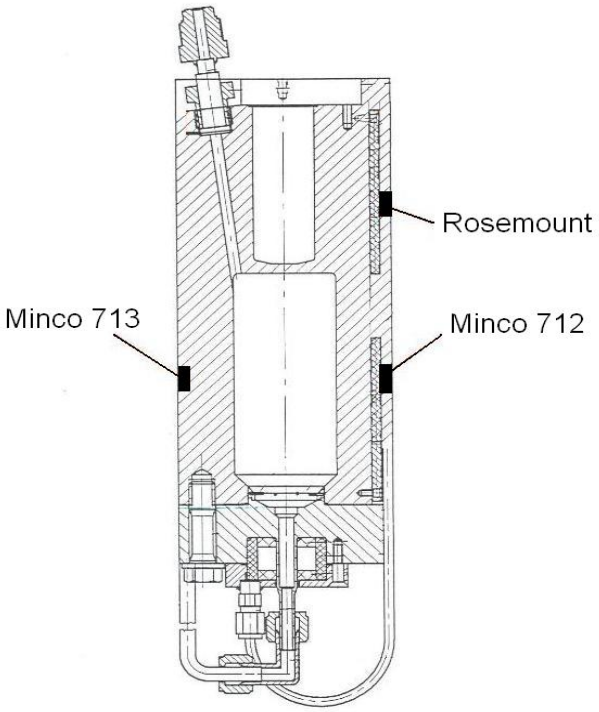

Figure 3.12. *Location of the PRT-25 temperature probes in the measuring cell.*

Temperature probes were calibrated in TERMOCAL, which is a metrology laboratory accredited by ENAC. Resistence ratios registered by probes were transformed in absolute temperature values by reference functions defined in the Absolute International Temperature Scale ITS90 [21] taking into account the constants of their respectives calibration certificates. The corrected temperature is expressed in Kelvin. The arithmetic average of the temperatures registered by Minco 712 and Minco 713 probes was used for the fluid density determination in each measurement point.

System for filling, evacuating and measuring the pressure

The pressure inside the cell is determined by two pressure transducers: Paroscientific 43KR-HHT-101 for pressure range from (2 to 20) MPa and Paroscientific 2300A-101 from (0 to 2) MPa. Both transducers are connected to two Digiquartz® intelligent displays (models 730 and 735, respectively) and to the filling system, according to Figure 3.13.

Figure 3.13. *Pressure transducers used to measure the pressure in the range (2 - 20) MPa (up) and (0 - 2) MPa (down).*

The transducer which works up to 2 MPa is separated from the network thanks to a manually operated valve to avoid overpressure of the equipment. Therefore, the manually operated valve must be opened when the fluid pressure is below 2 MPa for each isotherm.

The pressure values registered by the transducers are corrected by a polynomial function of fifth order from the parameters of the calibration certificates of each transducer. Pressure transducers were also calibrated at TERMOCAL.

The system for filling, evacuating and measuring the pressure , and all its components, is represented in Figure 3.14. The tubing of the pressurized network is made of stainless steel. The tubing connected to the measuring cell and to the vacuum line has an outer diameter of 1/4”. The cylinder with the measuring fluid is connected to the pressurized network by tubing with an outer diameter of 1/8”. The rest of the tubing has outer diameters of 1/16”. The network was designed to work up to 105 MPa and all its elements were supplied by HiP (*High Pressure Equipment Company*). The manual pump used to pressurize the measuring cell (HiP Model 87-6-5; 5000 psi) is made of stainless steel.

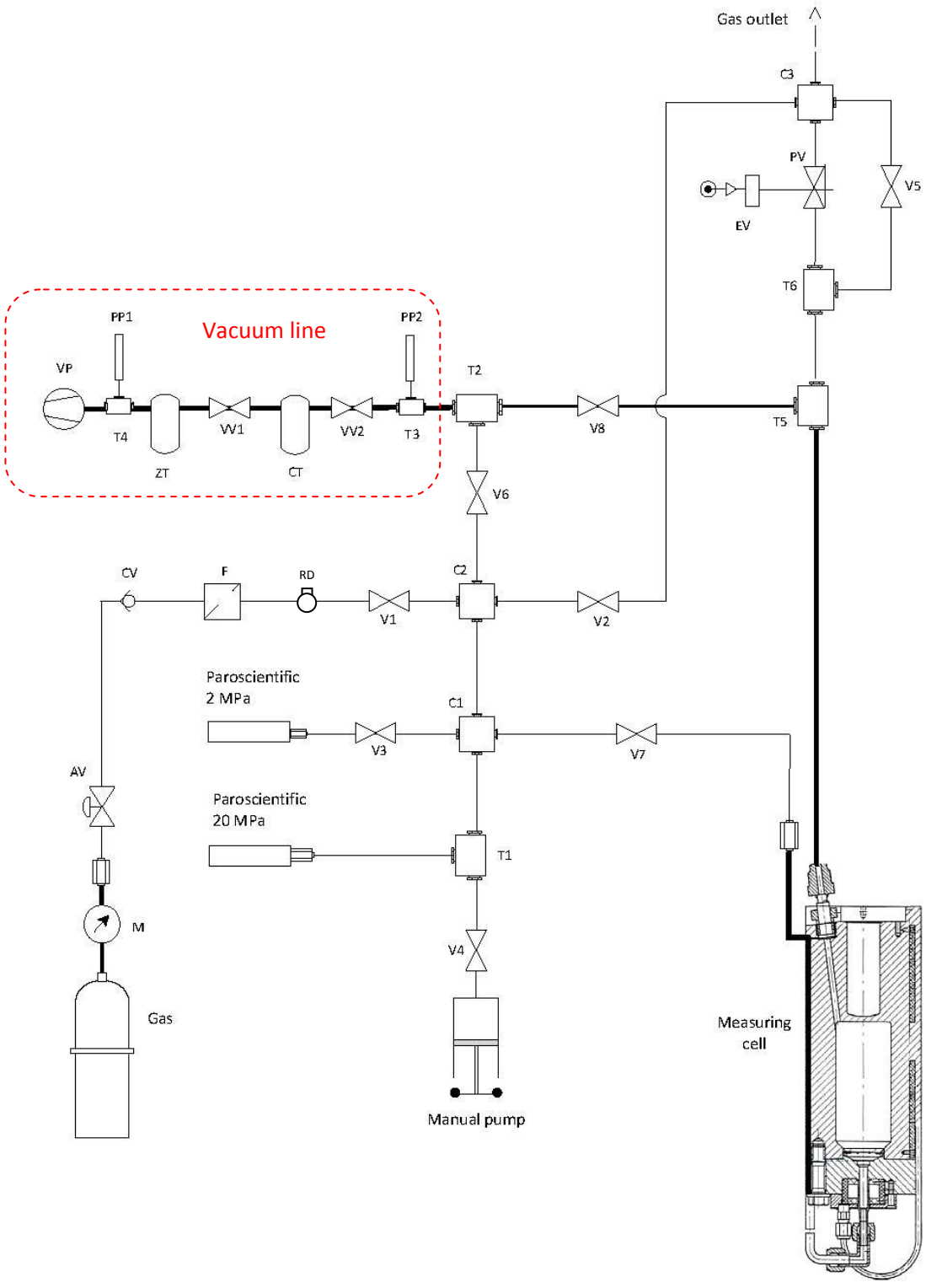

Figure 3.14. *Schematic flow diagram of the network used to fill and evacuate the measuring cell of the single-sinker densimeter. V1-V8: High pressure valves (20 MPa). EV: Electrovalve. PV: Piston air-operated valve. C1-C3: High pressure cross fittings. T1-T6: High pressure "T" fittings. VP: Vacuum pump. M: Manometer. VV1-VV2: Vacuum line valves. ZT: Zeolites trap. CT: Cryogenic trap. PP1-PP2: vacuum probes. AV: pressure reducer. F: filter. RD: ruptura disc. CV: check valve.*

Vacuum system

The vacuum system is connected to the filling and evacuating system through valve V6 and directly to the measuring cell through valve V8. Therefore, it is possible to evacuate the tubing or the measuring cell independently. The vacuum inside the cell is achieved by a two-stage rotator vacuum pump (Leybold TRIVAC D8B) which can create a vacuum of 0.5 Pa. There are two traps between the measuring cell and the vacuum pump to avoid the entry of impurities and damaging vapors into the measuring cell or the pump. The first trap is a zeolite trap (Leybold FA 2-4) which prevents the migration of water or hydrocarbon molecules from the pump to the measuring cell. The second trap is a cryogenic trap (Leybold TK 4-8) which protects the pump from damaging vapors. The trap must be filled with liquid nitrogen when the vacuum pump is working. The pressure during the evacuation process is controlled by two vacuum probes connected to a vacuometer (Thermovac TM22) which works in the pressure range from $5 \cdot 10^{-4}$ Pa to atmospheric pressure. Figure 3.15 shows the elements of the vacuum system.

Figure 3.15. *Elements of the vacuum system: zeolites trap, cryogenic trap, vacuometer and vacuum pump.*

3.4. MEASUREMENT PROCESS

The data collection process is carried out by logging the density of the fluid in isotherms at (250, 275, 300, 325, 350, 375 and 400) K. For each isotherm the pressure is decreased in 1 MPa steps from (20 to 1) MPa. The vacuum system is turned on after each isotherm to measure the sinker mass when the cell is evacuated. 30 (p, ρ, T) measurements are logged in each pressure step.

Filling and pressurization of the measuring cell

The filling of the measuring cell is carried out manually using the panel valves shown in Figure 3.14. The cylinder with the measuring gas is connected to the network through a valve which controls the filling process.

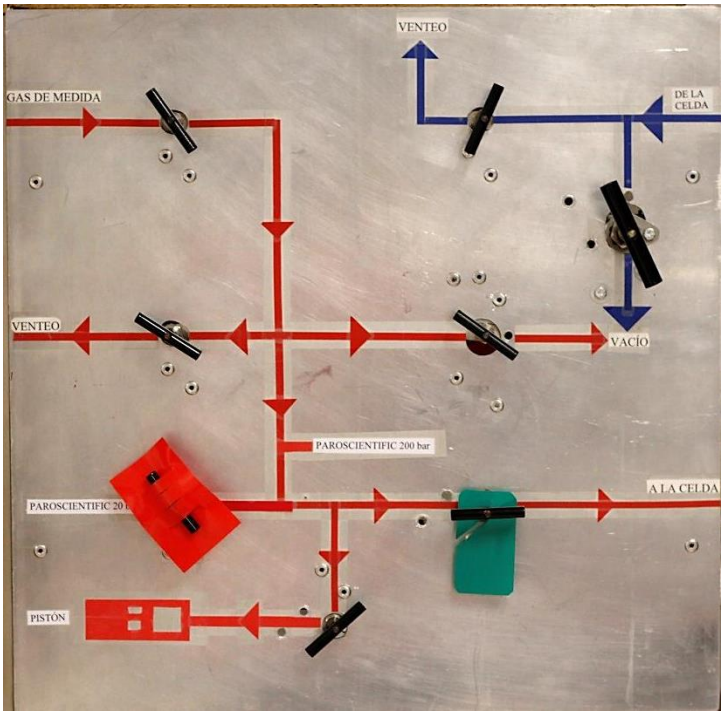

Figure 3.16. *Valves panel.*

The initial pressure of the cylinder must be considered before filling the measuring cell. If its pressure is 20 MPa or above, the measuring cell is filled by opening the valves V1 and V7, providing a continuous and moderate gas flow up to 20 MPa. If the cylinder pressure is less than 20 MPa, the manual pump must be used to fill the measuring cell. The first step is filling the measuring cell (V7) and the manual pump (V4) with the gas at the supplied

pressure. Then valve V1 is closed and the measuring cell is pressurized by the manual pump. If pressure inside the cell is still less than 20 MPa, it is necessary to do another manual pressurizing, closing valve V7 and opening valve V1, allowing the entry of fresh gas to the network and the manual pump. Then, valve V1 is closed and the pressure is increased by the manual pump up to the target pressure of the previous pressurizing step. In that moment valve V7 is opened, and the measuring cell is pressurized to a new pressure manually. This process has to be repeated until the required pressure inside the measuring is reached.

If pressurizing and heating of the measuring cell are performed at the same time, the increment of pressure inside the cell due to the increment of temperature must be considered to avoid overpressure. Nevertheless, there is an automatic evacuation system if pressure exceeds 20 MPa

Pressure control in the measuring cell

Evacuation of the measuring cell can be done manually or automatically by a pneumatic valve. Both systems are equivalent. The manual evacuation allows depressurizing the cell before measuring the sinker mass in vacuum at the end of each isotherm. It can be performed by valve V2 (from the pressurized network) and/or by valve V5 (directly from the measuring cell).

The automatic pressure control of the measuring cell is designed to vary the pressure in 1 MPa steps during the measurement of an isotherm, making the measurement process totally automatic. If the pressure inside the measuring cell is higher than 20 MPa, the automatic evacuation is also activated. A piston air-operated valve (Mini-Hippo Piston air-operated valve 50-90 psi) is remotely operated from the control computer. When the measurements of a pressure-step are over (30 measurements) the piston valve is automatically opened depressurizing the measuring cell. The transducer from (2 - 20) MPa (Paroscientific 43KR-HHT-101) controls the pressure and when the fitted pressure of the next pressure-step of the isotherm is reached, the valve is automatically closed and measurements start again.

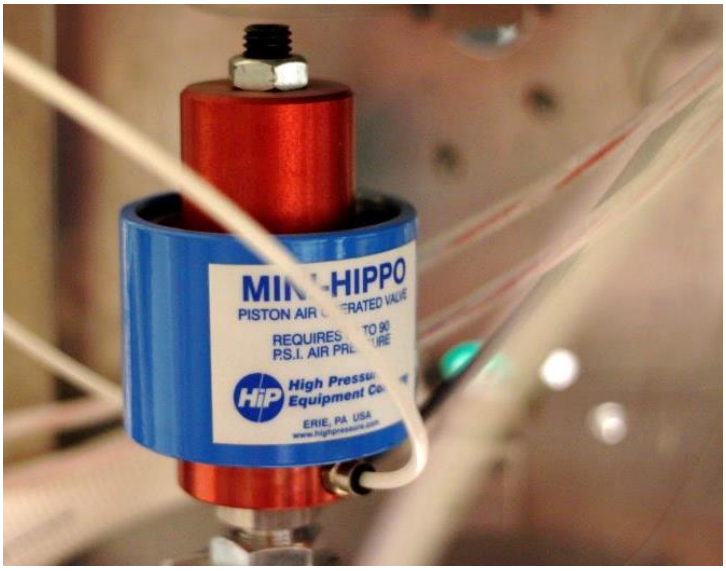

Figure 3.10. *Piston air-operated valve.*

Force transmission error

The magnetic coupling is of great advantage for the density measurements. However it is sensitive to deviations. The magnetic force transmitted between the electromagnet and the permanent magnet can be influenced by external magnetic fields or by the magnetic properties of the sinker, the measuring cell or the measured fluid. This effect is known as "force transmission error" (FTE) and it was described in detail by McLinden et al. [22]. The FTE affects both the single-sinker and the two-sinker densimeter.

In the case of the single-sinker densimeter, the FTE can be separated in two terms: error induced by the apparatus and error induced by the fluid, as is shown in equation 3.6.

$$\frac{\Delta\rho}{\rho_f} = \underbrace{\left(1-\phi_0\right)\cdot\frac{\rho_S-\rho_f}{\rho_f}}_{\text{Apparatus FTE}} - \overbrace{\varepsilon_\rho\cdot\frac{\chi_f}{\chi_{f0}}\cdot\left(\frac{\rho_S}{\rho_0}-\frac{\rho_f}{\rho_0}\right)}^{\text{Fluid FTE}} \qquad \textbf{Eq. 3.6}$$

where ρ_f and ρ_S are the fluid and sinker densities, respectively; ϕ_0 is the coupling factor; χ_f is the magnetic susceptibility of the fluid; ε_ρ is the apparatus specific constant; and ρ_0 = 1000 kg·m^{-3} y χ_{f0} = 10^{-8} m^3·kg^{-1} are reduced constants. The first term of the expression represents the relative effect of the FTE induced by the apparatus in terms of density. The

second term refers to the FTE induced by the fluid and it depends on the magnetic susceptibility of the fluid.

The FTE induced by the magnetic behavior of the components of the equipment can be determined when the cell is evacuated $(\rho_f = 0)$ and the magnetic influence of the fluid is null. Therefore, the difference between the real mass of the sinker and the reading of the balance is the FTE induced by the apparatus, according to equation 3.7.

$$W_{S0} = m_{S0} + FTE_{apparatus} \qquad \textbf{Eq. 3.7}$$

The FTE induced by the apparatus varies with temperature and also if spatial modifications have been carried out in the equipment, like the leveling of the balance or the centering of the rod of the electromagnet. For this reason, the experimental process includes the mass sinker measuring when the cell is evacuated after each isotherm recording. Thus, any influence of the FTE induced by the apparatus in density measurements is cancelled, according to McLinden et al. [22].

The FTE induced by the magnetic behavior of the fluid or "fluid specific effect" depends, as it can be seen in equation 3.6, on the magnetic susceptibility of the fluid χ_f, the density difference between the sinker $(\rho_S - \rho_f)$ and the fluid and the specific constant of the apparatus ε_ρ.

The magnetic susceptibility of the fluid χ_f affects the FTE induced by the fluid proportionally. Fluids with strong diamagnetic or paramagnetic behavior, like water and oxygen, respectively, affect significantly to the transmission of the weight by the magnetic coupling. The specific fluid effect will be higher when the difference between the density of the fluid and the density of the sinker is higher. This means that the FTE affects more at low densities than at high fluid densities. Finally, the apparatus specific constant ε_ρ depends on the configuration of the equipment. McLinden describes a methodology to calculate ε_ρ trought the comparison of measurements in the same densimeter, with the same fluid at the same temperature and pressure conditions with different sinkers [22]. The value of ε_ρ is then obtained by comparing the deviation of the experimental density data with the values obtained from the fluid reference equation of state. The value of the specific fluid effect with each sinker is expressed by equation 3.8 and 3.9.

$$\frac{\rho_{S1}-\rho_{EoS,1}}{\rho_{EoS,1}}=-\varepsilon_{\rho}\cdot\frac{\chi_f}{\chi_{f0}}\cdot\left(\frac{\rho_{S1}}{\rho_0}-\frac{\rho_{EoS,1}}{\rho_0}\right) \qquad \textbf{Eq. 3.8.}$$

$$\frac{\rho_{S1}-\rho_{EoS,2}}{\rho_{EoS,2}}=-\varepsilon_{\rho}\cdot\frac{\chi_f}{\chi_{f0}}\cdot\left(\frac{\rho_{S2}}{\rho_0}-\frac{\rho_{EoS,2}}{\rho_0}\right) \qquad \textbf{Eq. 3.9.}$$

The apparatus specific constant is calculated with equation 3.10, assuming that the density estimated from the equation of state is the same in both experiences $\left(\rho_{EoS,1}=\rho_{EoS,2}\right)$.

$$\varepsilon_{\rho}=\frac{\chi_f}{\chi_{f0}}\cdot\left(\frac{\rho_0}{\rho_{S2}-\rho_{S1}}\right)\cdot\left(\frac{\rho_1-\rho_2}{\rho_{EoS}}\right) \qquad \textbf{Eq. 3.10.}$$

Due to the measuring process followed in this work it is very complicated to compare the performance of different experiences at the exact same temperature and pressure conditions with different sinkers. However, Mondéjar et al. [Ref] estimated the apparatus specific constant ε_{ρ} comparing density results obtained with the current sinker of the densimeter with density data from previous experiences with the original sinker supplied with the densimeter at the same temperature and pressure conditions [23]. The average value for ε_{ρ} was 45.7 ppm. This is equivalent to a correction in density about 0.005 % (ρ = 300 kg·m^{-3}). Although the number of data was low, other authors reported silimar values (ε_{ρ} = 189 ppm, Cristancho et al. [24]; ε_{ρ} = 36 ppm Klimeck [25]). Since this value is not too significant, there is not a considerable lack of accuracy in the measurements due to the FTE. In addition, according to McLinden et al. [22], the FTE induced by the apparatus affects more than the FTE induced by the fluid (except for strongly paramagnetic fluids), and it is cancelled by measuring the sinker mass when the cell is evacuated. Therefore, the experimental data reported in this work were not corrected in relation to fluid specific effect. However, the estimation of the parameters and the justification about the influence of the fluid specific effect in the experimental density data are detailed in the chapters with the results of each measured mixture.

Apparent mass measuring process

The mass measuring process is carried out by combining the different positions of the magnetic suspension coupling system and the calibrated weight changing device. Therefore, the non-linearity effect of the balance is reduced in the sinker mass measuring

at pressure conditions or when the measuring cell is evacuated and the weights of the sinker support, the electromagnet and the balance hook are cancelled. Two different measurements are defined in function of the position of the magnetic coupling:

- **Zero point (ZP)**: The magnetic coupling is in null position (NP) and the tantalum mass is on the balance. The load of the balance is determined by equation 3.11.

$$m_{ZP} = m_{Ta} + m_{electromagnet} + m_{magnet} \qquad \textbf{Eq. 3.11.}$$

- **Measuring point (MP)**: The magnetic suspension coupling is in measuring position (MP) and the titanium mass is on the balance. The load of the balance is calculated by equation 3.12.

$$m_{MP} = m_{Ti} + m_{electromagnet} + m_{magnet} + m_{Sf} \qquad \textbf{Ec. 3.12.}$$

The steps of the mass measuring process are described as follows:

- **Step 1:** The magnetic coupling is switched on in the null position before each measuring point.
- **Step 2**: The calibration factor is determined. The tantalum mass is on the balance, and after the stabilization time, which takes around 25 seconds, the balance is tared. Afterwards, the tantalum mass is replaced by the titanium mass. The weight difference between both values is recorded and the software calculates the calibration factor CF by equation 3.4.
- **Step 3**: With the magnetic coupling still in null position, the tantalum mass is placed one more time on the balance and it is tared again. This is the “zero point” (ZP).
- **Step 4**: The tantalum mass is replaced by the titanium mass and the magnetic coupling is in the measuring position (MP). After the stabilization period, the apparent sinker mass is read by the balance and logged.
- **Step 5**: Finally, the calibrated weights and the magnetic coupling return to their initial positions.

The described process is valid for both measurements when the cell is pressurized or evacuated. Following this process, the unknown masses of the electromagnet and the permanent magnet are cancelled. In addition, the air buoyancy force acting on the

calibrated masses in the balance is cancelled by subtracting the balance reading in the measuring point (MP) and the zero point (ZP), according to equations 3.13 and 3.14.

$$(MP-ZP)(T,p)=(m_{Ti}-m_{Ta})+m_{Sf} \qquad \textbf{Eq. 3.13.}$$

$$(MP-ZP)(T,0)=(m_{Ti}-m_{Ta})+m_{S0} \qquad \textbf{Eq. 3.14.}$$

With the described process, the possible sorption effects of gas molecules in the measuring cell walls and in the sinker is the only known effect whicn is not compensated during the measuring process. This effect was evaluated for each measured mixture and is explained in detail in chapters 6, 7 and 8.

Finally, the density of the fluid can be calculated by subtracting equations 3.13 y 3.14, according to equation 3.15.

$$\rho(T,p)=\frac{(MP-ZP)(T,0)-(MP-ZP)(T,p)}{V_S(T,p)}=\frac{m_{S0}-m_{Sf}}{V_S(T,p)} \qquad \textbf{Eq. 3.15.}$$

Sinker volume calculation

The volume of the sinker $V_S(T,p)$ is not constant during the density measuring process. It is influenced by pressure and temperature of the measuring fluid. Therefore the sinker volume is calculated for each measuring point from the pressure, temperature and calibration sinker volume data.

The sinker used in this work is made of silicon. The size and material of the sinker depend on two factors: the densimeter operation range, in terms of density, and the maximum measuring fluid density. The buoyancy force has effect over the weight of the sinker and this variation has to be quantified by the balance using the magnetic suspension coupling system. Therefore the density of the sinker must be higher than the higher density of the fluid during the measurements. Thus, high density sinkers are needed for liquids or gases at ver high pressures, while low density sinkers give more accurate measurements at lower and moderate pressures. On the other hand, the buoyancy force acting on the sinker is proportional to the sinker volume. Due to the limited balance resolution, the higher buoyancy force the better balance reading, which yields in the end more accurate measurements. So, a sinker with higher volume provides higher accuracy of the density measurements.

Figure 3.18. *Silicon sinker and its support.*

The original sinker supplied with the densimeter was made of titanium (volume 13.26 cm^3 and density 4500 $kg \cdot m^{-3}$). The improvements developed by Mondéjar [19] to reduce measurement uncertainties included the evaluation of the suitability of the sinker in the temperature range from (250 to 400) K and up to 20 MPa. The best results were obtained with a lower density and higher volume sinker. Therefore the original titanium sinker was replaced by the current silicon sinker. This sinker has a volume of 26 cm^3 and an approximated density of 2300 $kg \cdot m^{-3}$.

The influence of the sinker in the fluid specific effect previously described is also lower with this sinker. According to equation 3.6, the FTE induced by the fluid is lower when the different between fluid and sinker densities is small. The silicon sinker has lower density than titanium sinker, so that the fluid specific effect is lower too.

The silicon sinker was made and supplied by Rubotherm and calibrated by DKD (*Deutscher Kalibrierdienst*) and CEM. Table 3.4 shows the calibration data and the expanded uncertainties (k = 2). Density calculations were carried out by considering the results obtained by CEM due to the reported lower volume uncertainties.

Table 3.4. *Calibration data of the silicon sinker.*

	DKD	CEM
Date	20/05/2009	17/09/2009
Volume (cm^3)	26.444 ± 0.015	26.444 ± 0.003
Real mass (g)	-	61.59181 ± 0.00016
Density ($kg \cdot m^{-3}$)	2329 ± 2	2329.12 ± 0.35
Calibration conditions		
Room temperature (°C)	(19.9 - 20.3)	21.3 ± 0.15
Room pressure (mbar)	(1011.37 - 1011.77)	934.17 ± 0.03
Room humidity (%)	(49 - 54)	46.0 ± 0.5

The volume of the sinker varies with pressure and temperature, so its value must be calculated as a function of these parameters and the thermal and mechanical properties of the silicon. The volume of the sinker in function of pressure and temperature is calculated by using equation 3.16.

$$V(T,p)=V_0(T_0,p_0)\cdot\left[1+3\cdot\alpha(T)\cdot(T-T_0)-\frac{3\cdot(p-p_0)}{E(T)}\cdot(1-2\nu(T))\right] \qquad \textbf{Eq. 3.16.}$$

This equation assumes that the material is isotropic and the lineal expansion coefficient $\alpha(T)$, the Young's module $E(T)$ and the Poisson's coeficient ν have the same values in the three spatial directions. Silicon is an anisotropic material, so the properties of the sinker may vary in function of the superficial direction of the material. An intensive analysis of the silicon properties was needed to calculate the average values for equation 3.16.

The thermal properties of silicon have been widely studied in the last years due to the great importance of this material in the ICT industry and the manufacturing of photovoltaic cells. The most accurate values to calculate the lineal expansion coefficient of silicon in the temperature range from (90 to 850) K is given by equation 3.17, where T is the temperature of the fluid [26].

$$\alpha(T)=\alpha+A\cdot\frac{\left(\frac{\Theta_E}{T}\right)^2\cdot e^{\frac{\Theta_E}{T}}}{\left(e^{\frac{\Theta_E}{T}}-1\right)^2}+B\cdot\frac{\left(\frac{T}{\Phi_0}-1\right)^2}{1+b\cdot\frac{T}{\Phi_0}} \qquad \textbf{Eq. 3.17.}$$

Parameters for calculating $\alpha(T)$ by equation 3.17 are detailed in Table 3.5. The uncertainty of this equation is $10^{-8}\ K^{-1}$.

Table 3.5. *Parameters of equation 3.17.*

Parameter	Value	Units
a	$-0.687\cdot10^{-6}$	K^{-1}
A	$5\cdot10^{-6}$	K^{-1}
Θ_E	685	K
B	$0.22\cdot10^{-6}$	K^{-1}
b	0.316	-
Φ_0	395	K

The variation of the sinker volume due to fluid pressure depends mainly on the Young's module E and on the Poisson's coefficient ν. Due to the anisotropy of silicon, properties vary in function of the direction of the structure. However, the orientation of the surfaces of the crystalline structure respect to the geometry of the sinker is unknown. Therefore average values have been used to calculate both coefficients.

Young's module and Poisson's coefficient are calculated as functions of the second order elastic constants of silicon C_{11}, C_{12} y C_{44} by equations 3.18 y 3.19, respectively; where $H = 2\cdot C_{44} + C_{12} - C_{11}$ is the anisotropy factor. Average values of the second order elastic constants are showed in Table 3.6.

$$E = 2\cdot\left(C_{44} - \frac{H}{5}\right)\cdot(1+\nu) \qquad \textbf{Eq. 3.18.}$$

$$\nu = \frac{C_{12} - \frac{H}{5}}{2\cdot\left(C_{12} + C_{44} - 2\frac{H}{5}\right)} \qquad \textbf{Eq. 3.19.}$$

Table 3.6. *Average values of the second order elastic constants of silicon.*

C_{ij}	C_{ij} (298.15 K) [27]	$\left(\frac{1}{C_{ij}}\right)\cdot\frac{\partial C_{ij}}{\partial T}$
	MPa	K^{-1}
C_{11}	$1.6564\cdot10^{5}$	$-9.4\cdot10^{-5}$
C_{12}	$0.6394\cdot10^{5}$	$-9.8\cdot10^{-5}$
C_{44}	$0.7951\cdot10^{5}$	$-8.3\cdot10^{-5}$

Young's module E and Poisson's coefficient ν depends on the temperature. Thus, a lineal regression in the temperature range of the densimeter (250 - 400) K was made from the literature data at 298.15 K. Equations 3.20 and 3.21 allow calculating E and ν for each measuring point in function of temperature.

$$E = 1.6681 \cdot 10^{5} - 1.4494 \cdot 10^{2} \cdot T \qquad \textbf{Eq. 3.20.}$$

$$\nu = 0.21788 - 2.3748 \cdot 10^{-5} \cdot T \qquad \textbf{Eq. 3.21.}$$

Finally, replacing the calculated values of $\alpha(T)$, E, ν and the experimental temperature and pressure in equation 3.11, sinker volume is determined after each measuring point.

Figure 3.19 shows how the sinker volume increases with temperature and decreases when pressure is increased.

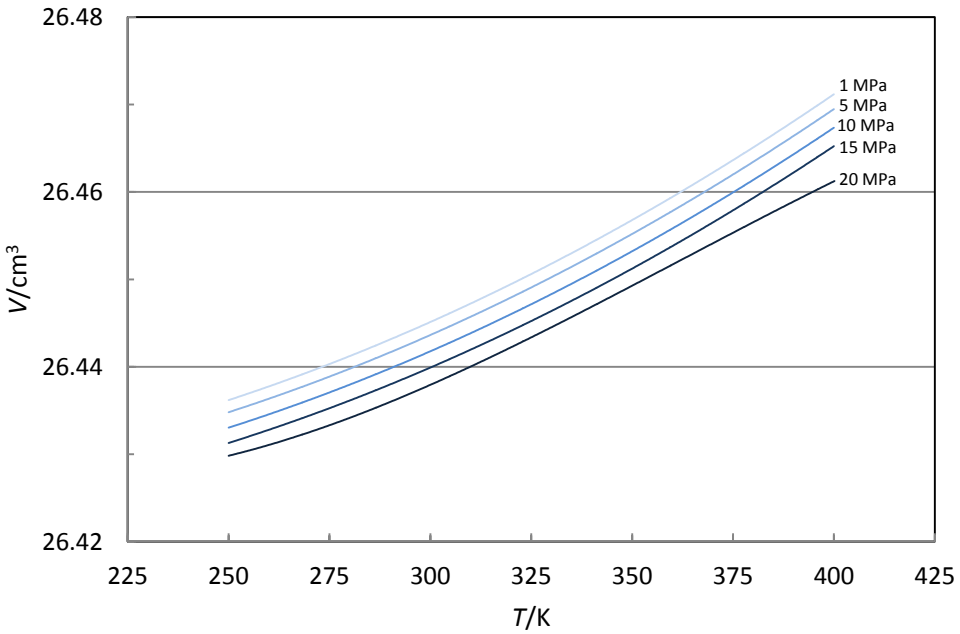

Figure 3.19. *Variation of the sinker volume with temperature and pressure.*

3.7. CONTROL AND DATA ACQUISITION SOFTWARE

The density measuring process with the single-sinker densimeter is completely automatic. The measurement control and the log of experimental data are carried out by a computer Intel Pentium® 4 powered by Microsoft Windows® XP. The controller of the magnetic suspension coupling , the weight changing device controller and the piston air-operated valve are connected to the computer by means of a data acquisition digital I/O counter module ECON series model DT9810. The balance, both pressure transducers and the AC

resistance bridge are directly connected to the serial ports of the computer. All the equipment, except for the refrigerated-heating circulator and the thermostatic bath, are connected to an uninterruptible power supply to avoid problems in the case of temporal failures of the electric network.

The control software of the densimeter was programmed in Agilent VEE Pro 7.0® virtual, software developed by Hewlett-Packard optimized to measuring equipment. This software allows controlling the measuring process through a simple graphical interface, even remotely from another computer. The developed control panel shows the main variables of the measuring process: temperature, pressure, mass and number of measuring point. Figure 3.20 shows a screenshot of the control panel during the record of an isotherm. The experimental data are registered in a Microsoft Excel® file.

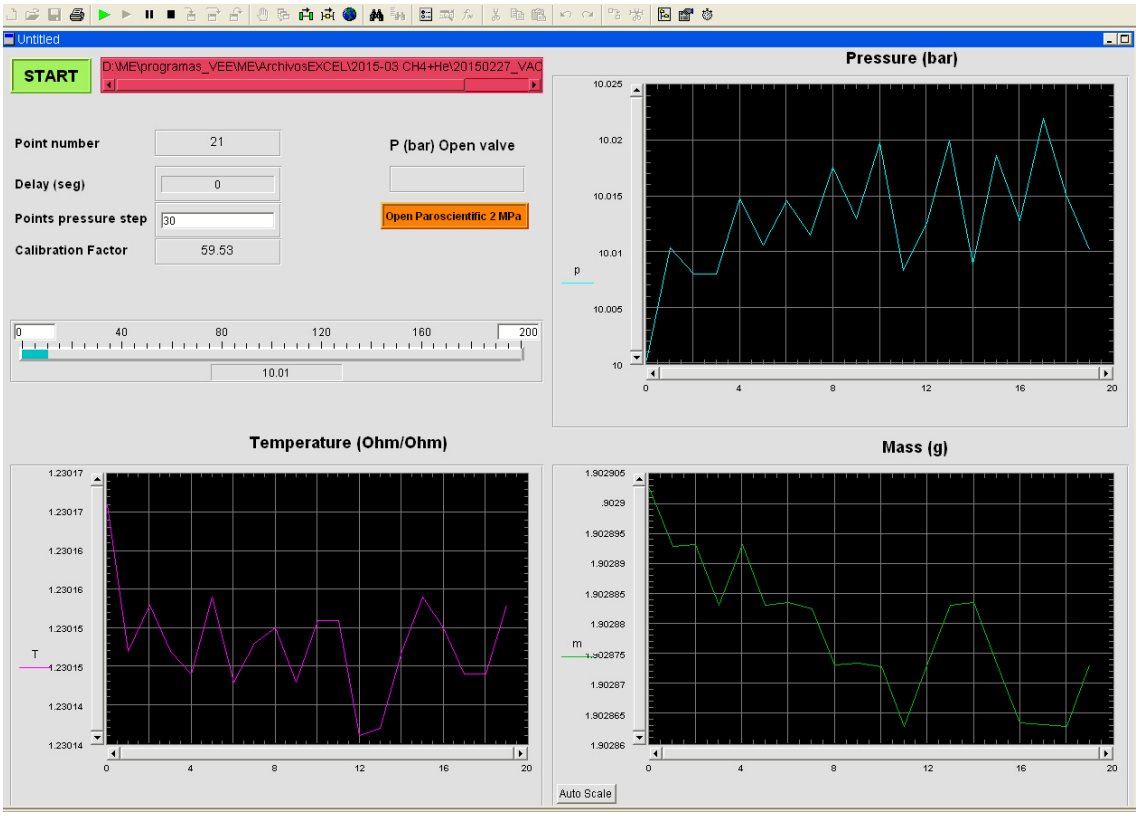

Figure 3.20. *Screenshot of the control and acqusition data software.*

The control panel is divided in two areas: “user‘s area” and “graphical area”.

The **user’s area** has control icons, information about measuring magnitudes and input boxes.

- **Options box**: Before a measuring, the user can modify the number of measuring points of each pressure step and the initial delay of the measuring process. The default values are 30 measurements per pressure step and zero seconds of delay.
- **"*Start*" button**: When the *start* button is clicked an input window asks where the Excel file with the isotherm data will be saved. Measurements start once this information has been introduced.
- **Information box**: The software shows to the user the number and the calibration factor of the current measuring point.
- **Pressure box**: The piston air-operated valve is automatically opened when the measurements of a pressure steps finish and the measuring cell is evacuated to the netx pressure step value. During this process, the pressure box shows the current pressure inside the cell registered by the presure transducer of (2 - 20) MPa. The control software stops automatically when the pressure cell is 2 MPa. In this moment the valve associated to the 2 MPa pressure transducer must be manually opened. After that, the user must be pressed the button "*Open Paroscientific: 2 MP*a" and the measurements stars again.

The **graphical area** shows different useful information to visually control the stability of the measuring process. The scale of the plots is automatic in function of the values registered.

- **Pressure plot**: This plot represents the pressure values registered in the pressure transducer of (2 - 20) MPa versus the number of measuring point. The shown value is not corrected with the calibration parameters. The plot is reset when a new pressure step starts.
- **Pressure progress bar**: It shows the current pressure step the number of the measurement inside a pressure step.
- **Temperature plot**: It shows the resistance ratio measured in the AC resistance bridge for the Minco 713 PRT-25 probe versus the number of the measurement. This plot is not reset when a new pressure step starts, so it is possible to check the stability of the temperature along the isotherm measuring process.
- **Mass plot**: It represents the sinker mass values measured by the balance (MP) corrected with the calibration factor CF calculated for each point. The plot is reset when a new pressure step starts.

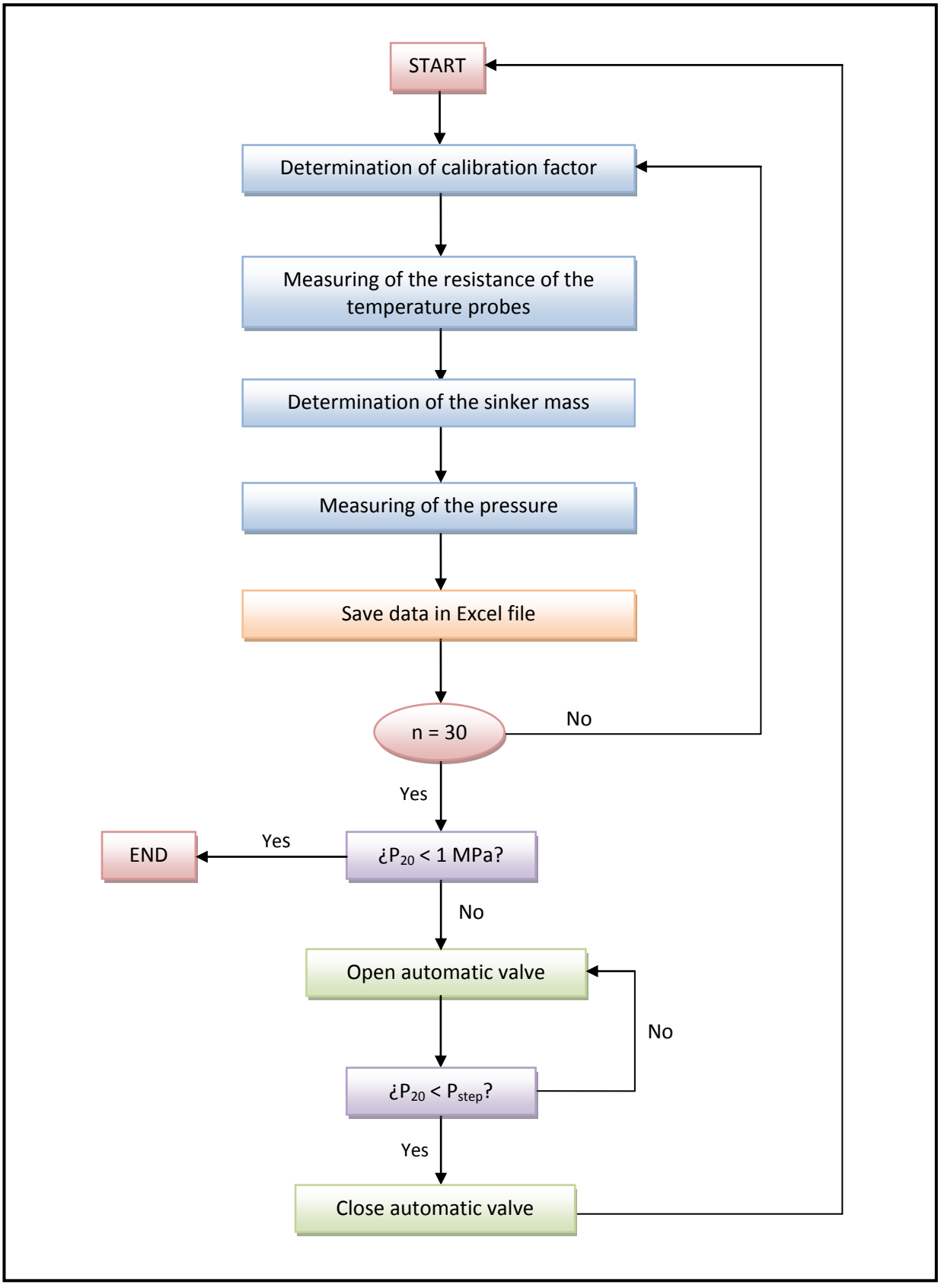

Figure 3.21. *Flow diagram of the control and data acquisition software.*

Figure 3.21 shows the flow diagram of the control and data acquisition software. The term P_{20} refers to pressure measured by pressure transducer of (2 - 20) MPa and P_{step} represent refers the pressure defined to the next pressure step.

The measuring process starts when the button 'start' is pressed. The measurements start once the Excel file has been created. The calibration factor is calculated in the first place by equation 3.4. Then, the resistance ratios of the three PRT-25 temperature probes are calculated by the AC resistance bridge. The apparent sinker mass calculation process starts with the tare of the balance with the magnetic coupling in null position and the tantalum mass on the balance (zero point, ZP); then the magnetic coupling is in the measuring position (MP) and the titanium mass replaces the tantalum mass on the balance. The sinker mass is calculated by subtracting the reading of the balance at ZP and at MP. The temperatures of the three PRT-100 probes and the pressure of the two pressure transduces are also registered. All data are saved for each measurement in an Excel file with the date, time and room temperature (from the temperature probe located inside the (2 - 20) MPa pressure transducer). Figure 3.22 shows the data of an isotherm saved in an Excel file.

	A	B	C	D	E	F	G	H	I	J	K	L	M	N	O
1	Time	Minco 713	Minco 712	Rosement	Tara	Masa	FC	A1	A2	S	Nom	P200	P20	T_Parosc	
2	20/02/2015 0:01:39	1.428823	1.426323	1.429764	0	-1.48851	59.5302	101.92	101.85	101.62	101.85	151.2401	9.95655	21.937	
3	20/02/2015 0:04:08	1.428824	1.426327	1.429762	0	-1.48827	59.53023	101.94	101.84	101.62	101.85	151.2297	9.94944	21.937	
4	20/02/2015 0:06:33	1.428819	1.42633	1.429766	0	-1.4884	59.5302	101.93	101.85	101.62	101.85	151.2351	9.95511	21.937	
5	20/02/2015 0:08:58	1.428812	1.426317	1.429761	0	-1.48799	59.53013	101.9	101.85	101.62	101.85	151.2139	9.93529	21.926	
6	20/02/2015 0:11:26	1.428838	1.426344	1.429779	0	-1.48819	59.53012	101.92	101.85	101.61	101.85	151.2249	9.95496	21.934	
7	20/02/2015 0:13:54	1.428811	1.426309	1.42974	0	-1.48794	59.53015	101.98	101.84	101.61	101.85	151.2127	9.93979	21.926	
8	20/02/2015 0:16:19	1.428819	1.426321	1.429756	0	-1.48819	59.53016	101.98	101.84	101.61	101.85	151.2239	9.95674	21.918	
9	20/02/2015 0:18:44	1.428823	1.426325	1.429759	0	-1.48793	59.53015	101.92	101.84	101.61	101.85	151.21	9.93897	21.912	
10	20/02/2015 0:21:09	1.428808	1.426309	1.429741	0	-1.48805	59.53014	101.99	101.84	101.62	101.85	151.2218	9.95844	21.91	
11	20/02/2015 0:23:35	1.428829	1.42633	1.42976	0	-1.48788	59.53011	101.92	101.84	101.62	101.85	151.207	9.93954	21.902	
12	20/02/2015 0:26:00	1.428813	1.426317	1.429756	0	-1.48804	59.53015	101.9	101.85	101.62	101.85	151.219	9.95635	21.902	
13	20/02/2015 0:28:25	1.428821	1.426322	1.429758	0	-1.48786	59.5301	101.93	101.84	101.62	101.85	151.2064	9.93966	21.893	
14	20/02/2015 0:30:51	1.428831	1.426333	1.429764	0	-1.48797	59.53014	102.11	101.85	101.61	101.85	151.215	9.95653	21.902	
15	20/02/2015 0:33:16	1.428806	1.426306	1.42974	0	-1.48775	59.53013	101.92	101.84	101.61	101.85	151.2012	9.93914	21.893	
16	20/02/2015 0:35:42	1.428805	1.426312	1.429742	0	-1.48793	59.53009	101.99	101.84	101.61	101.85	151.2116	9.95689	21.893	
17	20/02/2015 0:38:06	1.428816	1.42633	1.429771	0	-1.48768	59.53013	102.03	101.85	101.62	101.85	151.1984	9.94001	21.896	
18	20/02/2015 0:40:32	1.428838	1.426335	1.429764	0	-1.48775	59.53015	101.94	101.85	101.62	101.85	151.2087	9.9557	21.877	
19	20/02/2015 0:42:58	1.428828	1.426329	1.429764	0	-1.48771	59.5301	101.97	101.85	101.62	101.85	151.199	9.94094	21.891	
20	20/02/2015 0:45:25	1.428834	1.426331	1.429768	0	-1.48776	59.53013	101.92	101.85	101.62	101.85	151.2091	9.9572	21.877	
21	20/02/2015 0:47:50	1.428828	1.426334	1.429767	0	-1.48757	59.53013	101.92	101.84	101.61	101.85	151.1937	9.94001	21.888	
22	20/02/2015 0:50:15	1.428806	1.426301	1.429728	0	-1.48755	59.53014	101.99	101.84	101.6	101.85	151.1953	9.9528	21.871	
23	20/02/2015 0:52:40	1.428802	1.426304	1.429738	0	-1.48751	59.53013	102.02	101.84	101.61	101.85	151.1887	9.94269	21.88	
24	20/02/2015 0:55:05	1.428822	1.426323	1.429756	0	-1.48745	59.53013	102.02	101.85	101.62	101.85	151.1917	9.95096	21.871	
25	20/02/2015 0:57:30	1.428834	1.426338	1.429773	0	-1.48742	59.53013	101.94	101.85	101.62	101.85	151.1879	9.94461	21.874	
26	20/02/2015 0:59:55	1.42883	1.426326	1.429753	0	-1.48745	59.53011	102.02	101.84	101.61	101.85	151.1893	9.95092	21.869	
27	20/02/2015 1:02:20	1.428823	1.426325	1.429761	0	-1.48736	59.53012	101.96	101.84	101.61	101.85	151.1837	9.94387	21.86	
28	20/02/2015 1:04:45	1.428815	1.426319	1.429755	0	-1.48735	59.53013	101.97	101.85	101.62	101.85	151.1853	9.95065	21.858	
29	20/02/2015 1:07:10	1.428833	1.426334	1.429762	0	-1.4873	59.53011	101.97	101.84	101.61	101.85	151.1789	9.9429	21.858	
30	20/02/2015 1:09:34	1.428817	1.426325	1.429768	0	-1.48727	59.53014	101.93	101.85	101.62	101.85	151.1823	9.95251	21.86	
31	20/02/2015 1:12:03	1.428817	1.426315	1.429746	0	-1.48717	59.53013	101.98	101.84	101.61	101.85	151.1755	9.94379	21.852	
32	20/02/2015 1:28:45	1.42879	1.426311	1.429784	0	-1.25611	59.53017	101.99	101.84	101.62	101.85	140.0012	9.94708	21.83	
33	20/02/2015 1:31:10	1.428838	1.426343	1.429795	0	-1.25597	59.53015	101.93	101.85	101.62	101.85	140.0153	9.9487	21.825	
34	20/02/2015 1:33:35	1.428834	1.426337	1.429786	0	-1.25564	59.53013	101.93	101.85	101.62	101.85	140.0123	9.94557	21.836	
35	20/02/2015 1:36:00	1.428833	1.426332	1.429769	0	-1.25564	59.53013	101.93	101.84	101.62	101.85	140.0169	9.9488	21.822	
36	20/02/2015 1:38:28	1.428828	1.426334	1.429774	0	-1.25534	59.53011	101.88	101.85	101.62	101.85	140.0101	9.94618	21.83	
37	20/02/2015 1:40:52	1.428822	1.426331	1.429775	0	-1.25557	59.53013	101.89	101.85	101.62	101.85	140.0183	9.95432	21.822	

Hoja1

Figure 3.22. *Screenshot of the Excel file with an isotherm data.*

The data treatment is carried out using an Excel template designed especially to this process. In the measuring process 30 measurements points are recorded for each pressure

step, but for stability reasons, only the last ten measuring points are used for determining the experimental density of the fluid. The temperature and pressure are corrected in the data treatment step, according to the process explained in section 3.4. Also the sinker volume is calculated for each measuring point. Experimental density of the fluid is determined from these data.

In order to compare experimental density data with the values estimated from reference equations of state, the average experimental density value of the five last measured points of every pressure step is used. In other words, each isotherm has 20 experimental density values from (1 a 20) MPa, one for each pressure step. With these data, the deviation of the experimental densities between estimated values from the GERG-2008 and AGA8-DC92 equations of state is analyzed. The estimated values are calculated with the software REFPROP [28], which is installed as an addin in the Excel spreadsheet.

3.6. RESULTS OF THE MEASUREMENTS WITH NITROGEN

Nitrogen density measurements were carried out over the whole working range of the apparatus in order to validate the process and check for the correct operation of the densimeter. These measurements were carried out before and after of density measurements with a new mixture. Experimental results were compared with densities estimated from the reference equation of state for nitrogen developed by Span et al. [29]. More than 90 % of relative deviations were within 0.02 % band. This test confirmed that densimeter worked correctly.

Table 3.7 shows the statistical data of the results of the measurements with nitrogen.

Table 3.7. *Statistical parameters of relative deviation of experimental data from reference equation of state for nitrogen* [29].

Statistical parameter	04/2012	10/2012	03/2013	10/2013	11/2014	02/2015	11/2015
AAD	0.0087	0.0066	0.0103	0.0069	0.0072	0.0055	0.0058
Bias	0.0053	0.0055	0.0075	0.0048	0.0050	0.0028	0.0026
RMS	0.0104	0.0074	0.0119	0.0082	0.0082	0.0067	0.0074
MaxD/ %	–0.022	0.014	0.020	0.018	–0.026	–0.022	–0.023

The statistical analysis were performed by calculating the absolute average deviation (*AAD*), the average deviation (*Bias*) and the root mean square (*RMS*) by using equations 3.22, 3.23 y 3.24, respectively. Finally, the largest relative deviation (*MaxD*) was identified in each experience.

$$AAD = \frac{1}{n}\sum_{i=1}^{n}\left|10^2 \cdot \frac{\rho_{i,\exp} - \rho_{i,EoS}}{\rho_{i,EoS}}\right| \qquad \textbf{Eq. 3.22}$$

$$Bias = \frac{1}{n}\sum_{i=1}^{n}\left(10^2 \cdot \frac{\rho_{i,\exp} - \rho_{i,EoS}}{\rho_{i,EoS}}\right) \qquad \textbf{Eq. 3.23.}$$

$$RMS = \sqrt{\frac{1}{n}\sum_{i=1}^{n}\left(10^2 \cdot \frac{\rho_{i,\exp} - \rho_{i,EoS}}{\rho_{i,EoS}}\right)^2} \qquad \textbf{Eq. 3.24.}$$

3.7. IMPROVEMENTS ON THE EQUIPMENT

The improvements performed by Mondéjar [19] previous to this work were associated with redctions in the uncertainty in density, temperature and pressure. In this work some improvements related to pressure and temperature estability were carried out by adquisition of two new equipments.

A new climatization system (Daikin Inverter Room Air Conditioner model FTX50GV1B) was intalled in the room were the single-sinker densimeter and all auxiliary devices are located. The ambient temperature can affect the pressure transducers. In addition, room temperature can also be affected by thermostatic bath. For these reasons temperature room is permanently set at (23 ± 2) ^{o}C. The ideal solution for the improvement of the pressure transducers stability would be to make a thermostatization system. This is one of the future improvements suggested.

As it can be see in Figure 3.23, the room temperature stability with the old climatization system was worse than the new one. Ambient temperature in Figure 3.23 was registered by a termometer installed inside the (0 - 2) MPa pressure transducer case, so the shown values do not correspond with the real laboratory temperature, but however they give a good idea about room temperature variation during a whole density measurement (seven isotherms). The laboratory real temperature can be checked by using an independent termometer located in the room.

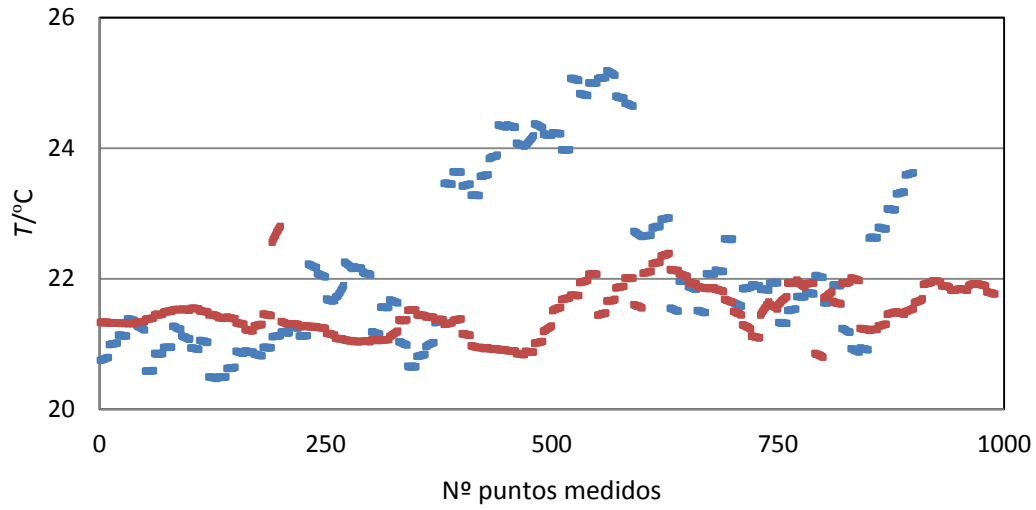

Figure 3.23. *Room ambient temperature during a whole density measurement by using "old" climatization system (blue) and new one (red). Temperature was recorded by using the termometer inside (0 - 2) MPa pressure transducer case.*

Another improvement related with temperature stability inside the measuring cell was the replacement of the thermostatic bath described in section 3.3. A new ultra-low refrigerated-heating circulator Julabo FP51-SL was installed to control the temperature inside the measuring cell. Table 3.8 shows the standard deviation of average temperature registered by Minco 712 and 713 probes inside the measuring cell.

Table 3.8. *Standard deviation of average temperature inside the measuring cell.*

T/K	Ultra-low refrigerated-heating circulator	"Old" refrigerated-heating circulator		
	11/2015	12/2012	05/2013	03/2015
240	0.0036	-	-	-
250	0.0033	0.0025	-	0.0051
260	0.0038	-	-	-
275	0.0031	0.0026	0.0043	0.0043
300	0.0024	0.0023	0.0021	0.0021
325	0.0004	0.0014	0.0026	0.0015
350	0.0006	0.0026	0.0019	0.0023
375	0.0009	0.0028	0.0024	0.0026
400	0.0010	0.0028	0.0026	0.0020

The new thermostatic bath was installed in October 2015. As it can be observed, the temperature stability inside the measuring cell is better with the new thermostatic bath than with the old one. In addition, this new equipment allows measuring (p, ρ, T) data at temperatures of 240 K (instead 250 K), so measurements closer to saturation curve (in some mixtures) will be carried out in future experiments.

3.8. REFERENCES

[1] W. Wagner and R. Kleinrahm, “Densimeters for very accurate density measurements of fluids over large ranges of temperature, pressure, and density,” *Metrologia*, vol. 41, no. 2, pp. S24–S39, 2004.

[2] A. R. H. Goodwin, K. N. Marsh, and W. A. y Wakeham, “Measurement of the thermodynamic properties of single phases,” 2003, pp. 127–219.

[3] R. Kleinrahm and W. Wagner, “Entwicklung und Aufbau einer Dichtemeßanlage zur Messung der Siede- und Taudichten reiner fluider Stoffe auf der gesamten Phasengrenzkurve,” *Forsch. im Ingenieurwes.*, vol. 50, no. 5, pp. 166–166, Sep. 1984.

[4] R. Kleinrahm and W. Wagner, “Measurement and correlation of the equilibrium liquid and vapour densities and the vapour pressure along the coexistence curve of methane,” *J. Chem. Thermodyn.*, vol. 18, no. 8, pp. 739–760, Aug. 1986.

[5] T. Gast and K. H. Behrndt, “Vacuum Microbalance Techniques,” vol. 3, pp. 45–54, 1963.

[6] H. W. Losch, R. Kleinrahm, and W. Wagner, “New Magnetic Suspension Weighers for Gravimetric Measurements In-Process Engineering,” *Chemie Ing. Tech.*, vol. 66, no. 8, pp. 1055–1058, Aug. 1994.

[7] K. Brachthäuser, R. Kleinrahm, H. W. Lösch, and W. Wagner, “Entwicklung eines neuen Dichtemeßverfahrens und Aufbau einer Hochtemperatur-Hochdruck-Dichtemeßanlage,” 1993.

[8] W. Wagner, K. Brachthäuser, R. Kleinrahm, and H. W. Lösch, “A new, accurate single-sinker densitometer for temperatures from 233 to 523 K at pressures up to 30 MPa,” *Int. J. Thermophys.*, vol. 16, no. 2, pp. 399–411, 1995.

[9] J. Klimeck, R. Kleinrahm, and W. Wagner, “An accurate single-sinker densimeter and measurements of the (p, ρ, T) relation of argon and nitrogen in the temperature range from (235 to 520) K at pressures up to 30 MPa,” *J. Chem. Thermodyn.*, vol. 30, no. 12, pp. 1571–1588, 1998.

[10] M. Richter, R. Kleinrahm, R. Span, and P. Schley, “A new apparatus for accurate measurements of the densities of liquefied natural gas (LNG),” in *International Gas Research Conference Proceedings*, 2011, vol. 4, pp. 2776–2790.

[11] W. Blanke, G. Klingenberg, and R. Weiss, “PVT Measurements on tetrafluoroethane (R134a) along the vapor-liquid equilibrium boundary between 288 and 373 K and in the liquid state from the triple point to 265 K,” *Int. J. Thermophys.*, vol. 16, no. 5, pp. 1143–1153, Sep. 1995.

[12] P. Patil, S. Ejaz, M. Atilhan, D. Cristancho, J. C. Holste, and K. R. Hall, “Accurate density measurements for a 91% methane natural gas-like mixture,” *J. Chem. Thermodyn.*, vol. 39, no. 8, pp. 1157–1163, Aug. 2007.

[13] K. Iwagai, T. Masuda, H. Sato, and K. Watanabe, “Proc. 20th Japan Symp. on Thermophysical Properties (Japan Society of Thermophysical Properties, Tokyo, 1999), pp. 197-200,” 1999.

[14] Y. Kano, Y. Kayukawa, K. Fujii, and H. Sato, “A new method for correcting a force transmission error due to magnetic effects in a magnetic levitation densimeter,” *Meas. Sci. Technol.*, vol. 18, no. 3, pp. 659–666, 2007.

[15] M. Gong, H. Li, H. Guo, X. Dong, and J. F. Wu, “Apparatus for accurate density measurements of fluids based on a magnetic suspension balance,” in *AIP Conference Proceedings*, 2012, vol. 1434, no. 57, pp. 1857–1864.

[16] X. Yang, M. Richter, Z. Wang, and Z. Li, “Density measurements on binary mixtures (nitrogen+carbon dioxide and argon+carbon dioxide) at temperatures from (298.15 to 423.15)K with pressures from (11 to 31)MPa using a single-sinker densimeter,” *J. Chem. Thermodyn.*, vol. 91, pp. 17–29, Dec. 2015.

[17] J. T. R. Watson, D. Ferguson, and G. Ryan, “Density Seminar Held in the James Watt Conference Centre (NEL, 24 October 1994), pp. 1-16. conjunction with the North Sea Flow Measurement Workshop, East Kilbride (Glasgow), National Engineering Laboratory,” 1994.

[18] C. R. Chamorro, J. J. Segovia, M. C. Martín, M. A. Villamañán, J. F. Estela-Uribe, and J. P. M. Trusler, “Measurement of the (pressure, density, temperature) relation of two (methane+nitrogen) gas mixtures at temperatures between 240 and 400K and pressures up to 20MPa using an accurate single-sinker densimeter,” *J. Chem. Thermodyn.*, vol. 38, no. 7, pp. 916–922, Jul. 2006.

[19] M. E. Mondéjar, J. J. Segovia, and C. R. Chamorro, “Improvement of the measurement uncertainty of a high accuracy single sinker densimeter via setup modifications based on a state point uncertainty analysis,” *Measurement*, vol. 44, no. 9, pp. 1768–1780, 2011.

[20] E. (European A. of N. M. Institutes), “Guidelines on the calibration of Non-Automatic Weighing Instruments,” vol. cg-18 / v., 2007.

[21] C. A. S. R L Rusby and R P Hudson and M Durieux and J F Schooley and P P M Steur and, “Thermodynamic Basis of the ITS-90,” *Metrologia*, vol. 28, no. 1, p. 9, 1991.

[22] M. O. McLinden, R. Kleinrahm, and W. Wagner, “Force transmission errors in magnetic suspension densimeters,” *Int. J. Thermophys.*, vol. 28, no. 2, pp. 429–448, 2007.

[23] M. E. Mondéjar Montagud, “Contribución al desarrollo e introducción de combustibles gaseosos renovables mediante la caracterización termodinámica de mezclas de sus componentes utilizando un densímetro de flotador de suspensión magnética optimizado,” 2012.

[24] D. E. Cristancho, I. D. Mantilla, S. Ejaz, K. R. Hall, G. A. Iglesias-Silva, and M. Atilhan, “Force transmission error analysis for a high-pressure single-sinker magnetic suspension densimeter,” *Int. J. Thermophys.*, vol. 31, no. 4–5, pp. 698–709, 2010.

[25] J. Klimeck, “Weiterentwicklung Einer Ein-Senkkörper- Dichtemessanlage Und Präzisionsmessungen Der Thermischen Zustandsgrößen Von Kohlendioxid, Argon, Stickstoff Und Methan,” 1997.

[26] C. A. Swenson, “Recommended Values for the Thermal Expansivity of Silicon from 0 to 1000 K,” *J. Phys. Chem. Ref. Data*, vol. 12, no. 2, pp. 179–182, 1983.

[27] Landolt-Börnstein, “Elastic Constants of Second Order: Temperature Coefficients Tc,” in *Springer Verlag*, vol. 225, no. III/29a 1.2.2., Berlin, 2001.

[28] “Lemmon, E.W., Huber, M.L., McLinden, M.O. NIST Standard Reference Database 23: Reference Fluid Thermodynamic and Transport Properties-REFPROP, Version 9.1, National Institute of Standards and Technology, Standard Reference Data Program, Gaithersburg, 2013.” .

[29] R. Span, E. W. Lemmon, R. T. Jacobsen, W. Wagner, and A. Yokozeki, “A reference equation of state for the thermodynamic properties of nitrogen for temperatures from 63.151 to 1000 K and pressures to 2200 MPa,” *J. Phys. Chem. Ref. Data*, vol. 29, no. 6, pp. 1361–1401, 2000.

CHAPTER 4

Uncertainty analysis of density measurements

4.1. Introduction 95
4.2. Uncertainty estimation method 95
4.3. Temperature uncertainty analysis 99
4.4. Pressure uncertainty analysis 100
4.5. Sinker mass uncertainty analysis 101
4.6. Density uncertainty analysis 102
4.7. Overall uncertainty of experimental density measurements 104
4.8. References 107

4.1. INTRODUCTION

The measurement process of the single-sinker densimeter with magnetic suspension coupling has been described in detail in chapter 3. Furthermore, the improvements carried out by M.E. Mondéjar as part of her thesis in the equipment in order to reduce the measurement uncertainties of temperature, pressure and density, are also commented [1][2]. This work uses these improvements as the starting point. The uncertainty analysis of the measuring magnitudes only calculates the current uncertainties, updates data of new calibrations and studies if any drift has appeared in comparison with previous measurements.

4.2. UNCERTAINTY CALCULATION METHOD

The purpose of a measurement is to determine the value of a measurand, in other words, the amount of a particular attribute associated to any substance, body or physical phenomenon that can be defined quantitatively and expressed by a number or reference [3].

Generally, the result of a measurement is an approximation to the real value of a magnitude. In this sense, a measurement is only completed when it is reported with an uncertainty statement of the estimation. *Measurement uncertainty* is defined as the parameter characterizing the dispersion of the values which could be attributed to the measurand [4]. The measurement uncertainty gives an idea of the quality of the measurement results.

In practice, the specification of the measurand is ruled by the *accuracy of the measurement* and it can be defined with enough integrity respect to the required accuracy, so its value is unique. In several cases, the result of a measurement is determined from a set of measurements with repeatability conditions. So, the mathematical model used to transform the measurement set in the measurement result is very important because, generally, the measurements results are influenced by other effects which cannot be quantified exactly. This lack of knowledge, along with the variation in the repetitions, the accuracy of the used instruments, the ambient conditions and the uncertainty associated with the mathematical model contribute to the overall uncertainty of the final result of the measurement. According to the International Office of Weights and Measures (BIPM, *Bureau International des Poids et Mesures*), the method to evaluate and state the

uncertainty of a measurement should be universal (applicable to all measurements), internally consistent (derivable directly from the components that contribute to the result) and transferable (it must be possible to use the uncertainty of a result directly as a component in evaluating the uncertainty of another measurement which uses the first result). According to INC-1 recommendation of the Work Group of Uncertainty Declaration, the uncertainty of a measure has some components that can be grouped for its evaluation [5]:

- **"A type"**: magnitudes whose estimated value and associated uncertainty are determined directly from the measurements. These values can be obtained from one measurement, repetitive measurements or be based on previous experiences. Their uncertainty is characterized by statistic methods, like standard deviation and number of degrees of freedom.
- **"B type"**: magnitudes whose estimated value and associated uncertainty are incorporated to the measurement from external sources, for example calibrated measurement standards, certified reference materials or handbook reference data.

"A type" standard uncertainty is a function of the probability density derived from the distribution observed, while "B type" uncertainties are function of probability density based on the probability that the "event" happens.

The most extended calculation method the *uncertainty propagation law* described in the Guide to the Expression of Uncertainty in Measurement (GUM) and in its transposition for calibration laboratories EA-4/02 "Evaluation of measurement uncertainty in calibrations" [6]. According to this methodology, the measurand Y is expressed as a function of the required input variables X_i, so the estimation of Y, expressed as y, is made from the estimations of the input variables, expressed as x_i. $y = f(x_1, x_2, ..., x_N)$.

For random variables of the "A type", the standard uncertainty of each input variable $u(x_i)$ is calculated as the standard deviation from the average $s(x)$ and it has the same dimensions of the measured magnitude. The estimation is performed from the variance distribution $s^2(x)$ divided by the number of measurements N, according to equation 4.1.

$$s^2(x) = u^2(x_i) = \frac{s^2(x)}{N} = \frac{\frac{1}{N-1}\sum_{j=1}^{N}(x_j - x)^2}{N} \qquad \textbf{Eq. 4.1.}$$

The standard deviation and therefore the standard uncertainty, because $s(x)=u(x_i)$, will be the square root of this value.

The evaluation of "B type" standard uncertainty associated to an estimated value x_i of the input variable X_i takes into account the following different cases:

- If a single value of X_i is known (e.g. because only one measurement was carried out or it is a reference value), this value will be used as x_i. If its standard uncertainty $u(x_i)$ is not given, it has to be calculated supposing the probability distribution followed by X_i. The standard uncertainty $u(x_i)$ will be the root square of the variance.
- If only the upper a_+ and lower a_- limits of X_i can be estimated (manufacturing specifications, temperature range…) a rectangular probability distribution in which x_i is the middle point of the interval has to be supposed. The standard uncertainty $u(x_i)$ is obtained by equation 4.2. If the difference between the limits is expressed as $2a$, equation 4.3 is used.

$$u(x_i)=\frac{(a_+ - a_-)}{2\sqrt{3}} \qquad \textbf{Eq. 4.2.}$$

$$u(x_i)=\frac{a}{\sqrt{3}} \qquad \textbf{Eq. 4.3.}$$

Once the standard uncertainties of the input variables $u(x_i)$ are determined, the standard combined uncertainty of the output variable $u(y)$ is calculated.

In the case of uncorrelated input variables, $u(y)$ is determined by equation 4.4.

$$u^2(y)=\sum_{i=1}^{N} c_i{}^2 \cdot u^2(x_i) \qquad \textbf{Eq. 4.4.}$$

where $c_i=\left(\partial f \big/ \partial x_i\right)$ is the sensitivity coefficient, indicator of the influence that variations in the estimated input variables x_i have in the output estimation y.

The standard combined uncertainty $u(y)$ in the case of correlated input variables is calculated by equation 4.5.

$$u^2(y)=\sum_{i=1}^{N}(c_i\cdot u(x_i))^2+2\sum_{i=1}^{N-1}\sum_{j=i+1}^{N}(c_i\cdot u(x_i))\cdot(c_j\cdot u(x_j))\cdot r(x_i,x_j) \qquad \textbf{Eq. 4.5.}$$

where $r(x_i,x_j)$ is the correlation coefficient. It depends on the standard deviations of the input variables $u(x_i)$, $u(x_j)$ and the covariance between them $u(x_i,x_j)$, according to equation 4.6. If input variables are independent (uncorrelated), $r(x_i,x_j)$ is zero; if not, it can vary between (–1 and 1).

$$r(x_i,x_j)=\frac{u(x_i,x_j)}{u(x_i)\cdot u(x_j)} \qquad \textbf{Eq. 4.6.}$$

in order to express the final estimated uncertainty of a measurement the *expanded uncertainty* $U(y)$ is used and it is calculated like the standard combined uncertainty $u(y)$ times the coverage factor k, according to equation 4.7.

$$U(y)=k\cdot u(y) \qquad \textbf{Eq. 4.7.}$$

The final result is expressed as $Y=y\pm U(y)$. The choice of coverage factor k depends on the confidence level required for this range and the probability distribution of the measurement result. If the uncertainty is not dominated by contributions of type A with few measurements o type B with rectangular distribution, the distribution can be considered like Gaussian distribution. In that case, the confidence level for $k=1$ is 68.27 %. For $k=2$ the confidence level is 95.45 %. For different distributions than Gaussian, to obtain the k value that gives a confidence level of 95 % it is necessary to calculate the number of degrees of freedom ν_i. If the variable follow a Student or *t*-distribution, the degrees of freedom are $\nu_i=N-1$; in a least squares fitting $\nu_i=N-M$; in rectangular distributions with known limits $\nu_i=\infty$; finally, if the overall uncertainty is the sum of two or more components, the number of effective degrees of freedom ν_{eff} must be calculated by Welch-Satterthwaite equation (eq. 4.8). Depends on ν_{eff} different values of k can be obtained for the required confidence level, according to statistic tables in annex G of GUM [4].

$$\frac{u^4(y)}{\nu_{eff}}=\sum_{i=1}^{N}\frac{u_i^4(y)}{\nu_i} \qquad \textbf{Ec. 4.8.}$$

The uncertainty analyses of the measurements of magnitudes involved in density determination are detailed in the next sections. These magnitudes are: pressure, temperature, mass of the sinker and density. The analyses are shown in tables where the sources of uncertainty associated with the output variable are detailed, showing their units and the estimated value (when it is different than zero), the standard uncertainty, the probability distribution, the type of uncertainty (A or B type), the sensitivity coefficient and the divisor (it is different than 1 depends on the interval defined for each magnitude according to equations 4.2 and 4.3). The last column indicates the contribution of each uncertainty source to the standard combined uncertainty $u(y)$. The expanded uncertainty $U(y)$ $(k=2)$ is also shown for each magnitude.

4.3. TEMPERATURE UNCERTAINTY ANALYSIS

The temperature inside the measuring cell is recorded by two temperature probes PRT-25 Minco (712 and 713) connected to an AC comparator resistance bridge through a multichannel switchbox. The bridge measures the resistance ratio between the PRT-25 probes and a calibrated external resistor. The temperature used to determine the fluid density is the average between the temperatures registered for both probes, which were calibrated in the calibration facility of TERMOCAL (accredited by ENAC, member of EA) for different temperature fixed points. The calibration values of PRT-25 probes for each fix point are showed in Table 4.1.

Table 4.1. *Calibration uncertainty and its drift for both PRT-25 Minco probes.*

Probe	Calibration expanded uncertainty $(k=2)$				Drift (K)
	505.077 K	429.748 K	302.913 K	234.317 K	
Minco 712	$6\cdot10^{-3}$	$5\cdot10^{-3}$	$4\cdot10^{-3}$	$4\cdot10^{-3}$	$2\cdot10^{-3}$
Minco 713	$6\cdot10^{-3}$	$5\cdot10^{-3}$	$4\cdot10^{-3}$	$4\cdot10^{-3}$	$2\cdot10^{-3}$

The calibration uncertainty for each probe is the highest value of Table 4.1 in the densimeter working range.

The uncertainty analysis of the fluid temperature measurement inside the measuring cell is shown in Table 4.2.

Table 4.2. *Uncertainty budget for temperature measurement.*

Uncertainty source	Units	Standard uncertainty	Distribution	Type	Sensitivity coefficient	Divisor	Contribution
Calibration uncertainty of Minco 712	K	$2.0\cdot10^{-3}$	Gaussian	B	0.5	1	$1.0\cdot10^{-3}$
Calibration uncertainty of Minco 713	K	$2.0\cdot10^{-3}$	Gaussian	B	0.5	1	$1.0\cdot10^{-3}$
Temperature reading	Ω	$6.7\cdot10^{-5}$	Gaussian	B	10.5	1	$7.04\cdot10^{-4}$
Repeatability	K	$6.3\cdot10^{-4}$	Gaussian	A	1	1	$6.3\cdot10^{-4}$
Uniformity	K	$2.5\cdot10^{-3}$	Rectangular	B	1	$2\sqrt{3}$	$7.22\cdot10^{-4}$
Drift	K	$1.0\cdot10^{-3}$	Rectangular	B	1	$\sqrt{3}$	$5.77\cdot10^{-4}$
					Standard combined uncertainty (K)		$1.94\cdot10^{-3}$
					Expanded uncertainty $(k=2)$ (K)		$3.87\cdot10^{-3}$

4.4. PRESSURE UNCERTAINTY ANALYSIS

The pressure inside the measuring cell is determined by two pressure transduces depending on the operation range. There is a transducer for pressures between (2 and 20) MPa and another transducer for the range pressure of (0 to 2) MPa isolated of the network through a manually-operated valve.

The main sources of uncertainty in pressure measurements are the correction of the transducers due to their calibration, resolution, repeatability and drift. Pressure transducers were calibrated in TERMOCAL and the correction parameters were estimated by a polynomial of degree five. The repeatability was estimated as the standard deviation of the mean of the ten measurements used to calculate each pressure point and drift was estimated from two consecutive calibrations.

Table 4.3 shows the uncertainty budget of the (2 - 20) MPa pressure transducer. The uncertainty budget of the (0 - 2) MPa pressure transducer is showed in Table 4.4.

Table 4.3. *Uncertainty Budget of the (2 - 20) MPa pressure transducer.*

Uncertainty source	Units	Standard uncertainty	Distribution	Type	Sensitivity coefficient	Divisor	Contribution
Transducer calibration	MPa	$38\cdot10^{-6}\cdot p + 1.74\cdot10^{-3}$	Gaussian	B	1	1	$38\cdot10^{-6}\cdot p + 1.74\cdot10^{-3}$
Resolution	MPa	$1.0\cdot10^{-3}$	Rectangular	B	1	$2\sqrt{3}$	$2.89\cdot10^{-6}$
Repeatability	MPa	$2.6\cdot10^{-4}$	Gaussian	A	1	1	$2.6\cdot10^{-4}$
Drift	MPa	$1.04\cdot10^{-6}$	Gaussian	B	1	$\sqrt{3}$	$8.1\cdot10^{-7}$
					Standard combined uncertainty (MPa)		$38\cdot10^{-6}\cdot p + 1.76\cdot10^{-3}$
					Expanded uncertainty $(k=2)$ (MPa)		$75\cdot10^{-6}\cdot p + 3.52\cdot10^{-3}$

Table 4.4. *Uncertainty Budget of the (0 - 2) MPa pressure transducer.*

Uncertainty source	Units	Standard uncertainty	Distribution	Type	Sensitivity coefficient	Divisor	Contribution
Transducer calibration	MPa	$30\cdot10^{-6}\cdot p + 5.32\cdot10^{-5}$	Gaussian	B	1	1	$30\cdot10^{-6}\cdot p + 5.32\cdot10^{-5}$
Resolution	MPa	$1.0\cdot10^{-6}$	Rectangular	B	1	$2\sqrt{3}$	$2.89\cdot10^{-7}$
Repeatability	MPa	$7.0\cdot10^{-5}$	Gaussian	A	1	1	$7.0\cdot10^{-5}$
Drift	MPa	$2.4\cdot10^{-5}$	Gaussian	B	1	$\sqrt{3}$	$1.39\cdot10^{-5}$
					Standard combined uncertainty (MPa)		$30\cdot10^{-6}\cdot p + 8.9\cdot10^{-5}$
					Expanded uncertainty $(k=2)$ (MPa)		$60\cdot10^{-6}\cdot p + 1.78\cdot10^{-4}$

Therefore the expanded uncertainty (k = 2) of experimental pressure will be calculated by equation 4.9 in the range of (2 - 20) MPa and by equation 4.10. in the range of (0 - 2) MPa.

$$U(p) = 75\cdot10^{-6}\cdot p + 3.52\cdot10^{-3} \qquad \textbf{Eq. 4.9.}$$

$$U(p) = 60\cdot10^{-6}\cdot p + 1.78\cdot10^{-4} \qquad \textbf{Eq. 4.10.}$$

4.5. SINKER MASS UNCERTAINTY ANALYSIS

The mass of the sinker is determined through the magnetic suspension coupling by using a precision microbalance, as described in chapter 3. The balance has a resolution of 0.01 mg and its uncertainty was determined in two different conditions: when the measuring cell is pressurized and evacuated. The main contributions to the balance uncertainty are shown

in Tables 4.5 and 4.6 when the measuring cell is pressurized and evacuated, respectively. The main contribution is the calibration of the balance itself.

Table 4.5. *Uncertainty budget for the mass reading when the measuring cell is pressurized.*

Uncertainty source	Units	Standard uncertainty	Distribution	Type	Sensitivity coefficient	Divisor	Contribution
Balance calibration	kg	$2.0\cdot10^{-7}$	Gaussian	B	1	1	$2.0\cdot10^{-7}$
Resolution	kg	$1.0\cdot10^{-8}$	Rectangular	B	1	$2\sqrt{3}$	$2.89\cdot10^{-9}$
Repeatability	kg	$3.0\cdot10^{-8}$	Gaussian	A	1	1	$3.0\cdot10^{-8}$
Drift	kg	$1.0\cdot10^{-7}$	Rectangular	B	1	$\sqrt{3}$	$5.77\cdot10^{-8}$
						Standard combined uncertainty (kg)	$2.10\cdot10^{-7}$
						Expanded uncertainty $(k=2)$ (kg)	$4.21\cdot10^{-7}$

Table 4.6. *Uncertainty budget for the mass reading when the measuring cell is evacuated.*

Uncertainty source	Units	Standard uncertainty	Distribution	Type	Sensitivity coefficient	Divisor	Contribution
Balance calibration	kg	$2.0\cdot10^{-7}$	Gaussian	B	1	1	$2.0\cdot10^{-7}$
Resolution	kg	$1.0\cdot10^{-8}$	Rectangular	B	1	$2\sqrt{3}$	$2.9\cdot10^{-9}$
Repeatability	kg	$8.0\cdot10^{-8}$	Gaussian	A	1	1	$8.0\cdot10^{-8}$
Drift	kg	$1.0\cdot10^{-7}$	Rectangular	B	1	$\sqrt{3}$	$5.8\cdot10^{-8}$
						Standard combined uncertainty (kg)	$2.23\cdot10^{-7}$
						Expanded uncertainty $(k=2)$ (kg)	$4.46\cdot10^{-7}$

4.6. DENSITY UNCERTAINTY ANALYSIS

The determination of the density of any fluid by a single-sinker densimeter with magnetic suspension coupling is carried out from the apparent mass and the volume of the sinker at determined pressure and temperature conditions by equation 3.15, as is described in chapter 3.

$$\rho(T,p)=\frac{m_{S0}-m_{Sf}}{V_S(T,p)} \qquad \textbf{Eq. 3.15.}$$

Therefore, density uncertainty depends on the uncertainty of the mass of the sinker when the measuring cell is evacuated m_{S0} and pressurized m_{Sf} and also depends on the uncertainty of the volume of the sinker V_S. According to the law of propagation of uncertainties (GUM) [4] and expressed in equation 4.4, the standard combined uncertainty of the density is calculated by equation 4.11.

$$u(\rho)=\frac{1}{V_S}\cdot\sqrt{u^2(m_{S0})+u^2(m_{Sf})+\rho^2\cdot u^2(V_S)} \qquad \textbf{Eq. 4.11.}$$

The density uncertainty depends on the balance reading uncertainty of the sinker mass. The weight of the sinker when the cell is evacuated and the weight when the cell pressurized are determined in independent measurements. Thus, the value of the coefficient of correlation was $r(m_{S0}, m_{Sf})$ = $-3\cdot10^{-5}$. Considering this value, and to simplify calculations, m_{S0} and m_{Sf} are considered uncorrelated variables. The balance is calibrated in situ using the certificate masses of tantalum and titanium. However, the uncertainty of these certificate masses does not affect the mass uncertainty value since the repeatability was taken as the standard deviation of the mean of balance readings.

Another contribution to density uncertainty is the sinker volume uncertainty. The calibration of the sinker was carried out by CEM and its certificate indicates the volume of the silicon sinker V_S = 26.444 ± 0.003 cm^3 $(k=2)$. The volume of the sinker varies because of the temperature and pressure according to the thermal and mechanical properties of the material, as described in chapter 3. However, the contribution of these magnitudes to the volume sinker uncertainty is negligible in comparison with the volume uncertainty of calibration certificate of the sinker. Therefore, combined volume uncertainty of the sinker was taken from the calibration certificate from CEM.

Table 4.7 shows the uncertainty budget for density.

Table 4.7. *Uncertainty budget for the density of the fluid.*

Uncertainty source	Units	Estimation	Standard uncertainty	Sensitivity coefficient	Degrees of freedom	Contribution
Sinker mass in vacuum	kg	$1.90\cdot10^{-3}$	$2.2\cdot10^{-7}$	$3.8\cdot10^{4}$	500	$8.4\cdot10^{-3}$
Sinker mass in fluid	kg	$-5.27\cdot10^{-3}$	$2.1\cdot10^{-7}$	$3.8\cdot10^{4}$	1200	$8.0\cdot10^{-3}$
Sinker volume	m^3	$2.64\cdot10^{-5}$	$1.5\cdot10^{-9}$	$3.8\cdot10^{4}\cdot\rho$	∞	$5.7\cdot10^{-5}\cdot\rho$
				Standard combined uncertainty ($kg\cdot m^{-3}$)		$1.16\cdot10^{-2} + 5.7\cdot10^{-5}\cdot\rho$
				Expanded uncertainty $(k=2)$ ($kg\cdot m^{-3}$)		$2.31\cdot10^{-2} + 1.14\cdot10^{-4}\cdot\rho$

The conclusion from the uncertainty analysis of the variables involved in density determination by the single-sinker densimeter with magnetic suspension coupling used in this work is that experimental density data have associated an expanded uncertainty $(k=2)$ that varies in function of the density range measured. According to equation 4.12, density uncertainty is directly proportional to experimental density.

$$U(\rho) = 2.31\cdot10^{-2} + 1.14\cdot10^{-4}\cdot\rho \qquad \textbf{Eq. 4.12.}$$

4.7. OVERALL UNCERTAINTY OF THE EXPERIMENTAL DENSITY MEASUREMENTS

According to GUM, the standard overall uncertainty $(k=1)$, expressed in density units $u_T(\rho)$ is calculated considering the standard combined uncertainties estimated to density, temperature, pressure and composition. As it is described before, uncertainties in density, pressure and temperature are estimated specifically for the used equipment and they value depends on the experimental data. The uncertainty in composition is estimated from uncertainties of the components of the mixture which was prepared by gravimetric method.

However, the composition inside the measuring cell can change due to different reasons, like sorption effects (see chapter 3.4) or due to an incorrect homogenization in the filling or emptying steps. These unpredictable effects are an additional source of uncertainty in composition. The molar density of a vapor mixture is constant for a given temperature,

pressure and composition. In other words, the mass density is proportional to the average molar mass. So the uncertainty in density due to uncertainties in the composition is proportional to the uncertainty in the molar mass M of the mixture. Molar mass uncertainty associated to unpredictable effects inside the measuring cell can be estimated from experimental data.

The standard overall uncertainty $(k=1)$ $u_T(\rho)$ of the experimental density measurements of this work were calculated according to two different methods.

The first method takes into account uncertainty contributions of density, pressure, temperature and gravimetric composition by using equation 4.13.

$$u_T(\rho)=\left[u(\rho)^2+\left(\left(\frac{\partial\rho}{\partial p}\right)_{T,x}u(p)\right)^2+\left(\left(\frac{\partial\rho}{\partial T}\right)_{p,x}u(T)\right)^2+\sum_i\left(\left(\frac{\partial\rho}{\partial x_i}\right)_{T,p,x_j\neq x_i}u(x_i)\right)^2\right]^{0.5} \quad \textbf{Eq. 4.13.}$$

where p is pressure, T s temperature and x_i is the molar fraction of each of the components of the mixture. Partial derivatives were calculated by GERG-2008 equation of state using REFPROP software [7].

The second method uses the uncertainty in the molar mass of the mixture instead the uncertainty in composition estimated directly from the gravimetric preparation. Thus, the uncertainty associated to sorption effects can be included. In this case, the standard overall uncertainty $(k=1)$ $u_T(\rho)$ of the experimental density measurements is given by equation 4.14.

$$u_T(\rho)=\left[u(\rho)^2+\left(\left(\frac{\partial\rho}{\partial p}\right)_{T}u(p)\right)^2+\left(\left(\frac{\partial\rho}{\partial T}\right)_{p}u(T)\right)^2+\left(\left(\frac{\partial\rho}{\partial M}\right)_{p,T}\cdot u(M)\right)^2\right]^{0.5} \quad \textbf{Ec. 4.14.}$$

Molar mass uncertainty analysis

The combined molar mass uncertainty $u(M)$ is given by equation 4.15 from three sources of uncertainty.

$$u(M)=\left[u(M_{atomic})^2+u(M_{grav})^2+u(M_{sorp})^2\right]^{0.5} \quad \textbf{Eq. 4.15.}$$

$u(M_{atomic})$ is the uncertainty of the molar mass of the mixture associated to the uncertainties of the molar weights related with the components of the mixture. This values

can be obtained from the IUPAC technical report of 2011 by Wieser et al. [8]. The uncertainty due to the uncertainties estimated in the gravimetric preparation of the mixture $u(M_{grav})$ is given by equation 4.16.

$$u(M_{grav}) = \left\{ \sum_{j=1}^{n} \left[\frac{\sum_{i=1}^{n} \frac{m_i}{M_i} - \left(\sum_{i=1}^{n} m_i \right) \Big/ M_j}{\left(\sum_{i=1}^{n} \frac{m_i}{M_i} \right)^2} \cdot u(m_j) \right]^2 \right\}^{0.5} \qquad \textbf{Eq. 4.16.}$$

where M_i are the molar masses of the mixture components and m_i are the masses of the n components used in the gravimetric preparation of the mixture. The derivation of expression 4.14 can be found in Ritcher and McLinden [9].

Finally, $u(M_{sorp})$ is the uncertainty associated to sorption effects and it is given by equation 4.17. These effects can be observed sometimes in the represented experimental data when the pressure is close to zero and the behavior tends to the ideal behavior. In other words, if the deviation of the experimental data at very low pressures does not tend to zero, the composition inside the measuring cell could be different than the reported gravimetric values. A fitting of the experimental data to the virial equation of state (equation 2.5) provides an independent estimation of M . The root-mean-square (RMS) of the difference between the molar mass from the gravimetric preparation M_{grav} and the molar mass determined from the virial analysis M_{virial} is taken as the standard uncertainty (*k* = 1) arising from the unpredictable effects mentioned above $u(M_{sorp})$.

$$u(M_{sorp}) = \left[\frac{\sum_{i=1}^{N} \left(M_{grav,i} - M_{virial,i} \right)^2}{N} \right]^{0.5} \qquad \textbf{Eq. 4.17.}$$

where N is the number of measured isotherms.

4.6. REFERENCES

[1] M. E. Mondéjar, C. R. Chamorro, and R. Span, “Contribution to the development and introduction of renewable gaseous fuels through the thermodynamic characterization of mixtures of their components by using an optimized single sinker densimeter whit magnetic suspension coupling (Phd thesis),” Valladolid, 2012.

[2] M. E. Mondéjar, J. J. Segovia, and C. R. Chamorro, “Improvement of the measurement uncertainty of a high accuracy single sinker densimeter via setup modifications based on a state point uncertainty analysis,” *Measurement*, vol. 44, no. 9, pp. 1768–1780, 2011.

[3] I. E. C. BIPM IFCC, ILAC, IUPAC, IUPAP, ISO and OOIML, “International Vocabulary of Metrology-Basic and General Concepts and Associated Terms (VIM), 3rd edn.,” *Int. Vocab. Metrol. Gen. Concepts Assoc. Terms*, 2008.

[4] I. E. C. BIPM IFCC, ISO, IUPAC, IUPAP and OIML, “Guide to the Expression of Uncertainty in Measurement,” *Guid. to Expr. Uncertain. Meas.*, 1995.

[5] *Recommendation INC-1 - Working Group on the Statement of Uncertainties*. Sévres, France: Bureau International des Poids et Mesures, 1980.

[6] Comité de Laboratorios de la Cooperación Europea para la Acreditación, “EA 4/02 - Evaluación de la incertidumbre de medida en las calibraciones,” 2013.

[7] “Lemmon, E.W., Huber, M.L., McLinden, M.O. NIST Standard Reference Database 23: Reference Fluid Thermodynamic and Transport Properties-REFPROP, Version 9.1, National Institute of Standards and Technology, Standard Reference Data Program, Gaithersburg, 2013.” .

[8] M. E. Wieser, N. Holden, T. B. Coplen, J. K. Böhlke, M. Berglund, W. A. Brand, P. De Bièvre, M. Gröning, R. D. Loss, J. Meija, T. Hirata, T. Prohaska, R. Schoenberg, G. O’Connor, T. Walczyk, S. Yoneda, and X.-K. Zhu, “Atomic weights of the elements 2011 (IUPAC Technical Report),” *Pure Appl. Chem.*, vol. 85, no. 5, pp. 1047–1078, Jan. 2013.

[9] M. Richter and M. O. McLinden, “Vapor-Phase (p, ρ, T, x) Behavior and Virial Coefficients for the (Methane + Propane) System,” *J. Chem. Eng. Data*, vol. 59, no. 12, pp. 4151–4164, Dec. 2014.

[10] J. T. R. Watson and National Engineering Laboratory-FPT Division, “‘A generalised fitting package for the least squares analysis of data’.” East Kilbride, Glasgow G75 0QU, Scotland., 1991.

CHAPTER 5

Preparation of gas mixtures for high accuracy density measurements

5.1. Introduction 111
5.2. The gravimetric method for mixtures preparation 111
5.3. Prepared mixtures for this work 118
5.4. References 119

5.1. INTRODUCTION

As it was stated in chapter 2, the accurate estimation of the thermophysical properties of the fuels from equations of state is an essential point in their applications. The development and the validation of equations of state need an important amount of experimental data over wide ranges of temperature and pressure with high accuracy. In the area of gas fuels, the experimental determination of density has a relevant importance because the formulation of the mixture model of the GERG-2008 equation of state, reference equation for natural gases and related mixtures, is based on multi-fluid approximations explicit in the Helmholtz energy $a(\rho,T,x)$, which is a function of state with the independent variables: density ρ, temperature T and molar composition vector x [1]. 70 % of the data used in the GERG-2008 development were (p,ρ,T) data from pure fluids and binary mixtures [2].

In this work, the density was determined by a single-sinker densimeter with magnetic suspension coupling. Its uncertainty analysis is on chapter 4. The calculation of the overall standard uncertainty $(k=1)$ expressed in density units $u_T(\rho)$ considers the standard combined uncertainties estimated for density, temperature, pressure and composition, according to equation 4.11.

$$u_T(\rho)=\left[\underbrace{u(\rho)^2}_{\text{Density}}+\overbrace{\left(\left(\frac{\partial\rho}{\partial p}\right)_{T,x}u(p)\right)^2}^{\text{Pressure}}+\underbrace{\left(\left(\frac{\partial\rho}{\partial T}\right)_{p,x}u(T)\right)^2}_{\text{Temperature}}+\overbrace{\sum_i\left(\left(\frac{\partial\rho}{\partial x_i}\right)_{T,p,x_j\neq x_i}u(x_i)\right)^2}^{\text{Composition}}\right]^{0.5} \quad \textbf{Eq. 4.11.}$$

As it can be observed, the uncertainty of the studied mixture composition influences directly in density overall uncertainty. Experimental needs require mixtures which composition is not usually available for commercial purposes. Therefore, specific preparation of certificated mixtures is required.

5.2. THE GRAVIMETRIC METHOD FOR MIXTURES PREPARATION

The gravimetric method is the main technique to prepare gaseous mixtures with the adequate traceability to be used as reference standards. The preparation of mixtures through the gravimetric method consists in the ordered addition of the different

components, also called mother gases (pure gases or premixtures with known composition, which are in turn gravimetrically prepared), in a evacuated cylinder. The amount of gas components added from a mother gas is determined by weighing the cylinder after each sequential addition. Once the mixture preparation is completed, the final composition is controlled by analytical methods. The mass fraction of each component in the final gas mixture is expressed as the quotient between the mass of this component and the total mass of the mixture. The international standard ISO 6142 [3] establishes a "process for the preparation of calibration gas mixtures" based on the final composition of the gas mixture is within a predefined uncertainty limits. The standard only has application in gas mixtures or vaporized components which cannot react among themselves and the walls of the cylinder. The process to verify the final mixture composition is also described in the standard.

The main characteristics of the gas mixtures prepared through the gravimetric method are:

- **Homogeneity**: The values determined in a sample must be applied to any other mixtures within the uncertainty limits.
- **Stability**: The mixture composition must be the same in the whole validity period through conservation and handling defined conditions.

The final accuracy of the prepared mixtures by gravimetric method is limited by the smallest amount of gas that can be measured and added to the final mixture with an adequate uncertainty. This physical restriction causes a limit in the most diluted mixture that can be prepared in one step. However, this limit is usually overtaken thanks to multiple-dilution methods in which gravimetrically-prepared premixtures are used as mother gases in different dilution steps. In addition, in recent years, techniques have been developed for handling gases that are capable of reducing the smallest mass that can be weighed and transferred to a mixture in a single step [4].

Mixture preparation

In order to prepare a gas mixture by gravimetric method, the target composition (ideal), uncertainty limits and final pressure of the homogenized mixture at 15 ^{o}C must be fitted in the first instance. The potential of any chemical reaction between mixture components or with cylinder or tubing materials during the process must be taken into account before starting the mixture preparation. The standard ISO 6142 does not specify any relation of

reactive combinations, so chemical knowledge is needed to evaluate the stability of a specific gas mixture.

Once the chemical stability of the mixture is known, the most adequate filling procedure is selected. The following parameters must be considered:

- Security of the filling process. Intermediate mixtures with components that can react in a violent way must be avoided.
- Available pressure of the mother gases. A minimum difference between mother gas and final cylinder pressures must exist in each filling process step. The use of compressors is not allowed in gravimetric method because the mixture could be contaminated. The availability of previous premixtures which are useful for the process must also be taken into account.
- Maximum filling pressure of the cylinder to avoid condensation. The composition of the gas mixture could be modified due to the condensation of the mixture components. To avoid condensation during the gas mixture preparation, filling pressure must be lower than that of the dew point of the final mixture at the filling temperature. This condition has to be fulfilled for each intermediate mixture and during the storage and handling. 15 ^{o}C is the usual temperature to secure the no-condensation of the mixture components.
- Composition and uncertainty of the used mother gas.
- Specifications of the balance used.
- Preparation tolerance requirements. Components with low concentrations will have higher uncertainties, so the acceptable value of uncertainty must be selected according to the composition of each component.

Starting from a target composition for a mixture (in molar fraction), mass values m_i of each component i are calculated by equation 5.2.

$$m_i = \frac{x_i \cdot M_i}{\sum_{j=1}^{N} x_j \cdot M_j} \cdot m_f \qquad \textbf{Eq. 5.2.}$$

where x_i and x_j are the molar fractions of the components i and j, respectively; M_i and M_j are the molar mass of the components i and j, respectively; N is the number of components in the final mixture, and m_f is the mass of the final mixture.

The filling process is selected after each component mass has been calculated and the process is simulated, estimating by equations of state the pressures of the intermediate steps as a function of the calculated masses. The associated uncertainties are calculated at the same time. If the estimated uncertainty for this process is unacceptable, another procedure should be adopted.

There are three main techniques for gas mixture preparation by the gravimetric method, but a combination of them is the most usual procedure, especially in multicomponent mixtures.

- **Direct method**: The final mass calculated for each component is added directly to the final cylinder. The gas amount is controlled by weighing. The sequence of filling and the filling pressures of the mother gases must be considered on each step. This method is used when a mixture or premixture with high concentrations of all components needs to be prepared. The exact amount depends on the accuracy of the balance and the final mass of the mixture, but it is approximate for components quantity higher than 50 g.

- **Transference method**: If small amounts of some components are needed (lower than 50 g), small cylinders (25, 50 or 75 ml) are used to weight the amount of these components in high resolution balances. The smallest amount that can be registered with an acceptable uncertainty is approximately 2 g. Then, pressure is increased by heating and the weighted quantity is introduced in the final mixture cylinder. This method is also used if any of the components of the final gas mixture is in the liquid phase at ambient temperature. In this case the volume of the cylinder must be appropriate for the liquid mass because when the pressure is increased by heating, and the volume is too small, the component does not change to the gas phase (overheated) and a violent release of liquid can occur.

- **Multi-dilution method**: According to the previous described specifications, the use of premixtures is very common. Premixtures can be prepared previously or be prepared as an intermediate step of a new mixture. Once the premixture is prepared the filling process is carried out following the direct method, weighting the amount of added premixture directly in a balance. Each filling step has its own

associated uncertainty, so keeping down the number of dilution steps uncertainties will be within the required limits.

The composition of the target mixture (ideal) can differ from the final prepared mixture. The composition of each component in the final mixture (real) is determined by weighting the final cylinder before each filling step with an accuracy balance. During the filling process, the amount of mother gas is controlled by weighting while the cylinder is filling. Once the step is over, the mixture must be rest around 24 hours to be stabilized. After this time the cylinder is weighted again, obtaining the exact amount of mother gas added in the previous step. Molar fractions of individual components in the final mixture are calculated by equation 5.3.

$$x_i = \frac{\sum_{A=1}^{P}\left(\frac{x_{i,A}\cdot m_A}{\sum_{i=1}^{N} x_{i,A}\cdot M_i}\right)}{\sum_{A=1}^{P}\left(\frac{m_A}{\sum_{i=1}^{N} x_{i,A}\cdot M_i}\right)} \qquad \textbf{Eq. 5.3.}$$

where P is the total number of mother gases, m_A is the mass of the mother gas A determined by weighting and $x_{i,A}$ is the mass of the component i in the mother gas A.

Depending on the number of components, the preparation procedure and the amount of steps, the preparation of a gas mixture following the gravimetric method can take up to two months.

Uncertainty calculation

The uncertainty of the composition of a gas mixture comes from three factors:

- The weighting process of the mother gases.
- The purity of the individual components of the mixture.
- The knowledge of the molar mass of the components.

The accuracy that can be obtained by gravimetric method depends significantly on the purity of the mother gases used in the mixture preparation. The impurities present in the mother gases are the most usual sources of uncertainty of the final composition. Thus, the

purity of the main gas component is essential. The impurities of a nominally “pure” mother gas are determined by analysis.

In order to evaluate the uncertainty of the mixture, all the factors that can affect the final composition must be identified on each step of the procedure. The combined uncertainty is the sum of squares of individual uncertainty contributions, so that all the contributions that are less than or equal to 1/10 from the higher contribution can be neglected.

Verification of the mixture composition

Once the reference gas mixture is prepared, its composition is analyzed to check that the calculated composition from the gravimetric process agrees the measurements carried out by independent devices. This verification allows discarding significant mistakes in the preparation process of an individual gas mixture. Moreover, later checks can be required to demonstrate the mixture stability.

According to standard ISO 6142, the verification of the composition of a gas mixture can be performed by the method described below:

a) Establishing coherence between premixtures and appropriate traceable standards.
b) Establishing coherence between mixtures prepared by the same method.
c) Monitoring the production of mixtures validated using an appropriate method of statistical process control.

The composition of the mixtures studied for this thesis was validated by direct comparison with available traceable standards, using the multi-point calibration according to the procedure described in the international standard ISO 6143 [5] and the single-point exact-match calibration according to ISO/CD 12963 [6]. In both cases a GC analyzer especially designed for natural gas samples was used.

Figure 5.1 shows a scheme of the gravimetric method steps.

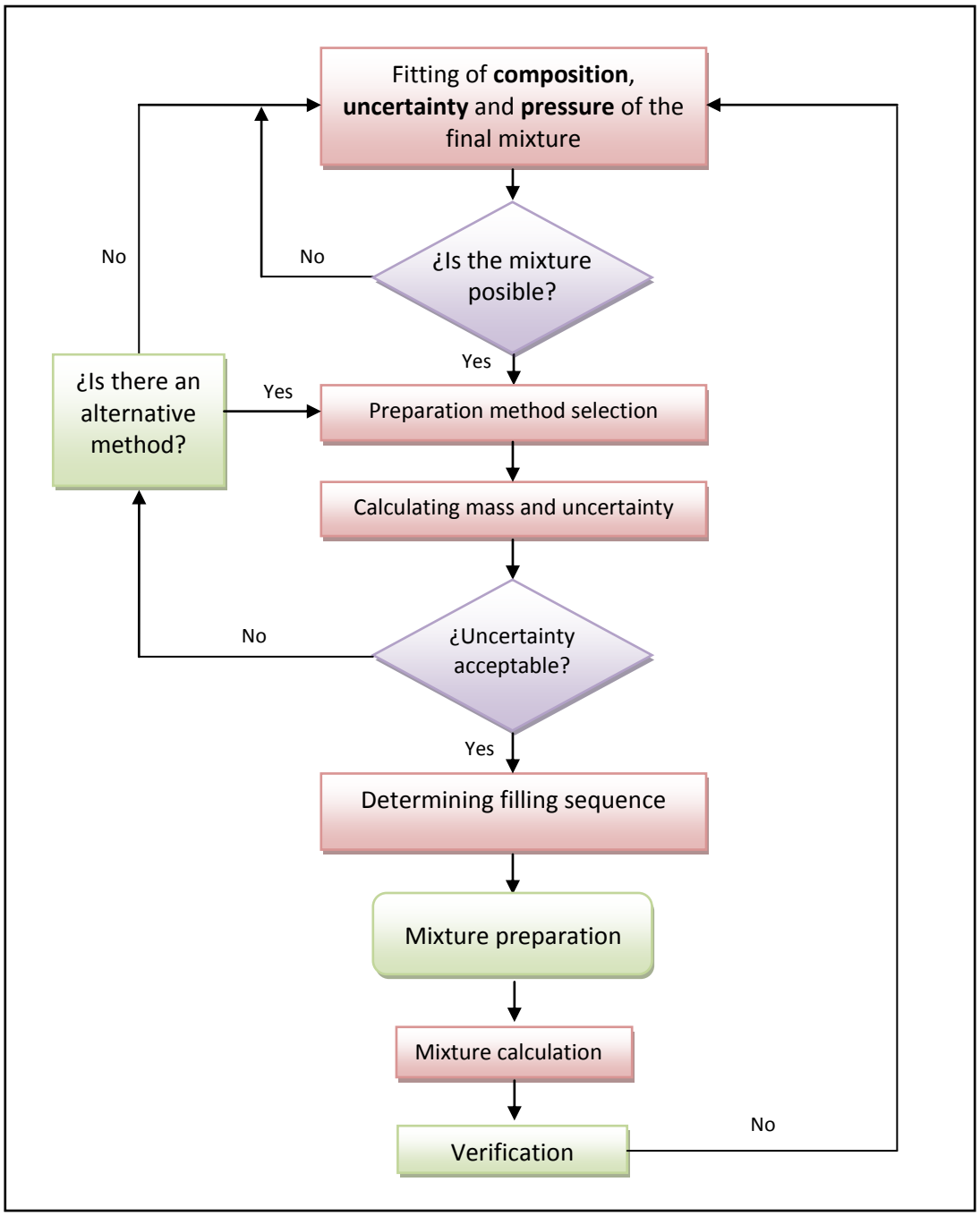

Figure 5.1. *Diagram of the process a gas mixture preparation by gravimetric method.*

5.3. PREPARED MIXTURES FOR THIS WORK

The studied mixtures were prepared specifically for density measurements by using a single-sinker densimeter. Five mixtures, three binary and two multicomponent mixtures, were prepared by two collaborating laboratories with TERMOCAL:

- The Federal Institute for Material research and Testing (*Bundesanstalt für Materialforschung und -prüfung*, BAM) [7].
- The Spanish Center of Metrology (*Centro Español de Metrología*, CEM) [8].

The mixtures were prepared within two European collaborative projects funded by the European Association of Metrology National Institutes (EURAMET) and the EU: "*Characterization of non-conventional energy gases"* [9] and "*Metrology for Biogas"* [10]. Table 5.1 shows the relation of the studied mixtures. Critical parameters were estimated from the GERG-2008 equation of state [2] by using REFPROP [11]. The procedure of the preparation of each mixture is detailed in the corresponding chapter.

Table 5.1. *Studied mixtures prepared by gravimetric method.*

Mixture	Components	Composition /mol-%	Laboratory	Starting pressure	Volume	Critical parameters
Methane + Helium (1)	CH_4 He	95.001470 4.998530	BAM	13.7 MPa	10 dm^3	T_c = 194.2 K p_c = 6.44 MPa
Methane + Helium (2)	CH_4 He	89.993256 10.006744	BAM	13.2 MPa	10 dm^3	T_c = 196.3 K p_c = 8.24 MPa
Methane + Helium (3)	CH_4 He	49.259240 50.740760	BAM	14.0 MPa	10 dm^3	-
CMM	CH_4 CO_2 N_2 C_2H_6 C_3H_8 *i*-C_4H_{10} *n*-C_4H_{10} *i*-C_5H_{12} *n*-C_5H_{12} O_2	64.207992 17.312271 17.031942 0.846613 0.078154 0.010716 0.005710 0.001723 0.000752 0.504128	BAM	4.9 MPa	10 dm^3	T_c = 207.1 K p_c = 6.86 MPa
Biogas	CH_4 CO_2 N_2 CO	49.8141 35.2028 9.9916 4.9915	CEM	10.0 MPa	5 dm^3	T_c = 224.8 K p_c = 8.9352 MPa

5.4. REFERENCES

[1] "ISO 20765-2 Natural gas -Calculation of thermodynamic properties -Part 2: Single-phase properties (gas, liquid, and dense fluid) for extended ranges of application," Geneva, 2015.

[2] O. Kunz and W. Wagner, "The GERG-2008 Wide-Range Equation of State for Natural Gases and Other Mixtures: An Expansion of GERG-2004," *J. Chem. Eng. Data*, 2012.

[3] "ISO 6142 - Preparation of calibration gas mixtures - Gravimetric method. International Organisation for Standardization, Geneva, 2001)." 2001.

[4] M. J. T. Milton, G. M. Vargha, and A. S. Brown, "Gravimetric methods for the preparation of standard gas mixtures," *Metrologia*, vol. 48, no. 5, pp. R1–R9, Oct. 2011.

[5] "ISO 6143 - Comparison methods for determining and checking the composition of calibration gas mixtures. International Organisation for Standardization, Geneva." 2001.

[6] "ISO/CD 12963 Gas analysis – Comparison methods for the determination of the composition of gas mixtures based on one- and two-point calibration, International Organization for Standardization, Geneva."

[7] "BAM Federal Institute for Materials Research and Testing." [Online]. Available: http://www.bam.de/en/index.htm. [Accessed: 12-Sep-2015].

[8] "CEM - Centro Español de Metrología." [Online]. Available: http://www.cem.es/. [Accessed: 12-Sep-2015].

[9] "Characterization of energy gases: EMRP ENG01 N 912/2009/EC (2010-2013)," European Metrology Research Programme.

[10] "JRP Summary Report for ENG54 Biogas 'Metrology for biogas.'" [Online]. Available: http://www.euramet.org/fileadmin/docs/EMRP/JRP/JRP_Summaries_2013/Energy_JRPs/ENG54_Publishable_JRP_Summary.pdf. [Accessed: 05-May-2014].

[11] "Lemmon, E.W., Huber, M.L., McLinden, M.O. NIST Standard Reference Database 23: Reference Fluid Thermodynamic and Transport Properties-REFPROP, Version 9.1, National Institute of Standards and Technology, Standard Reference Data Program, Gaithersburg, 2013." .

CHAPTER 6

Thermodynamic characterization of binary mixtures of methane and helium

6.1. Introduction 123
6.2. Mixture preparation 124
6.3. Experimental process 127
6.4. Experimental results 128
6.5. Virial coefficients determination 130
6.6. Uncertainty analysis of the measurements 136
6.7. Discussion 140
6.8. Table of results 152
6.9. References 167

6.1. INTRODUCTION

The knowledge of the thermophysical properties of natural gases and other related mixtures is of great importance for the design and estimation of the performance of technical processes. Depending on the source and the application, several components may be present in natural gases at different compositions. The raw natural gas needs to be processed due to the quality specifications for its commercial use as a fuel. Thus, the separation of undesirable components (e.g., carbon dioxide, water or hydrogen sulfide) or other components (e.g., lower and higher hydrocarbons) is required. In addition, the growing interest in alternative sources of energy gases and the diversity of composition of non-conventional fuels requires considering the presence of other minoritary components that are not found in standard natural gas. For all this reasons, property calculations over wide ranges of mixture compositions and operating conditions in the homogeneous gaseous, liquid, and supercritical regions and for vapor-liquid equilibrium (VLE) states are required. These particular data can be calculated from equations of state.

Different equations of state have been developed for various substances and applications, according to the requirements of precision and availability of experimental data. There are two main equations of state for estimating natural gas properties: AGA8-DC92 [1] and GERG-2008 [2]. The later one is the current reference equation of state for natural gas and other related mixtures, and was designated as an ISO Standard (ISO 20765-2) for the calculation of thermodynamic properties of natural gases [3]. More details on this equation are given in chapter 2.4.

The GERG-2008 equation of state is based on multi-fluid approximations and is explicit in the Helmholtz free energy $a(\rho,T,x)$ with density ρ, temperature T, and the vector of the molar composition of the mixture x as independent variables. The mixture model uses equations of state in the form of fundamental equations for each individual component along with further auxiliary correlations to consider the residual mixture behavior.

Experimental data for the 21 pure components of natural gas and for 210 binary combinations of these components were considered for the development of the GERG-2008 equation of state. For those binary mixtures for which sufficient accurate experimental data were available, binary specific departure functions or a generalized departure function were developed. Due to the lack of experimental data for most of the binary combinations and to the complexity of the process, a great number of the binary systems were accounted for by using adjusted reducing functions for density and

temperature. This is the case of the binary mixture (methane + helium), for which no departure function was established so far. In fact, the GERG-2008 report considers binary mixtures containing helium as one of the binary mixtures proposed to develop a generalized departure function in the future [2].

Helium is an inert gas with a very small molecular size present in most of the raw natural gases. Moreover, the only practical sources of helium come from certain natural gas fields. Helium has a wide range of important medical, scientific and industrial applications based on its extremely low boiling temperature and non-flammable nature. In the last years, the world demand for helium has increased significantly, and projections show a continued increase in demand for helium from (5 to 7) % per annum, so the value of natural gas fields that contain helium, even in very small amounts, is likely to rise significantly. In general, natural gas fields with helium contents above 0.3 mole-% are considered to be of commercial interest as helium sources, although the helium content can be up to 7 % [4]. This is estimated to represent about $8.6 \cdot 10^6$ tons of helium in the world, with US having the largest fraction of reserves (around 35 %), followed by Qatar (with 20 %) [5].

This part of the thesis provides accurate experimental (*p, ρ, T*) data in the temperature range from (240 to 400) K and up to 20 MPa of three binary mixtures of methane and helium, (0.95 CH_4 + 0.05 He), (0.90 CH_4 + 0.10 He) and (0.50 CH_4 + 0.50 He). The mixtures were prepared by following the gravimetric method by the Federal Institute for Materials Research and Testing (*Bundesanstalt für Materialforschung und –prüfung*, BAM) in Berlin, Germany. The second and third interaction virial coefficients of the mixtures were estimated from the experimental data. Overall uncertainties of the density measurements were also estimated through the two different methods which were described in chapter 4. Finally, the experimental density data were compared with the estimated densities from the GERG-2008 and AGA8-DC92 equations of state.

6.2. MIXTURE PREPARATION

The (CH_4 + He) binary mixtures were prepared by the Federal Institute for Materials Research and Testing (*Bundesanstalt für Materialforschung und –prüfung*, BAM) in Berlin, Germany according to the ISO 6142 [6]. The mixtures were supplied in aluminum cylinders of 10 dm^3. Table 6.1 shows the composition and the expanded uncertainty (k = 2) of the mixtures. Table 6.2 shows the purity, supplier, molar mass and critical parameters of the

samples of pure methane and helium. All substances were used without further purification.

Table 6.1. *Composition of the studied (CH_4 + He) mixtures.*

Component	(0.95 CH_4 + 0.05 He) BAM nº: 8036-150126		(0.90 CH_4 + 0.10 He) BAM nº: 8069-150127		(0.50 CH_4 + 0.50 He) BAM nº: 8092-141020	
	x_i (mol-%)	$U(x_i)$ (k = 2) (mol-%)	x_i (mol-%)	$U(x_i)$ (k = 2) (mol-%)	x_i (mol-%)	$U(x_i)$ (k = 2) (mol-%)
Methane	95.001470	0.009236	89.993256	0.008336	49.25924	0.0051291
Helium	4.998530	0.001365	10.006744	0.001702	50.74076	0.0057509

Table 6.2. *Purity, supplier, molar mass and critical parameters of the individuals components of the studied (CH_4 + He) mixtures.*

Components	Purity	Supplier	M/g·mol^{-1}	Critical parameters	
				T_c /K	P_c /MPa
Methane	≥ 99.9995 mol %	Linde[a]	16.043 [b]	190.564 [b]	4.599 [b]
Helium	≥ 99.9999 mol %	Linde[a]	4.003 [c]	5.195 [c]	0.228 [c]

[a] Linde AG, Unterschleißheim, Germany.

[b] Setzmann et al. [7]

[c] Ortiz-Vega et al. [8]

The preparation of the mixtures was effected in two steps as shown in Figure 6.1. First, the mixture of (0.50 CH_4 + 0.50 He) was prepared by a consecutive introduction of pure helium and pure methane into the evacuated recipient cylinder (BAM no.: 8092-141020, volume: 10 dm^3).

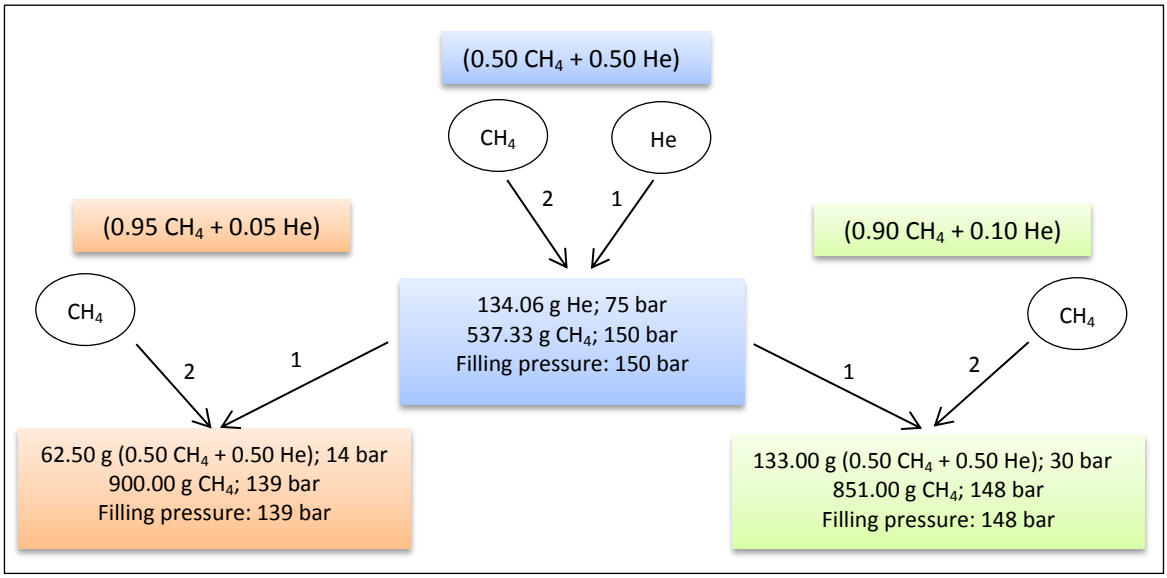

Figure 6.1. *Preparation scheme of the (CH_4 + He) binary mixtures.*

The substance transfer was actuated only by the pressure difference between the cylinder containing the pure compound and the recipient cylinder. The mass of the gas portion was determined after each filling step using a high-precision mechanical gas balance (Voland model HCE 25, Voland Corp., New Rochelle NY, USA). The resulting mixture had a pressure of approximately 15 MPa.

The other two binary mixtures were prepared in a similar way. A specified portion of the (0.50 CH_4 + 0.50 He) parent mixture was introduced into a new cylinder and diluted by a properly measured amount of methane to create the final composition. The two cylinders displayed a pressure of 13.9 MPa for the (0.95 CH_4 + 0.05 He) mixture and of 14.8 MPa for the (0.90 CH_4 + 0.10 He) mixture, respectively. Each mixture was finally homogenized by a procedure of subsequent heating and rolling.

Critical parameters of the mixtures were estimated from the GERG-2008 equation of state [2] by using REFPROP [9] and they are shown in Table 6.3.

Table 6.3. *Critical parameters and molar mass of the studied (CH_4 + He) binary mixtures.*

Parameters	(0.95 CH_4 + 0.05 He)	(0.90 CH_4 + 0.10 He)	(0.50 CH_4 + 0.50 He)
T_c /K	194.244	196.254	-
p_c /MPa	6.438	8.237	-
M/g·mol $^{-1}$	15.441	14.838	9.933

The samples of (0.95 CH_4 + 0.05 He) and (0.90 CH_4 + 0.10 He) were validated by gas chromatography (GC) against samples of similar composition following the single-point exact-match calibration according to ISO/CD 12963 [10]. The gas mixture used for validation matched the (0.90 CH_4 + 0.10 He) mixture, and the analysis was executed on a multichannel process GC (Siemens MAXUM II, Siemens AG, Karlsruhe, Germany) for the investigation of natural gases. The GC was equipped with customized packed columns particularly adapted for the analysis of synthetic natural gases and individual TCDs (thermal conductivity detectors) for each channel. The analysis was performed in an isothermal regime at 60 °C. Table 6.4 gives the results of the GC analysis. These measurements were entirely done at BAM prior to the density determination.

The GC analysis for the (0.50 CH_4 + 0.50 He) mixture was not performed due to the fact that the helium content was higher than the validated limit of the used method. However,

it was possible to validate its composition thanks to the concordance with the GC analysis of the other two mixtures.

Table 6.4. *Results of the GC analysis of the (CH_4 + He) binary mixtures and gravimetric composition of the validation mixture.*

	(0.95 CH_4 + 0.05 He)			(0.90 CH_4 + 0.10 He)		
Component	Concentration (molar fraction)		Relative deviation between gravimetric preparation GC analysis	Concentration (molar fraction)		Relative deviation between gravimetric preparation GC analysis
	x_i	$U(x_i)$ % (k = 2)	%	x_i	$U(x_i)$ % (k = 2)	%
Methane	94.7963	0.0306	–0.216	90,0192	0.0397	0.029
Helium	4.9742	0.0085	–0.487	10.0195	0.0146	0.127

Validation mixture BAM no.: 7065-100105	x_i	$U(x_i)$ % (k = 2)
Methane	90.438798	0.009165
Helium	9.559901	0.005987
Carbon monoxide	0.0002158	0.0000002
Carbon dioxide	0.0002164	0.0000002
Oxygen	0.0002139	0.0000002
Argon	0.0002169	0.0000002
Hydrogen	0.0002220	0.0000003
Nitrogen	0.0002166	0.0000002

6.3. EXPERIMENTAL PROCESS

Firstly, experimental (p, ρ, T) measurements were carried out for the (0.95 CH_4 + 0.05 He) and (0.90 CH_4 + 0.10 He) mixtures by using the single-sinker densimeter with magnetic suspension coupling at temperatures from (250 to 400) K and pressures up to 20 MPa. During the measurements of the (0.50 CH_4 + 0.50 He) mixture, there were some problems with the AC comparator resistance bridge. Therefore, measurements were cancelled and re-started after repairing the device a few months later. The new ultra-low refrigerating-heating circulator (Julabo FP51-SL), which is described in chapter 3.3, was installed during this interlude. With this thermostatic bath it is possible to obtain data at 240 K. Thus, the measurements for the (0.50 CH_4 + 0.50 He) mixture were carried out from (240 to 400) K

and pressures up to 20 MPa. Later, (*p, ρ, T*) data from (240 to 260) K were obtained for the (0.95 CH_4 + 0.05 He) and (0.90 CH_4 + 0.10 He) mixtures.

At the end, nine isotherms were measured at (240, 250, 260, 275, 300, 325, 350, 375 and 400) K for each (CH_4 + He) mixture. The pressure was decreased from (20 to 1) MPa in 1 MPa steps.

The sinker mass in vacuum was measured after each of the isotherms to check any misalignment suffered by the magnetic suspension coupling during the measurements and to cancel the apparatus effect of the FTE. The maximum difference between the replicates of the sinker mass in vacuum at the same temperature was 0.0001 % for all the (CH_4 + He) mixtures. This good repeatability of the measurements in vacuum confirmed that there was not any misalignment during the measurements.

Before and after carrying out the measurements on the studied (CH_4 + He) mixtures, test measurements with nitrogen were carried out in the whole working range of the apparatus to validate the operation by comparing the experimental results with the densities calculated from the reference equation of state for nitrogen by Span et al. [11]. Relative deviations of the experimental data from the calculated densities were within a ±0.02 % band, with an Absolute Average Deviation (*AAD*) of 0.0055 %. These results are shown in chapter 3.6.

6.4. EXPERIMENTAL RESULTS

Table 6.19 (section 6.8) shows the (*p, ρ, T*) data for the (0.95 CH_4 + 0.05 He) mixture and the relative deviation from the density values estimated by the GERG-2008 [2] and AGA8-DC92 [1] equations of state. The same data are shown in Tables 6.20 and 6.21 for the (0.90 CH_4 + 0.10 He) and the (0.50 CH_4 + 0.50 He) mixtures, respectively. Each pressure point of the isotherms is calculated as the average value of the last ten measurements on each pressure step. Tables 6.19, 6.20 and 6.21 also show the expanded uncertainty (k = 2) in density, both relative and absolute values, and the overall expanded uncertainty. The overall uncertainty was calculated by two alternative methods: from the gravimetric composition of the mixtures (equation 4.13) and from the virial fitting of the experimental data (equation 4.14), method which is described in chapter 4.7.

Although the single-sinker densimeter is one of the most accurate methodologies for the measurement of the density of fluids, it presents some systematic errors which affect the

final density result and must be evaluated. The two main effects are the force transmission error (FTE) due to the magnetic coupling and the possible sorption of gas molecules on the cell and sinker surfaces.

Force transmission error

The FTE consists of two terms: the apparatus effect and the fluid specific effect. In this work, the apparatus effect of the FTE was accounted for by measuring the sinker mass under vacuum for each isotherm [12]. In the case of the fluid specific effect, its magnitude depends on the magnetic behavior of the measured gas, the difference between the sinker and the fluids densities and the specific constant of the apparatus. The specific constant of the apparatus was estimated in 45.7 ppm. This corresponds with a correction of 0.005 % in density (see chapter 3.4 for further details).

The magnetic susceptibility of the mixtures χ_{mix} were estimated by using an additive law proposed by Bitter [13], from the magnetic susceptibility of the pure components χ_i and their molar fractions x_i, according to equation 6.1.

$$\chi_{mix} = \sum_{i=1}^{n} \left(x_i \cdot \chi_i \right) \qquad \textbf{Eq. 6.1.}$$

Magnetic susceptibility of (0.95 CH_4 + 0.05 He) mixture is $\chi_{He5\%} = -8.62 \cdot 10^{-9}$, for (0.90 CH_4 + 0.10 He) is $\chi_{He10\%} = -8.17 \cdot 10^{-9}$ and $\chi_{He50\%} = -4.64 \cdot 10^{-9}$ for (0.50 CH_4 + 0.50 He) mixture. According to McLinden et al. [12], the apparatus effect affects more than the fluid specific effect to the density measurements, except for strongly paramagnetic fluids. The magnetic susceptibility values estimated for (CH_4 + He) mixtures does not present paramagnetic behavior (i.e. magnetic susceptibility of oxygen is $\chi_{O_2} = 1.78 \cdot 10^{-6}$). Since the values of magnetic susceptibility of the mixture are relatively low, the fluids magnetic behavior would be negligible in relation to the apparatus effect and therefore the fluid specific effect was not considered in these measurements.

Sorption effects in the measuring cell

Adsorption of gas molecules can take place on the measuring cell walls or the sinker surface and it can produce deviations up to 0.1 % in density [14]. This effect is not

compensated for in the measurements performed on a single-sinker densimeter. Klimeck et al. [15] and Lösch-Will [16], among others, reported that this effect could only affect the accuracy of the measurements near the saturation curve or at very low gas densities, since only the adsorption on the sinker, and not that on the cell walls, had to be considered.

Test measurements to check for any adsorption effect on the experimental density value were carried out for the (0.95 CH_4 + 0.05 He) y (0.90 CH_4 + 0.10 He) mixtures at 1MPa and temperatures of 300 K and 400 K. The maximum difference observed in relative deviation along the isotherms was than 0.0014%, which is one order of magnitude lower than the uncertainty in density, and therefore it was concluded that the adsorption effect could be neglected in the measurements of (CH_4 + He) mixtures.

6.5. VIRIAL COEFFICIENTS DETERMINATION

The second and the third virial coefficients for (CH_4 + He) mixtures were calculated by fitting the experimental data to the virial expansion (equation 2.5).

$$Z = \frac{pM}{RT\rho} = 1 + B \cdot \frac{\rho}{M} + C \cdot \frac{\rho^2}{M^2} \qquad \textbf{Eq. 2.5.}$$

The fit was done for each measured isotherm by using a generalised fitting package for the least squares analysis of data developed by Watson at the National Engineering Laboratory in Glasgow [17]. The results are shown in Tables 6.5 (0.95 CH_4 + 0.05 He), 6.6 (0.90 CH_4 + 0.10 He) and 6.7 (0.50 CH_4 + 0.50 He) with the virial coefficients calculated by the GERG-2008. The uncertainties of the fitted parameters were calculated according to the GUM [18] from standard deviation values returned by the software.

In the fitting process, some experimental values were identified as outliers because considering them during the fitting could not be done within the tolerance limits. This limit was 0.02 %, which is approximately the uncertainty in density of the densimeter. Experimental values measured at pressures above 10 MPa were outliers, so they were not used for the fitting. A reason for this can be the number of parameters of the used virial expansion was inappropriate to model the experimental behavior over all the pressure range. The forth and even the fifth virial coefficients should be required, but in this case a new software tool and probably more experimental data would be needed.

Table 6.5. *Least mean squares fitting results for (0.95 CH_4 + 0.05 He) mixture (M_{virial}, B, C), with their uncertainties, and virial coefficients values estimated by the GERG-2008.*

T/K	M_{virial}/ g·mol^{-1}	ΔM/ g·mol^{-1}	U(M)/ g·mol^{-1}	B/ cm^3·mol^{-1}	U(B)/ cm^3·mol^{-1}	B_{GERG}/ cm^3·mol^{-1}	C/ cm^6·mol^{-2}	U(C)/ cm^6·mol^{-2}	C_{GERG}/ cm^6·mol^{-2}
240.047	15.437	0.004	0.0041	–62.69	0.04	–62.99	2857	4	2921
249.996	15.434	0.007	0.0042	–57.12	0.05	–57.53	2717	6	2765
260.005	15.440	0.001	0.0043	–52.04	0.06	–52.55	2595	7	2625
275.002	15.439	0.002	0.0084	–45.27	0.12	–45.91	2429	16	2442
299.958	15.438	0.003	0.0044	–35.96	0.09	–36.61	2240	14	2197
324.955	15.438	0.003	0.0040	–28.34	0.06	–28.99	2095	10	2010
349.938	15.436	0.005	0.0039	–22.00	0.04	–22.65	1980	7	1865
374.924	15.436	0.005	0.0039	–16.72	0.05	–17.29	1912	10	1752
399.997	15.428	0.013	0.0062	–12.47	0.30	–12.70	1909	67	1663

T is the average temperature of each isotherm. ΔM is the difference between the gravimetric molar mass of the mixture M_{grav} (15.441 g·mol^{-1}*) and the fitted molar mass value M_{virial}.*

Table 6.6. *Least mean squares fitting results for (0.90 CH_4 + 0.10 He) mixture (M_{virial}, B, C), with their uncertainties, and virial coefficients values estimated by the GERG-2008 equation of state.*

T/K	M_{virial}/ g·mol^{-1}	ΔM/ g·mol^{-1}	U(M)/ g·mol^{-1}	B/ cm^3·mol^{-1}	U(B)/ cm^3·mol^{-1}	B_{GERG}/ cm^3·mol^{-1}	C/ cm^6·mol^{-2}	U(C)/ cm^6·mol^{-2}	C_{GERG}/ cm^6·mol^{-2}
240.045	14.827	0.0107	0.0108	–54.24	0.22	–55.03	2601	23	2639
250.005	14.832	0.0057	0.0085	–49.00	0.14	–50.19	2454	17	2508
260.013	14.836	0.0017	0.0083	–44.40	0.13	–45.78	2343	17	2389
274.994	14.836	0.0017	0.0084	–38.32	0.16	–39.88	2201	22	2235
299.951	14.842	–0.0043	0.0083	–29.66	0.16	–31.60	2002	26	2029
324.958	14.836	0.0017	0.0077	–22.94	0.10	–24.78	1892	19	1871
349.939	14.830	0.0077	0.0079	–17.51	0.14	–19.11	1849	28	1749
374.923	14.836	0.0017	0.0079	–12.58	0.15	–14.30	1758	30	1653
400.006	14.833	0.0047	0.0078	–8.28	0.16	–10.17	1646	36	1576

T is the average temperature of each isotherm. ΔM is the difference between the gravimetric molar mass of the mixture M_{grav} (14.838 g·mol^{-1}*) and the fitted molar mass value M_{virial}.*

Table 6.7. *Least mean squares fitting results for (0.50 CH_4 + 0.50 He) mixture (M_{virial}, B, C), with their uncertainties, and virial coefficients values estimated by the GERG-2008 equation of state.*

T/K	M_{virial}/ g·mol^{-1}	ΔM/ g·mol^{-1}	U(M)/ g·mol^{-1}	B/ cm^3·mol^{-1}	U(B)/ cm^3·mol^{-1}	B_{GERG}/ cm^3·mol^{-1}	C/ cm^6·mol^{-2}	U(C)/ cm^6·mol^{-2}	C_{GERG}/ cm^6·mol^{-2}
240.032	9.926	0.008	0.0106	–2.98	0.57	–10.79	864	83	757
249.998	9.929	0.004	0.0082	–1.81	0.41	–9.12	938	62	734
259.991	9.932	0.001	0.0058	0.21	0.19	–7.58	824	30	714
275.007	9.935	–0.002	0.0068	2.29	0.31	–5.49	754	51	688
299.922	9.935	–0.002	0.0051	4.80	0.09	–2.52	778	17	653
324.970	9.930	0.003	0.0050	6.75	0.06	–0.02	794	11	625
349.914	9.921	0.012	0.0059	7.73	0.28	2.09	935	58	602
374.906	9.927	0.006	0.0069	9.76	0.46	3.90	816	24	583
399.990	9.929	0.004	0.0063	11.02	0.39	5.47	802	92	567

T is the average temperature of each isotherm. ΔM is the difference between the gravimetric molar mass of the mixture M_{grav} (9.933 g·mol^{-1}) and the fitted molar mass value M_{virial}.

Figures 6.2, 6.3 y 6.4 show the deviation of experimental pressure from pressure calculated trough virial fitting for the three (CH_4 + He) mixtures. Higher deviations of 0.02 % can be observed at pressures above 10 MPa and at low pressures in Figure 6.4. These points were considered outliers and were not used in the fitting.

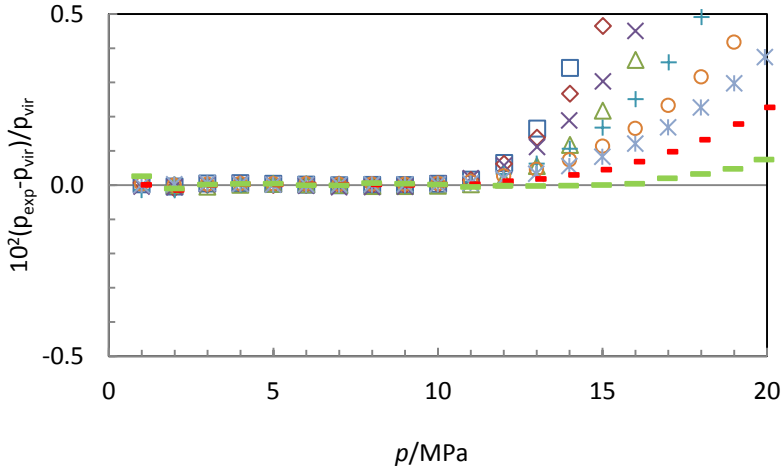

Figure 6.2. *Relative deviation of experimental pressure from pressure calculated by virial expansion p_{vir} (Eq. 4.16) by using the fitted parameters for the (0.95 CH_4 + 0.05 He) mixture. □ 240 K; ◇ 250 K; △ 260 K; × 275 K; + 300 K; ○ 325 K; ✳ 350 K; – 375 K; – 400 K.*

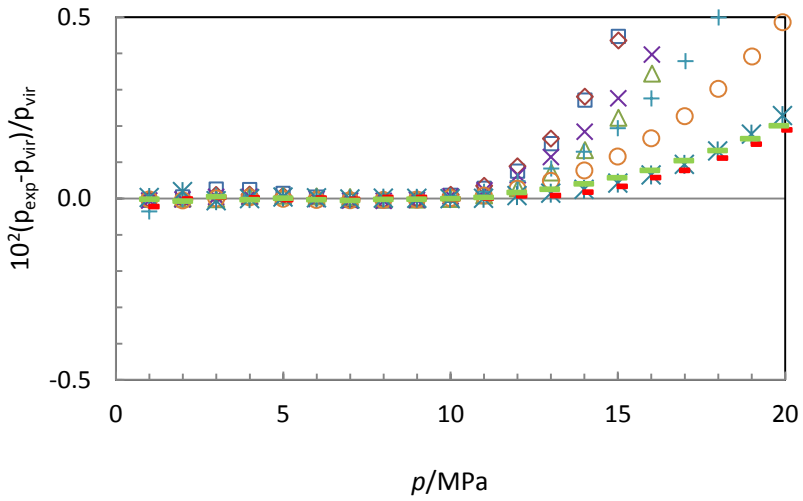

Figure 6.3. *Relative deviation of experimental pressure from pressure calculated by virial expansion p_{vir} (Eq. 4.16) by using the fitted parameters for the (0.90 CH_4 + 0.10 He) mixture. □ 240 K; ◇ 250 K; △ 260 K; × 275 K; + 300 K; ○ 325 K; ✳ 350 K; – 375 K; – 400 K.*

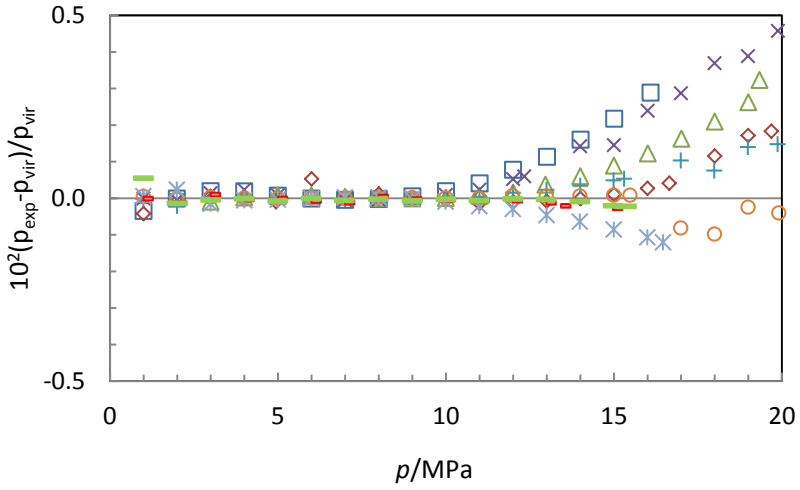

Figure 6.4. *Relative deviation of experimental pressure from pressure calculated by virial expansion p_{vir} (Eq. 4.16) by using the fitted parameters for the (0.50 CH_4 + 0.50 He) mixture. □ 240 K; ◇ 250 K; △ 260 K; × 275 K; + 300 K; ○ 325 K; ✳ 350 K; – 375 K; – 400 K.*

Virial composition of the mixtures

Estimating the "real composition" of the mixture loaded in the measuring cell is possible for binary mixtures from the obtained molar mass value in the virial fitting. The molar mass value of a mixture with n components is given by equation 6.2

$$M = \sum_{i=1}^{n} M_i \cdot x_i \qquad \textbf{Eq. 6.2.}$$

Knowing the molar mass value from the virial fitting and considering that the sum of the molar fraction of the mixture components $\sum_{i=1}^{n} x_i = 1$, the mixture composition inside the measuring cell can be obtained.

Table 6.8 shows the obtained results for the studied (CH_4 + He) mixtures.

Table 6.8. *Estimated composition of the studied (CH_4 + He) mixtures from virial fitting of the experimental results.*

Isotherm	240 K	250 K	260 K	275 K	300 K	325 K	350 K	375 K	400 K
(0.9500147 CH_4 + 0.0499853 He) M_{grav}= 15.441 g·mol^{-1}									
M_{virial} /g·mol^{-1}	15.437	15.434	15.440	15.439	15.438	15.438	15.436	15.436	15.428
x_{CH_4}	0.94969	0.94944	0.94993	0.94985	0.94977	0.94977	0.94960	0.94960	0.94894
x_{He}	0.05031	0.05056	0.05007	0.05015	0.05023	0.05023	0.05040	0.05040	0.05106
(0.89993256 CH_4 + 0.10006744 He) M_{grav}= 14.838 g·mol^{-1}									
M_{virial} /g·mol^{-1}	14.827	14.832	14.836	14.836	14.842	14.836	14.830	14.836	14.833
x_{CH_4}	0.89902	0.89944	0.89977	0.89977	0.90027	0.89977	0.89927	0.89977	0.89952
x_{He}	0.10098	0.10056	0.10023	0.10023	0.09973	0.10023	0.10073	0.10023	0.10048
(0.4925924 CH_4 + 0.5074076 He) M_{grav}= 9.933 g·mol^{-1}									
M_{virial} /g·mol^{-1}	9.9256	9.929	9.932	9.935	9.935	9.930	9.921	9.927	9.929
x_{CH_4}	0.49194	0.49222	0.49247	0.49272	0.49272	0.49230	0.49155	0.49205	0.49222
x_{He}	0.50806	0.50778	0.50753	0.50728	0.50728	0.50770	0.50845	0.50795	0.50778

Determination of interaction virial coefficients

The virial coefficients calculated for a mixture by equation 2.5 depend on the temperature and concentration of the components. In a mixture with n components, the second virial coefficient $B(T, x)$ is given by equation 2.6. In binary mixtures, the interaction virial coefficient $B_{12}(T)$ can be calculated from the estimated value of B by using equation 2.7. The obtained results for (CH_4 + He) mixtures are detailed in Table 6.9.

$$B_{12}(T) = \frac{B(T,x) - x_1^2 \cdot B_{11}(T) - x_2^2 \cdot B_{22}(T)}{2 \cdot x_1 \cdot x_2} \qquad \textbf{Eq. 2.7.}$$

Table 6.9. *Second interaction virial coefficients and expanded uncertainties (k = 2) for studied (CH_4 + He) binary mixtures.*

Isotherm	240 K	250 K	260 K	275 K	300 K	325 K	350 K	375 K	400 K
				(0.95 CH_4 + 0.05 He)					
$T_{average}$/K	240.047	249.996	260.005	275.002	299.958	324.955	349.938	374.924	399.997
B_{12}/ $cm^3 \cdot mol^{-1}$	21.43	21.44	22.60	23.06	22.01	21.29	20.66	19.56	15.35
$U(B_{12})$/ $cm^3 \cdot mol^{-1}$	0.84	0.85	0.85	0.85	1.72	1.72	1.72	1.66	1.68
B_{12} GERG/ $cm^3 \cdot mol^{-1}$	21.72	17.13	17.27	16.30	15.18	14.49	13.89	13.57	12.97
				(0.90 CH_4 + 0.10 He)					
$T_{average}$/K	240.045	250.005	260.013	274.994	299.951	324.958	349.939	374.923	400.006
B_{12}/ $cm^3 \cdot mol^{-1}$	20.26	22.12	22.86	23.19	24.77	23.46	21.53	22.31	23.10
$U(B_{12})$/ $cm^3 \cdot mol^{-1}$	0.88	0.87	0.87	0.87	1.74	1.73	1.73	1.67	1.67
B_{12} GERG/ $cm^3 \cdot mol^{-1}$	15.91	15.56	15.23	14.51	13.98	13.21	12.73	12.77	12.63
				(0.50 CH_4 + 0.50 He)					
$T_{average}$/K	240.032	249.998	259.991	275.007	299.922	324.970	349.914	374.906	399.990
B_{12}/ $cm^3 \cdot mol^{-1}$	22.58	22.00	23.38	23.99	24.03	23.80	22.32	23.58	23.68
$U(B_{12})$/ $cm^3 \cdot mol^{-1}$	1.09	1.02	0.95	0.98	1.77	1.77	1.79	1.77	1.75
B_{12} GERG/ $cm^3 \cdot mol^{-1}$	6.95	7.39	7.82	8.44	9.38	10.24	11.03	11.86	12.60

The expanded uncertainty $U(B_{12})$ was calculated according to the GUM [18] *from the uncertainties of interaction virial coefficients of the pure components* [19] *and the uncertainties of the gravimetric composition.*

There are two different values for the third interaction virial coefficient: $C_{112}(T)$, corresponds to the interaction between two molecules of “component 1” one molecule of

"component 2", and $C_{122}(T)$, interaction between one molecule of "component 1" and two molecules of "component 2". In the case of the (CH_4 + He) binary mixtures, methane was considered as "component 1" and helium as "component 2". The coefficients $C_{112}(T)$ and $C_{122}(T)$ are independent of composition, they only depend on temperature, and are related with the third virial coefficient of a mixture by equation 2.9.

$$C(T,x) = x_1^3 \cdot C_{111}(T) + x_1^2 \cdot x_2 \cdot C_{112}(T) + x_1 \cdot x_2^2 \cdot C_{122}(T) + x_2^3 \cdot C_{222}(T) \qquad \textbf{Eq. 2.9.}$$

The values of $C_{112}(T)$ and $C_{122}(T)$ were estimated by solving equation 2.9 simultaneously for the three studied compositions and minimizing the difference between the value of $C(T,x)$ calculated from the virial fitting and calculated by equation 2.9 from estimated values of interaction coefficients. Table 6.10 shows the results .

Table 6.10. *Third interaction virial coefficients and expanded uncertainties (k = 2) for (CH_4 + He) binary mixtures.*

T/K	240	250	260	275	300	325	350	375	400
C_{112}/ cm^6·mol^{-2}	1983	1551	1610	1760	2105	2934	3920	4430	4713
C_{122}/ cm^6·mol^{-2}	1688	2833	2020	1510	1631	1167	1508	197	-97
$U(C_{ijk})$/ cm^6·mol^{-2}	183	183	183	185	179	178	566	708	714

Interaction virial coefficients of methane (B_{11} and C_{111}) and helium (B_{22} and C_{222}) were obtained from reference equations of state of methane [25] and helium [26] at corresponding temperatures by using REFPROP [9].

6.6. UNCERTAINTY ANALYSIS OF THE MEASUREMENTS

The uncertainties associated to the single-sinker densimeter were evaluated by Mondéjar [20] after carrying out some improvements on the single sinker densimeter. These values were recalculated considering the last calibrations of the auxiliary devices. The results have not differed from those estimated in the past by Mondéjar. Chapter 4 contains a detailed uncertainty analysis which is summarized below.

The pressure uncertainty depends on the pressure transducer used. The pressure expanded uncertainty (k = 2) in the range of (2 - 20) MPa were calculated by equation 4.9 and pressure expanded uncertainty in the range of (0 - 2) MPa were calculated by equation 4.10. In the working range of the densimeter, the expanded uncertainties in temperature and pressure were less than 4 mK than 0.005 MPa, respectively.

The expanded uncertainty in density (k = 2) can be expressed as a density function by equation 4.12.

$$U(\rho) = 2.31 \cdot 10^{-2} + 1.14 \cdot 10^{-4} \cdot \rho \qquad \textbf{Eq. 4.12.}$$

Temperature, pressure and composition uncertainties expressed in density contributions must be considered for the calculation of the overall uncertainty of the measurements $u_T(\rho)$ of density. As it is expressed in chapter 4.7, the overall composition was calculated according to two different methods related to the calculation of the uncertainty of the composition.

The first method considers only the uncertainty of the concentration of the components given from the gravimetric preparation of the mixture. The overall standard uncertainty (k = 1) is given by equation 4.13.

$$u_{T1}(\rho) = \left[u(\rho)^2 + \left(\left(\frac{\partial \rho}{\partial p} \right)_{T,x} u(p) \right)^2 + \left(\left(\frac{\partial \rho}{\partial T} \right)_{p,x} u(T) \right)^2 + \sum_i \left(\left(\frac{\partial \rho}{\partial x_i} \right)_{T,p,x_j \neq x_i} u(x_i) \right)^2 \right]^{0.5} \qquad \textbf{Eq. 4.13.}$$

The second method considers the unpredictable composition deviations that could occur inside the measuring cell, due to sorption effects or an uncomplete homogenization of the mixture during the filling process, and also the uncertainty of the concentration of the components given from the gravimetric preparation of the mixture. In this case, the uncertainty in density due to uncertainties in the composition is calculated from the uncertainty in the molar mass of the mixture. The standard overall uncertainty in density is given by equation 4.14.

$$u_{T2}(\rho) = \left[u(\rho)^2 + \left(\left(\frac{\partial \rho}{\partial p} \right)_T u(p) \right)^2 + \left(\left(\frac{\partial \rho}{\partial T} \right)_p u(T) \right)^2 + \left(\left(\frac{\partial \rho}{\partial M} \right)_{p,T} \cdot u(M) \right)^2 \right]^{0.5} \qquad \textbf{Eq. 4.14.}$$

Molar mass uncertainty

Unpredictable effects above mixture composition inside the measuring cell can be accounnted for by estimating the molar mass of the mixture inside the measuring cell through the virial analysis M_{virial}.

The combined uncertainty of the mixture composition was calculated by using equation 4.15, and considering all sources of uncertainty related to the molar mass of the mixture (see chapter 4.7): uncertainty due to the atomic weights, uncertainty related to the gravimetric composition of the mixture, and uncertainty associated to changes in the composition inside the measuring cell.

The estimation of the uncertainty of the molar mass of the mixture due to uncertainties in the atomic weights of the involved components of the mixture $u(M_{atomic})$ was obtained from the 2011 IUPAC report by Wieser et al. [21]. Table 6.11 shows the molar mass uncertainties of the methane and helium.

Table 6.11. *Molar mass of methane and helium* [21].

Substance	M_i /g·mol-1	$u(M_i)$ /g·mol-1	$u(M_i)/M_i$ /ppm
Methane	16.0428	0.00085	53
Helium	4.002602	0.000002	0.50

The uncertainty of the molar mass due to uncertainties in the gravimetric composition of the mixture $u(M_{grav})$ was calculated by equation 4.16 [22].

$$u(M_{grav}) = \left\{ \sum_{j=1}^{n} \left[\frac{\sum_{i=1}^{n} \frac{m_i}{M_i} - \left(\sum_{i=1}^{n} m_i \right) \Big/ M_j}{\left(\sum_{i=1}^{n} \frac{m_i}{M_i} \right)^2} \cdot u(m_j) \right]^2 \right\}^{0.5} \qquad \textbf{Eq. 4.16.}$$

Finally, the uncertainty associated to changes in the composition inside the measuring cell $u(M_{sorp})$ was calculated by using equation 4.17 from the molar mass value estimated by the virial fitting.

The molar mass uncertainties for the (CH_4 + He) mixtures are summarized in Table 6.12.

$$u\left(M_{sorp}\right)=\left[\frac{\sum_{i=1}^{N}\left(M_{grav,i}-M_{virial,i}\right)^2}{N}\right]^{0.5} \qquad \textbf{Eq. 4.17.}$$

Table 6.12. *Uncertainty budget of the composition associated to the molar mass of the (CH_4 + He) mixtures.*

Source of uncertainty	Units	Contribution		
		(0.95 CH_4 + 0.05 He)	(0.90 CH_4 + 0.10 He)	(0.50 CH_4 + 0.50 He)
$u\left(M_{atomic}\right)$ (Table 7.6) [21]	g·mol^{-1}	0.0008	0.0008	0.0008
$u\left(M_{grav}\right)$ (Eq. 4.16) [22]	g·mol^{-1}	0.00008	0.0001	0.0002
$u\left(M_{sorp}\right)$(Eq. 4.17)	g·mol^{-1}	0.0055	0.0053	0.006
Standard combined uncertainty (k = 1)		0.005	0.005	0.006
Expanded combined uncertainty (k = 2)		0.011	0.011	0.012

Overall uncertainty of the measurements

Tables 6.13, 6.14 and 6.15 show the estimated contributions to the expanded overall uncertainty (k = 2) of the experimental magnitudes involved in density determination for the (0.95 CH_4 + 0.05 He), (0.90 CH_4 + 0.10 He) and (0.50 CH_4 + 0.50 He) mixtures. The contribution of each mixture component is detailed from gravimetric composition.

Table 6.13. *Contributions to the expanded overall uncertainty in density (k = 2) for the (0.95 CH_4 + 0.05 He) mixture.*

Source of uncertainty	Units	Contribution (k = 2)	Estimation in density (k = 2)	
			kg·m^{-3}	%
Temperature	K	0.004	< 0.004	< 0.005
Pressure	MPa	0.005	< 0.064	(0.007 - 0.189)
Density	kg·m^{-3}	(0.024 - 0.045)	(0.024 - 0.048)	(0.022 - 0.512)
Gravimetric composition	mol·mol^{-1}	< 0.0001	< 0.039	< 0.024
Virial fitting composition	g·mol^{-1}	0.020	< 0.158	0.073
		$U_{T1}(\rho)$ gravimetric	(0.024 - 0.081)	(0.032 - 0.552)
		$U_{T2}(\rho)$ virial	(0.024 - 0.169)	(0.078 - 0.517)

Table 6.14. *Contributions to the expanded overall uncertainty in density (k = 2) for the (0.90 CH_4 + 0.10 He) mixture.*

Source of uncertainty	Units	Contribution (k = 2)	Estimation in density (k = 2)	
			kg·m^{-3}	%
Temperature	K	0.004	< 0.007	< 0.004
Pressure	MPa	0.005	< 0.055	(0.007 - 0.189)
Density	kg·m^{-3}	(0.024 - 0.045)	(0.024 - 0.045)	(0.007 - 0.316)
Gravimetric composition	mol·mol^{-1}	< 0.0001	< 0.031	< 0.020
Virial fitting composition	g·mol^{-1}	0.010	< 0.141	0.073
		$U_{T1}(\rho)$ gravimetric	(0.024 - 0.072)	(0.034 - 0.565)
		$U_{T2}(\rho)$ virial	(0.024 - 0.153)	(0.079 - 0.537)

Table 6.15. *Contributions to the expanded overall uncertainty in density (k = 2) for the (0.50 CH_4 + 0.50 He) mixture.*

Source of uncertainty	Units	Contribution (k = 2)	Estimation in density (k = 2)	
			kg·m^{-3}	%
Temperature	K	0.004	< 0.002	0.002
Pressure	MPa	0.005	< 0.023	(0.007 - 0.185)
Density	kg·m^{-3}	(0.024 - 0.033)	(0.024 - 0.033)	(0.038 - 0.764)
Gravimetric composition	mol·mol^{-1}	< 0.00006	< 0.012	< 0.014
Virial fitting composition	g·mol^{-1}	0.012	< 0.106	0.119
		$U_{T1}(\rho)$ gravimetric	(0.024 - 0.042)	(0.047 - 0.795)
		$U_{T2}(\rho)$ virial	(0.024 - 0.113)	(0.127 - 0.803)

6.7. DISCUSSION

Relative deviation of the experimental data from the reference equations of state

Figures 6.5 y 6.6 show the relative deviations of the (0.95 CH_4 + 0.05 He) mixture from the values estimated with the GERG-2008 and AGA8-DC92 equations of state, respectively. Figures 6.7 and 6.8 show the relative deviations for the (0.90 CH_4 + 0.10 He) mixture and Figures 6.9 and 6.10 for the (0.50 CH_4 + 0.50 He) mixture.

As it can be observed, the relative deviations of the experimental data from the GERG-2008 are clearly higher than relative deviations from AGA8-DC92.

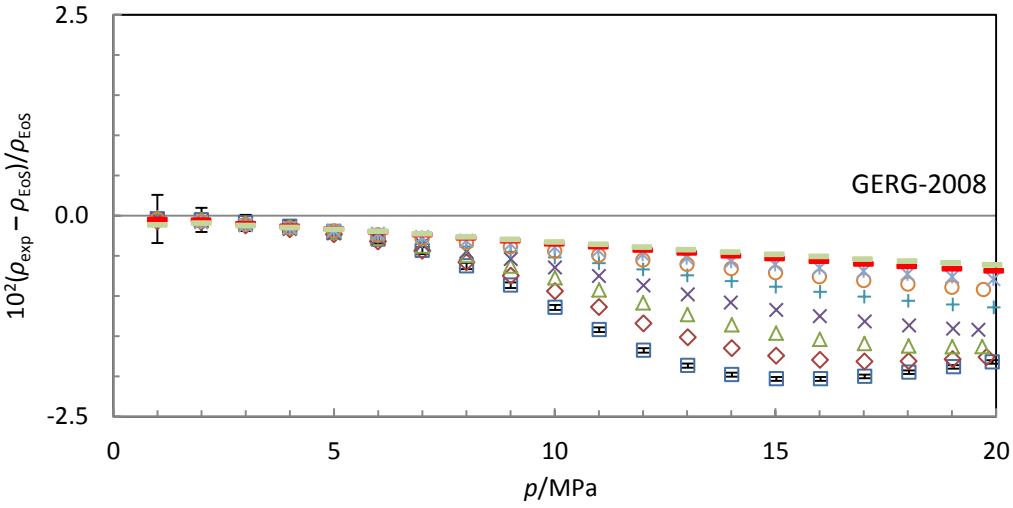

Figure 6.5. *Relative deviations in density of experimental (p, ρ, T) data of the (0.95 CH_4 + 0.05 He) mixture ρ_{exp} from density values calculated from the GERG-2008 equation of state ρ_{EoS} versus pressure: □ 240 K; ◇ 250 K; △ 260 K; × 275 K; + 300 K; ○ 325 K; ✳ 350 K; – 375 K; – 400 K. Error bars on the 240 K isotherm indicate the expanded uncertainty (k = 2) of the experimental data.*

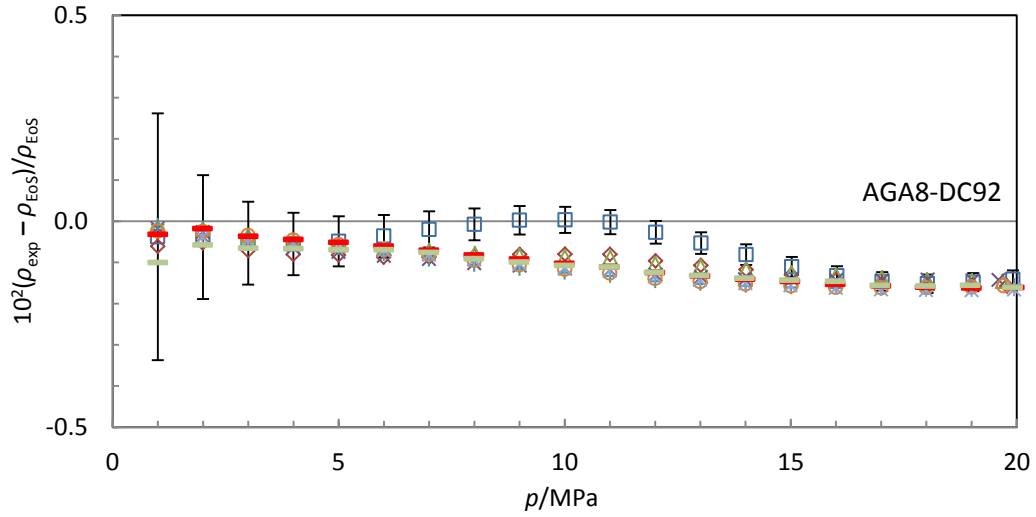

Figure 6.6. *Relative deviations in density of experimental (p, ρ, T) data of the (0.95 CH_4 + 0.05 He) mixture ρ_{exp} from density values calculated from the* AGA8-DC92 *equation of state ρ_{EoS} versus pressure*: □ *240 K; ◇ 250 K; △ 260 K; × 275 K; + 300 K; ○ 325 K; ✳ 350 K; – 375 K; – 400 K. Error bars on the 240 K isotherm indicate the expanded uncertainty (k = 2) of the experimental data.*

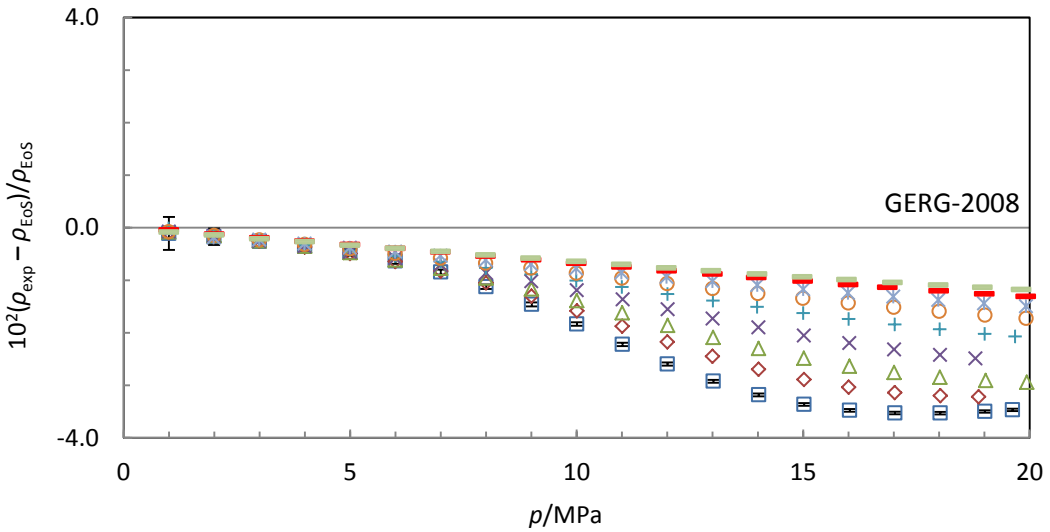

Figure 6.7. *Relative deviations in density of experimental (p, ρ, T) data of the (0.90 CH_4 + 0.10 He) mixture ρ_{exp} from density values calculated from the GERG-2008 equation of state ρ_{EoS} versus pressure: □ 240 K; ◇ 250 K; △ 260 K; × 275 K; + 300 K; ○ 325 K; ✳ 350 K; – 375 K; – 400 K. Error bars on the 240 K isotherm indicate the expanded uncertainty (k = 2) of the experimental data.*

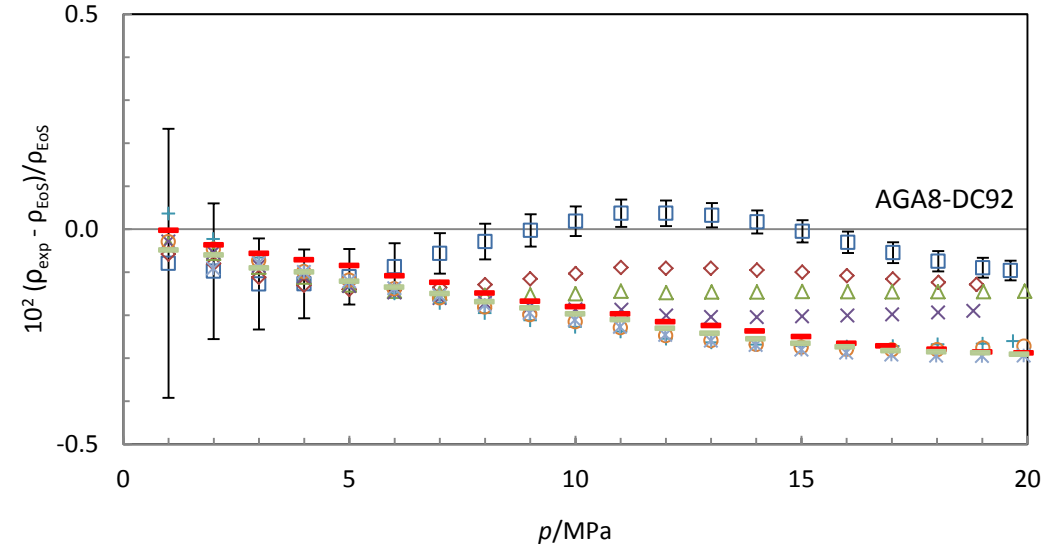

Figure 6.8. *Relative deviations in density of experimental (p, ρ, T) data of the (0.90 CH_4 + 0.10 He) mixture ρ_{exp} from density values calculated from the* AGA8-DC92 *equation of state ρ_{EoS} versus pressure*: □ *240 K; ◇ 250 K; △ 260 K; × 275 K; + 300 K; ○ 325 K; ✳ 350 K; – 375 K; – 400 K. Error bars on the 240 K isotherm indicate the expanded uncertainty (k = 2) of the experimental data.*

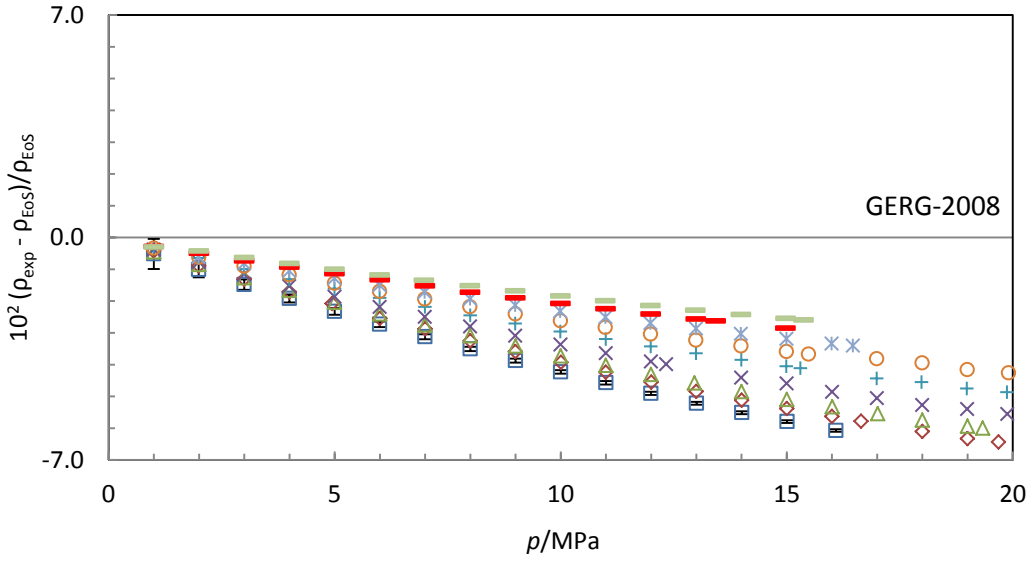

Figure 6.9. *Relative deviations in density of experimental (p, ρ, T) data of the (0.50 CH_4 + 0.50 He) mixture ρ_{exp} from density values calculated from the GERG-2008 equation of state ρ_{EoS} versus pressure: □ 240 K; ◇ 250 K; △ 260 K; × 275 K; + 300 K; ○ 325 K; ✳ 350 K; – 375 K; – 400 K. Error bars on the 240 K isotherm indicate the expanded uncertainty (k = 2) of the experimental data.*

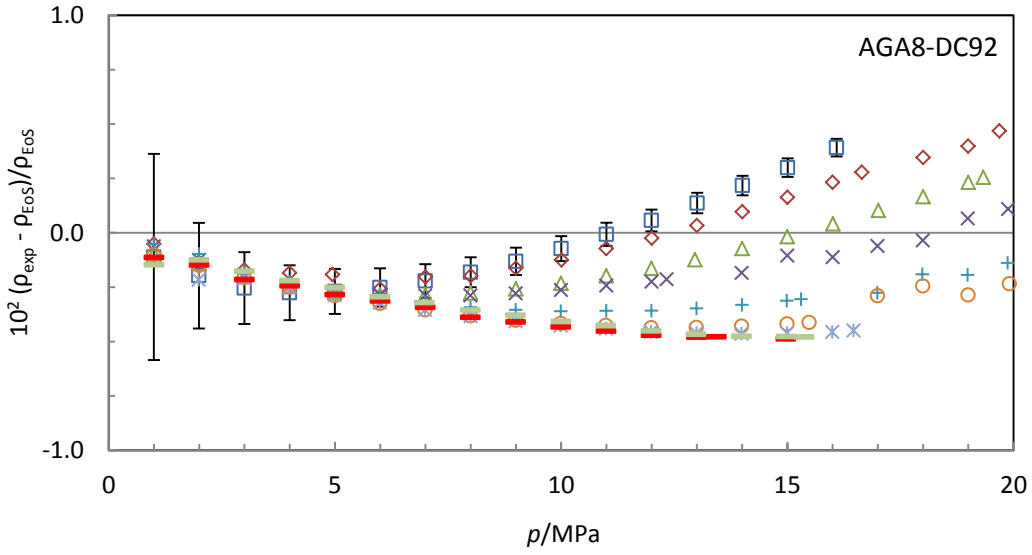

Figure 6.10. *Relative deviations in density of experimental (p, ρ, T) data of the (0.50 CH_4 + 0.50 He) mixture ρ_{exp} from density values calculated from the* AGA8-DC92 *equation of state ρ_{EoS} versus pressure*: □ *240 K; ◇ 250 K; △ 260 K; × 275 K; + 300 K; ○ 325 K; ✳ 350 K; – 375 K; – 400 K. Error bars on the 240 K isotherm indicate the expanded uncertainty (k = 2) of the experimental data.*

The relative deviations of experimental density data from the GERG-2008 equation of state are as large as –2 %, for the (0.95 CH_4 + 0.05 He) mixture. These deviations are higher at high pressures and low temperatures. The highest deviations were registered at 240 K and pressures around 15 MPa. In contrast, the highest relative deviation from the AGA8-DC92 is –0.2 % and relative deviations are lower at low temperatures.

For the (0.90 CH_4 + 0.10 He) mixture, relative deviations exceeded –3 % from the values estimated by the GERG-2008. The largest deviation was registered at 240 K and 17 MPa. In contrast to the GERG-2008, relative deviations from AGA8-DC92 exceeded –0.2 %, but they are lower at low temperatures. In fact, all data of the isotherms at (240 and 250) K are within the uncertainty of the AGA8-DC92 in the working range (0.1 %).

For the (0.50 CH_4 + 0.50 He) mixture, relative deviations from the GERG-2008 have maximum values close to –6.5 % at low temperatures and high pressures. Deviations from the AGA8-DC92 are, in this case, positive at high pressures and low temperatures and negative at high temperatures. The largest deviation is around 0.5 %.

A statistical comparison of the deviation data from GERG-2008 and AGA8-DC92 equations of state is given in Table 6.16. *AAD* is the average absolute deviation defined in equation 3.22, *Bias* is the average deviation defined in equation 3.23, *RMS* refers to the root mean squared defined in equation 3.24, and *MaxD* represents the maximum relative deviation in the considered data set.

Table 6.16. *Statistical parameters of the data set with respect to the GERG-2008 and AGA8-DC92 equations of state for the (CH_4 + He) mixtures.*

Statistical parameter	(0.95 CH_4 + 0.05 He)		(0.90 CH_4 + 0.10 He)		(0.50 CH_4 + 0.50 He)	
	GERG-2008	AGA8-DC92	GERG-2008	AGA8-DC92	GERG-2008	AGA8-DC92
AAD	0.655	0.101	1.170	0.159	2.849	0.262
Bias	–0.655	–0.101	–1.170	–0.157	-2.849	-0.212
RMS	0.853	0.111	1.483	0.178	3.277	0.291
MaxD/%	–2.031	–0.167	–3.529	–0.295	-6.439	-0.488

According to these data, the relative deviation of experimental density data from values calculated from both equations of state increases with the helium content of the mixture,

especially for deviations from the GERG-2008. The *AAD* from the GERG-2008 is 0.655 for the (0.95 CH_4 + 0.05 He) mixture, 1.170, almost double, for the (0.90 CH_4 + 0.10 He) and 2.849, four times greater, for the (0.50 CH_4 + 0.50 He) mixture.

The high deviation of the density data from the GERG-2008 agrees the claimed uncertainty of the equation of state. Formally, the GERG-2008 allows the estimation of thermophysical properties of any mixture consisting of an arbitrary combination of the 21 considered components in wide ranges of temperature and pressure. According to Kunz and Wagner, the uncertainty of GERG-2008 in density in the gas-phase is 0.1 % over the temperature range from (250 to 450) K at pressures up to 35 MPa [2]. This estimated uncertainty is valid for various types of natural gases, including natural gases rich in nitrogen, carbon dioxide or with considerable amounts of heavier hydrocarbons, carbon monoxide or oxygen. However, there are some mixtures of these 21 components which composition is considerably far from the standard composition of natural gas in any of the existing applications of this fuel composition. According to the GERG-2004 monograph, the usual amount of helium in natural gases is less than 0.1 mol-% [23].

The mixture models developed for the formulation of the GERG-2008 (described in chapter 2.4) are based in the Helmholtz free energy, expressed in its dimensionless form $a(\delta, \tau, \bar{x})$ which is not accessible through experimental measurements. The Helmholtz free energy is divided in two terms: the ideal behavior term and the residual term. When the critical parameters of any binary mixture are very asymmetric, the mixture has a behavior far from ideality. The difference between the critical temperatures of the pure components of a binary mixture can be used as a simplified indication of the extent of the real mixture behavior. When the critical temperatures of the components of a binary mixture differ by more than 150 K, uncertainties up to 1 % may exist [2]. This is the case of the (CH_4 + He) mixture.

The mixture model of the GERG-2008 does not have any (specific or generalized) departure function for the (CH_4 + He) mixture and, being a mixture with a strongly real behavior, the high deviations of the experimental density from the GERG-2008 can be associated to that.

Therefore, the thermodynamic behavior of the studied mixtures is agreed with the statements of the GERG-2008 equation of state.

In contrast, the deviation from AGA8-DC92 is distinctly lower. The AGA8-DC92 equation of state is written in terms of the compressibility factor [1] and it is dependent of

temperature, density and composition. However, the formulation does not depend on the critical parameters. This fact can explain why the AGA8-DC92 equation of state fits better than GERG-2008 to asymmetric mixtures with far compositions from the typical composition of natural gases like the studied (CH_4 + He) binary mixtures.

Virial fitting of experimental data

When the pressure trends to zero, all gases have ideal gas behavior, so that the compressibility factor is Z = 1. Thus, the deviation of experimental density data from equations of state, represented in Figures 6.5 to 6.10, must tend to zero when pressure is closed to zero. An opposite behavior indicates a possible error in the experimental data. A coherent interpretation of this kind of deviations is that the composition could change inside the measuring cell due to sorption effects, gas stratification or a poor homogenization of the mixture.

The estimated values of the relative deviation of density when the pressure is close to zero are shown in Table 6.17. They were calculated from the intersection with y-axis by using a polynomial of degree 2, 3 or 4, depending on reaching an acceptable value for R^2.

Table 6.17. *Estimated deviations of the experimental densities from the GERG-2008 equation of state when pressure is zero.*

Isotherm	(0.95 CH_4 + 0.05 He)		(0.90 CH_4 + 0.10 He)		(0.50 CH_4 + 0.50 He)	
	$10^2(\rho_{exp}-\rho_{EoS})/\rho_{EoS}$	R^2	$10^2(\rho_{exp}-\rho_{EoS})/\rho_{EoS}$	R^2	$10^2(\rho_{exp}-\rho_{EoS})/\rho_{EoS}$	R^2
240 K	0.1299	0.9994	0.1449	0.9999	–0.0580	1
250 K	0.0385	0.9998	–0.0932	0.9996	0.0124	1
260 K	0.0472	0.9999	–0.0617	0.9997	–0.0182	1
275 K	–0.0178	0.9998	–0.0803	0.9996	–0.0226	0.9999
300 K	–0.0160	0.9998	0.0385	0.9998	0.0111	0.9999
325 K	–0.0239	0.9981	–0.0430	0.9990	–0.0226	0.9997
350 K	–0.0095	0.9990	–0.0084	0.9990	–0.0984	0.9999
375 K	–0.0173	0.9997	–0.0318	0.9998	–0.0582	0.9999
400 K	–0.0890	0.9983	–0.0090	0.9997	–0.0681	0.9997

As it can be observed, the deviations are below 0.1 % (uncertainty of the GERG-2008), except at 240 K for the (0.95 CH_4 + 0.05 He) and (0.90 CH_4 + 0.10 He) mixtures. This means that the gravimetric composition of the mixture agrees with the composition inside the measuring cell. Therefore, there is no evidence of sorption effects or an incomplete homogenization of the mixture in the filling or evacuation processes. The estimated values for molar mass from the virial fitting, M_{virial}, confirm this. The differences between M_{virial} and the gravimetric molar mass are within the estimated uncertainty of M_{virial}. However, the composition of the mixture was recalculated from the value of M_{virial}. The results are shown in Table 6.8 and the maximum difference with the gravimetric composition was 0.001 %, which is within the uncertainty of the composition (Table 6.1).

Due to these small differences, the contribution of the expanded uncertainty in composition to the overall uncertainty of the measurements considering the value of molar mass from the virial fitting is approximately 25 % greater than the overall uncertainty from gravimetric composition. This can be checked in Tables 6.13 to 6.15.

Regarding the estimation of the virial coefficients, as it can be observed in Tables 6.5, 6.6 and 6.7, the values estimated from virial fitting (B_{virial} and C_{virial}) and values from the GERG-2008 (B_{GERG} and C_{GERG}) has larger differences than expected, considering the small differences between virial and gravimetric molar masses. Figures 6.11, 6.12 and 6.13 show the variation of the second and the third virial coefficients with temperature in the studied mixtures. Virial coefficients calculated from gravimetric molar mass values by least mean square are also shown (B_{grav} and C_{grav}).

Virial coefficients estimated from experimental data and virial coefficients calculated from the GERG-2008 are close for the (0.95 CH_4 + 0.05 He) mixture, but their differences are larger than the estimated uncertainty values. The same thing occurs with the values for B_{grav} and C_{grav}. For the other mixtures, it can be observed that when the helium content is higher, the differences between virial coefficients from experimental data and from the GERG-2008 are higher too, especially at high temperatures. In the (0.50 CH_4 + 0.50 He) the difference between B_{vir} and B_{GERG} is almost constant with temperature, however, the difference between C_{vir} and C_{GERG} increases with temperature. Finally, C_{vir} and C_{grav} present a peak at 350 K and 325 K, respectively, in contrast with the third virial coefficient estimated for the other mixtures, which decreases with temperature.

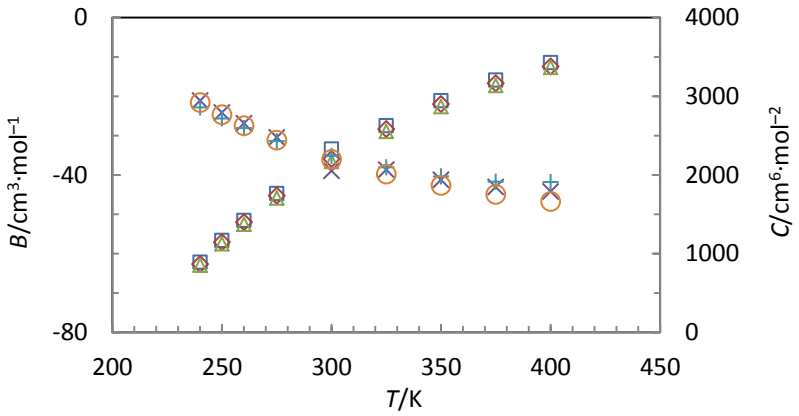

Figure 6.11. *Variation of the calculated virial coefficients with temperature for the (0.95 CH_4 + 0.05 He) mixture. □ B_{grav}; ◇ B_{virial}; △ B_{GERG}; × C_{grav}; + C_{virial}; ○ C_{GERG}.*

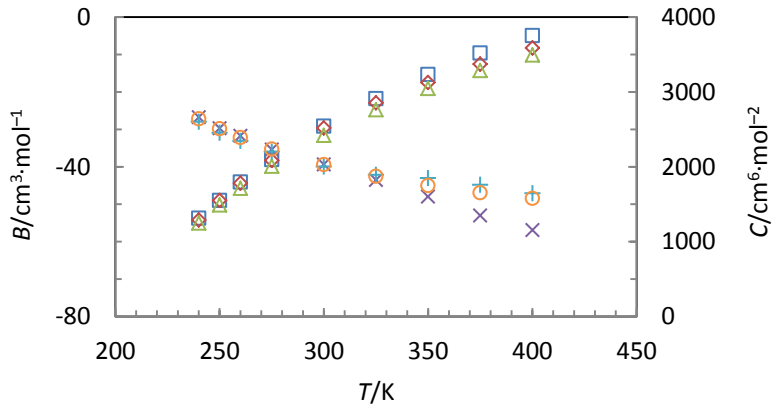

Figure 6.12 *Variation of the calculated virial coefficients with temperature for the (0.90 CH_4 + 0.10 He) mixture. □ B_{grav}; ◇ B_{virial}; △ B_{GERG}; × C_{grav}; + C_{virial}; ○ C_{GERG}.*

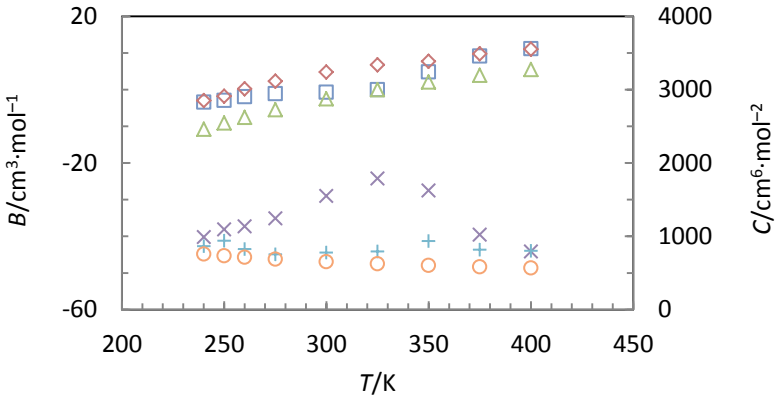

Figure 6.13. *Variation of the calculated virial coefficients with temperature for the (0.50 CH_4 + 0.50 He) mixture. □ B_{grav}; ◇ B_{virial}; △ B_{GERG}; × C_{grav}; + C_{virial}; ○ C_{GERG}.*

Analysis of the interaction virial coefficients

The interaction virial coefficient is independent of composition, so B_{12} only depends on temperature. The estimated values of B_{12} from the experimental data are agreed with that, however vsalues calculated from the GERG-2008 show dependence of composition, as it can be observed in Figure 6.14.

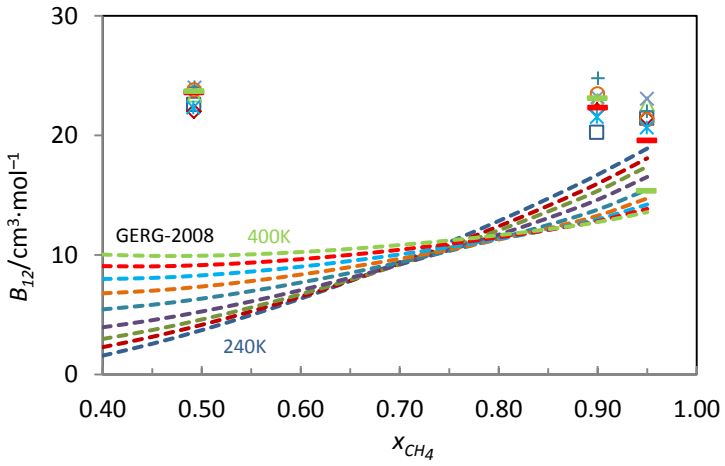

Figure 6.14. *Second interaction virial coefficient for the (CH_4 + He) mixture estimated from the experimental data. □ 240 K; ◇ 250 K; △ 260 K; × 275 K; + 300 K; ○ 325 K; ✳ 350 K; – 375 K; – 400 K. The dash lines represent the B_{12} values estimated from the GERG-2008 at different temperatures.*

The calculated values for B_{12} at different compositions and at the same temperature are within the estimated expanded uncertainty on the isotherms of (240 to 275) K and 350 K. It must be considered that B_{12} was calculated by using the average temperature values because the same isotherm can be a little bit different in each measured mixture. Therefore, the differences in B_{12} at the same temperature can be due to that.

Table 6.18 shows the standard deviation of the experimental data of B_{12}, the average temperatures used in each isotherm and the highest difference between the temperatures of the same isotherm. In most cases, the isotherms with higher difference between the average temperatures used to the virial coefficient estimation have associated higher standard deviations of B_{12}. However, the differences registered at (375 and 400) K are higher than expected.

Table 6.18. *Average temperatures of the isotherms and standard deviation of* B_{12}.

$T_{average}$/K (0.95 CH_4 + 0.05 He)	$T_{average}$/K (0.90 CH_4 + 0.10 He)	$T_{average}$/K (0.50 CH_4 + 0.50 He)	ΔT_{max}/K	Standard deviation B_{12}/cm^3·mol^{-1}
240.047	240.045	240.032	0.013	1.16
249.996	250.005	249.998	0.009	0.36
260.005	260.013	259.991	0.022	0.40
275.002	274.994	275.007	0.013	0.50
299.958	299.951	299.922	0.029	1.43
324.955	324.958	324.970	0.012	1.36
349.938	349.939	349.914	0.025	0.83
374.924	374.923	374.906	0.017	2.06
399.997	400.006	399.990	0.016	4.65

Figure 6.15 compares the calculated results of B_{12} with values reported by Bignell et al. [24] for the system (CH_4 + He) at temperatures between (290 and 310) K. As it can be observed, the results of this work agree those of Bignell et al.

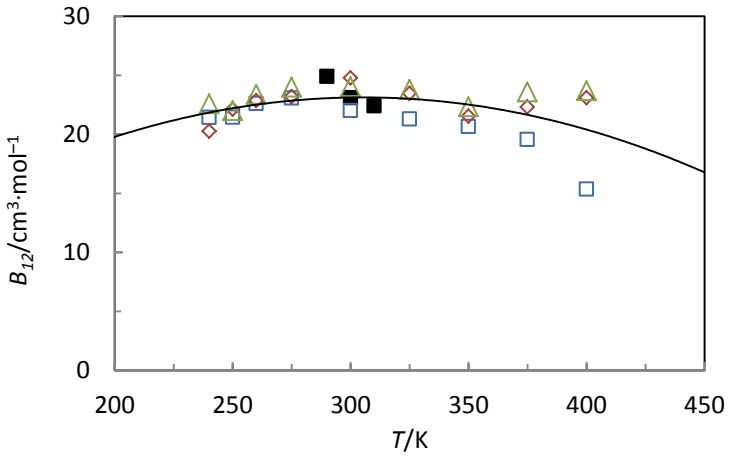

Figure 6.15. *Second interaction virial coefficient for the (CH_4 + He) binary mixture.* □ *(0.95 CH_4 + 0.05 He);* ◇ *(0.90 CH_4 + 0.10He);* △ *(0.50 CH_4 + 0.50 He). The solid line represents the polynomial of degree 2 fitted to experimental data of this work.* $B_{12}(T)/cm^3 \cdot mol^{-1} = -3 \cdot 10^{-4} \cdot T^2 + 0.1847 \cdot T - 5.0431$. ■ *Bignell et al* [24].

Figure 6.16 shows the values estimated for the third interaction virial coefficients C_{112} and C_{122}. Data to compare the results did not find in the literature.

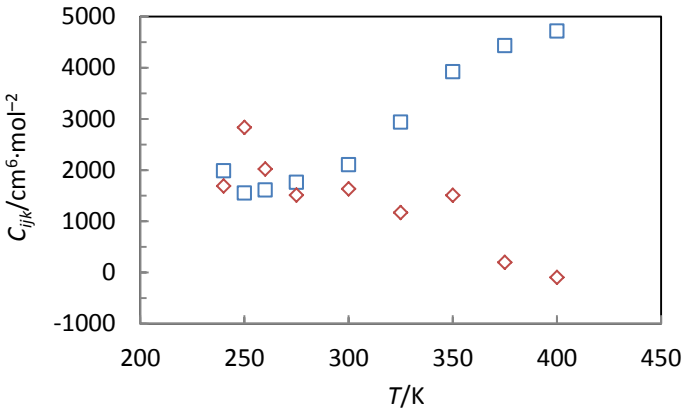

Figure 6.16. *Variation of the third interaction virial coefficients with temperature for the (CH_4 + He) binary mixture.* □ C_{112}; ◇ C_{122}.

Stability of the studied (CH_4 + He) mixtures

Due to the delay in the measurement of the density as a consequence of the failure of the AC comparator resistance bridge and the installation of the new ultra-low refrigerated-heating circulator, the experimental density values for the (0.95 CH_4 + 0.05 He) and (0.90 CH_4 + 0.10 He) mixtures were validated by calculating the compatibility index I given by equation 6.2.

$$I = \frac{x_1 - x_2}{\sqrt{U(x_1)^2 + U(x_2)^2}} \qquad \textbf{Eq. 6.2.}$$

where x_i is the property to compare, in this case the relative deviation of experimental density from density calculated by the GERG-2008, and $U(x_i)$ is their relative overall expanded uncertainty. Data are considered compatibles if $I < 1$. This condition was fulfilled for all measured points. The average values were $I = 0.222$ for the (0.95 CH_4 + 0.05 He) mixture and $I = 0.121$ for the (0.90 CH_4 + 0.10 He) mixture.

These results show the compatibility of experimental density data and also the correct work of the densimeter and the good stability of the (CH_4 + He) mixtures prepared by the gravimetric method.

6.8. TABLE OF RESULTS

Table 6.19. *Experimental (p, ρ, T) measurements for the (0.95 CH_4 + 0.05 He), mixture, relative and absolute expanded uncertainty in density (k = 2) U(ρ_{exp}), expanded overall uncertainty in density (k = 2) from gravimetric composition $U_{T1}(\rho_{exp})$ and from virial expansion $U_{T2}(\rho_{exp})$ and relative deviations from the GERG-2008 and AGA8-DC92 equations of state; where T is the temperature (ITS-90* [25]*), p the pressure, ρ_{exp} the experimental density and ρ_{EoS} the density calculated from both equations of state.*

T/K	*p*/MPa	ρ_{exp}/ kg·m^{-3}	$U(\rho_{exp})$ kg·m^{-3}	$U(\rho_{exp})$ %	$U_{T1}(\rho_{exp})$ kg·m^{-3}	$U_{T2}(\rho_{exp})$ (kg·m^{-3})	$10^2(\rho_{exp}-\rho_{EoS})/\rho_{EoS}$	
							GERG-2008	AGA8-DC92
240.045	19.915	217.591	0.047	0.022	0.032	0.078	–1.820	–0.141
240.046	19.037	211.432	0.046	0.022	0.033	0.078	–1.882	–0.148
240.047	18.026	203.713	0.045	0.022	0.035	0.079	–1.948	–0.152
240.047	17.023	195.305	0.044	0.023	0.038	0.079	–1.999	–0.146
240.047	16.022	186.059	0.043	0.023	0.041	0.081	–2.031	–0.132
240.047	15.023	175.881	0.042	0.024	0.044	0.082	–2.030	–0.111
240.047	14.013	164.584	0.041	0.025	0.048	0.084	–1.979	–0.081
240.048	13.016	152.406	0.040	0.026	0.053	0.087	–1.865	–0.053
240.047	12.015	139.257	0.038	0.028	0.059	0.090	–1.676	–0.027
240.049	11.009	125.326	0.037	0.029	0.064	0.094	–1.418	–0.002
240.047	10.010	111.115	0.035	0.032	0.069	0.098	–1.142	0.003
240.045	9.003	96.823	0.034	0.035	0.075	0.102	–0.865	0.002
240.045	8.003	83.039	0.032	0.039	0.081	0.107	–0.626	–0.007
240.046	7.001	69.896	0.031	0.044	0.089	0.113	–0.433	–0.020
240.046	6.000	57.586	0.029	0.051	0.099	0.122	–0.294	–0.036
240.047	4.999	46.133	0.028	0.061	0.113	0.134	–0.198	–0.049
240.047	3.998	35.506	0.027	0.076	0.135	0.153	–0.134	–0.055
240.047	2.998	25.657	0.026	0.101	0.172	0.187	–0.090	–0.053
240.048	1.998	16.504	0.025	0.150	0.153	0.169	–0.053	–0.039
240.046	0.998	7.970	0.024	0.300	0.304	0.312	–0.041	–0.038
250.000	19.784	200.072	0.045	0.022	0.034	0.078	–1.762	–0.157
249.997	19.016	194.396	0.044	0.023	0.035	0.079	–1.787	–0.158
249.995	18.017	186.477	0.044	0.023	0.037	0.080	–1.810	–0.157
249.995	17.019	177.898	0.043	0.024	0.040	0.081	–1.815	–0.151
249.996	16.011	168.529	0.042	0.025	0.043	0.082	–1.795	–0.141
249.994	15.017	158.560	0.040	0.026	0.046	0.083	–1.743	–0.130
249.994	14.013	147.789	0.039	0.027	0.050	0.085	–1.649	–0.118
249.993	13.013	136.403	0.038	0.028	0.054	0.088	–1.514	–0.107

249.994	12.011	124.468	0.037	0.029	0.058	0.090	–1.342	–0.096
249.991	11.003	112.149	0.035	0.032	0.062	0.094	–1.137	–0.080
249.992	10.007	99.845	0.034	0.034	0.067	0.097	–0.940	–0.080
249.993	9.004	87.584	0.033	0.037	0.073	0.101	–0.748	–0.080
249.992	8.002	75.669	0.031	0.041	0.079	0.106	–0.579	–0.085
249.992	7.000	64.219	0.030	0.047	0.087	0.112	–0.436	–0.087
249.989	5.997	53.324	0.029	0.054	0.098	0.121	–0.321	–0.087
249.999	4.998	43.065	0.028	0.064	0.113	0.133	–0.231	–0.082
250.000	3.997	33.379	0.027	0.080	0.135	0.153	–0.171	–0.081
250.001	2.997	24.270	0.026	0.106	0.108	0.188	–0.122	–0.071
250.002	1.992	15.655	0.025	0.158	0.161	0.176	–0.078	–0.053
250.001	0.998	7.617	0.024	0.313	0.487	0.325	–0.070	–0.061
260.005	19.685	184.360	0.043	0.023	0.035	0.079	–1.630	–0.146
260.007	19.008	179.270	0.043	0.024	0.037	0.080	–1.631	–0.144
260.006	18.018	171.413	0.042	0.024	0.039	0.080	–1.622	–0.142
260.005	17.017	162.926	0.041	0.025	0.041	0.082	–1.593	–0.137
260.006	16.008	153.819	0.040	0.026	0.044	0.083	–1.540	–0.131
260.006	15.015	144.337	0.039	0.027	0.047	0.084	–1.463	–0.125
260.006	14.014	134.298	0.038	0.028	0.050	0.086	–1.359	–0.118
260.006	13.009	123.820	0.037	0.030	0.053	0.088	–1.231	–0.110
260.006	12.003	113.023	0.035	0.031	0.057	0.091	–1.085	–0.103
260.008	11.008	102.188	0.034	0.034	0.061	0.093	–0.924	–0.088
260.005	10.005	91.250	0.033	0.036	0.066	0.097	–0.773	–0.086
260.006	9.000	80.421	0.032	0.040	0.071	0.101	–0.628	–0.083
260.004	8.013	70.021	0.031	0.044	0.078	0.105	–0.496	–0.078
260.005	7.006	59.750	0.030	0.049	0.086	0.112	–0.378	–0.071
260.004	6.004	49.933	0.028	0.057	0.097	0.121	–0.284	–0.066
260.004	4.999	40.507	0.027	0.068	0.113	0.134	–0.207	–0.058
260.005	3.997	31.566	0.026	0.084	0.136	0.154	–0.147	–0.049
260.005	2.998	23.076	0.026	0.111	0.113	0.190	–0.096	–0.035
260.005	1.997	14.985	0.025	0.164	0.167	0.182	–0.053	–0.019
260.005	0.997	7.297	0.024	0.326	0.495	0.338	–0.029	–0.015
275.006	19.598	164.546	0.041	0.025	0.037	0.080	–1.420	–0.142
275.009	19.027	160.360	0.041	0.025	0.038	0.081	–1.406	–0.144
275.010	18.027	152.751	0.040	0.026	0.040	0.081	–1.366	–0.142
275.008	17.024	144.735	0.039	0.027	0.042	0.083	–1.317	–0.143
275.008	16.005	136.235	0.038	0.028	0.045	0.084	–1.251	–0.143
275.008	15.019	127.693	0.037	0.029	0.047	0.085	–1.173	–0.141

275.000	13.990	118.505	0.036	0.030	0.050	0.087	–1.081	–0.141
275.000	13.015	109.579	0.035	0.032	0.053	0.089	–0.979	–0.135
275.000	12.010	100.248	0.034	0.034	0.057	0.091	–0.870	–0.130
275.000	11.003	90.832	0.033	0.036	0.061	0.093	–0.752	–0.118
275.000	10.007	81.538	0.032	0.039	0.065	0.097	–0.645	–0.115
275.001	9.005	72.274	0.031	0.043	0.071	0.100	–0.541	–0.108
275.001	7.999	63.141	0.030	0.047	0.078	0.105	–0.446	–0.102
275.001	6.999	54.270	0.029	0.053	0.086	0.112	–0.359	–0.092
275.001	5.998	45.638	0.028	0.061	0.098	0.121	–0.285	–0.084
275.001	4.999	37.306	0.027	0.073	0.114	0.135	–0.222	–0.074
274.998	3.998	29.247	0.026	0.090	0.138	0.156	–0.168	–0.064
274.997	2.997	21.492	0.025	0.118	0.120	0.193	–0.118	–0.048
274.997	1.997	14.036	0.025	0.175	0.178	0.192	–0.068	–0.026
274.995	0.997	6.868	0.024	0.346	0.507	0.358	–0.036	–0.017
299.958	19.947	142.569	0.039	0.027	0.039	0.081	–1.142	–0.154
299.957	19.019	136.456	0.038	0.028	0.040	0.082	–1.106	–0.158
299.958	18.012	129.617	0.037	0.029	0.042	0.083	–1.060	–0.161
299.958	17.014	122.639	0.036	0.030	0.044	0.084	–1.008	–0.163
299.958	16.012	115.449	0.036	0.031	0.046	0.085	–0.949	–0.162
299.957	15.009	108.100	0.035	0.032	0.048	0.086	–0.885	–0.161
299.958	14.009	100.634	0.034	0.034	0.051	0.088	–0.816	–0.157
299.959	13.003	93.029	0.033	0.036	0.054	0.089	–0.744	–0.153
299.960	12.004	85.416	0.032	0.038	0.057	0.092	–0.671	–0.146
299.960	11.004	77.780	0.032	0.041	0.061	0.094	–0.592	–0.133
299.958	10.001	70.115	0.031	0.044	0.066	0.097	–0.520	–0.125
299.959	9.001	62.524	0.030	0.048	0.072	0.101	–0.451	–0.116
299.960	8.000	55.004	0.029	0.053	0.079	0.107	–0.385	–0.106
299.957	6.998	47.579	0.028	0.059	0.088	0.113	–0.323	–0.094
299.956	5.998	40.294	0.027	0.068	0.100	0.123	–0.263	–0.080
299.956	5.008	33.227	0.027	0.080	0.117	0.137	–0.209	–0.065
299.955	4.021	26.333	0.026	0.098	0.142	0.159	–0.161	–0.052
299.956	2.999	19.372	0.025	0.130	0.132	0.199	–0.115	–0.038
299.957	2.002	12.753	0.024	0.191	0.194	0.280	–0.062	–0.014
299.957	0.997	6.264	0.024	0.378	0.529	0.389	–0.030	–0.008
324.954	19.715	123.531	0.037	0.030	0.040	0.079	–0.920	–0.157
324.954	19.000	119.317	0.036	0.030	0.042	0.083	–0.894	–0.160
324.955	18.002	113.320	0.035	0.031	0.043	0.084	–0.853	–0.161
324.955	17.003	107.193	0.035	0.032	0.045	0.085	–0.809	–0.162

324.956	15.998	100.920	0.034	0.034	0.047	0.086	–0.762	–0.161
324.956	15.005	94.630	0.033	0.035	0.049	0.087	–0.712	–0.157
324.956	14.000	88.182	0.033	0.037	0.052	0.089	–0.660	–0.153
324.956	12.999	81.698	0.032	0.039	0.055	0.090	–0.607	–0.147
324.955	12.000	75.193	0.031	0.042	0.059	0.093	–0.553	–0.139
324.956	10.998	68.639	0.031	0.045	0.063	0.095	–0.494	–0.126
324.955	10.002	62.122	0.030	0.048	0.068	0.099	–0.442	–0.117
324.954	8.999	55.577	0.029	0.052	0.073	0.103	–0.389	–0.106
324.955	8.000	49.095	0.028	0.058	0.081	0.108	–0.338	–0.095
324.954	6.996	42.630	0.028	0.065	0.090	0.116	–0.286	–0.081
324.955	5.997	36.261	0.027	0.074	0.103	0.126	–0.239	–0.069
324.955	4.997	29.964	0.026	0.088	0.121	0.141	–0.193	–0.056
324.955	3.996	23.752	0.026	0.108	0.148	0.165	–0.150	–0.046
324.956	2.997	17.648	0.025	0.141	0.144	0.206	–0.110	–0.034
324.956	1.991	11.608	0.024	0.209	0.212	0.224	–0.073	–0.025
324.955	0.997	5.755	0.024	0.411	0.552	0.422	–0.046	–0.024
349.937	19.941	111.598	0.035	0.032	0.042	0.083	–0.791	–0.166
349.937	19.004	106.652	0.035	0.033	0.043	0.084	–0.762	–0.167
349.937	17.994	101.235	0.034	0.034	0.045	0.085	–0.727	–0.167
349.939	16.998	95.804	0.034	0.035	0.047	0.086	–0.690	–0.165
349.938	15.998	90.270	0.033	0.036	0.049	0.087	–0.651	–0.162
349.939	14.995	84.662	0.032	0.038	0.051	0.088	–0.610	–0.156
349.939	13.996	79.008	0.032	0.040	0.054	0.090	–0.569	–0.151
349.939	12.990	73.276	0.031	0.042	0.057	0.092	–0.525	–0.142
349.939	11.994	67.563	0.030	0.045	0.060	0.094	–0.483	–0.134
349.938	10.993	61.799	0.030	0.048	0.065	0.097	–0.435	–0.120
349.938	9.999	56.060	0.029	0.052	0.070	0.100	–0.394	–0.113
349.939	9.000	50.297	0.029	0.057	0.076	0.105	–0.352	–0.104
349.938	7.997	44.519	0.028	0.063	0.084	0.110	–0.310	–0.093
349.937	6.996	38.775	0.027	0.070	0.094	0.118	–0.267	–0.081
349.937	5.996	33.066	0.027	0.081	0.107	0.129	–0.226	–0.071
349.935	4.995	27.399	0.026	0.095	0.126	0.145	–0.186	–0.060
349.937	3.997	21.795	0.025	0.117	0.154	0.170	–0.151	–0.052
349.936	2.997	16.237	0.025	0.153	0.200	0.213	–0.118	–0.047
349.939	1.989	10.705	0.024	0.226	0.229	0.240	–0.084	–0.039
349.936	0.997	5.331	0.024	0.442	0.447	0.453	–0.054	–0.033
374.925	19.944	101.307	0.034	0.034	0.043	0.084	–0.687	–0.161
374.924	18.996	96.766	0.034	0.035	0.044	0.085	–0.662	–0.162

374.923	17.973	91.800	0.033	0.036	0.046	0.086	–0.631	–0.160
374.926	16.992	86.972	0.033	0.037	0.048	0.087	–0.601	–0.157
374.924	15.983	81.950	0.032	0.039	0.050	0.088	–0.569	–0.153
374.923	14.981	76.903	0.031	0.041	0.053	0.089	–0.534	–0.146
374.924	13.990	71.871	0.031	0.043	0.056	0.091	–0.500	–0.141
374.923	12.991	66.756	0.030	0.045	0.059	0.093	–0.465	–0.133
374.925	11.991	61.606	0.030	0.048	0.062	0.095	–0.429	–0.125
374.926	10.985	56.398	0.029	0.052	0.067	0.098	–0.387	–0.111
374.926	9.988	51.222	0.029	0.056	0.072	0.102	–0.351	–0.102
374.926	8.990	46.028	0.028	0.061	0.079	0.107	–0.313	–0.092
374.925	7.989	40.819	0.027	0.067	0.087	0.113	–0.277	–0.082
374.925	6.995	35.650	0.027	0.076	0.097	0.121	–0.238	–0.070
374.926	5.994	30.458	0.026	0.087	0.111	0.132	–0.202	–0.060
374.926	4.995	25.296	0.026	0.102	0.131	0.149	–0.167	–0.052
374.927	3.996	20.159	0.025	0.125	0.160	0.175	–0.134	–0.044
374.926	2.998	15.064	0.025	0.164	0.209	0.221	–0.102	–0.037
374.924	1.985	9.932	0.024	0.243	0.246	0.256	–0.059	–0.018
374.923	0.997	4.962	0.024	0.475	0.480	0.485	–0.051	–0.032
399.998	19.908	92.835	0.033	0.036	0.045	0.085	–0.615	–0.161
399.996	18.968	88.715	0.033	0.037	0.046	0.085	–0.588	–0.156
399.996	17.980	84.322	0.032	0.038	0.048	0.086	–0.567	–0.158
399.997	16.970	79.783	0.032	0.040	0.050	0.088	–0.542	–0.156
399.998	15.982	75.296	0.031	0.042	0.052	0.089	–0.509	–0.146
399.996	14.971	70.659	0.031	0.044	0.055	0.090	–0.482	–0.143
399.998	13.973	66.035	0.030	0.046	0.057	0.092	–0.454	–0.139
399.997	12.972	61.369	0.030	0.048	0.061	0.094	–0.424	–0.132
399.997	11.976	56.692	0.029	0.052	0.065	0.097	–0.393	–0.125
399.999	10.988	52.036	0.029	0.055	0.069	0.100	–0.357	–0.111
399.997	9.990	47.301	0.028	0.060	0.075	0.104	–0.329	–0.107
399.999	8.986	42.531	0.028	0.065	0.082	0.109	–0.297	–0.099
399.997	7.987	37.772	0.027	0.072	0.090	0.115	–0.265	–0.091
399.998	6.992	33.027	0.027	0.081	0.101	0.124	–0.226	–0.076
399.997	5.994	28.272	0.026	0.092	0.115	0.136	–0.196	–0.069
399.998	4.996	23.520	0.026	0.109	0.136	0.154	–0.173	–0.069
399.997	3.996	18.766	0.025	0.134	0.166	0.181	–0.147	–0.067
399.999	2.996	14.035	0.025	0.175	0.217	0.229	–0.123	–0.066
399.998	1.988	9.288	0.024	0.259	0.262	0.272	–0.094	–0.058
399.999	0.997	4.638	0.024	0.507	0.512	0.517	–0.116	–0.100

Table 6.20. *Experimental (p, ρ, T) measurements for the (0.90 CH_4 + 0.10 He), mixture, relative and absolute expanded uncertainty in density (k = 2) $U(\rho_{exp})$, expanded overall uncertainty in density (k = 2) from gravimetric composition $U_{T1}(\rho_{exp})$ and from virial expansion $U_{T2}(\rho_{exp})$ and relative deviations from the GERG-2008 and AGA8-DC92 equations of state; where T is the temperature (ITS-90* [25]*), p the pressure, ρ_{exp} the experimental density and ρ_{EoS} the density calculated from both equations of state.*

T/K	*p*/MPa	ρ_{exp}/ kg·m^{-3}	$U(\rho_{exp})$ kg·m^{-3}	$U(\rho_{exp})$ %	$U_{T1}(\rho_{exp})$ kg·m^{-3}	$U_{T2}(\rho_{exp})$ (kg·m^{-3})	$10^2(\rho_{exp}-\rho_{EoS})/\rho_{EoS}$	
							GERG-2008	AGA8-DC92
240.042	19.625	194.079	0.044	0.023	0.034	0.079	–3.467	–0.096
240.043	19.012	189.597	0.044	0.023	0.035	0.079	–3.499	–0.090
240.043	18.027	181.952	0.043	0.024	0.037	0.080	–3.529	–0.075
240.044	17.027	173.595	0.042	0.024	0.040	0.081	–3.526	–0.055
240.045	16.029	164.619	0.041	0.025	0.043	0.082	–3.476	–0.030
240.046	15.022	154.900	0.040	0.026	0.046	0.084	–3.364	–0.005
240.045	14.021	144.595	0.039	0.027	0.050	0.086	–3.181	0.017
240.046	13.019	133.681	0.038	0.028	0.054	0.088	–2.923	0.032
240.045	12.005	122.134	0.036	0.030	0.058	0.091	–2.595	0.037
240.045	11.012	110.482	0.035	0.032	0.062	0.094	–2.221	0.037
240.046	10.006	98.519	0.034	0.034	0.067	0.097	–1.833	0.019
240.046	9.009	86.730	0.033	0.038	0.073	0.101	–1.460	–0.003
240.045	8.002	75.062	0.031	0.042	0.079	0.106	–1.123	–0.029
240.045	7.001	63.844	0.030	0.047	0.087	0.112	–0.845	–0.056
240.046	6.000	53.119	0.029	0.054	0.098	0.121	–0.632	–0.087
240.046	4.998	42.934	0.028	0.065	0.113	0.133	–0.472	–0.111
240.046	3.998	33.318	0.027	0.080	0.135	0.153	–0.356	–0.127
240.047	2.998	24.247	0.026	0.106	0.174	0.188	–0.263	–0.127
240.047	1.996	15.681	0.025	0.158	0.160	0.176	–0.171	–0.098
240.046	0.998	7.620	0.024	0.313	0.317	0.325	–0.109	–0.079
250.004	18.875	173.914	0.042	0.024	0.037	0.080	–3.221	–0.128
250.003	18.031	167.361	0.041	0.025	0.039	0.081	–3.199	–0.123
250.003	17.022	159.082	0.040	0.025	0.041	0.082	–3.139	–0.116
250.004	16.006	150.232	0.040	0.026	0.044	0.083	–3.037	–0.108
250.004	15.019	141.163	0.039	0.027	0.047	0.085	–2.890	–0.100
250.004	14.018	131.510	0.037	0.028	0.050	0.086	–2.695	–0.095
250.004	13.000	121.315	0.036	0.030	0.053	0.088	–2.449	–0.091
250.005	12.003	111.033	0.035	0.032	0.057	0.091	–2.175	–0.091
250.006	11.009	100.603	0.034	0.034	0.061	0.094	–1.876	–0.089
250.004	10.008	90.050	0.033	0.037	0.066	0.097	–1.586	–0.103

250.005	9.003	79.524	0.032	0.040	0.071	0.101	–1.304	–0.115
250.005	8.002	69.239	0.031	0.044	0.078	0.106	–1.051	–0.129
250.007	7.001	59.226	0.030	0.050	0.086	0.112	–0.828	–0.136
250.006	6.000	49.568	0.028	0.057	0.097	0.121	–0.645	–0.142
250.006	4.998	40.290	0.027	0.068	0.113	0.134	–0.493	–0.140
250.004	3.997	31.436	0.026	0.084	0.136	0.154	–0.368	–0.130
250.005	2.997	22.993	0.026	0.111	0.113	0.190	–0.263	–0.112
250.007	1.998	14.960	0.025	0.165	0.167	0.182	–0.167	–0.080
250.005	0.997	7.285	0.024	0.327	0.496	0.339	–0.095	–0.058
260.015	19.940	168.802	0.042	0.025	0.036	0.080	–2.942	–0.144
260.014	19.031	162.300	0.041	0.025	0.038	0.081	–2.909	–0.145
260.015	18.020	154.700	0.040	0.026	0.040	0.081	–2.848	–0.145
260.013	17.010	146.708	0.039	0.027	0.042	0.082	–2.758	–0.145
260.014	16.023	138.537	0.038	0.028	0.045	0.084	–2.639	–0.145
260.013	15.018	129.866	0.037	0.029	0.047	0.085	–2.485	–0.145
260.012	14.018	120.922	0.036	0.030	0.050	0.087	–2.302	–0.146
260.014	13.014	111.695	0.035	0.032	0.053	0.089	–2.091	–0.146
260.013	12.010	102.273	0.034	0.033	0.057	0.091	–1.862	–0.147
260.014	11.007	92.773	0.033	0.036	0.061	0.094	–1.621	–0.144
260.013	10.003	83.236	0.032	0.039	0.066	0.097	–1.388	–0.150
260.013	9.003	73.809	0.031	0.042	0.071	0.101	–1.165	–0.153
260.013	8.001	64.503	0.030	0.047	0.078	0.106	–0.960	–0.154
260.012	7.000	55.420	0.029	0.053	0.086	0.112	–0.774	–0.149
260.012	5.998	46.581	0.028	0.060	0.098	0.121	–0.616	–0.144
260.012	5.001	38.068	0.027	0.071	0.113	0.134	–0.475	–0.130
260.012	4.000	29.826	0.026	0.088	0.138	0.155	–0.354	–0.111
260.011	2.998	21.898	0.025	0.116	0.118	0.192	–0.249	–0.088
260.010	1.998	14.290	0.025	0.172	0.175	0.189	–0.152	–0.056
260.009	0.997	6.987	0.024	0.340	0.504	0.352	–0.078	–0.035
274.999	18.804	144.712	0.039	0.027	0.040	0.082	–2.488	–0.190
274.999	18.024	139.174	0.038	0.028	0.041	0.082	–2.421	–0.193
274.999	17.008	131.721	0.037	0.028	0.043	0.083	–2.317	–0.198
274.999	16.019	124.219	0.037	0.030	0.045	0.084	–2.195	–0.200
274.998	15.016	116.391	0.036	0.031	0.048	0.086	–2.055	–0.203
274.997	14.013	108.363	0.035	0.032	0.050	0.087	–1.899	–0.204
274.995	13.002	100.126	0.034	0.034	0.054	0.089	–1.729	–0.204
274.993	12.009	91.938	0.033	0.036	0.057	0.091	–1.553	–0.200
274.992	11.018	83.711	0.032	0.038	0.061	0.094	–1.366	–0.187

274.992	10.003	75.270	0.031	0.042	0.066	0.097	–1.190	–0.186
274.991	8.999	66.981	0.030	0.045	0.071	0.101	–1.020	–0.180
274.991	8.002	58.832	0.029	0.050	0.078	0.106	–0.862	–0.171
274.991	6.999	50.769	0.029	0.056	0.087	0.113	–0.714	–0.160
274.992	5.998	42.884	0.028	0.065	0.099	0.122	–0.582	–0.147
274.992	4.997	35.184	0.027	0.076	0.115	0.136	–0.464	–0.132
274.992	3.997	27.702	0.026	0.094	0.140	0.158	–0.353	–0.110
274.992	2.997	20.437	0.025	0.124	0.126	0.196	–0.254	–0.085
274.991	1.991	13.357	0.024	0.183	0.186	0.199	–0.158	–0.054
274.990	0.998	6.585	0.024	0.360	0.517	0.372	–0.077	–0.029
299.950	19.681	130.063	0.037	0.029	0.040	0.082	–2.071	–0.260
299.950	19.009	125.943	0.037	0.029	0.041	0.083	–2.022	–0.266
299.951	18.016	119.734	0.036	0.030	0.043	0.083	–1.935	–0.268
299.952	17.022	113.365	0.035	0.031	0.044	0.084	–1.842	–0.272
299.951	16.006	106.706	0.035	0.033	0.047	0.085	–1.738	–0.273
299.950	15.003	100.010	0.034	0.034	0.049	0.087	–1.627	–0.272
299.950	13.987	93.126	0.033	0.036	0.052	0.088	–1.508	–0.268
299.949	13.009	86.415	0.033	0.038	0.055	0.090	–1.390	–0.263
299.951	12.007	79.484	0.032	0.040	0.058	0.092	–1.264	–0.255
299.952	11.000	72.492	0.031	0.043	0.062	0.095	–1.131	–0.238
299.950	9.995	65.501	0.030	0.046	0.067	0.098	–1.008	–0.227
299.951	9.002	58.607	0.029	0.050	0.073	0.102	–0.885	–0.212
299.950	7.997	51.678	0.029	0.056	0.080	0.108	–0.767	–0.195
299.951	7.000	44.863	0.028	0.062	0.089	0.115	–0.649	–0.172
299.951	5.998	38.093	0.027	0.071	0.102	0.125	–0.539	–0.149
299.951	4.998	31.436	0.026	0.084	0.119	0.139	–0.434	–0.124
299.953	3.997	24.884	0.026	0.103	0.145	0.162	–0.331	–0.095
299.952	2.997	18.458	0.025	0.136	0.138	0.202	–0.235	–0.066
299.950	1.989	12.112	0.024	0.201	0.204	0.287	–0.130	–0.023
299.951	0.997	6.006	0.024	0.394	0.540	0.405	–0.014	0.036
324.957	19.926	116.277	0.036	0.031	0.041	0.079	–1.728	–0.272
324.958	19.015	111.310	0.035	0.032	0.042	0.083	–1.667	–0.276
324.958	18.005	105.694	0.035	0.033	0.044	0.084	–1.595	–0.280
324.957	17.002	100.013	0.034	0.034	0.046	0.085	–1.516	–0.281
324.956	15.999	94.246	0.033	0.035	0.048	0.086	–1.434	–0.279
324.957	14.998	88.403	0.033	0.037	0.050	0.088	–1.345	–0.274
324.957	14.003	82.534	0.032	0.039	0.053	0.089	–1.255	–0.268
324.957	13.003	76.570	0.031	0.041	0.056	0.091	–1.162	–0.259

324.958	12.000	70.552	0.031	0.044	0.060	0.093	–1.065	–0.248
324.958	10.999	64.520	0.030	0.047	0.064	0.096	–0.963	–0.229
324.959	9.998	58.468	0.029	0.050	0.069	0.100	–0.867	–0.215
324.959	8.995	52.405	0.029	0.055	0.075	0.104	–0.772	–0.199
324.959	7.994	46.366	0.028	0.061	0.083	0.110	–0.677	–0.181
324.958	6.998	40.385	0.027	0.068	0.092	0.117	–0.582	–0.160
324.959	5.996	34.403	0.027	0.078	0.105	0.128	–0.491	–0.138
324.958	4.997	28.498	0.026	0.092	0.124	0.143	–0.404	–0.118
324.956	3.997	22.640	0.025	0.113	0.151	0.167	–0.321	–0.099
324.957	2.998	16.862	0.025	0.147	0.150	0.210	–0.235	–0.073
324.957	1.997	11.149	0.024	0.217	0.220	0.232	–0.150	–0.046
324.956	0.997	5.523	0.024	0.427	0.565	0.438	–0.079	–0.029
349.940	19.921	104.600	0.035	0.033	0.043	0.084	–1.495	–0.294
349.940	18.995	100.043	0.034	0.034	0.044	0.084	–1.441	–0.295
349.940	17.984	94.992	0.033	0.035	0.046	0.085	–1.378	–0.294
349.941	16.992	89.961	0.033	0.037	0.048	0.086	–1.312	–0.291
349.940	15.993	84.830	0.032	0.038	0.050	0.087	–1.243	–0.287
349.938	15.003	79.680	0.032	0.040	0.052	0.089	–1.172	–0.280
349.941	13.990	74.360	0.031	0.042	0.055	0.091	–1.095	–0.269
349.939	12.999	69.108	0.031	0.044	0.058	0.092	–1.019	–0.259
349.939	11.988	63.714	0.030	0.047	0.062	0.095	–0.940	–0.246
349.940	10.989	58.360	0.029	0.050	0.066	0.098	–0.856	–0.227
349.940	9.989	52.977	0.029	0.054	0.071	0.101	–0.776	–0.211
349.940	8.992	47.601	0.028	0.059	0.078	0.106	–0.696	–0.195
349.939	7.995	42.220	0.028	0.065	0.086	0.112	–0.616	–0.176
349.941	6.993	36.826	0.027	0.073	0.096	0.120	–0.532	–0.154
349.939	5.995	31.461	0.026	0.084	0.110	0.131	–0.457	–0.137
349.939	4.996	26.119	0.026	0.099	0.129	0.148	–0.383	–0.121
349.939	3.995	20.798	0.025	0.122	0.157	0.173	–0.305	–0.099
349.939	2.997	15.529	0.025	0.159	0.205	0.218	–0.229	–0.078
349.937	1.989	10.253	0.024	0.235	0.238	0.249	–0.188	–0.091
349.937	0.997	5.112	0.024	0.461	0.466	0.471	–0.111	–0.065
374.922	19.912	95.374	0.033	0.035	0.044	0.084	–1.311	–0.288
374.922	18.997	91.271	0.033	0.036	0.046	0.085	–1.262	–0.285
374.923	17.991	86.700	0.033	0.038	0.047	0.086	–1.205	–0.279
374.924	16.856	81.471	0.032	0.039	0.050	0.087	–1.138	–0.271
374.923	15.992	77.441	0.032	0.041	0.051	0.089	–1.086	–0.265
374.924	14.990	72.730	0.031	0.043	0.054	0.090	–1.017	–0.250

374.922	13.966	67.866	0.030	0.045	0.057	0.092	–0.949	–0.237
374.924	12.998	63.225	0.030	0.047	0.060	0.094	–0.885	–0.224
374.923	11.986	58.341	0.029	0.050	0.064	0.096	–0.821	–0.215
374.922	10.989	53.503	0.029	0.054	0.068	0.099	–0.749	–0.197
374.926	9.991	48.640	0.028	0.058	0.074	0.103	–0.679	–0.180
374.920	8.994	43.761	0.028	0.064	0.081	0.108	–0.613	–0.168
374.923	7.988	38.828	0.027	0.070	0.089	0.115	–0.541	–0.149
374.924	6.992	33.941	0.027	0.079	0.100	0.123	–0.464	–0.124
374.923	5.995	29.050	0.026	0.090	0.114	0.135	–0.397	–0.108
374.923	4.996	24.159	0.026	0.106	0.134	0.152	–0.322	–0.084
374.922	3.993	19.262	0.025	0.130	0.164	0.179	–0.258	–0.071
374.924	2.996	14.413	0.025	0.171	0.214	0.226	–0.194	–0.056
374.924	1.997	9.577	0.024	0.251	0.254	0.264	–0.126	–0.037
374.923	0.997	4.766	0.024	0.494	0.499	0.504	–0.045	–0.003
400.005	19.812	87.449	0.033	0.037	0.046	0.085	–1.178	–0.291
400.005	18.956	83.913	0.032	0.038	0.047	0.086	–1.137	–0.287
400.005	17.982	79.843	0.032	0.040	0.049	0.087	–1.093	–0.285
400.006	16.970	75.567	0.031	0.041	0.051	0.088	–1.045	–0.282
400.005	15.958	71.246	0.031	0.043	0.053	0.090	–0.991	–0.274
400.005	14.977	67.013	0.030	0.045	0.056	0.091	–0.939	–0.265
400.006	13.983	62.689	0.030	0.048	0.059	0.093	–0.883	–0.255
400.006	12.965	58.225	0.029	0.051	0.062	0.095	–0.824	–0.242
400.007	11.979	53.869	0.029	0.054	0.066	0.098	–0.767	–0.230
400.006	10.985	49.453	0.028	0.058	0.071	0.101	–0.701	–0.210
400.006	9.991	45.009	0.028	0.062	0.077	0.105	–0.642	–0.197
400.008	8.984	40.487	0.027	0.068	0.084	0.111	–0.581	–0.183
400.006	7.987	35.996	0.027	0.075	0.092	0.117	–0.520	–0.168
400.005	6.994	31.514	0.026	0.084	0.104	0.126	–0.455	–0.150
400.006	5.990	26.977	0.026	0.096	0.119	0.139	–0.395	–0.135
400.007	4.993	22.465	0.025	0.113	0.139	0.157	–0.335	–0.121
400.007	3.997	17.962	0.025	0.139	0.171	0.185	–0.269	–0.099
400.007	2.996	13.446	0.024	0.182	0.223	0.235	–0.215	–0.090
400.006	1.996	8.941	0.024	0.268	0.271	0.281	–0.141	–0.060
400.005	0.997	4.458	0.023	0.527	0.532	0.537	–0.087	–0.048

Table 6.21. *Experimental (p, ρ, T) measurements for the (0.50 CH_4 + 0.50 He), mixture, relative and absolute expanded uncertainty in density (k = 2) U(ρ_{exp}), expanded overall uncertainty in density (k = 2) from gravimetric composition $U_{T1}(\rho_{exp})$ and from virial expansion $U_{T2}(\rho_{exp})$ and relative deviations from the GERG-2008 and AGA8-DC92 equations of state; where T is the temperature (ITS-90* [25]*), p the pressure, ρ_{exp} the experimental density and ρ_{EoS} the density calculated from both equations of state.*

T/K	*p*/MPa	ρ_{exp}/ kg·m^{-3}	$U(\rho_{exp})$ kg·m^{-3}	$U(\rho_{exp})$ %	$U_{T1}(\rho_{exp})$ kg·m^{-3}	$U_{T2}(\rho_{exp})$ (kg·m^{-3})	$10^2(\rho_{exp}-\rho_{EoS})/\rho_{EoS}$ GERG-2008	AGA8-DC92
240.032	16.089	77.505	0.032	0.041	0.053	0.130	–6.072	0.392
240.029	15.008	72.695	0.031	0.043	0.056	0.131	–5.791	0.299
240.029	14.007	68.168	0.030	0.045	0.058	0.132	–5.512	0.217
240.030	13.007	63.573	0.030	0.047	0.061	0.133	–5.216	0.137
240.031	11.997	58.869	0.029	0.050	0.065	0.135	–4.904	0.057
240.031	11.002	54.180	0.029	0.053	0.070	0.137	–4.571	–0.007
240.030	10.001	49.403	0.028	0.058	0.075	0.140	–4.229	–0.073
240.031	9.001	44.581	0.028	0.063	0.081	0.144	–3.874	–0.131
240.031	8.000	39.712	0.027	0.069	0.089	0.148	–3.505	–0.181
240.032	6.999	34.803	0.027	0.077	0.100	0.155	–3.124	–0.221
240.032	5.997	29.862	0.026	0.088	0.114	0.164	–2.732	–0.251
240.033	4.998	24.905	0.026	0.103	0.133	0.178	–2.330	–0.269
240.033	3.998	19.928	0.025	0.126	0.162	0.201	–1.917	–0.275
240.033	2.998	14.943	0.025	0.165	0.211	0.242	–1.481	–0.254
240.033	1.992	9.928	0.024	0.243	0.246	0.273	–1.009	–0.197
240.033	0.997	4.969	0.024	0.474	0.479	0.494	–0.515	–0.111
250.005	19.686	88.663	0.033	0.037	0.047	0.127	–6.439	0.468
249.964	18.997	85.915	0.032	0.038	0.048	0.128	–6.329	0.398
250.017	18.002	81.885	0.032	0.039	0.050	0.128	–6.106	0.346
249.994	16.646	76.317	0.031	0.041	0.053	0.129	–5.782	0.278
249.997	15.999	73.600	0.031	0.042	0.054	0.130	–5.630	0.232
249.994	15.003	69.361	0.031	0.044	0.056	0.131	–5.384	0.163
249.997	14.005	65.051	0.030	0.046	0.059	0.132	–5.123	0.096
249.998	12.999	60.647	0.030	0.049	0.063	0.134	–4.843	0.034
249.999	12.002	56.224	0.029	0.052	0.066	0.136	–4.553	–0.025
249.999	11.000	51.722	0.029	0.055	0.071	0.138	–4.242	–0.073
250.000	10.006	47.205	0.028	0.060	0.076	0.141	–3.930	–0.125
249.999	8.999	42.584	0.028	0.065	0.083	0.145	–3.593	–0.162
250.000	8.001	37.957	0.027	0.072	0.091	0.149	–3.253	–0.198
250.053	7.001	33.286	0.027	0.080	0.102	0.156	–2.877	–0.203

250.000	6.000	28.574	0.026	0.091	0.116	0.166	–2.551	–0.258
249.991	4.945	23.600	0.026	0.108	0.137	0.181	–2.082	–0.192
249.989	3.997	19.095	0.025	0.131	0.166	0.204	–1.712	–0.185
249.989	2.997	14.323	0.025	0.172	0.174	0.246	–1.314	–0.170
249.990	1.991	9.521	0.024	0.253	0.256	0.282	–0.894	–0.135
249.989	0.997	4.769	0.024	0.493	0.617	0.512	–0.431	–0.051
259.986	19.334	83.513	0.032	0.039	0.048	0.128	–6.001	0.255
259.987	19.000	82.229	0.032	0.039	0.049	0.128	–5.940	0.232
259.987	18.001	78.346	0.032	0.040	0.051	0.129	–5.750	0.166
259.986	17.011	74.435	0.031	0.042	0.053	0.130	–5.548	0.103
259.986	16.009	70.413	0.031	0.044	0.055	0.131	–5.329	0.041
259.986	15.001	66.310	0.030	0.046	0.058	0.132	–5.096	–0.018
259.985	14.000	62.178	0.030	0.048	0.060	0.133	–4.851	–0.073
259.985	12.960	57.824	0.029	0.051	0.064	0.135	–4.580	–0.124
259.992	11.996	53.738	0.029	0.054	0.068	0.136	–4.314	–0.164
259.993	10.997	49.455	0.028	0.058	0.072	0.139	–4.023	–0.198
259.994	9.998	45.124	0.028	0.062	0.078	0.142	–3.727	–0.232
259.994	9.000	40.749	0.027	0.067	0.085	0.146	–3.417	–0.258
259.995	7.999	36.324	0.027	0.074	0.093	0.151	–3.094	–0.277
259.995	6.996	31.852	0.027	0.083	0.104	0.158	–2.757	–0.286
259.994	5.997	27.365	0.026	0.095	0.119	0.168	–2.410	–0.286
259.995	4.997	22.844	0.026	0.112	0.139	0.183	–2.048	–0.275
259.995	3.997	18.303	0.025	0.137	0.170	0.207	–1.669	–0.248
259.995	2.997	13.742	0.025	0.178	0.181	0.251	–1.270	–0.202
259.996	1.997	9.169	0.024	0.262	0.265	0.290	–0.853	–0.141
259.997	0.997	4.578	0.024	0.513	0.633	0.532	–0.452	–0.097
275.092	19.880	80.485	0.032	0.040	0.049	0.128	–5.556	0.109
275.103	18.991	77.268	0.031	0.041	0.050	0.129	–5.400	0.066
274.973	17.996	73.619	0.031	0.042	0.052	0.129	–5.274	–0.035
275.033	16.993	69.886	0.031	0.044	0.054	0.130	–5.057	–0.061
275.013	16.003	66.148	0.030	0.046	0.057	0.131	–4.863	–0.112
275.137	14.998	62.299	0.030	0.048	0.059	0.132	–4.596	–0.105
275.030	13.992	58.399	0.029	0.050	0.062	0.134	–4.411	–0.184
274.981	12.333	51.873	0.029	0.055	0.068	0.137	–3.990	–0.214
274.982	11.998	50.535	0.029	0.057	0.070	0.137	–3.906	–0.224
274.983	10.998	46.513	0.028	0.060	0.074	0.140	–3.641	–0.242
274.984	9.997	42.440	0.028	0.065	0.080	0.143	–3.372	–0.263
274.984	8.996	38.323	0.027	0.071	0.087	0.147	–3.092	–0.278

274.985	7.996	34.172	0.027	0.078	0.096	0.153	–2.802	–0.288
274.984	6.996	29.987	0.026	0.088	0.107	0.160	–2.500	–0.288
274.984	5.997	25.777	0.026	0.100	0.123	0.171	–2.189	–0.284
274.984	4.997	21.529	0.025	0.118	0.144	0.186	–1.865	–0.270
274.980	3.997	17.256	0.025	0.144	0.176	0.212	–1.534	–0.252
274.979	2.997	12.967	0.024	0.188	0.191	0.258	–1.165	–0.199
274.980	1.997	8.655	0.024	0.277	0.280	0.304	–0.771	–0.124
274.978	0.997	4.329	0.023	0.542	0.657	0.561	–0.386	–0.062
299.999	19.872	73.326	0.031	0.042	0.051	0.129	–4.869	–0.139
299.938	18.984	70.381	0.031	0.044	0.053	0.130	–4.754	–0.194
300.048	17.984	67.021	0.030	0.045	0.054	0.130	–4.553	–0.191
299.893	16.990	63.637	0.030	0.047	0.057	0.131	–4.439	–0.276
299.910	15.304	57.804	0.029	0.051	0.061	0.133	–4.114	–0.305
299.912	14.990	56.703	0.029	0.052	0.062	0.134	–4.053	–0.313
299.910	13.998	53.196	0.029	0.054	0.065	0.135	–3.855	–0.332
299.911	12.994	49.608	0.028	0.057	0.069	0.137	–3.646	–0.347
299.910	11.994	45.991	0.028	0.061	0.073	0.139	–3.429	–0.358
299.911	10.999	42.355	0.028	0.065	0.078	0.142	–3.197	–0.359
299.908	9.994	38.640	0.027	0.071	0.084	0.145	–2.960	–0.361
299.910	8.995	34.912	0.027	0.077	0.092	0.150	–2.712	–0.354
299.910	7.998	31.158	0.026	0.085	0.101	0.156	–2.456	–0.343
299.910	6.997	27.355	0.026	0.095	0.113	0.164	–2.184	–0.322
299.910	5.995	23.517	0.026	0.109	0.130	0.176	–1.906	–0.298
299.909	4.996	19.658	0.025	0.128	0.152	0.193	–1.615	–0.264
299.909	3.996	15.769	0.025	0.157	0.186	0.221	–1.314	–0.225
299.908	2.997	11.860	0.024	0.205	0.208	0.270	–1.000	–0.178
299.908	1.997	7.922	0.024	0.301	0.305	0.376	–0.649	–0.097
299.910	0.997	3.963	0.023	0.591	0.698	0.609	–0.330	–0.053
325.139	19.910	67.575	0.030	0.045	0.053	0.128	–4.261	–0.234
325.052	18.996	64.771	0.030	0.047	0.055	0.131	–4.161	–0.286
325.262	17.996	61.669	0.030	0.048	0.057	0.131	–3.948	–0.245
325.183	16.993	58.519	0.029	0.050	0.059	0.132	–3.819	–0.289
324.920	15.482	53.698	0.029	0.054	0.063	0.134	–3.674	–0.412
324.921	14.996	52.129	0.029	0.055	0.065	0.135	–3.592	–0.419
324.921	13.989	48.856	0.028	0.058	0.068	0.137	–3.416	–0.429
324.921	12.990	45.572	0.028	0.061	0.072	0.139	–3.232	–0.435
324.921	11.991	42.251	0.028	0.065	0.077	0.141	–3.041	–0.437
324.922	10.989	38.891	0.027	0.070	0.082	0.144	–2.833	–0.425

324.922	9.995	35.519	0.027	0.076	0.089	0.148	–2.626	–0.417
324.923	8.996	32.100	0.027	0.083	0.097	0.153	–2.408	–0.403
324.924	7.994	28.637	0.026	0.091	0.107	0.159	–2.180	–0.383
324.924	6.995	25.153	0.026	0.102	0.119	0.168	–1.942	–0.355
324.924	5.996	21.639	0.025	0.117	0.137	0.181	–1.697	–0.325
324.923	4.996	18.094	0.025	0.138	0.161	0.200	–1.442	–0.289
324.924	3.995	14.517	0.025	0.169	0.197	0.230	–1.179	–0.248
324.924	2.996	10.922	0.024	0.222	0.224	0.283	–0.909	–0.205
324.923	1.997	7.302	0.024	0.326	0.330	0.350	–0.624	–0.150
324.922	0.997	3.654	0.023	0.640	0.741	0.658	–0.338	–0.101
349.914	16.463	52.660	0.029	0.055	0.063	0.134	–3.408	–0.449
349.915	15.995	51.273	0.029	0.056	0.065	0.135	–3.342	–0.456
349.914	14.995	48.291	0.028	0.059	0.068	0.137	–3.190	–0.461
349.914	13.986	45.249	0.028	0.062	0.071	0.138	–3.031	–0.464
349.916	12.995	42.230	0.028	0.065	0.076	0.141	–2.867	–0.462
349.914	11.987	39.127	0.027	0.070	0.080	0.143	–2.694	–0.456
349.915	10.991	36.033	0.027	0.075	0.086	0.147	–2.511	–0.440
349.915	9.989	32.885	0.027	0.081	0.093	0.151	–2.325	–0.427
349.914	8.995	29.735	0.026	0.088	0.101	0.156	–2.132	–0.407
349.913	7.997	26.543	0.026	0.098	0.112	0.163	–1.931	–0.384
349.912	6.991	23.297	0.026	0.110	0.126	0.173	–1.719	–0.354
349.913	5.993	20.048	0.025	0.126	0.144	0.187	–1.501	–0.320
349.913	4.995	16.770	0.025	0.148	0.169	0.207	–1.280	–0.286
349.913	3.996	13.462	0.024	0.182	0.208	0.239	–1.054	–0.252
349.913	2.996	10.130	0.024	0.238	0.272	0.296	–0.817	–0.210
349.914	1.989	6.742	0.024	0.352	0.356	0.375	–0.622	–0.216
349.913	0.997	3.390	0.023	0.690	0.696	0.706	–0.369	–0.165
374.904	14.969	44.946	0.028	0.062	0.071	0.138	–2.856	–0.488
374.906	13.428	40.599	0.027	0.068	0.077	0.141	–2.629	–0.479
374.905	12.989	39.345	0.027	0.069	0.079	0.142	–2.568	–0.480
374.906	11.988	36.471	0.027	0.074	0.084	0.145	–2.414	–0.471
374.906	10.992	33.585	0.027	0.079	0.090	0.149	–2.249	–0.452
374.906	9.992	30.659	0.026	0.086	0.097	0.154	–2.080	–0.433
374.905	8.993	27.711	0.026	0.094	0.106	0.159	–1.905	–0.410
374.905	7.993	24.728	0.026	0.104	0.118	0.167	–1.729	–0.389
374.904	6.993	21.725	0.025	0.117	0.132	0.177	–1.526	–0.343
374.904	5.995	18.697	0.025	0.134	0.151	0.192	–1.337	–0.314
374.906	4.995	15.636	0.025	0.158	0.178	0.214	–1.145	–0.285

374.903	3.996	12.555	0.024	0.194	0.219	0.249	–0.938	–0.244
374.908	2.996	9.447	0.024	0.254	0.286	0.310	–0.740	–0.215
374.906	1.997	6.319	0.024	0.375	0.379	0.397	–0.501	–0.148
374.905	0.997	3.165	0.023	0.738	0.745	0.754	–0.290	–0.113
399.992	15.369	43.172	0.028	0.064	0.072	0.139	–2.602	–0.479
399.991	14.974	42.136	0.028	0.066	0.074	0.140	–2.551	–0.477
399.990	13.984	39.520	0.027	0.069	0.078	0.142	–2.427	–0.476
399.990	12.978	36.835	0.027	0.073	0.083	0.144	–2.291	–0.467
399.989	11.984	34.161	0.027	0.078	0.088	0.148	–2.149	–0.451
399.989	10.983	31.443	0.026	0.084	0.094	0.152	–1.995	–0.427
399.989	9.992	28.726	0.026	0.091	0.102	0.156	–1.847	–0.409
399.989	8.991	25.954	0.026	0.100	0.111	0.163	–1.683	–0.379
399.989	7.990	23.158	0.026	0.110	0.123	0.171	–1.524	–0.356
399.991	6.972	20.293	0.025	0.124	0.139	0.183	–1.350	–0.321
399.990	5.992	17.506	0.025	0.142	0.159	0.198	–1.186	–0.295
399.991	4.993	14.646	0.025	0.168	0.187	0.222	–1.001	–0.252
399.991	3.996	11.762	0.024	0.207	0.230	0.259	–0.824	–0.220
399.992	2.996	8.853	0.024	0.271	0.301	0.323	–0.634	–0.177
399.990	1.993	5.910	0.024	0.400	0.404	0.421	–0.431	–0.125
399.991	0.997	2.964	0.023	0.787	0.795	0.803	–0.301	–0.148

6.9. REFERENCES

[1] K. E. Starling and J. L. Savidge, “Compressibility factors of natural gas and other related hydrocarbon gases - AGA Transmission Measurement Committee Report 8,” 1992.

[2] O. Kunz and W. Wagner, “The GERG-2008 Wide-Range Equation of State for Natural Gases and Other Mixtures: An Expansion of GERG-2004,” *J. Chem. Eng. Data*, 2012.

[3] “ISO 20765-2 Natural gas -Calculation of thermodynamic properties -Part 2: Single-phase properties (gas, liquid, and dense fluid) for extended ranges of application,” Geneva, 2015.

[4] T. Rufford, K. Chan, S. Huang, and E. May, “A Review of Conventional and Emerging Process Technologies for the Recovery of Helium from Natural Gas,” *Adsorpt. Sci. Technol.*, vol. 32, no. 1, pp. 49–72, Jan. 2014.

[5] R. F. Broadhead, “Helium in New Mexico—geologic distribution, resource demand, and exploration possibilities,” *New Mex. Geol.*, vol. 27, pp. 93–101, 2005.

[6] “ISO 6142 - Preparation of calibration gas mixtures - Gravimetric method. International Organisation for Standardization, Geneva, 2001).” 2001.

[7] U. Setzmann and W. Wagner, “A New Equation of State and Tables of Thermodynamic Properties for Methane Covering the Range from the Melting Line to 625 K at Pressures up to 1000 MPa,” *J. Phys. Chem. Ref. Data*, vol. 20, no. 6, pp. 1061–1151, 1991.

[8] D. O. Ortiz Vega, K. R. Hall, J. C. Holste, V. D. Arp, and E. W. Lemmon, “A New Wide Range Equation of State for Helium-4,” *J. Phys. Chem. Ref. Data*, Dec. 2013.

[9] “Lemmon, E.W., Huber, M.L., McLinden, M.O. NIST Standard Reference Database 23: Reference Fluid Thermodynamic and Transport Properties-REFPROP, Version 9.1, National Institute of Standards and Technology, Standard Reference Data Program, Gaithersburg, 2013.” .

[10] “ISO/CD 12963 Gas analysis – Comparison methods for the determination of the composition of gas mixtures based on one- and two-point calibration, International Organization for Standardization, Geneva.”

[11] R. Span, E. W. Lemmon, R. T. Jacobsen, and W. Wagner, “A reference quality equation of state for nitrogen,” *Int. J. Thermophys.*, vol. 19, no. 4 SPEC.ISS., pp. 1121–1132, 1998.

[12] M. O. McLinden, R. Kleinrahm, and W. Wagner, “Force transmission errors in magnetic suspension densimeters,” *Int. J. Thermophys.*, vol. 28, no. 2, pp. 429–448, 2007.

[13] F. Bitter, “The Magnetic Susceptibilities of Several Organic Gases,” *Phys. Rev.*, vol. 33, no. 3, pp. 389–397, Mar. 1929.

[14] M. Richter and R. Kleinrahm, “Influence of adsorption and desorption on accurate density measurements of gas mixtures,” *J. Chem. Thermodyn.*, Mar. 2014.

[15] J. Klimeck, R. Kleinrahm, and W. Wagner, “An accurate single-sinker densimeter and measurements of the (p, ρ, T) relation of argon and nitrogen in the temperature range from (235 to 520) K at pressures up to 30 MPa,” *J. Chem. Thermodyn.*, vol. 30, no. 12, pp. 1571–1588, 1998.

[16] M. O. McLinden and C. Lösch-Will, “Apparatus for wide-ranging, high-accuracy fluid (p, ρ, T) measurements based on a compact two-sinker densimeter,” *J. Chem. Thermodyn.*, vol. 39, no. 4, pp. 507–530, 2007.

[17] J. T. R. Watson and National Engineering Laboratory-FPT Division, “‘A generalised fitting package for the least squares analysis of data’.” East Kilbride, Glasgow G75 0QU, Scotland., 1991.

[18] I. E. C. BIPM IFCC, ISO, IUPAC, IUPAP and OIML, “Guide to the Expression of Uncertainty in Measurement,” *Guid. to Expr. Uncertain. Meas.*, 1995.

[19] J. H. Dymond and E. B. Smith, *The Virial Coefficients of Pure Gases and Mixtures. A Critical Compilation*. 1980.

[20] M. E. Mondéjar, J. J. Segovia, and C. R. Chamorro, “Improvement of the measurement uncertainty of a high accuracy single sinker densimeter via setup modifications based on a state point uncertainty analysis,” *Measurement*, vol. 44, no. 9, pp. 1768–1780, 2011.

[21] M. E. Wieser, N. Holden, T. B. Coplen, J. K. Böhlke, M. Berglund, W. A. Brand, P. De Bièvre, M. Gröning, R. D. Loss, J. Meija, T. Hirata, T. Prohaska, R. Schoenberg, G. O’Connor, T. Walczyk, S. Yoneda, and X.-K. Zhu, “Atomic weights of the elements 2011 (IUPAC Technical Report),” *Pure Appl. Chem.*, vol. 85, no. 5, pp. 1047–1078, Jan. 2013.

[22] M. Richter and M. O. McLinden, “Vapor-Phase (p, ρ, T, x) Behavior and Virial Coefficients for the (Methane + Propane) System,” *J. Chem. Eng. Data*, vol. 59, no. 12, pp. 4151–4164, Dec. 2014.

[23] O. Kunz, R. Klimeck, W. Wagner, and M. Jaeschke, “The GERG-2004 Wide-Range Reference Equation of State for Natural Gases and Other Mixtures,” *GERG Tech. Monogr. Fortschritt-Berichte VDI*, 2007.

[24] C. M. Bignell and P. J. Dunlop, “Second virial coefficients for fluoromethanes and their binary mixtures with helium and argon,” *J. Chem. Eng. Data*, vol. 38, no. 1, pp. 139–140, Jan. 1993.

[25] C. A. S. R L Rusby and R P Hudson and M Durieux and J F Schooley and P P M Steur and, “Thermodynamic Basis of the ITS-90,” *Metrologia*, vol. 28, no. 1, p. 9, 1991.

CHAPTER 7

Thermodynamic characterization of a synthetic mixture of coal mine methane (CMM)

7.1. Introduction 171
7.2. Mixture preparation 173
7.3. Experimental process 178
7.4. Experimental results 179
7.5. Virial coefficients determination 181
7.6. Uncertainty analysis of the measurements 182
7.7. Discussion 185
7.8. Table of results 193
7.9. References 196

7.1. INTRODUCTION

Coalbed methane (CBM) refers to all methane originated in coal seams by geological or biological processes. Depending on the production source of this fuel gas, it can be classified in several groups, each of them with specific reservoir characteristics, composition and extraction process. Thus, sorted in order from highest to lowest methane concentration, we can identify the following types: virgin coalbed methane (VCBM), abandoned mine methane (AMM), coal mine methane (CMM) and ventilation air methane (VAM) [1]:

- VCBM (virgin coalbed methane) refers to gas extracted from surface surveys before the exploitation of coal mines.
- The VCBM recovering in surveys of coal deposits can be stimulated by injecting N_2 or CO_2, obtaining ECBM (enhanced coalbed methane). This method can be combined with CCS (carbon capture storage).
- AMM (abandoned mine methane).
- CMM (coal mine methane) is obtained during the extraction of coal.
- VAM (ventilation air methane) is also obtained during the extraction.

The differentiation of the types of CBM is not defined in a rigorous way, so confused terms are often found in the literature. The classification described above can be seen schematically in Figure 7.1.

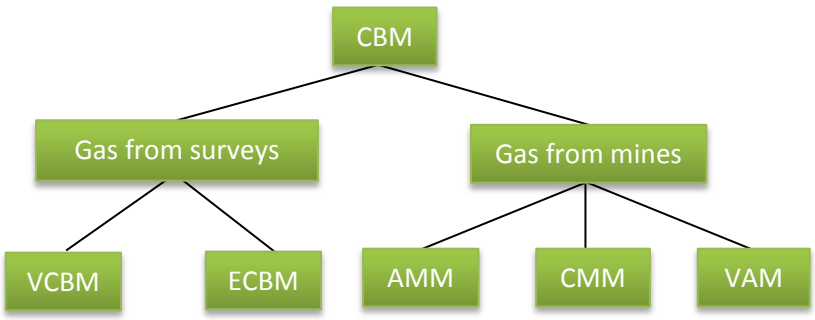

Figure 7.1. *Coalbed methane (CBM) types in function of their source.*

Table 7.1 shows the usual methane amount and the typical gas flows depending on the source of production.

***Table 7.1**. Usual concentrations and flows of the different types of CMB* [1].

CBM source	Methane concentration / %	Gas flow / x10^3 m^3/day
VCBM	>95	1 - 18
AMM	35 - 90	11 - 86
CMM	35 - 75	6 - 195
VAM	0.05 - 0.08	4 - 140

CMM is obtained from working coal mines, either in advance to the mining works or from worked seams, by using drainage techniques. Although its composition depends significantly on the reservoir characteristics, it generally consists of a mixture of methane as the main compound (35% to 75% molar fraction) and higher alkanes, together with nitrogen, oxygen, carbon dioxide and, occasionally, water vapor [1].

Due to the rise of fuel prices in the last few years caused by the advanced depletion of their reserves and the increasing demand by the global economy, non-conventional and renewable fuels are gaining importance as alternatives to fossil fuels and also as a way to reduce the CO_2 emissions to the atmosphere. Among non-conventional fuels, coalbed methane arises as a potential energy resource in countries with an important coal production. As a by-product of mining, coalbed methane was traditionally used in local small-scale power production, but it can also contribute to the domestic and commercial gas supply.

The presence of CMM in coal mining is a challenge for working safety and for environmental reasons. On the one hand, the accumulation of the gas due to desorption from the distressed coal seam can affect the safety of the mine with an increase of the explosion risk. On the other hand, the uncontrolled release of this gas to the atmosphere can be even more harmful to the environment than CO_2 emissions, since the global warming potential (GWP) of methane is 25 times that of carbon dioxide [2]. Therefore, apart from the exploitation of a coal mining by-product, the controlled use of CMM reduces the overall greenhouse gases emissions and ensures safety in coal mines.

The significant difference in composition between CMM and natural gas, which manifests in a lower methane content and a corresponding higher content of carbon dioxide, nitrogen and other components of the first, makes it necessary to validate the performance of the existing equations of state for natural gases for gases with deviating compositions employing accurate experimental data of their thermophysical properties.

Experimental density data of different multi-component gas mixtures with common natural gas compositions have been previously measured by different authors. However no previous density data of synthetic mixtures with similar compositions to that of non-conventional gas fuels, such as biogas or CMM, can be found in the literature.

In this work, accurate experimental (p, ρ, T) data of a synthetic CMM mixture in the supercritical and gaseous state at temperatures ranging from (250 to 400) K and pressures up to 15 MPa are presented. Densities were measured by using the single-sinker densimeter with magnetic suspension coupling. The synthetic CMM mixture was prepared gravimetrically at the Bundesanstalt für Materialforschung und -prüfung (BAM) in Berlin, Germany. The second and the third virial coefficients of the mixture were calculated from experimental results. Moreover, the overall uncertainty of density measurements was estimated according to two different methods described in chapter 4.7. Experimental data were compared with the corresponding densities calculated from the GERG-2008 and AGA8-DC92 [3] equations of state [4]. The study of this mixture was part of the research project EMRP ENG01 - European Metrology Research Program for the characterization of non-conventional energy gases [5], in which comparison of traceable methods for determining the calorific value of non-conventional fuel gases were also carried out [6].

7.2. MIXTURE PREPARATION

The synthetic CMM mixture was prepared gravimetrically at the Bundesanstalt für Materialforschung und -prüfung (BAM) in Berlin, Germany. It was supplied in a 5 dm^3 aluminum cylinder (BAM no.: 087) at 4.9 MPa of pressure. The composition of the mixture from gravimetric preparation according to ISO 6142 [7] is given in Table 7.2, together with the expanded uncertainty in composition for each component (k = 2), the certified purity, supplier, molar mass and critical parameters of each of the component gases. All substances were used without further purification.

The critical parameters of the mixture and its molar mass were estimated by using the GERG-2008 equation of state [4] through REFPROP software [8].

- T_c = 207.1 K
- p_c = 6.86 MPa
- M = 23.153 $g \cdot mol^{-1}$

Table 7.2. *Composition of the synthetic coal mine methane (CMM) mixture and purity, supplier, critical parameters and molar mass of the individual component gases.*

Component	Concentration (molar fraction) x_i	$U(x_i)$ %	Purity	Supplier	M g·mol^{-1}	Critical parameters	
						T_c / K	P_c / MPa
Methane	0.64207992	0.008	99.9995 mol-%	Linde[f]	16.043[g]	190.56[g]	4.60[g]
Carbon dioxide	0.17312271	0.010	99.9995 vol-%	Air Liquide[d]	44.010[h]	304.13[h]	7.38[h]
Nitrogen	0.17031942	0.011	99.9999 vol-%	Westfalen[a]	28.013[i]	126.19[i]	3.39[i]
Ethane	0.00846613	0.053	99.990 vol-%	Scott Specialty Gases	30.069[j]	305.32[j]	4.87[j]
Propane	0.00078154	0.052	99.990 vol-%	Scott Specialty Gases[b]	44.096[k]	369.89[k]	4.25[k]
i-Butane	0.00010716	0.052	99.95 vol-%	Messer[c]	58.122[l]	407.81[l]	3.63[l]
n-Butane	0.00005710	0.053	99.98 vol-%	Scott Specialty Gases	58.122[l]	425.13[l]	3.80[l]
i-Pentane	0.00001723	0.200	> 99.7 % (GC)	Sigma-Aldrich	72.149[m]	460.35[m]	3.38[m]
n-Pentane	0.00000752	0.200	> 99.8 % (GC)	Sigma-Aldrich[e]	72.149[n]	469.70[n]	3.37[n]
Oxygen	0.00504128	0.026	99.9995 vol-%	Westfalen	31.999[o]	154.58[o]	5.04[o]

[a] *Westfalen AG, Hörstel, Germany*
[b] *Scott Specialty Gases Nederlands BV, Breda, The Nederlands*
[c] *Messer Group GmbH, Krefeld, Germany*
[d] *Air Liquide AG, Düsseldorf, Germany*
[e] *Sigma-Aldrich Chemie GmbH, Steinheim, Germany*
[f] *Linde AG, Unterschleißheim, Germany*
[g] Setzmann et al. [24]
[h] Span et al. [25]
[i] Span et al. [26]
[j] Buecker et al. [27]
[k] Lemmon et al. [28]
[l] Buecker et al. [29]
[m] Lemmon et al. [30]
[n] Span et al. [31]
[o] Schmidt et al. [32]

In order to obtain the uncertainties given in Table 7.2, the preparation of the CMM mixture required a multi-step method via pre-mixtures. Altogether, four pre-mixtures were prepared in 10 dm^3 aluminum cylinders which contained all the required components (except carbon dioxide and methane) that could be introduced directly into the final cylinder with the target composition (BAM no.: 7078-111005, volume: 10 dm^3). The corresponding compositions are given in Table 7.2. Pre-mixture A (BAM no.: 7039-110912)

contained n-pentane and isopentane in methane. The liquid pentanes were introduced into evacuated minicylinders (volume: 25 cm^3, arranged in a parallel configuration according to ISO 6142 [7]) and transferred into the recipient cylinder by evaporation that is directly followed by purging the transfer system with the calculated amount of methane. In the next step, pre-mixture A was diluted with methane which resulted in pre-mixture B (BAM no.: 7064-110920). Pre-mixture C (BAM no.: 7083-110926) contributed ethane, propane, n-butane, and isobutane. Propane, n-butane, and isobutane were filled in the same way via minicylinders and ethane as purging gas. In the next step, pre-mixture C was completed with methane. Pre-mixture D (BAM no.: 7045-110823) was a binary mixture of oxygen and nitrogen. The filling sequence of the final CMM mixture (BAM no.: 7078-111005) was: carbon dioxide, pre-mixture B, pre-mixture C, pre-mixture D, methane (balance gas). Figure 7.2 shows the preparation scheme of the synthetic CMM mixture.

All substance transfers during the filling procedure were done by using temperature and pressure (or saturation pressure) differences only. No mechanical devices like, for example, a compressor, were employed. The mass of the gas portions added directly into the 10 dm^3 recipient cylinders during the filling was determined by using a high-precision mechanical gas balance (Voland model HCE 25, Voland Corp., New Rochelle NY, USA), whereas an electronic analytical balance (Sartorius CCE 2004, Sartorius AG, Göttingen, Germany) was used to determine the mass of minor components in smaller containers.

After the last gas portion had been added and weighed, the respective cylinder was finally homogenized by a procedure of subsequent heating and rolling. The target composition of the synthetic CMM was considered to be sufficiently stable based on the experience with mixtures of the same compounds and similar composition. The prepared final CMM mixture was decanted into the mentioned evacuated 5 dm^3 aluminum cylinder (BAM no.: 087). At this stage, the composition of the sample cylinder was validated for the first time. The applied analytical method was the so-called “bracketing method” according to the measurement protocol described in ISO 12963 [9].

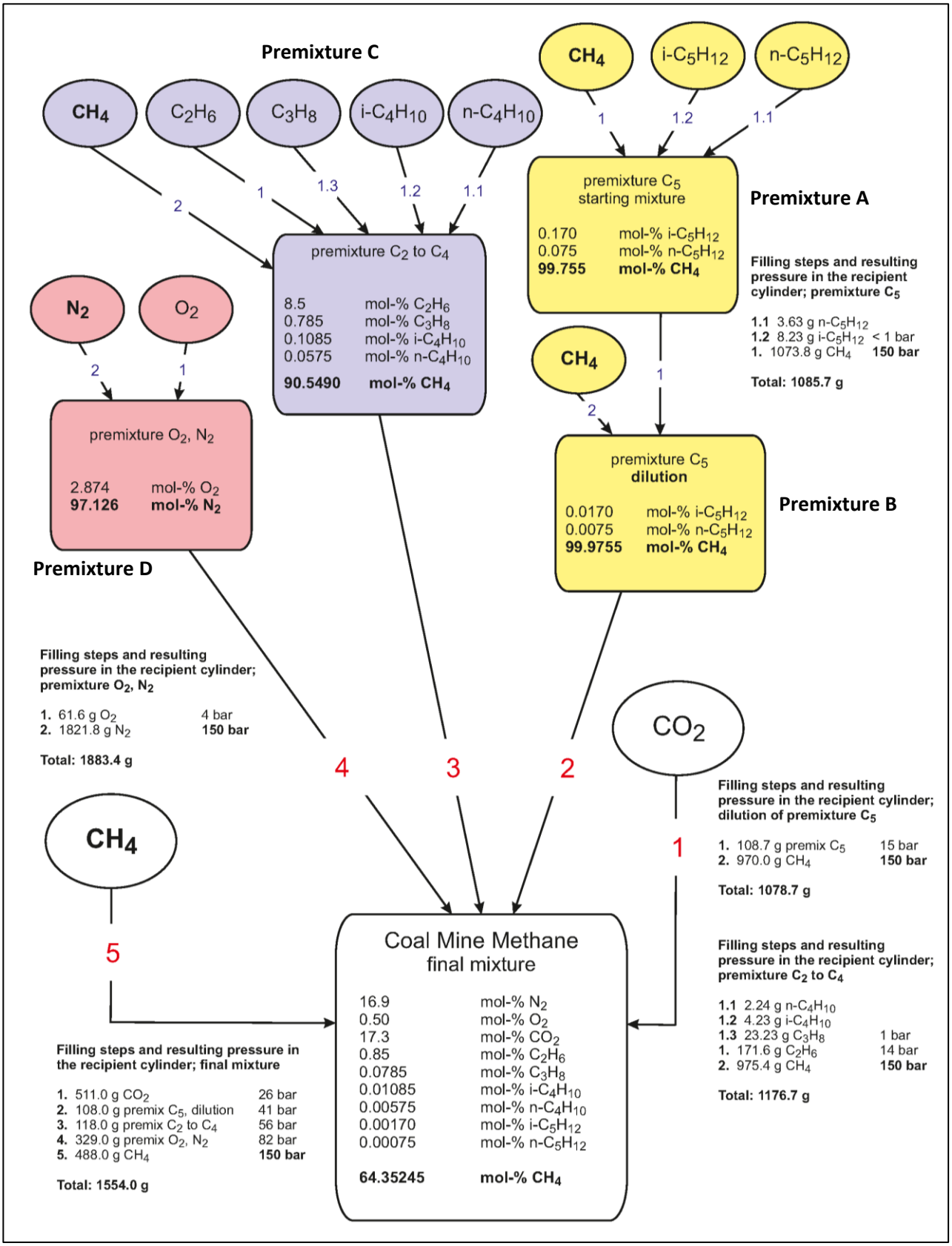

Figure 7.2. *Preparation scheme of the synthetic CMM mixture. BAM, Berlín, Germany.*

The composition of the samples was approximately ±5 % of the targeted composition. In the validation procedure, two GC analyzers were employed. The first instrument was a process GC (Siemens MAXUM II, Siemens AG, Karlsruhe, Germany) with a set of packed columns and TCDs designed for the analysis of natural gas samples. All compounds of the CMM sample could be analyzed. Table 7.3 gives the results of the GC analysis together with the expanded uncertainty.

Table 7.3. *Results of the first GC analysis of the synthetic CMM mixture.*

Componente	Concentration (molar fraction)		Relative deviation between gravimetric preparation and first GC analysis
	x_i	$U(x_i)$/% (k = 2)	%
Methane	0.64258731	0.047	0.079
Carbon dioxide	0.17352375	0.702	0.232
Nitrogen	0.16981633	0.098	–0.295
Ethane	0.00856491	0.738	1.167
Propane	0.00079081	0.862	1.187
i-Butane	0.00010760	2.503	0.412
n-Butane	0.00005800	1.729	1.579
i-Pentane	0.00001728	0.988	0.286
n-Pentane	0.00000757	1.639	0.620
Oxygen	0.00503861	0.257	–0.053

Due to the low content of C_4 and C_5, these compounds were analyzed a second time with higher resolution by a laboratory GC (Perkin-Elmer AutoSystem XL, The Perkin-Elmer Corp., Norwalk CT, USA) that was equipped with a CD-SIL-8-CB capillary column and a FID in addition to a TCD. Table 7.4 shows the results of a subsequent re-analysis at BAM that had been done after the comparison did not indicate any significant changes in the composition of the mixture.

Table 7.4. *Results of the second GC analysis of the synthetic CMM mixture.*

Component	Concentration (molar fraction)		Relative deviation between gravimetric preparation and second GC analysis
	x_i	$U(x_i)$/% (k = 2)	%
Methane	0.64275301	0.410	0.105
Carbon dioxide	0.17296253	0.461	–0.093
Nitrogen	0.16974036	0.626	–0.340
Ethane	0.00854686	0.955	0.954
Propane	0.00078875	1.167	0.923
i-Butane	0.00010862	1.328	1.363
n-Butane	0.00005807	1.057	1.690
i-Pentane	0.00001722	0.839	–0.043
n-Pentane	0.00000754	1.534	0.299
Oxygen	0.00503083	0.491	–0.207

7.3. EXPERIMENTAL PROCEDURE

The measurements reported in this work were carried out over the temperature range from (250 to 400) K and pressures up to 15 MPa. Seven isotherms were logged at (250, 275, 300, 325, 350, 375 and 400) K and decreasing pressure steps of 1 MPa between 1 and 15 MPa. the measured points of the studied CMM mixture are represented in Figure 7.3 together with the saturation curve and the range of validity of the GERG-2008 equation of state and the range of importance for the gas industry. Measurements could be done at the lowest limit of the temperature range since it was not close to the saturation curve of the studied mixture, thus avoiding any change in the composition due to the possible condensation of any of the mixture components in the colder parts of the densimeter. The maximum pressure achieved on each of the isotherms was determined by the initial pressure of the compressed mixture (which amounted to 4.9 MPa) that only allowed the pressurization of the measuring cell up to maximum 15 MPa by means of a manual pump. Each isotherm was measured from the highest pressure down to 1 MPa and was then followed by measurements of the sinker mass in vacuum.

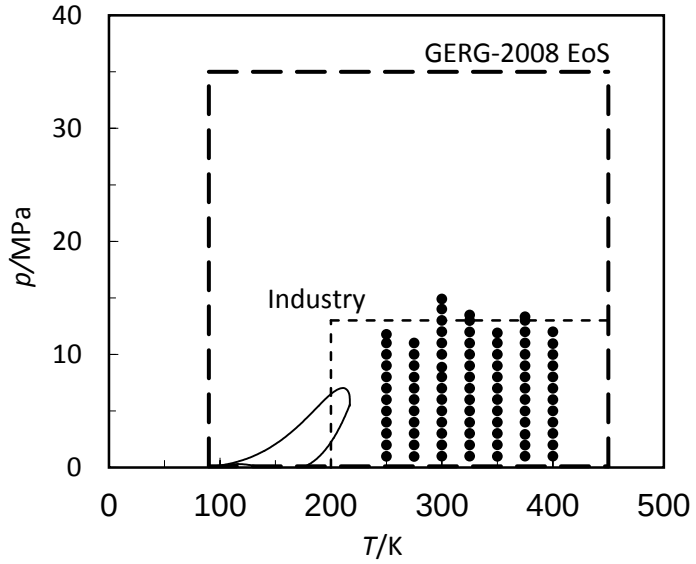

Figure 7.3. *pT-phase diagram showing the experimental points measured (●), the calculated saturation curve for the synthetic coal mine methane mixture, the temperature and pressure ranges of validity of the GERG-2008 equation of state (dashed line) and the area of interest for the storage, transport and utilization of gas fuels (thin dashed line).*

Test measurements with nitrogen were carried out in the whole working range of the apparatus, before and after measurements on the CMM mixture, to validate its operation by comparing the experimental results with the densities calculated from the reference equation of state for nitrogen by Span et al. [10]. Relative deviations of the experimental data from the calculated densities were within a less than 0.02% band, with an Absolute Average Deviation (*AAD*) of 0.011%. Results are shown in chapter 3.

The sinker mass in vacuum was measured after each of the isotherms performed for both nitrogen and the CMM mixture. The results showed that the maximum difference between the replicates of the sinker mass in vacuum at the same temperature was of 0.009%, corresponding to a temperature of 400K. This good repeatability of the measurements in vacuum confirmed that the magnetic coupling did not suffer any misalignment during the measurements.

7.4. EXPERIMENTAL RESULTS

Table 7.13 (section 7.8) shows the experimental results of the (p, ρ, T) measurements of the synthetic CMM mixture. Relative deviations from density values estimated by GERG-2008 [4] and AGA8-DC92 [3] equations of state, expanded uncertainty in density, and

overall expanded uncertainties (*k* = 2) are also included. Each pressure point of the isotherm is calculated as the average value of the last ten measurements on each pressure step.

Although the single-sinker densimeter is one of the most accurate methodologies for the measurement of the density of fluids, it presents some systematic errors which affect the final density result and must be evaluated. The two main effects are the force transmission error due to the magnetic coupling and the possible adsorption of gas molecules on the cell and sinker surfaces.

Force transmission error

This FTE consists of two terms: the apparatus effect and the fluid specific effect. In this work, the apparatus effect of the FTE was accounted for by measuring the sinker mass under vacuum for each isotherm. In the case of the fluid specific effect, its magnitude depends on the magnetic behavior of the measured gas, the difference between the sinker and the fluids densities and the specific constant of the apparatus. The specific constant of the apparatus was estimated in 45.7 ppm; that corresponds with a density correction of 0.005 % (see chapter 3.4 for further details). The magnetic susceptibility of the CMM mixture was estimated by using an additive law proposed by Bitter [11], according to equation 6.1. Magnetic susceptibility of CMM was $\chi_{CMM} = -2.9182 \cdot 10^{-10}$. According to this value, the CMM mixture does not present paramagnetic behavior (magnetic susceptibility of oxygen is $\chi_{O_2} = 1.78 \cdot 10^{-6}$). Since the value of magnetic susceptibility of the mixture is relatively low, the fluid magnetic behavior would be negligible in relation to the apparatus effect and therefore the fluid specific effect was not considered in our measurements.

Sorption effects in the measuring cell

On the other hand, adsorption of gas molecules can take place on the measuring cell walls or the sinker surface [12]. This effect is not compensated in the measurements performed on a single-sinker densimeter. Klimeck et al. [13] and Lösch-Will [14], among others, reported that this effect could only affect the accuracy of the measurements near the saturation curve or at very low gas densities, since only the adsorption on the sinker, and not that on the cell walls, had to be considered.

Test measurements to check for any adsorption effect on the experimental density value were carried out. These tests consisted in measuring 300 replicates (which corresponds approximately to 12 hours) of the density of the fluid at seven isotherms at (250, 275, 300, 325, 350, 375 and 400) K and relatively high pressures (10 - 11 MPa). Relative deviations of the experimental values from the GERG-2008 equation of state were analyzed for the adsorption test, instead of density values, to cancel any influence of the temperature or pressure of the fluid. For every isotherm the deviation of the experimental densities from the GERG-2008 equation of state along the duration of the test was constant. The maximum difference observed in relative deviation along the isotherms was less than 0.002%, which is one order of magnitude lower than the uncertainty in density, and therefore it was concluded that the adsorption effect could be neglected in our measurements.

7.5. VIRIAL COEFFICIENTS DETERMINATION

The second and the third virial coefficients for CMM mixture were calculated by fitting the experimental data to the virial expansion (equation 2.5). The fitting was done for each measured isotherm by using a generalised fitting package for the least squares analysis of data developed by Watson at the National Engineering Laboratory in Glasgow [15]. Results are detailed in Table 7.5 with the virial coefficients calculated by GERG-2008. The uncertainties of the fitted parameters were calculated according to the GUM [16] from standard deviation values returned by the software.

Table 7.5. *Least mean squares fitting results for synthetic CMM mixture (M_{virial}, B, C), with their uncertainties, and virial coefficients values estimated by the GERG-2008.*

T/K	M_{virial}/ g·mol^{-1}	ΔM/ g·mol^{-1}	$U(M)$/ g·mol^{-1}	B/ cm^3·mol^{-1}	$U(B)$/ cm^3·mol^{-1}	B_{GERG}/ cm^3·mol^{-1}	C/ cm^6·mol^{-2}	$U(C)$/ cm^6·mol^{-2}	C_{GERG}/ cm^6·mol^{-2}
250.034	23.124	0.029	0.019	-68.25	0.25	-68.62	3115	24	2976
275.001	23.133	0.019	0.012	-54.49	0.04	-54.72	2757	5	2719
299.947	23.142	0.010	0.012	-43.53	0.08	-43.71	2487	12	2495
324.963	23.141	0.011	0.013	-34.57	0.15	-34.76	2275	25	2312
349.952	23.134	0.018	0.013	-27.20	0.19	-27.37	2118	35	2166
374.941	23.134	0.018	0.013	-20.93	0.23	-21.17	1975	49	2048
400.005	23.129	0.023	0.014	-15.80	0.30	-15.88	1900	67	1953

T is the average temperature of each isotherm. ΔM is the difference between the gravimetric molar mass of the mixture M_{grav} (23.153 g·mol^{-1}*) and the fitted molar mass value* M_{virial}.

In the fitting process, some experimental values were identified as outliers because considering them during the fitting could not be done within the tolerance limits. This limit was 0.02 %, which is approximately the uncertainty in density of the densimeter. Experimental values measured at pressures above 10 MPa were outliers, so they were not used for the fitting. This can be because the number of parameters of the used virial expansion was inappropriate to model the experimental behavior over all the pressure range. The forth and even the fifth virial coefficients should be required, but in this case a new software tool and probably more experimental data would be needed.

In order to validate the fitted parameters, experimental pressure data were represented versus pressure calculated by the virial expansion. Figure 7.4 shows the results. As it can be observed, pressures above 10 MPa have higher deviations. Three "outliers" points were also identified below 10 MPa at 250 K, which were not used in the fitting. Therefore, the estimated virial coefficients are only valid for pressures up to 10 MPa.

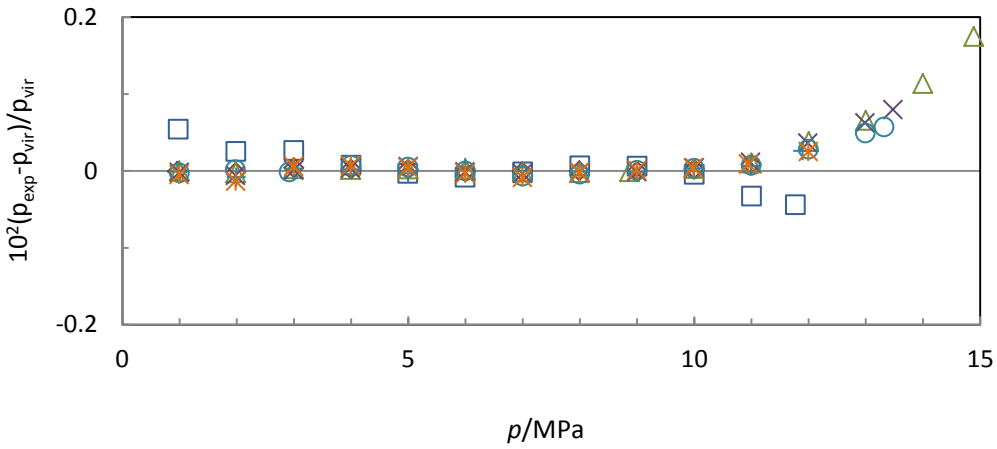

Figure 7.4. *Relative deviation of experimental pressure from pressure calculated by virial expansion (Eq. 4.16) by using the fitted parameters.* □ *250 K;* ◇ *275 K;* △ *300 K;* × *325;* + *350 K;* ○ *375 K;* ✳ *400 K.*

7.6. UNCERTAINTY ANALYSIS OF THE MEASUREMENTS

Chapter 4 contains a detailed uncertainty analysis which is summarized below.

The expanded uncertainty in temperature and pressure in the working range of the densimeter were less than 4 mK and 0.005 MPa, respectively. In terms of density, these values correspond to 0.0026 % and 0.070 % of the measured density, respectively.

The pressure uncertainty depends on the pressure transducer used. The pressure expanded uncertainty (k = 2) in the range of (2 - 20) MPa were calculated by equation 4.9 and pressure expanded uncertainty in the range of (0 - 2) MPa were calculated by equation 4.10.

Furthermore, the expanded uncertainty in density can be expressed as a density function by equation 4.12. According to the values of experimental density, the uncertainty in density was within (0.024 and 0.047) kg· m^{-3} or (0.023 and 0.345) %.

Temperature, pressure and composition uncertainties expressed in density units must be considered for the calculation of the overall uncertainty of the measurements $u_T(\rho)$ uncertainties in density. As it is expressed in chapter 4.7, the overall composition was calculated according to two different methods related to the calculation of the uncertainty of the composition.

The first one considers only the uncertainty of the concentration of the components given from the gravimetric preparation of the mixture. The overall standard uncertainty (k = 1) is given by equation 4.13.

The second method takes into account the unpredictable composition deviations that could occur inside the measuring cell, like sorption effects or an uncomplete homogenization of the mixture during the filling process, and also the uncertainty of the concentration of the components given from the gravimetric preparation of the mixture. In this case, the uncertainty in density due to uncertainties in the composition is calculated from the uncertainty in the molar mass of the mixture. The standard overall uncertainty in density is given by equation 4.14.

Molar mass uncertainty

Unpredictable effects above mixture composition inside the measuring cell can be taken into account by estimating the molar mass of the mixture inside the measuring cell through the virial analysis M_{virial}.

The combined uncertainty of the mixture composition was calculated by using equation 4.15, and considering all sources of uncertainty related to the molar mass of the mixture (see chapter 4.7).

The estimation of the uncertainty of the molar mass of the mixture due to uncertainties in the atomic weights of the involved components of the mixture $u(M_{atomic})$ was obtained from the 2011 IUPAC report by Wieser et al. [17]. Table 7.6 shows the molar mass uncertainties of the CMM mixture components.

Table 7.6. *Molar mass of CMM mixture components and their uncertainties* [17].

Substance	M_i /g·mol-1	$u(M_i)$ /g·mol-1	$u(M_i)/M_i$ /ppm
Methane	16.0428	0.00085	53
Nitrogen	28.01348	0.00040	14
Oxygen	31.9988	0.00060	19
Carbon dioxide	44.0098	0.00100	23
Ethane	30.06904	0.00165	55
Propane	44.09562	0.00246	56
Butane	58.1222	0.00328	56
Isobutane	58.1222	0.00328	56
Pentane	72.14878	0.00409	57
Isopentane	72.14878	0.00409	57

The uncertainty of the molar mass due to uncertainties in the gravimetric composition of the mixture $u(M_{grav})$ was calculated by equation 4.16 [18]. Finally, the uncertainty associated to changes in the composition inside the measuring cell $u(M_{sorp})$ was calculated by equation 4.17 from molar mass value estimated by the virial fitting. Molar mass uncertainties are summarized in Table 7.7.

Table 7.7. *Uncertainty budget of the composition associated to the molar mass of the synthetic CMM mixture.*

Source of uncertainty	Units	Contribution
$u(M_{atomic})$ (Table 7.6) [17]	g·mol^{-1}	0.0008
$u(M_{grav})$ (Eq. 4.16) [18]	g·mol^{-1}	0.0128
$u(M_{sorp})$ (Eq. 4.17)	g·mol^{-1}	0.0194
Standard combined uncertainty (k = 1) (Eq. 4.15)		0.023
Expanded combined uncertainty (k = 2)		0.047

Overall uncertainty of the measurements

Table 7.8 shows the contributions to the expanded overall uncertainty (k = 2) of the experimental magnitudes involved in density determination. The contribution of the mixture composition is detailed from gravimetric composition uncertainties and also from the virial expansion analysis described in chapter 4.7.

Table 7.8. *Contributions to the expanded overall uncertainty in density (k = 2) for synthetic CMM mixture.*

Source of uncertainty	Units	Contribution (k = 2)	Estimation in density (k = 2)	
			kg·m^{-3}	%
Temperature	K	0.004	< 0.001	< 0.015
Pressure	MPa	0.005	(0.005 - 0.048)	(0.005 - 0.140)
Density	kg·m^{-3}	(0.024 - 0.047)	(0.023 - 0. 047)	(0.023 - 0.345)
Gravimetric composition	mol·mol^{-1}	<0.003	< 0.074	(0.001 - 0.018)
Virial expansion composition	g·mol^{-1}	0.0465	(0.007 - 0.206)	0.101
		$U_{T1}(\rho)$ gravimetric	(0.027 - 0.400)	(0.148 - 0.388)
		$U_{T2}(\rho)$ virial	(0.028 - 0.425)	(0.028 - 0.425)

The overall expanded uncertainty (k = 2) $U_{T1}(\rho)$, calculated by Eq. 4.13, is within (0.027 and 0.400) kg·m^{-3} or (0.148 and 0.388) %, expressed in percentage. The overall expanded uncertainty from virial fitting and calculated from Eq. 4.14 $U_{T2}(\rho)$ is within (0.028 y 0.425) kg·m^{-3} or (0.205 y 0.540) %.

7.7. DISCUSSION

Virial fitting of experimental data

When the pressure trends to zero, all gases have ideal gas behavior, so that the compressibility factor is Z = 1. Thus, the deviation of experimental density data from equations of state, represented in Figures 7.6 and 7.7, must tend to zero when pressure is closed to zero. An opposite behavior indicates a possible error in the experimental data. A coherent interpretation of this kind of deviations is that the composition could change

inside the measuring cell due to sorption effects, gas stratification or a poor homogenization of the mixture.

The estimated values for the measured CMM synthetic mixtures when the pressure is closed to zero (intersection with ordinate axis) are shown in Table 7.9.

Table 7.9. *Estimated deviations of the experimental densities from the GERG-2008 equation of state when pressure is zero.*

Isotherm	250 K	275 K	300 K	325 K	350 K	375 K	400 K
$10^2(\rho_{exp}-\rho_{EoS})/\rho_{EoS}$	–0.206	–0.074	–0.034	–0.033	–0.067	–0.076	–0.080
R^2	0.996	0.999	0.996	0.982	0.940	0.927	0.771

The largest deviation was registered in the 250 K isotherm with a value of –0.206 %, while the rest of isotherms had absolute deviations lower than 0.08 %. This deviation could be a consequence of an imperfect homogenization of the mixture in the measuring cell during the recording of the isotherm due to the stratification of the gases in the cylinder. The deviation can also be observed in Table 7.5 attending to the difference between the estimated molar mass by virial fitting and the calculated molar mass calculated from the gravimetric composition at 250 K (0.029 $g \cdot mol^{-1}$). Therefore, the expanded overall uncertainty of the measurements considering the virial fitted value for molar mass is slightly higher than the overall uncertainty calculated with gravimetric composition uncertainty, especially at low pressures. This difference is smaller in the rest of the isotherms.

Regarding the estimation of the virial coefficients, it can be observed, in Table 7.5, that the virial coefficients estimated from experimental data and the virial coefficients calculated from GERG-2008 are very close, but their differences are slightly larger than the estimated uncertainties for most of the isotherms. Figure 7.5 shows the variation of the calculated virial coefficients with temperature.

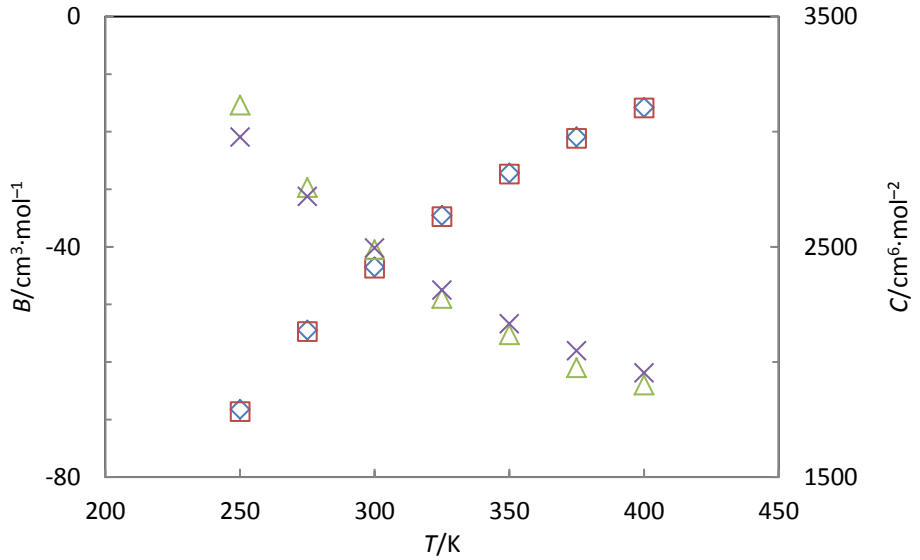

Figure 7.5 *Variation of the calculated virial coefficients with temperature.* ◇ B_{Virial}, □ B_{GERG}, △ C_{Virial} *y* × C_{GERG}.

Relative deviation of experimental data from reference equations of state

Figure 7.6 and 7.7 show the relative deviations of the experimental density from the estimated densities from the GERG-2008 equation of state and the AGA8-DC92, respectively.

As it can be observed in Figure 7.6, relative deviations are within a 0.2 % band for isotherms between (300 and 400) K. The same behavior can be observed for the isotherm of 275 K at pressures below 10 MPa. However, data measured at 250 K and at 275 K and pressures above 10 MPa show increasing negative deviations from the equation of state with pressure, reaching a maximum relative deviation of -0.545 %. About 86 % of the data are within a ±0.2 % band.

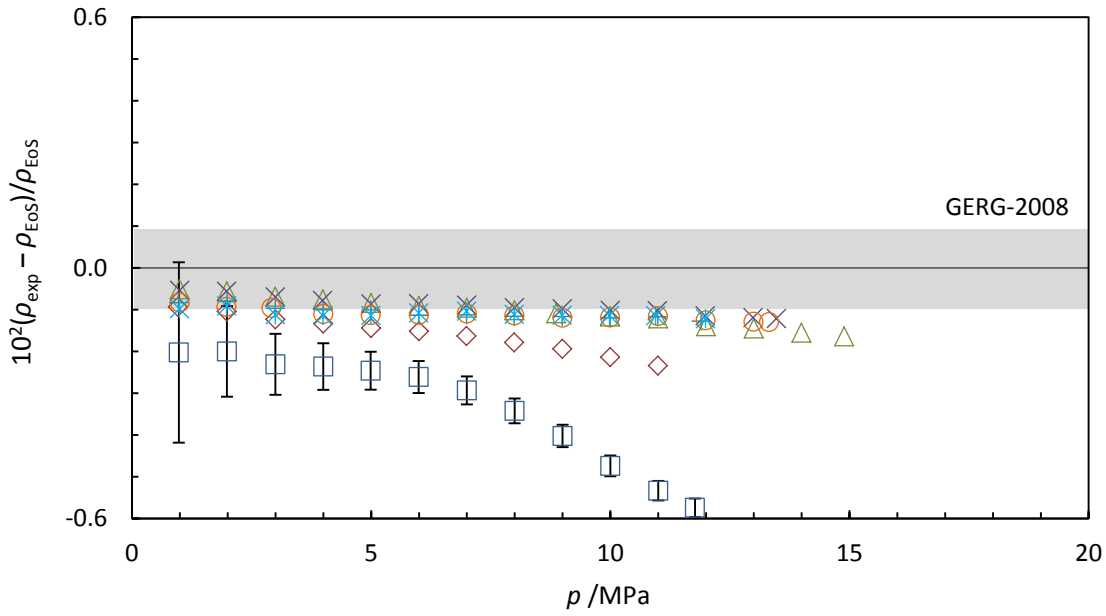

Figure 7.6. *Relative deviations in density of experimental (p, ρ, T) data of the synthetic CMM mixture ρ_{exp} from density values calculated from the GERG-2008 equation of state ρ_{EoS} versus pressure: □ 250 K; ◇ 275 K; △ 300 K; × 325; + 350 K; ○ 375 K; ✳ 400 K. Error bars on the 250 K isotherm indicate the expanded uncertainty (k = 2) of the experimental data. Dark bar corresponds to the uncertainty of the GERG-2008 (0.1 %)* [4].

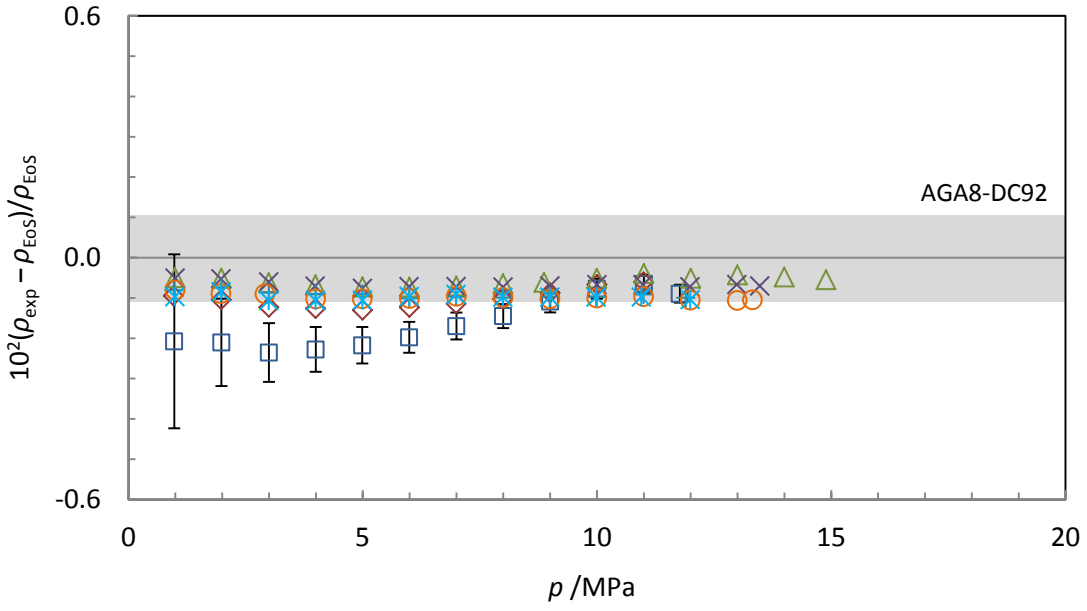

Figure 7.7. *Relative deviations in density of experimental (p, ρ, T) data of the synthetic CMM mixture ρ_{exp} from density values calculated from the AGA8-DC92 equation of state ρ_{EoS} versus pressure: □ 250 K; ◇ 275 K; △ 300 K; × 325; + 350 K; ○ 375 K; ✳ 400 K. Error bars on the 250 K isotherm indicate the expanded uncertainty (k = 2) of the experimental data. Dark bar corresponds to the uncertainty of the AGA8-DC92* [3].

According to Kunz and Wagner [4], the uncertainty of GERG-2008 equation of state for gas mixtures in the temperature range of (250 to 450) K and pressures up to 35 MPa is 0.1 %. This uncertainty is valid for enriched natural gases with nitrogen, carbon dioxide, oxygen, carbon monoxide or considerable amounts of heavy hydrocarbons. However, systematic deviations exceeding 0.3 % had been previously observed for rich natural gases with carbon dioxide contents higher than 0.14 % [19]. Therefore, this behavior was expected. Results also show that only 7 % of the data have higher deviations than 0.3 % and all of these data were registered at 250 K.

Deviations from the AGA8-DC92 were very similar to those of the GERG-2008, and even lower. In this case, about 94 % of data are within ±0.2 % band and 69 % are within ±0.1 % band. The maximum registered deviation was –0.235 %.

The AGA8-DC92 equation of state is designed for the estimation of thermophysical properties of different natural gases. The reported uncertainty in density is 0.1 % at temperatures above 290 K and pressures up to 12 MPa. However, it recognizes higher uncertainties for enriched gases, especially at lower temperatures [4]. Therefore, experimental data agreed also with the uncertainty of this equation.

A statistical analysis was carried out on the density deviation data from both equations of state. The average absolute deviation (*AAD*), average deviation (*Bias*), and root mean squared (*RMS*) were calculated by using equations 3.22, 3.23 and 3.24. The maximum relative deviation (*MaxD*) in the data set was also calculated. Results are given in Table 7.10.

Table 7.10. *Statistical parameters of the data set with respect to the GERG-2008 and AGA8-DC92 equations of state.*

Statistical parameter	GERG-2008	AGA8-DC92
AAD	0.140	0.095
Bias	–0.140	–0.095
RMS	0.166	0.103
MaxD/%	–0.545	–0.235

Comparison with literature data

As it has been mentioned in section 7.1, (p, ρ, T) data of mixtures of CMM type or mixtures with similar compositions were not found on the literature. Therefore results were compared to three synthetic natural gas mixtures with similar components but different composition. These works were performed by Patil et al. [20] and Atilhan et al. [21], by using a single-sinker densimeter, and by McLinden [22] by using a two-sinker densimeter.

Table 7.11. *Working range and composition of the synthetic CMM mixture of this work and synthetic samples of natural gas studied by* Patil, *Atilhan and McLinden.*

Component	CMM	Patil et al. [20]	Atilhan et al. [21]	McLinden [22]
	(250 - 400) K 15 MPa	(270 - 340) K 34.5 MPa	(250, 350 and 400) K 37 MPa	
	x_i	x_i	x_i	x_i
Methane	0.64208	0.90991	0.89982	0.89990
Carbon dioxide	0.17312	0.00403	0.01701	0.01707
Nitrogen	0.17032	0.02031	0.01697	0.01699
Ethane	0.00847	0.02949	0.03009	0.03150
Propane	0.00078	0.01513	0.01506	0.01583
Isobutane	0.00011	0.00755	0.00752	0.00781
Butane	0.00006	0.00755	0.00753	0.00790
Isopentane	0.00002	0.00299	0.00300	0.00150
Pentane	0.00001	0.00304	0.00300	0.00150
Oxygen	0.00504	-	-	-

The working ranges of the experiments and the composition of the studied mixtures are detailed in Table 7.11. The main difference between the selected mixtures, apart from a lower methane content, is the absence of oxygen. Moreover, the concentration of CO_2 in the CMM mixture is ten times higher than that in the natural gas samples.

Figure 7.8 shows deviations of experimental densities of each mixture from the values estimated by GERG-2008 equation of state in a pressure range up to 20 MPa.

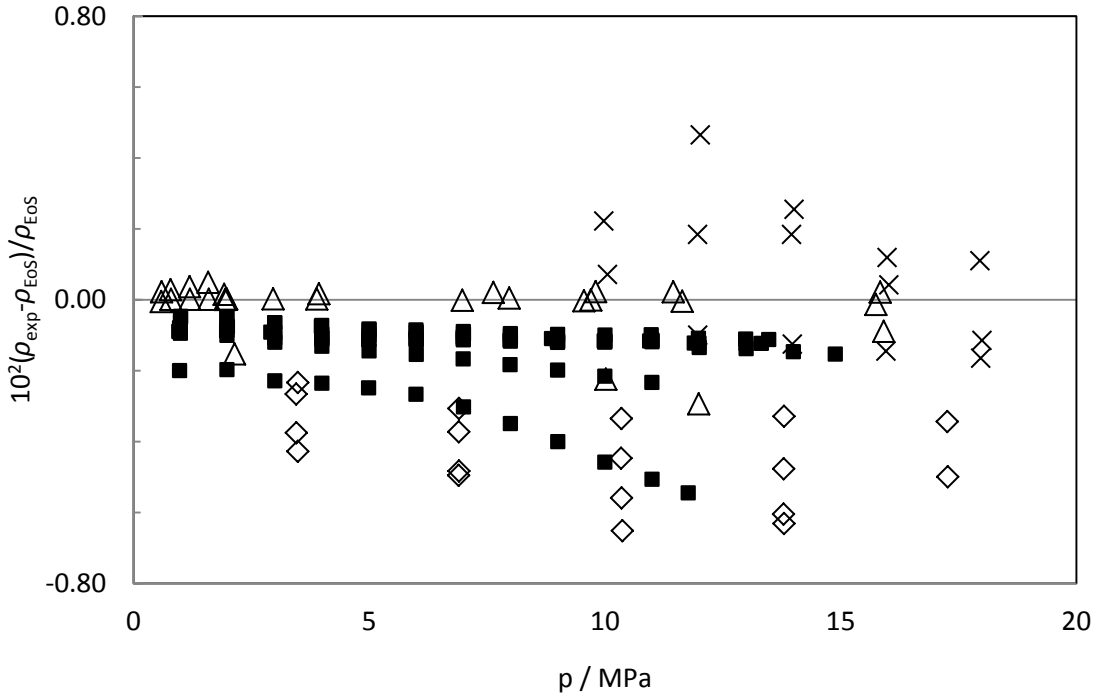

Figure 7.8. *Deviations of experimental densities from GERG-2008 equation of state:* ■ *CMM* this work, ◇ *Patil et al.,* × *Atilhan et al.* [21] *and* △ *McLinden* [22].

As it can be observed, in the three natural gas mixtures the qualitative behavior detected in the data of CMM is reproduced, finding lower deviations at high temperatures and lower pressures. Deviations of natural gas at high pressures deviations are higher, reaching maximum values from 0.29 % (McLinden) to 0.60 % (Patil). Negative deviations prevail in the experiences of McLinden and Patil, as in the case of CMM mixture. In summary, all experimental data of the natural gas mixtures are in the same range of deviation than the values of the CMM mixture. According to this, it can be assumed that there are not systematic errors in the data set of this work.

Finally, a comparative analysis of the uncertainties and statistical data of these experiences is presented in Table 7.12. It shows the amount of methane, the year of publication of the studies, the expanded uncertainty in density (k = 2) $U\left(\rho_{\exp}\right)$ calculated by equation 4.11, the number of evaluated points *n,* the average absolute deviation (*AAD)* and the root mean squared (*RMS*), calculated by equations 3.22 and 3.24, respectively, and the maximum relative deviation (*MaxD*).

Table 7.12. *Statistical comparison of density measurements of mixtures represented in Figure 7.7.*

Experiment	Year	x_{CH_4}	$U(\rho_{exp})$ (k =2)	*n*	*AAD*	*RMS*	*MaxD*/%
This work	2013	0.64208	0.38%	90	0.1395	0.1664	–0.545
Patil et al. [20]	2007	0.90991	0.12%	18	0.4354	0.4519	–0.652
Atilhan et al. [21]	2011	0.89982	0.13%	17	0.1724	0.1959	0.465
McLinden [22]	2011	0.89990	0.02%	28	0.0379	0.0792	–0.294

In view of these data, it can be concluded that the most accurate results were obtained by the two-sinker densimeter of McLinden, given that the uncertainty and the dispersion of data are smaller. However, focusing only on the data obtained from single-sinker densimeters, the dispersion of the data for the CMM mixture is less than the others, even for a higher data-set. In any case, the obtained results are within the expected deviations for a fluid with the characteristics of the studied synthetic CMM mixture.

7.8. TABLE OF RESULTS

Table 7.13. *Experimental (p, ρ, T) measurements for the synthetic CMM mixture, relative and absolute expanded uncertainty in density (k = 2) $U(\rho_{exp})$, expanded overall uncertainty in density (k = 2) from gravimetric composition $U_{T1}(\rho_{exp})$ and from virial expansion $U_{T2}(\rho_{exp})$ and relative deviations from the GERG-2008 and AGA8-DC92 equations of state; where T is the temperature (ITS-90* [23]*), p the pressure, ρ_{exp} the experimental density and ρ_{EoS} the density calculated from both equations of state.*

T/K	*p*/MPa	ρ_{exp}/ kg·m^{-3}	$U(\rho_{exp})$ kg·m^{-3}	$U(\rho_{exp})$ %	$U_{T1}(\rho_{exp})$ kg·m^{-3}	$U_{T2}(\rho_{exp})$ (kg·m^{-3})	$10^2(\rho_{exp}-\rho_{EoS})/\rho_{EoS}$	
							GERG-2008	AGA8-DC92
250.034	11.769	204.657	0.023	0.023	0.400	0.425	–0.545	–0.089
250.033	11.002	188.047	0.022	0.024	0.362	0.393	–0.506	–0.066
250.033	9.999	165.832	0.021	0.025	0.307	0.350	–0.458	–0.077
250.032	9.001	143.853	0.020	0.028	0.253	0.306	–0.401	–0.109
250.032	7.998	122.572	0.019	0.030	0.207	0.264	–0.349	–0.145
250.037	7.000	102.676	0.017	0.034	0.172	0.224	–0.302	–0.170
250.035	5.992	84.052	0.016	0.039	0.145	0.186	–0.267	–0.197
250.035	4.989	66.990	0.015	0.046	0.122	0.152	–0.249	–0.217
250.033	3.998	51.496	0.015	0.056	0.102	0.122	–0.236	–0.228
250.034	2.998	37.099	0.014	0.074	0.083	0.095	–0.229	–0.235
250.035	1.984	23.628	0.013	0.110	0.047	0.072	–0.198	–0.210
250.035	0.977	11.229	0.012	0.218	0.031	0.054	–0.200	–0.207
275.005	10.997	145.092	0.020	0.027	0.224	0.302	–0.233	–0.060
275.004	10.000	129.474	0.019	0.029	0.201	0.271	–0.216	–0.067
275.004	8.999	114.041	0.018	0.032	0.179	0.241	–0.199	–0.087
275.003	7.991	98.899	0.017	0.035	0.159	0.211	–0.183	–0.103
275.003	6.995	84.470	0.016	0.039	0.141	0.182	–0.167	–0.114
275.001	6.000	70.637	0.016	0.044	0.123	0.155	–0.155	–0.123
275.000	4.998	57.338	0.015	0.052	0.106	0.129	–0.145	–0.130
274.999	3.998	44.693	0.014	0.063	0.090	0.105	–0.131	–0.126
274.999	2.999	32.680	0.013	0.082	0.074	0.084	–0.120	–0.123
274.999	1.983	21.055	0.013	0.122	0.044	0.064	–0.101	–0.104
274.999	0.961	9.952	0.012	0.245	0.030	0.049	–0.089	–0.094
299.947	14.891	169.317	0.021	0.025	0.251	0.348	–0.154	–0.055
299.945	13.999	158.524	0.021	0.026	0.236	0.326	–0.147	–0.048

299.947	12.999	146.248	0.020	0.027	0.219	0.302	–0.138	–0.043
299.947	12.004	133.932	0.019	0.029	0.203	0.278	–0.135	–0.051
299.946	11.002	121.532	0.019	0.030	0.187	0.253	–0.119	–0.039
299.945	9.998	109.144	0.018	0.033	0.171	0.228	–0.116	–0.051
299.945	8.871	95.403	0.017	0.036	0.154	0.201	–0.110	–0.061
299.948	7.998	84.943	0.016	0.039	0.140	0.181	–0.103	–0.065
299.946	7.001	73.225	0.016	0.043	0.125	0.158	–0.097	–0.070
299.947	6.000	61.751	0.015	0.049	0.110	0.135	–0.091	–0.073
299.949	4.998	50.587	0.014	0.057	0.096	0.114	–0.083	–0.073
299.951	3.993	39.726	0.014	0.070	0.081	0.094	–0.073	–0.067
299.951	2.995	29.291	0.013	0.091	0.067	0.075	–0.065	–0.062
299.949	1.985	19.069	0.013	0.133	0.041	0.059	–0.051	–0.051
299.949	0.997	9.413	0.012	0.258	0.029	0.046	–0.047	–0.049
324.963	13.475	131.488	0.019	0.029	0.201	0.271	–0.113	–0.070
324.963	12.987	126.456	0.019	0.030	0.194	0.261	–0.111	–0.066
324.964	11.987	116.116	0.018	0.031	0.181	0.241	–0.109	–0.072
324.964	10.985	105.759	0.018	0.033	0.168	0.220	–0.099	–0.067
324.964	10.003	95.616	0.017	0.036	0.154	0.200	–0.100	–0.067
324.963	8.998	85.302	0.016	0.039	0.141	0.180	–0.098	–0.070
324.962	7.997	75.123	0.016	0.042	0.128	0.160	–0.096	–0.073
324.961	6.997	65.087	0.015	0.047	0.114	0.140	–0.090	–0.071
324.962	5.992	55.151	0.015	0.053	0.101	0.121	–0.086	–0.072
324.962	4.998	45.499	0.014	0.062	0.088	0.103	–0.085	–0.076
324.962	3.986	35.864	0.014	0.076	0.074	0.085	–0.076	–0.070
324.962	2.997	26.649	0.013	0.098	0.062	0.069	–0.065	–0.060
324.963	1.979	17.383	0.013	0.145	0.039	0.054	–0.051	–0.053
324.963	0.997	8.647	0.012	0.280	0.029	0.043	–0.050	–0.051
349.950	11.898	102.688	0.017	0.034	0.165	0.213	–0.123	–0.099
349.951	10.997	94.605	0.017	0.036	0.154	0.197	–0.114	–0.091
349.951	9.999	85.640	0.016	0.038	0.142	0.179	–0.119	–0.097
349.950	8.998	76.673	0.016	0.042	0.130	0.162	–0.117	–0.097
349.949	7.997	67.752	0.015	0.046	0.118	0.144	–0.117	–0.099
349.952	6.997	58.906	0.015	0.051	0.105	0.127	–0.114	–0.097
349.952	5.998	50.147	0.014	0.058	0.093	0.110	–0.114	–0.101

349.953	4.997	41.473	0.014	0.067	0.081	0.094	–0.100	–0.090
349.955	3.997	32.914	0.013	0.082	0.069	0.079	–0.098	–0.090
349.956	2.998	24.481	0.013	0.106	0.058	0.064	–0.093	–0.087
349.954	1.993	16.133	0.013	0.155	0.037	0.051	–0.076	–0.074
349.955	0.978	7.846	0.012	0.307	0.028	0.041	–0.079	–0.080
374.944	13.319	104.451	0.018	0.034	0.169	0.216	–0.123	–0.104
374.942	12.993	101.862	0.017	0.034	0.165	0.211	–0.124	–0.106
374.939	11.994	93.907	0.017	0.036	0.154	0.195	–0.123	–0.105
374.942	10.996	85.936	0.016	0.038	0.143	0.179	–0.115	–0.096
374.941	9.996	77.924	0.016	0.041	0.132	0.164	–0.120	–0.100
374.940	8.997	69.928	0.016	0.045	0.121	0.148	–0.121	–0.102
374.941	7.996	61.931	0.015	0.049	0.110	0.132	–0.116	–0.099
374.940	6.999	53.999	0.015	0.054	0.098	0.117	–0.111	–0.096
374.940	5.998	46.067	0.014	0.062	0.087	0.102	–0.113	–0.101
374.941	4.990	38.140	0.014	0.072	0.076	0.087	–0.112	–0.102
374.941	3.998	30.398	0.013	0.088	0.065	0.073	–0.107	–0.102
374.943	2.915	22.028	0.013	0.117	0.054	0.059	–0.092	–0.090
374.943	1.975	14.842	0.012	0.168	0.036	0.048	–0.088	–0.089
374.941	0.996	7.441	0.012	0.323	0.027	0.039	–0.079	–0.080
400.004	11.994	86.193	0.017	0.038	0.144	0.179	–0.123	–0.104
400.002	10.949	78.637	0.016	0.041	0.134	0.164	–0.117	–0.097
400.006	9.984	71.632	0.016	0.044	0.124	0.151	–0.117	–0.097
400.003	8.995	64.443	0.015	0.047	0.113	0.137	–0.116	–0.098
400.003	7.995	57.168	0.015	0.052	0.103	0.122	–0.114	–0.098
400.004	6.995	49.914	0.014	0.058	0.092	0.108	–0.106	–0.091
400.005	5.996	42.669	0.014	0.066	0.082	0.095	–0.108	–0.096
400.003	4.996	35.442	0.014	0.077	0.071	0.081	–0.113	–0.105
400.007	3.996	28.250	0.013	0.094	0.061	0.068	–0.112	–0.106
400.006	2.997	21.113	0.013	0.121	0.052	0.056	–0.108	–0.106
400.006	1.982	13.911	0.012	0.178	0.035	0.046	–0.086	–0.085
400.007	0.994	6.948	0.012	0.345	0.027	0.038	–0.095	–0.097

7.9. REFERENCES

[1] D. Creedy and H. Tilley, “Coalbed methane extraction and utilization,” *Proc. Inst. Mech. Eng. Part A J. Power Energy*, vol. 217, no. 1, pp. 19–25, Jan. 2003.

[2] O. Boucher, P. Friedlingstein, B. Collins, and K. P. Shine, “The indirect global warming potential and global temperature change potential due to methane oxidation,” *Environ. Res. Lett.*, vol. 4, no. 4, 2009.

[3] K. E. Starling and J. L. Savidge, “Compressibility factors of natural gas and other related hydrocarbon gases - AGA Transmission Measurement Committee Report 8,” 1992.

[4] O. Kunz and W. Wagner, “The GERG-2008 Wide-Range Equation of State for Natural Gases and Other Mixtures: An Expansion of GERG-2004,” *J. Chem. Eng. Data*, 2012.

[5] “Characterization of energy gases: EMRP ENG01 N 912/2009/EC (2010-2013),” European Metrology Research Programme.

[6] F. Haloua, E. Foulon, E. El-Harti, S. M. Sarge, J. Rauch, M. Neagu, A. S. Brown, and D. Tuma, “Comparison of traceable methods for determining the calorific value of non-conventional fuel gases,” *Int. J. Therm. Sci.*, vol. 100, pp. 438–447, Feb. 2016.

[7] “ISO 6142 - Preparation of calibration gas mixtures - Gravimetric method. International Organisation for Standardization, Geneva, 2001).” 2001.

[8] “Lemmon, E.W., Huber, M.L., McLinden, M.O. NIST Standard Reference Database 23: Reference Fluid Thermodynamic and Transport Properties-REFPROP, Version 9.1, National Institute of Standards and Technology, Standard Reference Data Program, Gaithersburg, 2013.” .

[9] “ISO/CD 12963 Gas analysis – Comparison methods for the determination of the composition of gas mixtures based on one- and two-point calibration, International Organization for Standardization, Geneva.”

[10] R. Span, E. W. Lemmon, R. T. Jacobsen, and W. Wagner, “A reference quality equation of state for nitrogen,” *Int. J. Thermophys.*, vol. 19, no. 4 SPEC.ISS., pp. 1121–1132, 1998.

[11] F. Bitter, “The Magnetic Susceptibilities of Several Organic Gases,” *Phys. Rev.*, vol. 33, no. 3, pp. 389–397, Mar. 1929.

[12] M. Richter and R. Kleinrahm, “Influence of adsorption and desorption on accurate density measurements of gas mixtures,” *J. Chem. Thermodyn.*, Mar. 2014.

[13] J. Klimeck, R. Kleinrahm, and W. Wagner, “An accurate single-sinker densimeter and measurements of the (p, ρ, T) relation of argon and nitrogen in the temperature range from (235 to 520) K at pressures up to 30 MPa,” *J. Chem. Thermodyn.*, vol. 30, no. 12, pp. 1571–1588, 1998.

[14] M. O. McLinden and C. Lösch-Will, “Apparatus for wide-ranging, high-accuracy fluid (p, ρ, T) measurements based on a compact two-sinker densimeter,” *J. Chem. Thermodyn.*, vol. 39, no. 4, pp. 507–530, 2007.

[15] J. T. R. Watson and National Engineering Laboratory-FPT Division, “‘A generalised fitting package for the least squares analysis of data’.” East Kilbride, Glasgow G75 0QU, Scotland., 1991.

[16] I. E. C. BIPM IFCC, ISO, IUPAC, IUPAP and OIML, “Guide to the Expression of Uncertainty in Measurement,” *Guid. to Expr. Uncertain. Meas.*, 1995.

[17] M. E. Wieser, N. Holden, T. B. Coplen, J. K. Böhlke, M. Berglund, W. A. Brand, P. De Bièvre, M. Gröning, R. D. Loss, J. Meija, T. Hirata, T. Prohaska, R. Schoenberg, G. O’Connor, T. Walczyk, S. Yoneda, and X.-K. Zhu, “Atomic weights of the elements 2011 (IUPAC Technical Report),” *Pure Appl. Chem.*, vol. 85, no. 5, pp. 1047–1078, Jan. 2013.

[18] M. Richter and M. O. McLinden, “Vapor-Phase (p, ρ, T, x) Behavior and Virial Coefficients for the (Methane + Propane) System,” *J. Chem. Eng. Data*, vol. 59, no. 12, pp. 4151–4164, Dec. 2014.

[19] O. Kunz, R. Klimeck, W. Wagner, and M. Jaeschke, “The GERG-2004 Wide-Range Reference Equation of State for Natural Gases and Other Mixtures,” *GERG Tech. Monogr. Fortschritt-Berichte VDI*, 2007.

[20] P. Patil, S. Ejaz, M. Atilhan, D. Cristancho, J. C. Holste, and K. R. Hall, “Accurate density measurements for a 91% methane natural gas-like mixture,” *J. Chem. Thermodyn.*, vol. 39, no. 8, pp. 1157–1163, Aug. 2007.

[21] M. Atilhan, S. Aparicio, S. Ejaz, D. Cristancho, I. Mantilla, and K. R. Hall, “p –ρ– T Behavior of Three Lean Synthetic Natural Gas Mixtures Using a Magnetic Suspension Densimeter and Isochoric Apparatus from (250 to 450) K with Pressures up to 150 MPa: Part II,” *J. Chem. Eng. Data*, vol. 56, no. 10, pp. 3766–3774, Oct. 2011.

[22] M. O. McLinden, “P-ρ- T behavior of four lean synthetic natural-gas-like mixtures from 250 K to 450 K with pressures to 37 MPa,” *J. Chem. Eng. Data*, vol. 56, no. 3, pp. 606–613, 2011.

[23] C. A. S. R L Rusby and R P Hudson and M Durieux and J F Schooley and P P M Steur and, “Thermodynamic Basis of the ITS-90,” *Metrologia*, vol. 28, no. 1, p. 9, 1991.

[24] Setzmann, U. and Wagner, W.,"A New Equation of State and Tables of Thermodynamic Properties for Methane Covering the Range from the Melting Line to 625 K at Pressures up to 1000 MPa," *J. Phys. Chem. Ref. Data*, 20(6):1061-1151, 1991.

[25] Span, R. and Wagner, W., "A New Equation of State for Carbon Dioxide Covering the Fluid Region from the Triple-Point Temperature to 1100 K at Pressures up to 800 MPa," *J. Phys. Chem. Ref. Data*, 25(6):1509-1596, 1996.

[26] Span, R., Lemmon, E.W., Jacobsen, R.T, Wagner, W., and Yokozeki, A. "A Reference Equation of State for the Thermodynamic Properties of Nitrogen for Temperatures from 63.151 to 1000 K and Pressures to 2200 MPa," J. Phys. Chem. Ref. Data, 29(6):1361-1433, 2000.

[27] Buecker, D. and Wagner, W. "A Reference Equation of State for the Thermodynamic Properties of Ethane for Temperatures from the Melting Line to 675 K and Pressures up to 900 MPa,"J. Phys. Chem. Ref. Data, 35(1): 205-266, 2006.

[28] Lemmon, E.W., McLinden, M.O., Wagner, W. "Thermodynamic Properties of Propane. III. A Reference Equation of State for Temperatures from the Melting Line to 650 K and Pressures up to 1000 MPa,"J. Chem. Eng. Data, 54: 3141-3180, 2009.

[29] Buecker, D. and Wagner, W., "Reference Equations of State for the Thermodynamic Properties of Fluid Phase n-Butane and Isobutane,"J. Phys. Chem. Ref. Data, 35(2): 929-1019, 2006.

[30] Lemmon, E.W. and Span, R.,"Short Fundamental Equations of State for 20 Industrial Fluids,"J. Chem. Eng. Data, 51: 785-850, 2006.

[31] Span, R. and Wagner, W. "Equations of State for Technical Applications. II. Results for Nonpolar Fluids,"Int. J. Thermophys., 24(1): 41-109, 2003.

[32] Schmidt, R. and Wagner, W., "A New Form of the Equation of State for Pure Substances and its Application to Oxygen,"Fluid Phase Equilibria, 19:175-200, 1985.

CHAPTER 8

Thermodynamic characterization of a synthetic biogas-like mixture (50 mol-% methane)

8.1. Introduction 201
8.2. Mixture preparation 202
8.3. Experimental process 204
8.4. Experimental results 205
8.5. Virial coefficients determination 207
8.6. Uncertainty analysis of the measurements 208
8.7. Discussion 211
8.8. Table of results 218
8.9. References 222

8.1. INTRODUCTION

The European Union has established that 20% of the energy consumption should come from renewable sources by 2020, and that biofuels should provide at least 10% of the transport fuel consumption by the same year [1]. This directive describes a framework for the promotion of energy from renewable sources, reducing CO_2 emissions and establishes the need to integrate renewable energy in existing transmission and distribution grids. The increase of the amount of biogas injected into natural gas networks is an important strategy to achieve this goal.

Due to the diversity of sources of biogas and other non-conventional energy gases, their composition may vary significantly. The main difference in composition between biogas and natural gas is the lower methane content of the biogas, within (50 to 80) %, and the corresponding higher content of carbon dioxide (20 to 50) %, with small amounts of other components as nitrogen, carbon monoxide and hydrogen. The biogas matrix presents serious challenges concerning its applicability for the devices used in the natural gas industry for measuring the moisture content and calculating gas properties, such as the density and calorific value. These problems are linked to the substantially higher carbon dioxide content of biogas.

Therefore it is essential to have a detailed knowledge of the thermophysical properties of biogas in order to solve the technical and design problems that may arise during the transport and exploitation stages. The current models are based on binary mixture data and accurate experimental data of multicomponent mixtures are relatively scarce yet. A large number of very high accuracy experimental data over wide temperature and pressure ranges are needed to develop and validate methods for the estimation of the density, heat capacity and calorific value of biogas and biomethane. Experimental density data of multicomponent natural-gas-like mixtures have been previously measured by other authors. However, no previous accurate density data of synthetic biogas-like mixtures with a content of methane less than 60% can be found in the literature. Moreover, CO is not present in any of the studied mixtures. The composition of biogas may vary significantly due to diversity of sources of production and, according to the different processes of biogas production, it is not unusual to find small amounts of CO, mainly in processes like biomass gasification [2].

This work studies the thermodynamic behavior of a synthetic biogas-like mixture, composed by methane, carbon dioxide, nitrogen and carbon monoxide through accurate

(*p, ρ, T*) experimental data at temperatures ranging from (275 to 400) K and pressures up to 20 MPa obtained by using a single sinker densimeter with magnetic suspension coupling. The experimental data are compared with the corresponding densities calculated from the GERG-2008 equation of state [3], which is the current reference equation of state for natural gas and other related mixtures and designated as ISO Standard (ISO 20765-2 [4]) for the calculation of the thermodynamic properties of natural gases. To achieve the highest accuracy in composition, the gas mixture was prepared by the gravimetric method according to ISO 6143 [5] by the Spanish National Metrology Institute (*Centro Español de Metrología*, CEM).

Using the same technique, TERMOCAL reported in the past density measurements of binary mixtures of the four components of this synthetic biogas-like mixture: : CH_4 + CO_2 [6], CH_4 + N_2 [7], N_2 + CO_2 [8][9] and N_2 + CO [10]. For some of these mixtures also speed of sound measurements were carried out s [11].

This work was part of the Joint Research Project ‘Metrology for Biogas’, funded by the European Metrology Research Program (EMRP) [12].

8.2. MIXTURE PREPARATION

The synthetic biogas-like mixture was prepared gravimetrically at the Spanish National Metrology Institute (Centro Español de Metrología, CEM) and was supplied in a 5 dm^3 aluminum alloy cylinder (CEM no.: 51858). The goal was to obtain a representative mixture of actual biogas, with known composition, and with the smallest achievable uncertainty in composition. The composition of the mixture from gravimetric preparation according to ISO 6143 [5] is given in Table 8.1, together with the expanded uncertainty for each component (k = 2), the certified purity, supplier and critical parameters of each of the component gases. All substances were used without further purification.

The critical parameters of the mixture were estimated with the GERG-2008 equation of state [3] by using REFPROP [13]:

- T_c = 224.8 K
- p_c = 8.9352 MPa
- M = 27.681 g·mol^{-1}

Table 8.1. *Composition of the synthetic biogas-like mixture, and purity, supplier, critical parameters and molar mass of the individual component gases.*

Component	Concentration (molar fraction)		Purity	Supplier	M g·mol^{-1}	Critical parameters	
	x_i	$U(x_i)$ /%				T_c / K	P_c / MPa
Methane	0.498141	0.014	> 99.999 5 mol %	Praxair	16.043[d]	16.043[d]	4.60[d]
Carbon dioxide	0.352028	0.040	> 99.999 9 mol %	Air Liquide[a]	44.010[e]	44.010[e]	7.38[e]
Nitrogen	0.099916	0.0062	> 99.99 5 mol %	Carburos Metálicos[b]	28.013[f]	28.013[f]	3.39[f]
Carbon monoxide	0.049915	0.10	> 99.998 mol %	Praxair[c]	28.010[g]	30.069[g]	3.49[g]

[a] AL Air Liquide España S.A., Madrid, Spain
[b] Air Products Group, Barcelona, Spain
[c] Praxair España S.L., Madrid, Spain
[d] Setzmann et al. [26]
[e] Span et al. [27]
[f] Span et al. [28]
[g] Lemmon et al. [29]

All components were introduced directly, without the need of premixtures, into the cylinder. The filling order was: carbon dioxide, carbon monoxide, nitrogen and methane (balance gas). The mass of the gas portions were determined using a high-precision balance (Mettler Toledo PR10003, Mettler-Toledo GmbH, Greifensee, Switzerland). After the last gas portion had been added and weighed, the cylinder was finally homogenized by a rolling procedure. The target composition of the synthetic mixture was considered to be sufficiently stable due to previous experience with mixtures of the same compounds and similar composition.

The composition of the mixture was validated by using the multi-point calibration according to the procedure described in ISO 6143 [5]. The composition of the three calibration reference materials were in the range of ±5 % of the targeted composition. In the validation procedure, a GC analyzer was used with a set of packed columns and TCDs designed for the analysis of natural gas samples (Agilent 6890N, Agilent Technologies, Santa Clara CA, USA). Table 8.2 shows the results of this analysis together with their expanded uncertainty (k = 2). Since the chromatographic method used is not optimized for CO analysis, large relative uncertainty and deviation are obtained for this component.

Table 8.2. *Results of the GC analysis of the synthetic biogas-like mixture.*

Component	Concentration (molar fraction)		Relative deviation between gravimetric preparation and GC analysis
	x_i	$U(x_i)$/% (k = 2)	%
Methane	0.500220	2.9	0.417
Nitrogen	0.099905	1.7	–0.011
Carbon dioxide	0.352260	0.48	0.066
Carbon monoxide	0.051236	5.2	2.646

8.3. EXPERIMENTAL PROCEDURE

Six isotherms were logged for this work at (275, 300, 325, 350, 375 and 400) K. Each isotherm was measured from a pressure of 20 MPa to 1 MPa, in 1 MPa steps, followed by measurements of the sinker mass in vacuum. All measured points of the studied biogas-like mixture are represented in Figure 8.1 together with the saturation curve and the range of validity of the GERG-2008 equation of state and the range of importance for gas industry.

Measurements could not be done at the lowest limit of the temperature range of densimeter (250 K) because it was close to the saturation curve of the studied mixture and the composition may change due to the condensation of the mixture components in the colder parts of the densimeter. The maximum pressure achieved on each of the isotherms was 20 MPa.

Before and after measurements on the studied biogas-like mixture, test measurements with nitrogen were carried out in the whole working range of the apparatus to validate its operation by comparing the experimental results with the densities calculated from the reference equation of state for nitrogen by Span et al. [16]. Relative deviations of the experimental data from the calculated densities were within a ±0.02 % band, with an Absolute Average Deviation (*AAD*) of 0.011% for the measurements with nitrogen, before biogas, and 0.007% after.

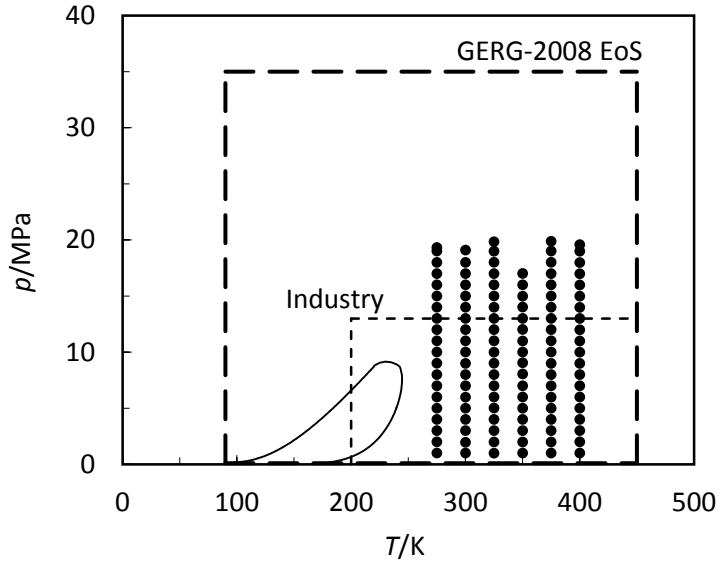

Figure 8.1. *pT-phase diagram showing the experimental points measured in this work (●), the calculated saturation curve for the synthetic biogas-like mixture, the temperature and pressure ranges of validity of the GERG-2008 equation of state (dashed line) and the area of interest for storage, transport and utilization processes of gas fuels (thin dashed line).*

The sinker mass in vacuum was measured after each of the isotherms to check any misalignment suffered by the magnetic suspension coupling during the measurements. The maximum difference between the replicates of the sinker mass in vacuum at the same temperature was of 0.0065 %, corresponding to a temperature of 400K. This good repeatability of the measurements in vacuum confirmed that there was not any misalignment during the measurements.

8.4. EXPERIMENTAL RESULTS

Measurements were carried out at six different temperatures (275, 300, 325, 350, 375 and 400) K and decreasing pressure steps of 1 MPa from 20 to 1 MPa. The state point magnitudes on each isotherm were calculated as the average of the last ten measured values of the corresponding magnitude for each pressure step. Table 8.9 (section 8.8) presents the experimental (p, ρ, T) data of the synthetic biogas-like mixture measured, the relative deviation in density from the values calculated with the GERG-2008 equation of state [3] and AGA8-DC92 [14] (zero line) and the expanded uncertainties in density (k = 2) of the experimental data calculated by equations 4.11 and 4.15, which are given in absolute value and relative value like a percentage of the measured density.

The single sinker densimeter is one of the most accurate methodologies for the measurement of the density of fluids. However this methodology presents some systematic errors, which affect the final density results. There are two main effects that must be evaluated: the force transmission error (FTE) due to the magnetic coupling and the adsorption of gas molecules on the cell and sinker surfaces.

Force transmission error

As it has been described in chapter 3.4, FTE consists in two terms: the apparatus effect and the fluid specific effect. The apparatus effect was accounted for by measuring the sinker mass under vacuum at the end of each isotherm.

In the case of the fluid specific effect, its magnitude depends on the magnetic behavior of the measured gas and on the apparatus specific constant (estimated in 45.7 ppm, see chapter 3.4). The magnetic susceptibility of the biogas-like mixture used in this work was estimated by using an additive law proposed by Bitter [15] from the magnetic susceptibilities of the pure components and their molar fractions. The magnetic susceptibility of the synthetic biogas-like mixture was $\chi_{BIOGÁS} = -9.52 \cdot 10^{-9}$. Since this value is relatively low, according to criteria expressed in the previous chapters, the magnetic behavior of the fluid would be negligible in relation to the apparatus effect and therefore the fluid specific effect was not considered in our measurements.

Sorption effects in the measuring cell

Adsorption and desorption of gas molecules on the measuring cell walls or the sinker surface was recently study by Richter et al. [16]. Previously, Wagner et al. [17] and Klimeck et al. [18] reported that this effect could only affect the accuracy of the measurements near the saturation curve or at very low gas densities, since only the adsorption on the sinker, and not that on the cell walls, had to be considered. However, Richter reported that due to sorption effects the composition of the measured gas could be modified inside the cell and significant errors up to about 0.1 % in density measurements could occur. Therefore, test measurements to check any adsorption effect on the experimental density value were carried out.

According to the experimental procedure, each isotherm was recorded in 120 hours, approximately. After that, the cell was evacuated and fresh mixture was introduced for measuring another isotherm. To check the sorption effects on the mixture composition for an isotherm measurement time, an adsorption test was carried out by measuring a large number of replicates of one selected point. The test was performed at temperature of 350 K and pressure of 1 MPa and density measurements were continuously recorded during 120 hours. The results showed that the relative deviation in density from the GERG-2008 equation was nearly constant along the whole test. The difference observed in the trend of the relative deviation in density from the GERG-2008 equation of state between the first and the last measurement was 0.0045 %, which is one order of magnitude lower than the uncertainty in density at the work pressure. Therefore it was concluded that the adsorption effect could be neglected in our measurements.

8.5. VIRIAL COEFFICIENTS DETERMINATION

The value of the molar mass of the synthetic biogas-like mixture inside the measuring cell M_{virial} and the second and the third virial coefficients, B and C respectively, were calculated by fitting the experimental data to the virial expansion (equation 2.5) by using a fitting package for the least squares [19]. Table 8.3 shows the obtained results with virial coefficients calculated by GERG-2008.

Table 8.3. *Least mean squares fitting results for synthetic biogas-like mixture (M_{virial}, B, C), with their uncertainties, and virial coefficients values estimated by GERG-2008 equation of state.*

T/K	M_{virial}/ g·mol^{-1}	ΔM/ g·mol^{-1}	$U(M)$/ g·mol^{-1}	B/ cm^3·mol^{-1}	$U(B)$/ cm^3·mol^{-1}	B_{GERG}/ cm^3·mol^{-1}	C/ cm^6·mol^{-2}	$U(C)$/ cm^6·mol^{-2}	C_{GERG}/ cm^6·mol^{-2}
275.006	27.692	-0.011	0.016	-68.29	0.12	-68.17	3146	14	3235
299.970	27.687	-0.006	0.014	-55.006	0.057	-55.18	2772	8	2987
324.982	27.644	0.037	0.014	-44.35	0.075	-44.70	2496	12	2752
349.970	27.680	0.001	0.014	-35.66	0.080	-36.10	2277	15	2549
374.956	27.678	0.003	0.015	-28.59	0.15	-28.92	2130	30	2379
400.017	27.692	-0.011	0.019	-22.39	0.41	-22.82	1997	90	2237

T is the average temperature of each isotherm. ΔM is the difference between the gravimetric molar mass of the mixture M_{grav} (27.681 g·mol^{-1}) and the fitted molar mass value M_{virial}.

The fitting was carried out for each isotherm using experimental data of pressures below 10 MPa. The uncertainties of the fitted parameters were calculated according to the GUM [20] from standard deviation values returned by the software.

Figure 8.2 shows the deviation of pressure data from virial expansion fitting versus experimental pressure. As it can be observed, deviations are not within the defined tolerance (0.02 %) at pressures above 10 MPa. Two "outliers" points were also identified below 10 MPa at 400 K, which were not used in the fitting.

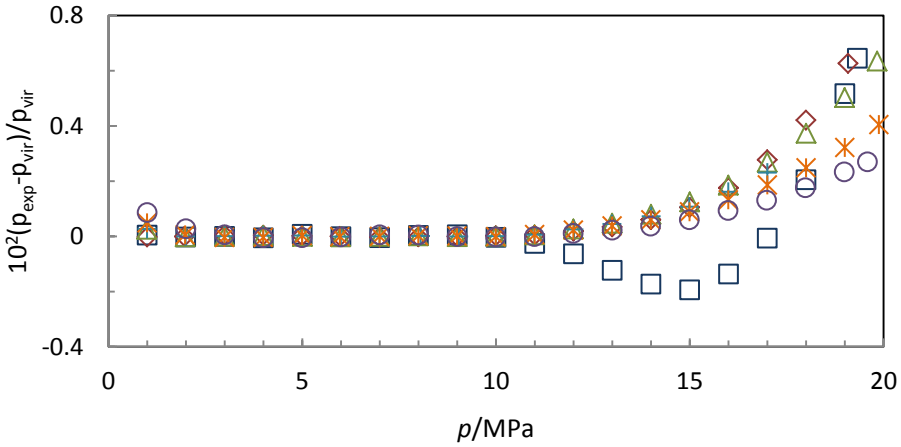

Figure 8.2. *Relative deviation of experimental pressure from pressure calculated by virial expansion (Eq. 4.16) by using the fitted parameters.* □ *275 K;* ◇ *300 K;* △ *325 K;* + *350 K;* ✳ *375 K;* ○ *400 K.*

In order to reproduce the experimental behavior in the whole pressure range, the forth and even the fifth virial coefficients should be required, but for that more experimental data would be required too.

8.6. UNCERTAINTY ANALYSIS OF THE MEASUREMENTS

A detailed analysis of the measurement uncertainty is shown in chapter 4.

Expanded uncertainty in temperature (k = 2) was evaluated to be less than 4 mK. It corresponds to a maximum contribution in density of 0.005 %, according to the density range measured.

The expanded uncertainties in pressure (k = 2) were estimated by equations 4.9 and 4.10, depending on the pressure transducer used: (2 - 20) MPa or (0 - 2) MPa, respectively. The

largest deviation was 0.05 MPa. This corresponds to a correction within (0.015 and 0.138) % in terms of density.

The expanded uncertainty in density (k = 2) was determined by equation 4.12. According to the experimental density range, its value was within (0.024 y 0.064) kg· m^{-3}, which corresponds to (0.018 y 0.289) %, expressed in percentage.

As it is detailed in chapter 4.7, the overall uncertainty of the measurements was estimated by two methods, according to the estimation of the uncertainty in composition of the mixture. Thus, standard overall uncertainty (k = 1) of measurements expressed in density units $u_T(\rho)$ was calculated by equations 4.13 and 4.14 from combined uncertainties in density, temperature, pressure and composition.

Molar mass uncertainty

The combined uncertainty of the mixture composition was calculated by equation 4.15, taking into account all sources of uncertainty related with the molar mass of the mixture (see chapter 4.7).

The estimation of the uncertainty of the molar mass of the mixture due to uncertainties in the atomic weights of the involved components of the mixture $u(M_{atomic})$ was obtained from the 2011 IUPAC report by Wieser et al. [21]. Table 8.4 shows molar mass uncertainties of the components of the synthetic biogas-like mixture.

Table 8.4. *Molar mass of biogas-like mixture components and their uncertainties* [21].

Substance	M_i /g·mol-1	$u(M_i)$ /g·mol-1	$u(M_i)/M_i$ /ppm
Methane	16.0428	0.00085	53
Nitrogen	28.01348	0.00040	14
Carbon dioxide	44.0098	0.00100	23
Carbon monoxide	28.0101	0.00010	4

The uncertainty of the molar mass due to uncertainties in the gravimetric composition of the mixture $u(M_{grav})$ was calculated by equation 4.16 [22] and uncertainty associated to changes in the composition inside the measuring cell $u(M_{sorp})$ was calculated by equation

4.17 from the molar mass value estimated by the virial fitting. The contributions to the molar mass combined uncertainty of the mixture are summarized in Table 8.5.

Table 8.5. *Uncertainty budget of the composition associated to the molar mass of the synthetic biogas-like mixture.*

Source of uncertainty	Units	Contribution
$u(M_{atomic})$ (Table 8.4) [21]	g·mol^{-1}	0.0008
$u(M_{grav})$ (Eq. 4.16) [22]	g·mol^{-1}	0.0029
$u(M_{sorp})$ (Eq. 4.17)	g·mol^{-1}	0.0165
Incertidumbre combinada estándar (k = 1) (Eq. 4.15)		0.017
Incertidumbre combinada expandida (k = 2)		0.034

Overall uncertainty of the measurements

The overall expanded uncertainty (k = 2) and the estimated contributions for temperature, pressure, density and composition are detailed in Table 8.6.

Table 8.6. *Contributions to expanded overall uncertainty in density (k = 2) for synthetic biogas-like mixture.*

Source of uncertainty	Units	Contribution (k = 2)	Estimation in density (k = 2)	
			kg·m^{-3}	%
Temperature	K	0.004	< 0.006	< 0.005
Pressure	MPa	0.005	(0.001 - 0.053)	(0.015 - 0.138)
Density	kg·m^{-3}	(0.024 - 0.064)	(0.024 - 0.064)	(0.018 - 0.289)
Gravimetric composition	mol·mol^{-1}	< 0.0004	< 0.029	< 0.009
Virial expansion composition	g·mol^{-1}	0.034	(0.005 - 0.219)	0.122
	$U_{T1}(\rho)$ gravimetric		(0.025 - 0.259)	(0.043 - 0.465)
	$U_{T2}(\rho)$ virial		(0.026 - 0.448)	(0.124 - 0.315)

The expanded overall uncertainty $U_{T1}(\rho)$ (k = 2) calculated from equation 4.13 is within (0.025 and 0.259) kg·m^{-3}, or (0.043 y 0.465) %, expressed in percentage. The expanded overall uncertainty $U_{T2}(\rho)$ calculated from equation 4.14 is within (0.026 y 0.448) kg·m^{-3}, or (0.124 y 0.315) %.

8.7. DISCUSSION

Virial fitting of experimental data

When the pressure tends to zero, all gases have ideal gas behavior. Experimental density deviations were estimated when pressure tends to zero by fitting the experimental data to a third degree polynomial and calculating the intersection with ordinate axis. Results are shown in Table 8.7.

Table 8.7. *Estimated deviations of experimental densities from the GERG-2008 equation of state when pressure is zero.*

Isotherm	275 K	300 K	325 K	350 K	375 K	400 K
$10^2(\rho_{exp}-\rho_{EoS})/\rho_{EoS}$	0.138	0. 012	–0. 154	–0. 044	–0. 074	–0. 071
R^2	0. 9806	0. 9591	0. 9202	0. 8828	0. 7534	0. 7243

The largest deviation was –0.1545 % at 325 K, while the rest of the isotherms, except 275 K, had deviations below 0.1 %. This deviation is also identifiable in Table 8.3. The difference between molar mass from virial fitting and molar mass from gravimetric composition at 325 K is larger than at the other temperatures. The value of 0.037 g·mol^{-1} is higher than its estimated uncertainty. The rest of the deviations present values within the uncertainty limits. These deviations are probably a consequence of the incomplete homogenization of biogas inside the measuring cell during the filling process, because the whole 325 K isotherm is “displaced”.

The expanded overall uncertainty of the measurements considering the virial fitted value for molar mass (Eq 4.14) is usually slightly higher than the overall uncertainty calculated with gravimetric composition uncertainty (Eq 4.13), especially at 325 K. However, since the uncertainty contribution of the molar mass to the overall uncertainty is constant for all isotherms (see Table 8.5) the overall uncertainty from gravimetric values can be larger than

the overall uncertainty from virial fitting. This can be observed in the isotherms from (350 to 400) K at pressures below 2 MPa.

Regarding the estimation of the virial coefficients shown in Table 8.3, the deviations between the second virial coefficients estimated from virial fitting and the second virial coefficients calculated by GERG-2008 are very close, but their differences are slightly larger than estimated uncertainties for most of the isotherms. However, differences of the third virial coefficients calculated from virial fitting and by GERG-2008 are much larger than estimated uncertainties. Figure 8.3 shows the variation with temperature of the calculated virial coefficients from virial fitting and from the GERG-2008 equation of state.

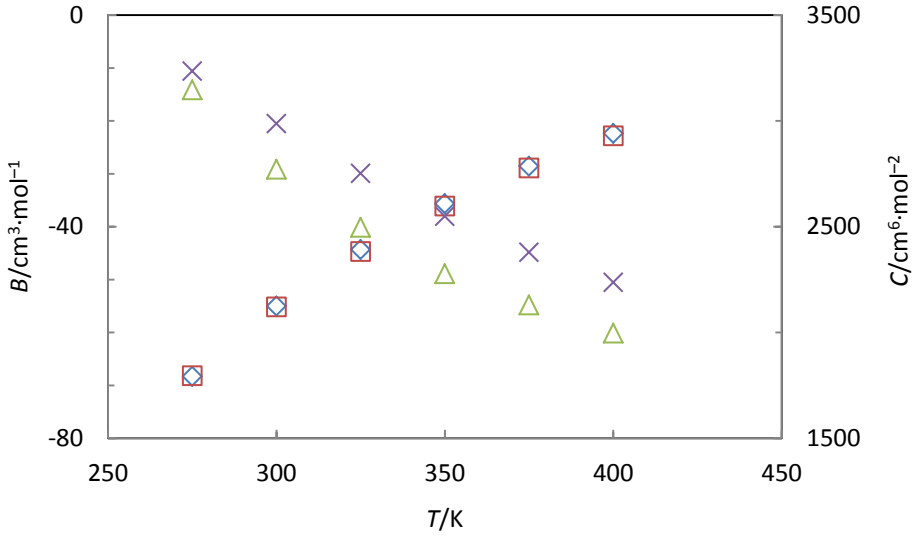

Figure 8.3. *Variation of the calculated virial coefficients with temperature.* ◇ B_{Virial}, □ B_{GERG}, △ C_{Virial} *y* × C_{GERG}.

Relative deviations of experimental data from reference equations of state

The relative deviations of experimental density data from the densities calculated by the GERG-2008 and AGA8-DC92 [14] equations of state for each of the isotherms are shown in Figures 8.4 and 8.5, respectively.

As it can be observed, the relative deviations are within a ±0.2 % band. Only the pressure range from (6 to 15) MPa at the temperature of 275 K are out of these limits. The 275 K isotherm shows a peak in which the highest relative deviation from densities calculated from the GERG-2008 equation of state is 0.41% and it can be observed at 10 MPa.

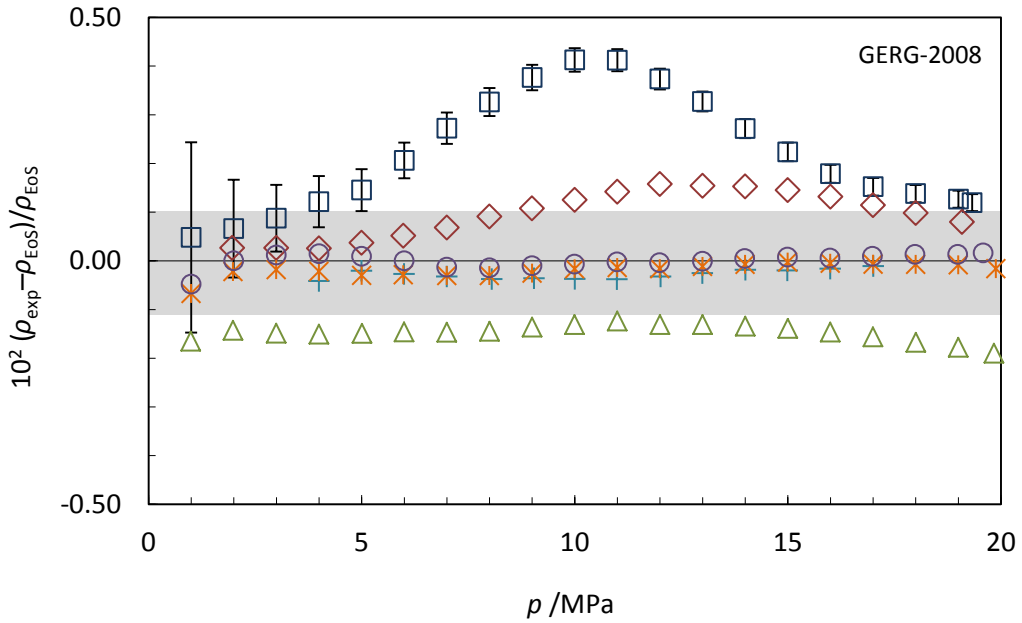

Figure 8.4. *Relative deviations in density of experimental (p, ρ, T) data of the synthetic biogas-like mixture ρ_{exp} from density values calculated from the GERG-2008 equation of state ρ_{EoS} versus pressure: □ 275 K; ◇ 300 K; △ 325 K; + 350 K; ✳ 375 K; ○ 400 K. Error bars on the 275 K isotherm indicate the expanded uncertainty (k = 2) of the experimental data. Dark bar corresponds to the uncertainty of the GERG-2008 (0.1 %)* [3].

Results also showed that only the isotherms at (275 and 300) K have positive deviations from the equation of state. Data belonging to the isotherms over 300 K showed negative deviations in density. However these isotherms are close to zero line, independently of pressure. Measurements at 325K revealed the highest negative deviation, but always below a 0.2% band. According to Kunz and Wagner, the uncertainty of GERG-2008 in the gas-phase density is 0.1% over the temperature range from (250 to 450) K at pressures up to 35 MPa [3]. This uncertainty estimate is valid for various types of natural gases, including natural gases rich in nitrogen, carbon dioxide or considerable amounts of heavier hydrocarbons, carbon monoxide or oxygen. In the case of gas mixtures with carbon dioxide mole fractions of 0.14 and more, GERG-2008 states that systematic deviations exceeding 0.3 % may be observed at some states. The synthetic biogas-like mixture studied in this work has a high content of CO_2 (35 mol-%). About 60 % of the data are within the expected uncertainty limits estimated for the GERG-2008 equation of state. Experimental data present deviations larger than 0.3 % are found only at 275 K and pressures above 10 MPa. Therefore the behavior registered in the measurements agrees with the uncertainty claimed by GERG-2008 equation of state.

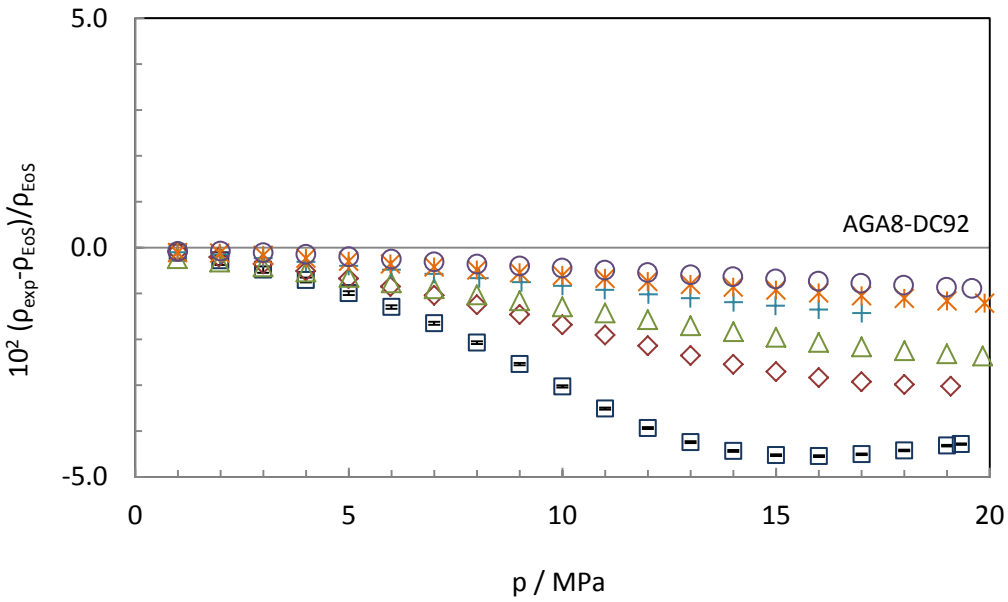

Figure 8.5. *Relative deviations in density of experimental (p, ρ, T) data of the synthetic biogas-like mixture ρ_{exp} from density values calculated from the AGA8-DC92 equation of state ρ_{EoS} versus pressure: □ 275 K; ◇ 300 K; △ 325 K; + 350 K; ✳ 375 K; ○ 400 K.*

Regarding AGA8-DC92, deviation of experimental density from estimated values is larger than deviations from GERG-2008, especially at high pressures and low temperatures. The highest deviation is –4.5 % at 275 K and at 16 MPa. The AGA8-DC92 equation of state was designed to estimate thermophysical properties of natural gases. The range of validity is limited to the gas phase at temperatures between (143 and 673) K and pressures up to 280 MPa. However, due to the limited amount of experimental data used for its development, the uncertainty in density is only estimated at temperatures within (250 y 350) K and pressures up to 30 MPa. At temperatures above 290 K and pressures up to 12 MPa, the uncertainty in density is 0.1 %. Higher uncertainties were reported for enriched gases, especially at lower temperatures [3]. The studied biogas-like mixture presents high carbon dioxide content, so the large deviations at low temperatures and high pressures observed for the experimental data agree the uncertainty of AGA8-DC92 equation of state. Deviations at high temperatures and low pressures are smaller but they are always below the uncertainty estimated to the equation for this working range.

An statistical comparison of the data measured is given in Table 8.8, where *AAD* is the average absolute deviation defined in equation 3.22, *Bias* is the average deviation defined in equation 3.23, *RMS* refers to the root mean squared defined in equation 3.24, and *MaxD* represents the maximum relative deviation in the considered data set.

Table 8.8. *Statistical parameters of the data set with respect to the GERG-2008 and AGA8-DC92 equations of state.*

Statistical parameter	GERG-2008	AGA8-DC92
AAD	0.088	1.290
Bias	0.021	–1.290
RMS	0.129	1.761
MaxD/%	0.413	–4.546

Comparison with literature data

The qualitative behavior observed for the experimental density deviations from the GERG-2008 equation of state is similar to that observed for the binary mixtures (CH_4 + CO_2) [6] and (CH_4 + N_2) [7]. The density of these binary mixtures was reported previously by TERMOCAL. Measurements were carried out with the same single-sinker densimeter.

Figures 8.6 and 8.7 show the experimental results for the (CH_4 + CO_2) binary mixture at different compositions (20 and 40) mol-% of CO_2. As it can be observed, deviations increase significantly at the lowest temperatures and pressures around 10 MPa. The synthetic biogas-like mixture (35 mol-% CO_2) presents at the same conditions qualitatively similar deviations.

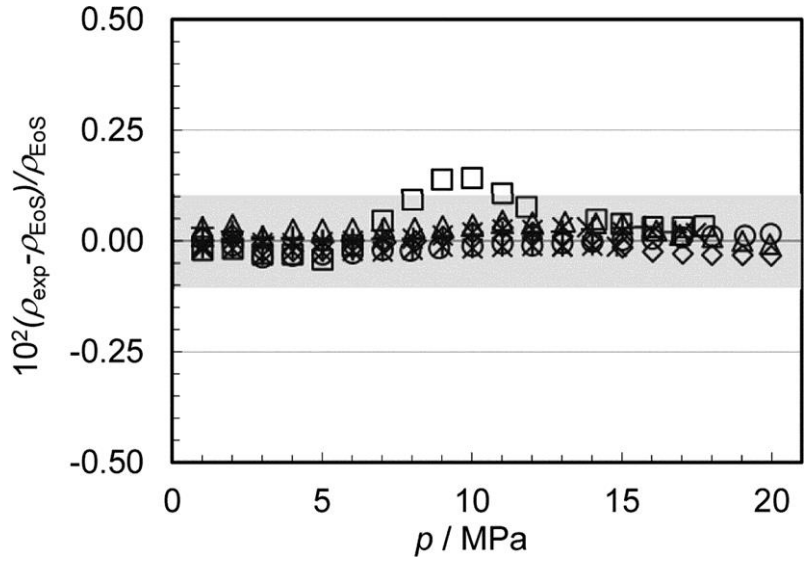

Figure 8.6. *Relative deviation of experimental density from density estimated by GERG-2008 equation of state for (0.20 CO_2 + 0.80 CH_4) binary mixture versus pressure: □ 250 K; ◇ 275 K; △ 300 K; × 325; + 350 K; ○ 375 K; ∗ 400 K* [6].

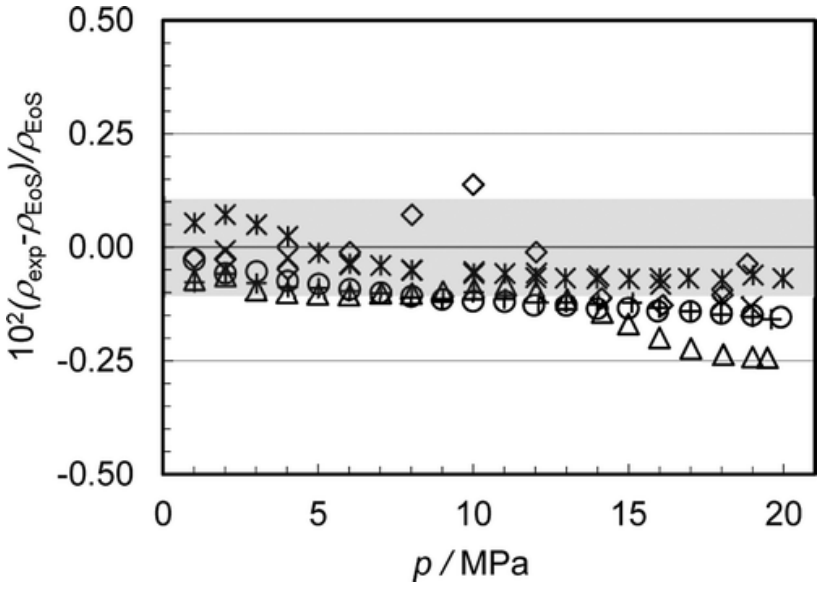

Figure 8.7. *Relative deviation of experimental density from density estimated by GERG-2008 equation of state for (0.40 CO_2 + 0.60 CH_4) versus pressure: ◇ 275 K; △ 300 K; × 325; + 350 K; ○ 375 K; ✳ 400 K* [6].

The same behavior is observed in (CH_4 + N_2) binary mixture in figures 8.8 and 8.9 with concentrations of 10 mol-% and 20 mol-% of N_2, respectively. In this case data are compared with AGA8-DC92 equation of state. The largest deviations were registered at the lowest temperatures and 10 MPa, similar to the case of biogas-like mixture (10 mol-% N_2).

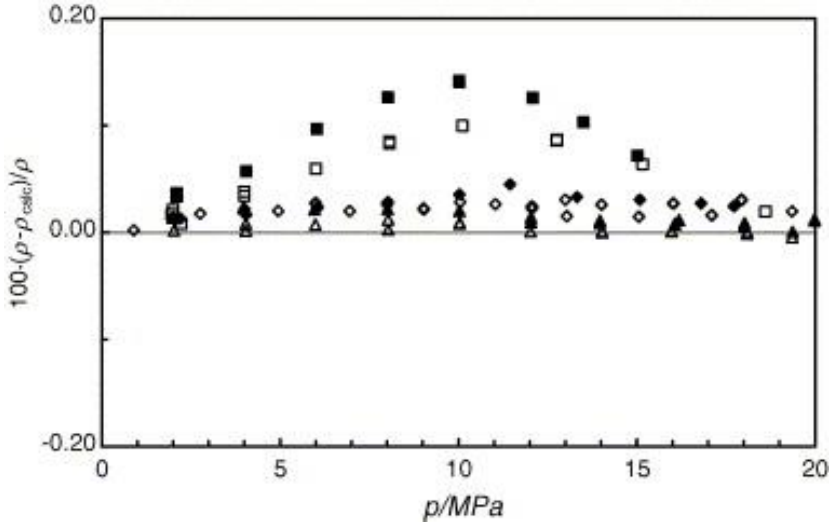

Figure 8.8. *Relative deviation of experimental density from density estimated by AGA8-DC92 equation of state for (0.89984 CH_4 + 0.10016 N_2) binary mixture versus pressure at different temperatures: ■ 240 K; □ 250 K; ♦ 275 K; ◊ 300 K; ▲ 350 K; and △ 400 K* [7].

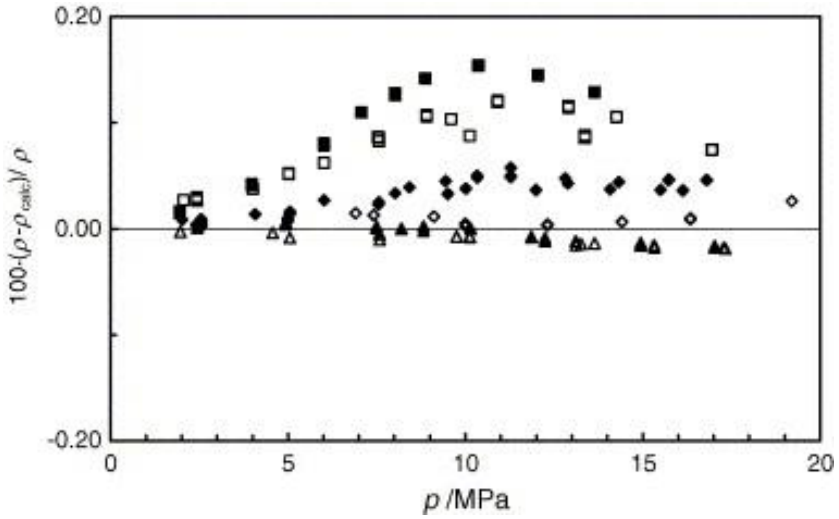

Figure 8.9. *Relative deviation of experimental density from density estimated by AGA8-DC92 equation of state for (0.79998 CH_4 + 0.20002 N_2) binary mixture versus pressure at different temperatures:* ■ *240 K;* □ *250 K;* ♦ *275 K;* ◊ *300 K;* ▲ *350 K; and* △ *400 K* [7].

8.8. TABLE OF RESULTS

Table 8.9. *Experimental (p, ρ, T) measurements for the synthetic CMM mixture, relative and absolute expanded uncertainty in density (k = 2) U(ρ_{exp}), expanded overall uncertainty in density (k = 2) from gravimetric composition $U_{T1}(\rho_{exp})$ and from virial expansion $U_{T2}(\rho_{exp})$ and relative deviations from the GERG-2008 and AGA8-DC92 equations of state; where T is the temperature (ITS-90* [23]*), p the pressure, ρ_{exp} the experimental density and ρ_{EoS} the density calculated from both equations of state.*

T/K	*p*/MPa	ρ_{exp}/ kg·m^{-3}	$U(\rho_{exp})$/ kg·m^{-3}	$U(\rho_{exp})$/ %	$U_{T1}(\rho_{exp})$/ kg·m^{-3}	$U_{T2}(\rho_{exp})$/ (kg·m^{-3})	$10^2(\rho_{exp}-\rho_{EoS})/\rho_{EoS}$	
							GERG-2008	AGA8-DC92
275.007	19.324	360.865	0.032	0.009	0.258	0.448	0.115	–4.284
275.002	19.002	356.476	0.032	0.009	0.259	0.443	0.122	–4.317
275.000	17.998	341.807	0.031	0.009	0.259	0.427	0.131	–4.422
275.002	17.001	325.781	0.030	0.009	0.258	0.409	0.145	–4.506
275.001	16.000	308.168	0.029	0.009	0.255	0.389	0.168	–4.546
274.999	14.998	288.893	0.028	0.010	0.249	0.368	0.209	–4.524
275.007	13.998	267.942	0.027	0.010	0.239	0.345	0.251	–4.433
275.008	12.997	245.547	0.026	0.010	0.224	0.320	0.305	–4.241
275.009	11.997	222.071	0.024	0.011	0.205	0.294	0.353	–3.934
275.012	10.998	198.123	0.023	0.012	0.182	0.266	0.397	–3.510
275.012	9.999	174.283	0.022	0.012	0.159	0.238	0.405	–3.027
275.009	8.999	151.158	0.020	0.013	0.137	0.211	0.377	–2.539
275.008	7.999	129.186	0.019	0.015	0.117	0.184	0.331	–2.072
275.006	6.999	108.589	0.018	0.016	0.101	0.158	0.276	–1.650
275.004	5.998	89.433	0.017	0.019	0.088	0.135	0.212	–1.295
275.001	4.998	71.694	0.016	0.022	0.078	0.114	0.148	–0.993
275.004	3.996	55.230	0.015	0.027	0.069	0.095	0.121	–0.707
275.007	2.998	39.984	0.014	0.035	0.063	0.079	0.083	–0.480
275.008	1.995	25.730	0.013	0.051	0.027	0.041	0.062	–0.281
275.014	0.999	12.470	0.012	0.099	0.025	0.029	0.040	–0.113
299.976	19.086	289.280	0.028	0.010	0.194	0.363	0.052	–3.024
299.973	18.000	273.672	0.027	0.010	0.188	0.345	0.067	–2.988
299.972	16.998	258.475	0.026	0.010	0.180	0.327	0.083	–2.926
299.969	15.998	242.593	0.025	0.010	0.172	0.309	0.100	–2.836
299.969	14.998	226.084	0.024	0.011	0.162	0.290	0.117	–2.708
299.968	13.998	209.120	0.024	0.011	0.151	0.270	0.134	–2.546
299.969	12.997	191.822	0.023	0.012	0.139	0.250	0.142	–2.355
299.971	11.998	174.424	0.022	0.012	0.127	0.230	0.152	–2.142
299.971	10.998	157.097	0.021	0.013	0.116	0.209	0.157	–1.908

299.970	9.998	140.008	0.020	0.014	0.105	0.189	0.149	–1.685
299.968	8.998	123.323	0.019	0.015	0.095	0.169	0.132	–1.463
299.971	7.997	107.139	0.018	0.017	0.086	0.150	0.111	–1.247
299.969	6.998	91.571	0.017	0.018	0.078	0.132	0.096	–1.042
299.971	5.977	76.312	0.016	0.021	0.071	0.114	0.072	–0.850
299.969	4.997	62.315	0.015	0.024	0.065	0.098	0.051	–0.676
299.969	3.997	48.660	0.014	0.030	0.060	0.083	0.035	–0.513
299.968	2.997	35.626	0.014	0.038	0.056	0.070	0.022	–0.360
299.971	1.963	22.782	0.013	0.057	0.027	0.038	0.022	–0.211
299.967	0.997	11.312	0.012	0.108	0.025	0.028	0.027	–0.087
324.982	19.836	251.082	0.026	0.010	0.149	0.315	–0.202	–2.364
324.984	18.999	240.804	0.025	0.011	0.144	0.303	–0.189	–2.317
324.982	18.004	228.234	0.025	0.011	0.138	0.289	–0.182	–2.250
324.981	17.000	215.189	0.024	0.011	0.131	0.273	–0.167	–2.167
324.980	15.996	201.844	0.023	0.011	0.124	0.258	–0.161	–2.067
324.983	14.999	188.339	0.022	0.012	0.117	0.242	–0.149	–1.956
324.981	14.003	174.683	0.022	0.012	0.110	0.226	–0.141	–1.836
324.980	13.000	160.847	0.021	0.013	0.103	0.209	–0.138	–1.706
324.980	11.999	147.023	0.020	0.014	0.096	0.193	–0.134	–1.572
324.980	10.997	133.261	0.019	0.014	0.089	0.177	–0.127	–1.427
324.981	9.997	119.644	0.018	0.015	0.082	0.161	–0.130	–1.295
324.982	8.999	106.264	0.018	0.017	0.076	0.145	–0.128	–1.162
324.980	8.000	93.115	0.017	0.018	0.071	0.130	–0.139	–1.034
324.980	6.998	80.238	0.016	0.020	0.066	0.115	–0.142	–0.902
324.983	5.997	67.692	0.015	0.023	0.062	0.101	–0.143	–0.772
324.985	5.007	55.631	0.015	0.027	0.058	0.087	–0.147	–0.651
324.986	3.998	43.686	0.014	0.032	0.054	0.075	–0.153	–0.536
324.986	2.997	32.221	0.013	0.042	0.051	0.064	–0.152	–0.424
324.987	1.983	20.959	0.013	0.061	0.026	0.036	–0.148	–0.317
324.986	0.989	10.281	0.012	0.119	0.025	0.028	–0.165	–0.246
349.970	17.004	187.005	0.022	0.012	0.104	0.238	–0.024	–1.431
349.970	15.997	175.555	0.022	0.012	0.099	0.224	–0.020	–1.352
349.968	14.988	163.964	0.021	0.013	0.094	0.211	–0.016	–1.270
349.970	14.007	152.587	0.020	0.013	0.089	0.197	–0.015	–1.191
349.969	12.996	140.818	0.020	0.014	0.084	0.183	–0.023	–1.107
349.969	12.014	129.390	0.019	0.015	0.079	0.170	–0.023	–1.020
349.969	10.991	117.515	0.018	0.016	0.074	0.156	–0.013	–0.924
349.971	10.002	106.099	0.018	0.017	0.070	0.142	–0.020	–0.839

349.970	9.044	95.137	0.017	0.018	0.066	0.130	–0.027	–0.757
349.969	8.054	83.936	0.016	0.020	0.062	0.117	–0.033	–0.671
349.969	6.997	72.151	0.016	0.022	0.059	0.103	–0.033	–0.575
349.969	5.997	61.194	0.015	0.025	0.055	0.091	–0.034	–0.486
349.969	4.999	50.445	0.014	0.029	0.052	0.080	–0.038	–0.402
349.970	3.998	39.894	0.014	0.035	0.050	0.069	–0.035	–0.315
349.970	2.998	29.569	0.013	0.045	0.047	0.059	–0.034	–0.232
349.969	1.992	19.417	0.013	0.065	0.045	0.035	–0.031	–0.153
349.972	0.997	9.601	0.012	0.127	0.043	0.027	–0.042	–0.100
374.957	19.882	194.414	0.023	0.012	0.099	0.245	–0.034	–1.214
374.954	19.001	185.997	0.022	0.012	0.083	0.235	–0.023	–1.163
374.957	18.002	176.300	0.022	0.012	0.079	0.224	–0.023	–1.110
374.956	17.002	166.458	0.021	0.013	0.088	0.212	–0.019	–1.053
374.955	15.996	156.468	0.021	0.013	0.084	0.200	–0.014	–0.991
374.956	14.997	146.445	0.020	0.014	0.080	0.188	–0.010	–0.926
374.956	13.998	136.360	0.019	0.014	0.076	0.176	–0.015	–0.866
374.958	12.998	126.219	0.019	0.015	0.072	0.164	–0.017	–0.805
374.956	11.998	116.060	0.018	0.016	0.069	0.152	–0.017	–0.742
374.953	10.998	105.923	0.018	0.017	0.065	0.141	–0.007	–0.673
374.956	9.998	95.796	0.017	0.018	0.062	0.129	–0.011	–0.609
374.957	8.999	85.730	0.016	0.019	0.059	0.117	–0.020	–0.552
374.957	7.998	75.725	0.016	0.021	0.056	0.106	–0.025	–0.490
374.957	6.998	65.812	0.015	0.023	0.054	0.095	–0.026	–0.426
374.956	5.976	55.783	0.015	0.026	0.051	0.083	–0.027	–0.360
374.957	5.000	46.329	0.014	0.031	0.049	0.073	–0.030	–0.302
374.957	3.998	36.750	0.014	0.037	0.046	0.064	–0.024	–0.234
374.956	2.998	27.330	0.013	0.048	0.044	0.055	–0.026	–0.173
374.956	1.981	17.903	0.013	0.070	0.042	0.033	–0.028	–0.123
374.957	0.997	8.929	0.012	0.136	0.041	0.027	–0.072	–0.116
400.017	19.583	173.337	0.021	0.012	0.085	0.219	–0.002	–0.888
400.015	18.986	168.193	0.021	0.013	0.072	0.213	–0.004	–0.866
400.015	17.983	159.462	0.021	0.013	0.068	0.203	0.001	–0.821
400.016	16.984	150.669	0.020	0.013	0.077	0.192	–0.001	–0.778
400.015	15.987	141.817	0.020	0.014	0.074	0.182	–0.002	–0.734
400.017	14.989	132.885	0.019	0.014	0.071	0.171	0.004	–0.683
400.017	13.988	123.875	0.019	0.015	0.068	0.161	0.004	–0.636
400.018	12.996	114.906	0.018	0.016	0.065	0.150	–0.003	–0.592
400.017	11.991	105.789	0.018	0.017	0.062	0.139	–0.001	–0.544

400.017	10.992	96.729	0.017	0.018	0.059	0.129	0.004	–0.492
400.017	9.992	87.655	0.017	0.019	0.057	0.118	0.000	–0.448
400.017	8.998	78.654	0.016	0.020	0.054	0.108	–0.004	–0.403
400.018	7.999	69.635	0.016	0.022	0.052	0.098	–0.009	–0.359
400.018	6.997	60.644	0.015	0.025	0.050	0.087	–0.010	–0.310
400.018	5.997	51.732	0.015	0.028	0.048	0.078	0.002	–0.251
400.018	4.997	42.892	0.014	0.033	0.046	0.068	0.007	–0.197
400.018	3.997	34.120	0.014	0.040	0.044	0.060	0.012	–0.148
400.017	2.997	25.434	0.013	0.051	0.042	0.052	0.004	–0.108
400.019	1.997	16.842	0.013	0.075	0.040	0.033	–0.006	–0.079
400.019	0.997	8.351	0.012	0.145	0.039	0.026	–0.056	–0.089

8.9. REFERENCES

[1] "DIRECTIVE 2009/28/EC OF THE EUROPEAN PARLIAMENT AND OF THE COUNCIL of 23 April 2009 on the promotion of the use of energy from renewable sources and amending and subsequently repealing Directives 2001/77/EC and 2003/30/EC." [Online].
Available: http://eur-lex.europa.eu/legal-content/EN/ALL/?uri=CELEX:32009L0028. [Accessed: 04-Mar-2015].

[2] N. Itoh, H. Nomura, M. Sato, and T. Sato, "Efficient hydrogen production process from biogas using a palladium membrane reactor," in *ACS National Meeting Book of Abstracts*, 2011.

[3] O. Kunz and W. Wagner, "The GERG-2008 Wide-Range Equation of State for Natural Gases and Other Mixtures: An Expansion of GERG-2004," *J. Chem. Eng. Data*, 2012.

[4] "ISO/DIS 20765-2 - Natural gas -- Calculation of thermodynamic properties -- Part 2: Single-phase properties (gas, liquid, and dense fluid) for extended ranges of application." [Online]. Available:
http://www.iso.org/iso/home/store/catalogue_tc/catalogue_detail.htm?csnumber=59222&commid=54448. [Accessed: 03-Mar-2014].

[5] "ISO 6143 - Comparison methods for determining and checking the composition of calibration gas mixtures. International Organisation for Standardization, Geneva." 2001.

[6] M. E. Mondéjar, T. E. Fernández-Vicente, F. Haloua, and C. R. Chamorro, "Experimental Determination of (p , ρ, T) Data for Three Mixtures of Carbon Dioxide with Methane for the Thermodynamic Characterization of Nonconventional Energy Gases," *J. Chem. Eng. Data*, vol. 57, no. 9, pp. 2581–2588, Sep. 2012.

[7] C. R. Chamorro, J. J. Segovia, M. C. Martín, M. A. Villamañán, J. F. Estela-Uribe, and J. P. M. Trusler, "Measurement of the (pressure, density, temperature) relation of two (methane+nitrogen) gas mixtures at temperatures between 240 and 400K and pressures up to 20MPa using an accurate single-sinker densimeter," *J. Chem. Thermodyn.*, vol. 38, no. 7, pp. 916–922, Jul. 2006.

[8] M. E. Mondéjar, M. C. Martín, R. Span, and C. R. Chamorro, "New (p, ρ, T) data for carbon dioxide – Nitrogen mixtures from (250 to 400) K at pressures up to 20 MPa," *J. Chem. Thermodyn.*, vol. 43, no. 12, pp. 1950–1953, 2011.

[9] M. E. Mondéjar, R. M. Villamañán, R. Span, and C. R. Chamorro, "Accurate (p, ρ, T) data for two new (carbon dioxide nitrogen) mixtures from (250 to 400) K at pressures up to 20MPa," *J. Chem. Thermodyn.*, vol. 48, pp. 254–269, 2012.

[10] M. E. Mondéjar, M. A. Villamañán, R. Span, and C. R. Chamorro, "(p, ρ, T) behavior of two mixtures of carbon monoxide with nitrogen in the temperature range from (250 to 400) K and pressures up to 20 MPa," *J. Chem. Eng. Data*, vol. 56, no. 10, pp. 3933–3939, 2011.

[11] J. F. Estela-Uribe, J. P. M. Trusler, C. R. Chamorro, J. J. Segovia, M. C. Martín, and M. A. Villamañán, "Speeds of sound in {(1−x)CH4+xN2} with x=(0.10001, 0.19999, and 0.5422) at temperatures between 170K and 400K and pressures up to 30MPa," *J. Chem. Thermodyn.*, vol. 38, no. 7, pp. 929–937, Jul. 2006.

[12] "JRP Summary Report for ENG54 Biogas 'Metrology for biogas.'" [Online]. Available: http://www.euramet.org/fileadmin/docs/EMRP/JRP/JRP_Summaries_2013/Energy_JRPs/ENG54_Publishable_JRP_Summary.pdf. [Accessed: 05-May-2014].

[13] "Lemmon, E.W., Huber, M.L., McLinden, M.O. NIST Standard Reference Database 23: Reference Fluid Thermodynamic and Transport Properties-REFPROP, Version 9.1, National Institute of Standards and Technology, Standard Reference Data Program, Gaithersburg, 2013." .

[14] K. E. Starling and J. L. Savidge, "Compressibility factors of natural gas and other related hydrocarbon gases - AGA Transmission Measurement Committee Report 8," 1992.

[15] F. Bitter, "The Magnetic Susceptibilities of Several Organic Gases," *Phys. Rev.*, vol. 33, no. 3, pp. 389–397, Mar. 1929.

[16] M. Richter and R. Kleinrahm, "Influence of adsorption and desorption on accurate density measurements of gas mixtures," *J. Chem. Thermodyn.*, Mar. 2014.

[17] W. Wagner, K. Brachthäuser, R. Kleinrahm, and H. W. Lösch, "A new, accurate single-sinker densitometer for temperatures from 233 to 523 K at pressures up to 30 MPa," *Int. J. Thermophys.*, vol. 16, no. 2, pp. 399–411, 1995.

[18] J. Klimeck, R. Kleinrahm, and W. Wagner, "Measurements of the (p, ρ, T) relation of methane and carbon dioxide in the temperature range 240 K to 520 K at pressures up to 30 MPa using a new accurate single-sinker densimeter," *J. Chem. Thermodyn.*, vol. 33, no. 3, pp. 251–267, 2001.

[19] J. T. R. Watson and National Engineering Laboratory-FPT Division, "'A generalised fitting package for the least squares analysis of data'." East Kilbride, Glasgow G75 0QU, Scotland., 1991.

[20] I. E. C. BIPM IFCC, ISO, IUPAC, IUPAP and OIML, "Guide to the Expression of Uncertainty in Measurement," *Guid. to Expr. Uncertain. Meas.*, 1995.

[21] M. E. Wieser, N. Holden, T. B. Coplen, J. K. Böhlke, M. Berglund, W. A. Brand, P. De Bièvre, M. Gröning, R. D. Loss, J. Meija, T. Hirata, T. Prohaska, R. Schoenberg, G. O'Connor, T. Walczyk, S. Yoneda, and X.-K. Zhu, "Atomic weights of the elements 2011 (IUPAC Technical Report)," *Pure Appl. Chem.*, vol. 85, no. 5, pp. 1047–1078, Jan. 2013.

[22] M. Richter and M. O. McLinden, "Vapor-Phase (p, ρ, T, x) Behavior and Virial Coefficients for the (Methane + Propane) System," *J. Chem. Eng. Data*, vol. 59, no. 12, pp. 4151–4164, Dec. 2014.

[23] C. A. S. R L Rusby and R P Hudson and M Durieux and J F Schooley and P P M Steur and, "Thermodynamic Basis of the ITS-90," *Metrologia*, vol. 28, no. 1, p. 9, 1991.

[26] Setzmann, U. and Wagner, W.,"A New Equation of State and Tables of Thermodynamic Properties for Methane Covering the Range from the Melting Line to 625 K at Pressures up to 1000 MPa," J. Phys. Chem. Ref. Data, 20(6):1061-1151, 1991.

[27] Span, R. and Wagner, W., "A New Equation of State for Carbon Dioxide Covering the Fluid Region from the Triple-Point Temperature to 1100 K at Pressures up to 800 MPa," J. Phys. Chem. Ref. Data, 25(6):1509-1596, 1996.

[28] Span, R., Lemmon, E.W., Jacobsen, R.T, Wagner, W., and Yokozeki, A. "A Reference Equation of State for the Thermodynamic Properties of Nitrogen for Temperatures from 63.151 to 1000 K and Pressures to 2200 MPa," J. Phys. Chem. Ref. Data, 29(6):1361-1433, 2000.

[29] Lemmon, E.W. and Span, R., "Short Fundamental Equations of State for 20 Industrial Fluids," *J. Chem. Eng. Data*, 51:785-850, 2006.

CHAPTER 9

Conclusions and future work

9.1. Scientific contribution of the thesis 227
9.2. Future challenges 230

9.1. SCIENTIFIC CONTRIBUTION OF THE THESIS

The results of this doctoral thesis contribute to extend the knowledge of the thermophysical properties of alternative gas fuels and the introduction of their use in the global energy mix. This work is supported by some national and European research projects.

- *Gases energéticos: biogás y gas natural enriquecido con hidrógeno* (ENE2013-47812-R). Funded by Ministerio de Economía y Competitividad of Spain.
- *Biogás renovable y procesos de captura del CO_2 de combustión asociados como base a la sostenibilidad energética ambiental: Investigación termodinámica experimental* (VA391A12-1). Funded by Consejería de Educación of the Junta de Castilla y León.
- *Characterization of non-conventional energy gases* (EMRP ENG01). Funded by the European Association of National Metrology Institutes (EURAMET) and the EU.
- *Metrology for Biogas* (JRP ENG54). Funded by the European Association of National Metrology Institutes (EURAMET) and the EU.

The main contributions of this work are enumerated as follows.

Analysis of the potential alternatives to traditional fossil fuels

The current situation of the production and use of natural gas and its sustainable alternatives was reviewed in order to evaluate the technical challenges for the introduction of these alternative fuels, and the role of thermodynamics in this process.

Biomethane is one the most promising alternative fuels. However, political and technical challenges must be still overcome in order to promote its use, and some technologies and models designed for natural gas (i.e. reference equation of state of natural gases) should be adapted to these new innovative fuels.

Review of the current methods for the experimental determination of gas densities over wide ranges of temperature and pressure.

Density is one of the most important properties in the development of equations of state. The available methodologies for the experimental determination of gas densities were reviewed, identifying the most adequate techniques to obtain high accuracy density data in order to develop and validate new equations of state.

The single-sinker and the two-sinker densimeter with magnetic suspension coupling are still the most accurate techniques for the experimental determination of gas densities over wide ranges of temperature and pressure.

Tune up of the single-sinker densimeter with magnetic suspension coupling

The single-sinker densimeter with magnetic suspension coupling, which is installed in the laboratory of TERMOCAL, was tuned up by using nitrogen as the reference fluid. Several improvements were also carried out in the measuring process/environment. Firstly, a new air conditioning system was installed in the laboratory to improve the stability of the pressure transducers. Secondly, the temperature operational range of the densimeter was increased thanks to a new thermostatic bath, which allows measuring at lower temperatures with good stability. Finally, the Microsoft Excel® templates used for the data treatment were improved. The experimental results, deviations from the reference equations of state, uncertainties, plots, virial coefficients, etc. can be obtained faster and easier with the new templates.

Estimation of the uncertainty of the density measurements

The uncertainties of the magnitudes involved in the measuring process (temperature, pressure, density and composition) were analyzed and the overall uncertainty of the measurements was calculated by following two alternative methods: i) considering the gravimetric composition, or ii) considering the composition inside the measuring cell from the virial fitting of the experimental data. The estimation of the overall uncertainty from the virial fitting of the experimental data is a good method if the correct homogenization of the mixture cannot be ensured, or sorption effects can occur in the walls of the measuring cell.

The obtained results show similar values for the overall uncertainty estimated by both methods. Therefore, the variation of the composition inside the measuring cell can be

considered as negligible. Moreover, the results of the molar mass of the mixtures obtained from the virial fitting are compatible with the values obtained from the gravimetric composition.

Thermodynamic characterization of binary mixtures of methane (CH_4) and helium (He) at different compositions

The GERG-2008 equation of state claims the future development of a generalized departure function for mixtures containing helium. In order to compensate the lack of experimental data of these kind of mixtures, and motivated by the continuous increase in the helium worldwide demand, the characterization of methane and helium binary mixtures at different composition were performed. This work provides 522 accurate experimental (*p, ρ, T*) data for three (CH_4 + He) mixtures with (5, 10 y 50 mol-% He) at nine temperatures between (240 and 400) K and up to 20 MPa. The estimation of the second B_{12} and third virial coefficients C_{112} y C_{122} is also presented. These results will be of great importance for the future improvement of the GERG-2008 equation of state.

Thermodynamic characterization of a synthetic coal mine methane (CMM) mixture

The thermodynamic characterization of a synthetic mixture emulating a non-conventional fuel gas, known as coal mine methane (CMM), were carried out within the project *"Characterization of non-conventional energy gases"*. The mixture was composed by ten components, with a concentration of 64 mol-% of methane, and it was prepared by the Federal Institute for Materials Research and Testing (BAM) in Berlin, Germany. This work provides 90 high accuracy (*p, ρ, T*) data in a temperature range from (250 to 400) K and pressures up to 15 MPa. The second and third virial coefficients of the CMM mixture were estimated from the experimental data.

Thermodynamic characterization of a synthetic biogas mixture

The thermodynamic characterization of a synthetic biogas-like mixture was carried out during the first period of the project "*Metrology for Biogas*". The mixture was prepared by the Spanish Metrology Center (CEM) with four components, and a concentration of 50

mol-% methane. This work provides 116 accurate (*p, ρ, T*) data in a temperature range from (275 to 400) K and at pressures up to 20 MPa. The second and third virial coefficients of the biogas-like mixture were estimated from the experimental data.

Evaluation of the performance of the reference equation of state for natural gases to represent the behavior of the studied mixtures

The GERG-2008 and, previously, the AGA8-DC92 are the reference equations of state for natural gases. The experimental data from the studied mixtures were compared to estimated values from these equations of state at the same working conditions.

Regarding the (CH_4 + He) mixtures, the relative deviations of experimental data from the GERG-2008 were found to be larger, especially at low temperatures (240 - 260 K) and pressures above 10 MPa. The deviations were greater than 6 % for the 50 mol-% He mixture at pressures above 16 MPa for 240 K, 18 MPa for 250 K and 19 MPa for 260 K. These large deviations could be due to the large difference in the critical temperatures of the individual components of the mixture. On the other hand the composition of the studied mixtures is far from the typical composition of natural gas, independently of its origin. Therefore, we could conclude that the GERG-2008 cannot estimate the thermophysical properties of this mixture with enough accuracy.

The relative deviations of the experimental data for the synthetic CMM and synthetic biogas mixtures were within a 0.2 % band at temperatures below 275 K. The results showed higher deviations at pressures above 10 MPa (up to 0.55 % for the CMM mixture and up to 0.41 % for the biogas) probably due to the high carbon dioxide content.

The identification and quantification of the magnitude of the deviations will contribute to the development of improved versions of the equation of state, customized for alternative fuels and their mixtures with natural gas.

9.2. FUTURE CHALLENGES

As a continuation of this work, an approach to the future research oriented to increase the knowledge of the thermophysical properties of alternative gas fuels by using the single-sinker densimeter is provided in this section. Furthermore, some improvements for the

equipment, in order to measure more accurate experimental density data, are also proposed.

Thermodynamic characterization of new binary mixtures for the development of equations of state

As it was described in chapter 2.4, the mixture model of the GERG-2008 equation of state is based in correlations which simulate the residual behavior of the binary combinations of the 21 components covered by the equation. Due to the lack of high accuracy thermodynamic data for most of the binary systems, the properties for these mixtures are simulated by using adjusted reducing functions for density and temperature. Only 15 of the 210 binary mixtures considered in the GERG-2008 equation of state have associated binary specific or generalized departure functions. However, the report of the GERG-2008 identifies some mixtures whose thermodynamic characterization will be of great interest to improve the equation of state through new specific or generalized departure functions.

- Binary mixtures of the air components: $N_2 + O_2$, $N_2 + Ar$, $O_2 + Ar$…
- Binary mixtures of carbon dioxide with other hydrocarbons.
- Binary hydrocarbon mixtures containing heavy hydrocarbons (from *n*-pentane to *n*-decane).
- Binary mixtures with hydrogen.
- Binary mixtures of water with nitrogen, argon, and carbon dioxide.
- Other binary mixtures containing helium: $N_2 + He$, $CO_2 + He$, $Ar + He$…

Thermodynamic characterization of mixtures related with the production of biomethane from syngas (bioSNG)

The synthetic biogas (bioSNG) is essentially methane (95 mol-%) generated through methanation of syngas from biomass gasification. This technology is still under development, but could be an important sustainable alternative to traditional fossil fuels. In this technology, the methane is produced by two reactions:

$$CO + 3H_2 \rightarrow CH_4 + H_2O$$

$$CO_2 + 4H_2 \rightarrow CH_4 + 2H_2O$$

The thermodynamic characterization of the binary mixtures involved in the process of generation of bioSNG ($CO + H_2$; $CO_2 + H_2$; and $CH_4 + H_2O$) will contribute to improve the scaling and the introduction of this technology. Moreover, the involved binary mixtures lack also of sspecified departure functions in the GERG-2008 equation of state.

Density measurements close to the saturation curve

The new ultra-low refrigerating-heating circulator installed in the laboratory allows obtaining experimental (*p, ρ, T*) data at temperatures from 240 K. Thus, density measurements closer to the saturation curve of gas mixtures can be measured with accuracy. This kind of data are very interesting for the development of equations of state and also to carry out sorption studies. As it was decribed in chapters 6, 7 and 8, the sorption effects on the sinker and the walls of the measuring cell are stronger in regions close to the saturation curve. Therefore, test measurements in that region would be interesting. However the potential condensation of some components in the measured mixture at the lowest temperature should be carefully considered.

Improvements in the thermal isolation of the densimeter auxiliary devices

The pressure transducers and the performance of the thermostatic bath are influenced by the ambient temperature of the laboratory. During this work, a new air conditioning system was installed to improve the situation, but still futher improvements can be carry out.

The thermal isolation of the pressure transducers used for the (2 - 20) MPa and (0 - 2) MPa ranges could be a good solution. Thus, the temperature of the laboratory would not influence in the reading of the pressure inside the measuring cell. Furthermore, the whole isolation of the tubing of the equipment will be considered. These changes could provoke a reorganization of all the devices and tubing, but the benefit will be a better stability of the pressure and temperature measurements.

Analysis of the force transmission error (FTE) induced by the fluid

The FTE induced by the magnetic behavior of the fluid depends on the magnetic susceptibility of the fluid χ_f, the difference between the densities of the sinker and the fluid $(\rho_S - \rho_f)$, and the apparatus specific constant ε_ρ. According to literature, only fluids with a strong diamagnetic or paramagnetic behavior, like water and oxygen, respectively, produce significant deviations in the sinker weight reading of the balance through the magnetic coupling. In this sense, carrying out measurements of this effect would be interesting.

Preparation of gas mixtures in the laboratory

The necessary equipment to prepare mixtures by the gravimetric method in the laboratory of TERMOCAL and the training for the staff would have high costs. However, the laboratory would have a higher capacity in the election of the studied mixtures, decreasing its dependence from external laboratories. Moreover, there are other equipments, like the sferic resonator, which could benefit from a mixture preparation facility.

Updating the data acquisition software

The current data acquisition software, described in chapter 3.5, allows the completly automation of the process. However, unexpected errors occur frecuently, making harder to export of the experimental data to the data treatment templates, and forcing, sometimes, to reset the measuring process. The update of the data acquisition software would avoid these errors and it could allow the development of a new program that can link up the data acquisition with the data treatment. Therefore, the most relevant information about measurements could be obtained automatically.

APPENDIX

A.1. List of tables 237
A.2. List of figures 243
A.3. Publications 249

A.1. LIST OF TABLES

Table 1.1. Natural gas demand per area (10^{12} m^3) [4] 3

Table 2.1. Percentage of fuel imports in the EU-28 in the period (1995 – 2012) [1] 17

Table 2.2. Estimation of technically recoverable reserves of conventional and non-conventional gases (10^{12} m^3) [4] 19

Table 2.3. Usual methane concentration in CMB and flow rates [5] 21

Table 2.4. Components and usual composition ranges of methane in biogas [10] 24

Table 2.5. List of the 21 main and secondary natural gas components and their equations of state used for the GERG-2008 equation of state [22] 33

Table 2.6. List of the binary mixtures for which binary specific or generalized departure functions were developed [22] 36

Table 3.1. Single-sinker densimeters used for researching 54

Table 3.2. Technical specifications of the microbalance Mettler Toledo AT261 DeltaRange 57

Table 3.3. Results from the mass and volume calibration of the weights of tantalum and titanium used in the changing device 59

Table 3.4. Calibration data of the silicon sinker 78

Table 3.5. Parameters of equation 3.17 79

Table 3.6. Average values of the second order elastic constants of silicon 79

Table 3.7. Statistical parameters of relative deviation of experimental data from reference equation of state for nitrogen [29] 85

Table 3.8. Standard deviation of average temperature inside the measuring cell 87

Table 4.1. Calibration uncertainty and its drift for both PRT-25 Minco probes 99

Table 4.2. Uncertainty budget for temperature measurement 100

Table 4.3. Uncertainty Budget of the (2 - 20) MPa pressure transducer 101

Table 4.4. Uncertainty Budget of the (0 - 2) MPa pressure transducer 101

Table 4.5. Uncertainty budget for the mass reading when the measuring cell is pressurized 102

Table 4.6. Uncertainty budget for the mass reading when the measuring cell is evacuated 102

Table 4.7. Uncertainty budget for the density of the fluid 104

Table 5.1. Studied mixtures prepared by gravimetric method 118

Table 6.1. Composition of the studied (CH_4 + He) mixtures 125

Table 6.2. Purity, supplier, molar mass and critical parameters of the individuals components of the studied (CH_4 + He) mixtures 125

Table 6.3. Critical parameters and molar mass of the studied (CH_4 + He) binary mixtures. 126

Table 6.4. Results of the GC analysis of the (CH_4 + He) binary mixtures and gravimetric composition of the validation mixture 127

Table 6.5. Least mean squares fitting results for (0.95 CH_4 + 0.05 He) mixture (M_{virial}, *B, C*), with their uncertainties, and virial coefficients values estimated by the GERG-2008..... 131

Table 6.6. Least mean squares fitting results for (0.90 CH_4 + 0.10 He) mixture (M_{virial}, *B, C*), with their uncertainties, and virial coefficients values estimated by the GERG-2008 equation of state 131

Table 6.7. Least mean squares fitting results for (0.50 CH_4 + 0.50 He) mixture (M_{virial}, *B, C*), with their uncertainties, and virial coefficients values estimated by the GERG-2008 equation of state 132

Table 6.8. Estimated composition of the studied (CH_4 + He) mixtures from virial fitting of the experimental results 134

Table 6.9. Second interaction virial coefficients and expanded uncertainties (k = 2) for studied (CH_4 + He) binary mixtures 135

Table 6.10. Third interaction virial coefficients and expanded uncertainties (k = 2) for (CH_4 + He) binary mixtures 136

Table 6.11. Molar mass of methane and helium [21] 138

Table 6.12. Uncertainty budget of the composition associated to the molar mass of the (CH_4 + He) mixtures 139

Table 6.13. Contributions to the expanded overall uncertainty in density (k = 2) for the (0.95 CH_4 + 0.05 He) mixture 139

Table 6.14. Contributions to the expanded overall uncertainty in density (k = 2) for the (0.90 CH_4 + 0.10 He) mixture 140

Table 6.15. Contributions to the expanded overall uncertainty in density (k = 2) for the (0.50 CH_4 + 0.50 He) mixture..... 140

Table 6.16. Statistical parameters of the data set with respect to the GERG-2008 and AGA8-DC92 equations of state for the (CH_4 + He) mixtures..... 144

Table 6.17. Estimated deviations of the experimental densities from the GERG-2008 equation of state when pressure is zero..... 146

Table 6.18. Average temperatures of the isotherms and standard deviation of B_{12} 150

Table 6.19. Experimental (p, ρ, T) measurements for the (0.95 CH_4 + 0.05 He), mixture, relative and absolute expanded uncertainty in density (k = 2) $U(\rho_{exp})$, expanded overall uncertainty in density (k = 2) from gravimetric composition $U_{T1}(\rho_{exp})$ and from virial expansion $U_{T2}(\rho_{exp})$ and relative deviations from the GERG-2008 and AGA8-DC92 equations of state; where T is the temperature (ITS-90 [25]), p the pressure, ρ_{exp} the experimental density and ρ_{EoS} the density calculated from both equations of state 152

Table 6.20. Experimental (p, ρ, T) measurements for the (0.90 CH_4 + 0.10 He), mixture, relative and absolute expanded uncertainty in density (k = 2) $U(\rho_{exp})$, expanded overall uncertainty in density (k = 2) from gravimetric composition $U_{T1}(\rho_{exp})$ and from virial expansion $U_{T2}(\rho_{exp})$ and relative deviations from the GERG-2008 and AGA8-DC92 equations of state; where T is the temperature (ITS-90 [25]), p the pressure, ρ_{exp} the experimental density and ρ_{EoS} the density calculated from both equations of state 157

Table 6.21. Experimental (p, ρ, T) measurements for the (0.50 CH_4 + 0.50 He), mixture, relative and absolute expanded uncertainty in density (k = 2) $U(\rho_{exp})$, expanded overall uncertainty in density (k = 2) from gravimetric composition $U_{T1}(\rho_{exp})$ and from virial expansion $U_{T2}(\rho_{exp})$ and relative deviations from the GERG-2008 and AGA8-DC92 equations of state; where T is the temperature (ITS-90 [25]), p the pressure, ρ_{exp} the experimental density and ρ_{EoS} the density calculated from both equations of state 162

Table 7.1. Usual concentrations and flows of the different types of CMB [1] 172

Table 7.2. Composition of the synthetic coal mine methane (CMM) mixture and purity, supplier, critical parameters and molar mass of the individual component gases 174

Table 7.3. Results of the first GC analysis of the synthetic CMM mixture 177

Table 7.4. Results of the second GC analysis of the synthetic CMM mixture 178

Table 7.5. Least mean squares fitting results for synthetic CMM mixture (M_{virial}, B, C), with their uncertainties, and virial coefficients values estimated by the GERG-2008 181

Table 7.6. Molar mass of CMM mixture components and their uncertainties [17] 184

Table 7.7. Uncertainty budget of the composition associated to the molar mass of the synthetic CMM mixture..... 184

Table 7.8. Contributions to the expanded overall uncertainty in density (k = 2) for synthetic CMM mixture 185

Table 7.9. Estimated deviations of the experimental densities from the GERG-2008 equation of state when pressure is zero..... 186

Table 7.10. Statistical parameters of the data set with respect to the GERG-2008 and AGA8-DC92 equations of state 189

Table 7.11. Working range and composition of the synthetic CMM mixture of this work and synthetic samples of natural gas studied by Patil, Atilhan and McLinden..... 190

Table 7.12. Statistical comparison of density measurements of mixtures represented in Figure 7.7..... 192

Table 7.13. Experimental (p, ρ, T) measurements for the synthetic CMM mixture, relative and absolute expanded uncertainty in density (k = 2) $U(\rho_{exp})$, expanded overall uncertainty in density (k = 2) from gravimetric composition $U_{T1}(\rho_{exp})$ and from virial expansion $U_{T2}(\rho_{exp})$ and relative deviations from the GERG-2008 and AGA8-DC92 equations of state; where T is the temperature (ITS-90 [23]), p the pressure, ρ_{exp} the experimental density and ρ_{EoS} the density calculated from both equations of state..... 193

Table 8.1. Composition of the synthetic biogas-like mixture, and purity, supplier, critical parameters and molar mass of the individual component gases..... 203

Table 8.2. Results of the GC analysis of the synthetic biogas-like mixture 204

Table 8.3. Least mean squares fitting results for synthetic biogas-like mixture (M_{virial}, B, C), with their uncertainties, and virial coefficients values estimated by GERG-2008 equation of state..... 207

Table 8.4. Molar mass of biogas-like mixture components and their uncertainties [21].. 209

Table 8.5. Uncertainty budget of the composition associated to the molar mass of the synthetic biogas-like mixture 210

Table 8.6. Contributions to expanded overall uncertainty in density (k = 2) for synthetic biogas-like mixture..... 210

Table 8.7. Estimated deviations of experimental densities from the GERG-2008 equation of state when pressure is zero 211

Table 8.8. Statistical parameters of the data set with respect to the GERG-2008 and AGA8-DC92 equations of state..... 215

Table 8.9. Experimental (p, ρ, T) measurements for the synthetic CMM mixture, relative and absolute expanded uncertainty in density (k = 2) $U(\rho_{exp})$, expanded overall uncertainty in density (k = 2) from gravimetric composition $U_{T1}(\rho_{exp})$ and from virial expansion $U_{T2}(\rho_{exp})$ and relative deviations from the GERG-2008 and AGA8-DC92 equations of state; where T is the temperature (ITS-90 [23]), p the pressure, ρ_{exp} the experimental density and ρ_{EoS} the density calculated from both equations of state 218

A.2. LIST OF FIGURES

Figure 2.1. Consumption of primary energy products: a) worldwide; b) in the EU-28 [1]... 17

Figure 2.2. Map of basins with proven reserves of shale gas in May 2013. The red colored basins have been quantified on an estimated basis. Source EIA [7] 22

Figure 2.3. Use of biogas depending on the level of purification [10] 26

Figure 2.4. Biogas plants in the EU [13] 27

Figure 2.5. Overall production of biogas in the EU in 2013 (ktoe) according to the origin of the organic substrate. Eurobserv'ER 2014 [14] 28

Figure 2.6. Biomethane plants in the UE-28 [13] 29

Figure 2.7. General description of the 210 binary combinations from the 21 natural gas components considered in the development of the GERG-2008 equation of state. Diagram illustrates the different types of functions used for the description of the binary mixtures [22] 36

Figure 3.1. Scheme of methods for density determination in fluids 49

Figure 3.2. Basic design of the two-sinker densimeter [1] 52

Figure 3.3. Scheme of the single-sinker densimeter 56

Figure 3.4. Microbalance Mettler Toledo AT261 DeltaRange inside the insulation bell and adjustable support 58

Figure 3.5. Weight changing device controller 59

Figure 3.6. "Non-linearity effect" of the real curve of a balance between two calibrated points (A and B). W_{load} refers to loaded weight and $W_{indication}$ indicates the balance reading 60

Figure 3.7. Calibrated weight changing device 61

Figure 3.8. Magnetic suspension coupling controller 62

Figure 3.9. Magnetic suspension coupling positions 63

Figure 3.10 Double-walled stainless steel cylinder and refrigerated-heating circulator Julabo FP50-HE 64

Figure 3.11. Scheme of the inner thermostatic system with the location of the temperature controlled probes in the measuring cells, the electrical heating cylinder and the Julabo MC-E controller 65

Figure 3.12. Location of the PRT-25 temperature probes in the measuring cell..... 66

Figure 3.13. Pressure transducers used to measure the pressure in the range (2 - 20) MPa (up) and (0 - 2) MPa (down) 67

Figure 3.14. Schematic flow diagram of the network used to fill and evacuate the measuring cell of the single-sinker densimeter. *V1-V8*: High pressure valves (20 MPa). *EV*: Electrovalve. *PV*: Piston air-operated valve. *C1-C3*: High pressure cross fittings. *T1-T6*: High pressure "*T*" fittings. *VP*: Vacuum pump. *M*: Manometer. *VV1-VV2*: Vacuum line valves. *ZT*: Zeolites trap. *CT*: Cryogenic trap. *PP1-PP2*: vacuum probes. *AV*: pressure reducer. *F*: filter. *RD*: ruptura disc. *CV*: check valve 68

Figure 3.15. Elements of the vacuum system: zeolites trap, cryogenic trap, vacuometer and vacuum pump..... 69

Figure 3.16. Valves panel 70

Figure 3.10. Piston air-operated valve 72

Figure 3.18. Silicon sinker and its support 77

Figure 3.19. Variation of the sinker volume with temperature and pressure 80

Figure 3.20. Screenshot of the control and acquisition data software 81

Figure 3.21. Flow diagram of the control and data acquisition software..... 83

Figure 3.22. Screenshot of the Excel file with an isotherm data 84

Figure 3.23. Room ambient temperature during a whole density measurement by using "old" climatization system (blue) and new one (red). Temperature was recorded by using the termometer inside (0 - 2) MPa pressure transducer case 87

Figure 5.1. Diagram of the process a gas mixture preparation by gravimetric method..... 117

Figure 6.1. Preparation scheme of the (CH_4 + He) binary mixtures..... 125

Figure 6.2. Relative deviation of experimental pressure from pressure calculated by virial expansion p_{vir} (Eq. 4.16) by using the fitted parameters for the (0.95 CH_4 + 0.05 He) mixture. ☐ 240 K; ◇ 250 K; △ 260 K; × 275 K; + 300 K; ○ 325 K; ✳ 350 K; – 375 K; – 400 K..... 132

Figure 6.3. Relative deviation of experimental pressure from pressure calculated by virial expansion p_{vir} (Eq. 4.16) by using the fitted parameters for the (0.90 CH_4 + 0.10 He) mixture. ☐ 240 K; ◇ 250 K; △ 260 K; × 275 K; + 300 K; ○ 325 K; ✳ 350 K; – 375 K; – 400 K..... 133

Figure 6.4. Relative deviation of experimental pressure from pressure calculated by virial expansion p_{vir} (Eq. 4.16) by using the fitted parameters for the (0.50 CH_4 + 0.50 He) mixture. ☐ 240 K; ◇ 250 K; △ 260 K; × 275 K; + 300 K; ○ 325 K; ✳ 350 K; – 375 K; – 400 K 133

Figure 6.5. Relative deviations in density of experimental (*p, ρ, T*) data of the (0.95 CH_4 + 0.05 He) mixture ρ_{exp} from density values calculated from the GERG-2008 equation of state ρ_{EoS} versus pressure: ☐ 240 K; ◇ 250 K; △ 260 K; × 275 K; + 300 K; ○ 325 K; ✳ 350 K; – 375 K; – 400 K. Error bars on the 240 K isotherm indicate the expanded uncertainty (*k* = 2) of the experimental data 141

Figure 6.6. Relative deviations in density of experimental (*p, ρ, T*) data of the (0.95 CH_4 + 0.05 He) mixture ρ_{exp} from density values calculated from the AGA8-DC92 equation of state ρ_{EoS} versus pressure: ☐ 240 K; ◇ 250 K; △ 260 K; × 275 K; + 300 K; ○ 325 K; ✳ 350 K; – 375 K; – 400 K. Error bars on the 240 K isotherm indicate the expanded uncertainty (*k* = 2) of the experimental data 141

Figure 6.7. Relative deviations in density of experimental (*p, ρ, T*) data of the (0.90 CH_4 + 0.10 He) mixture ρ_{exp} from density values calculated from the GERG-2008 equation of state ρ_{EoS} versus pressure: ☐ 240 K; ◇ 250 K; △ 260 K; × 275 K; + 300 K; ○ 325 K; ✳ 350 K; – 375 K; – 400 K. Error bars on the 240 K isotherm indicate the expanded uncertainty (*k* = 2) of the experimental data 142

Figure 6.8. Relative deviations in density of experimental (*p, ρ, T*) data of the (0.90 CH_4 + 0.10 He) mixture ρ_{exp} from density values calculated from the AGA8-DC92 equation of state ρ_{EoS} versus pressure: ☐ 240 K; ◇ 250 K; △ 260 K; × 275 K; + 300 K; ○ 325 K; ✳ 350 K; – 375 K; – 400 K. Error bars on the 240 K isotherm indicate the expanded uncertainty (*k* = 2) of the experimental data 142

Figure 6.9. Relative deviations in density of experimental (*p, ρ, T*) data of the (0.50 CH_4 + 0.50 He) mixture ρ_{exp} from density values calculated from the GERG-2008 equation of state ρ_{EoS} versus pressure: ☐ 240 K; ◇ 250 K; △ 260 K; × 275 K; + 300 K; ○ 325 K; ✳ 350 K; – 375 K; – 400 K. Error bars on the 240 K isotherm indicate the expanded uncertainty (*k* = 2) of the experimental data 143

Figure 6.10. Relative deviations in density of experimental (*p, ρ, T*) data of the (0.50 CH_4 + 0.50 He) mixture ρ_{exp} from density values calculated from the AGA8-DC92 equation of state ρ_{EoS} versus pressure: ☐ 240 K; ◇ 250 K; △ 260 K; × 275 K; + 300 K; ○ 325 K; ✳ 350 K; – 375 K; – 400 K. Error bars on the 240 K isotherm indicate the expanded uncertainty (*k* = 2) of the experimental data 143

Figure 6.11. Variation of the calculated virial coefficients with temperature for the (0.95 CH_4 + 0.05 He) mixture. ☐ B_{grav}; ◇ B_{virial}; △ B_{GERG}; × C_{grav}; + C_{virial}; ○ C_{GERG} 148

Figure 6.12 Variation of the calculated virial coefficients with temperature for the (0.90 CH_4 + 0.10 He) mixture. ☐ B_{grav}; ◇ B_{virial}; △ B_{GERG}; × C_{grav}; + C_{virial}; ○ C_{GERG} 148

Figure 6.13. Variation of the calculated virial coefficients with temperature for the (0.50 CH_4 + 0.50 He) mixture. ☐ B_{grav}; ◇ B_{virial}; △ B_{GERG}; × C_{grav}; + C_{virial}; ○ C_{GERG} 148

Figure 6.14. Second interaction virial coefficient for the (CH_4 + He) mixture estimated from the experimental data. ☐ 240 K; ◇ 250 K; △ 260 K; × 275 K; + 300 K; ○ 325 K; ✳ 350 K; – 375 K; – 400 K. The dash lines represent the B_{12} values estimated from the GERG-2008 at different temperatures 149

Figure 6.15. Second interaction virial coefficient for the (CH_4 + He) binary mixture. ☐ (0.95 CH_4 + 0.05 He); ◇ (0.90 CH_4 + 0.10He); △ (0.50 CH_4 + 0.50 He). The solid line represents the polynomial of degree 2 fitted to experimental data of this work. $B_{12}(T)/cm^3 \cdot mol^{-1} = -3 \cdot 10^{-4} \cdot T^2 + 0.1847 \cdot T - 5.0431$. ■ Bignell et al [24] 150

Figure 6.16. Variation of the third interaction virial coefficients with temperature for the (CH_4 + He) binary mixture. ☐ C_{112}; ◇ C_{122} 151

Figure 7.1. Coalbed methane (CBM) types in function of their source 171

Figure 7.2. Preparation scheme of the synthetic CMM mixture. BAM, Berlín, Germany .. 176

Figure 7.3. *pT*-phase diagram showing the experimental points measured (●), the calculated saturation curve for the synthetic coal mine methane mixture, the temperature and pressure ranges of validity of the GERG-2008 equation of state (dashed line) and the area of interest for the storage, transport and utilization of gas fuels (thin dashed line)... 179

Figure 7.4. Relative deviation of experimental pressure from pressure calculated by virial expansion (Eq. 4.16) by using the fitted parameters. ☐ 250 K; ◇ 275 K; △ 300 K; × 325; + 350 K; ○ 375 K; ✳ 400 K..... 182

Figure 7.5 Variation of the calculated virial coefficients with temperature. ◇ B_{Virial}, ☐ B_{GERG}, △ C_{Virial} y × C_{GERG} 187

Figure 7.6. Relative deviations in density of experimental (*p, ρ, T*) data of the synthetic CMM mixture ρ_{exp} from density values calculated from the GERG-2008 equation of state ρ_{EoS} versus pressure: ☐ 250 K; ◇ 275 K; △ 300 K; × 325; + 350 K; ○ 375 K; ✳ 400 K. Error bars on the 250 K isotherm indicate the expanded uncertainty (*k* = 2) of the experimental data. Dark bar corresponds to the uncertainty of the GERG-2008 (0.1 %) [3] 188

Figure 7.7. Relative deviations in density of experimental (*p, ρ, T*) data of the synthetic CMM mixture ρ_{exp} from density values calculated from the AGA8-DC92 equation of state ρ_{EoS} versus pressure: ☐ 250 K; ◇ 275 K; △ 300 K; × 325; + 350 K; ○ 375 K; ✳ 400 K.

Error bars on the 250 K isotherm indicate the expanded uncertainty (k = 2) of the experimental data. Dark bar corresponds to the uncertainty of the AGA8-DC92 [5] 188

Figure 7.8. Deviations of experimental densities from GERG-2008 equation of state: ■ CMM this work, ◇ Patil et al., × Atilhan et al. [21] and △ McLinden [22]..... 191

Figure 8.1. *pT*-phase diagram showing the experimental points measured in this work (●), the calculated saturation curve for the synthetic biogas-like mixture, the temperature and pressure ranges of validity of the GERG-2008 equation of state (dashed line) and the area of interest for storage, transport and utilization processes of gas fuels (thin dashed line) 205

Figure 8.2. Relative deviation of experimental pressure from pressure calculated by virial expansion (Eq. 4.16) by using the fitted parameters. □ 275 K; ◇ 300 K; △ 325 K; + 350 K; ✳ 375 K; ○ 400 K 208

Figure 8.3. Variation of the calculated virial coefficients with temperature. ◇ B_{Virial}, □ B_{GERG}, △ C_{Virial} y × C_{GERG} 212

Figure 8.4. Relative deviations in density of experimental (p, ρ, T) data of the synthetic biogas-like mixture ρ_{exp} from density values calculated from the GERG-2008 equation of state ρ_{EoS} versus pressure: □ 275 K; ◇ 300 K; △ 325 K; + 350 K; ✳ 375 K; ○ 400 K. Error bars on the 275 K isotherm indicate the expanded uncertainty (k = 2) of the experimental data. Dark bar corresponds to the uncertainty of the GERG-2008 (0.1 %) [3] 213

Figure 8.5. Relative deviations in density of experimental (p, ρ, T) data of the synthetic biogas-like mixture ρ_{exp} from density values calculated from the AGA8-DC92 equation of state ρ_{EoS} versus pressure: □ 275 K; ◇ 300 K; △ 325 K; + 350 K; ✳ 375 K; ○ 400 K..... 214

Figure 8.6. Relative deviation of experimental density from density estimated by GERG-2008 equation of state for (0.20 CO_2 + 0.80 CH_4) binary mixture versus pressure: □ 250 K; ◇ 275 K; △ 300 K; × 325; + 350 K; ○ 375 K; ✳ 400 K [6]..... 215

Figure 8.7. Relative deviation of experimental density from density estimated by GERG-2008 equation of state for (0.40 CO_2 + 0.60 CH_4) versus pressure: ◇ 275 K; △ 300 K; × 325; + 350 K; ○ 375 K; ✳ 400 K [6]..... 216

Figure 8.8. Relative deviation of experimental density from density estimated by AGA8-DC92 equation of state for (0.89984 CH_4 + 0.10016 N_2) binary mixture versus pressure at different temperatures: ■ 240 K; □ 250 K; ♦ 275 K; ◊ 300 K; ▲ 350 K; and ▵ 400 K [7] 216

Figure 8.9. Relative deviation of experimental density from density estimated by AGA8-DC92 equation of state for (0.79998 CH_4 + 0.20002 N_2) binary mixture versus pressure at different temperatures: ■ 240 K; □ 250 K; ♦ 275 K; ◊ 300 K; ▲ 350 K; and ▵ 400 K [7]..... 217

A.3. PUBLICATIONS RELATED TO THE THESIS

The most relevant results of this thesis have been published at the Journal of Chemical Thermodynamics (impact factor: 2.679, first quartile: Q1).

1. **Accurate thermodynamic characterization of a synthetic coal mine methane mixture**. R. Hernández-Gómez, D. Tuma, M. a. Villamañán, M. E. Mondéjar, and C. R. Chamorro. Journal of Chemical Thermodynamics, vol. 68, pp. 253–259, Jan. 2014. DOI: 10.1016/j.jct.2013.09.023.
2. **Integration of biogas in the natural gas grid: thermodynamic characterization of a biogas-like mixture**. R. Hernández-Gómez, T. E. Fernández-Vicente, M. C. Martín González, M. E. Mondéjar, and C. R. Chamorro. Journal of Chemical Thermodynamics, vol. 84, pp. 60–66, May 2015. DOI: 10.1016/j.jct.2014.12.028.
3. **Experimental determination of (p, ρ, T) data for binary mixtures of methane and helium**. R. Hernández-Gómez, D. Tuma, J. J. Segovia, and C. R. Chamorro. Journal of Chemical Thermodynamics. DOI: 10.1016/j.jct.2015.12.006.

Furthermore, the results obtained for the (0.50 CH_4 + 0.50 He) mixture and the interaction virial coefficients of the methane and helium binary mixtures will be also sent for publication in the next months.

On the other hand, some results of this thesis were also presented in international seminars.

1. **Challenges in the European Area: Young Scientist's 1st International Baku Forum**. Baku, Azerbaijan. 20-25/05/2013.

   Abstract: Integration of non-conventional gases in the natural gas grid: thermodynamic characterization of synthetic coal mine methane (CMM) mixture. Roberto Hernández Gómez.
2. **EGATEC. European Gas Technology Conference**. Paris, France. 30-31/05/2013.

   Poster: Integration of bio-methane in the natural gas grid: thermodynamic characterization of non-conventional energy gases. Roberto Hernández Gómez, César R. Chamorro Camazón, María E. Mondéjar.
3. **II Congreso Latinoamericano de Ingeniería Petrolera, Gas, Minas y Afines**. Quito, Ecuador. 21-22/11/2013.

Poster: Integración de biometano en la red de gas natural; caracterización termodinámica de combustibles no-convencionales. Roberto Hernández Gómez, César R. Chamorro Camazón.

4. **ECTP 2014. 20th European Conference on Thermophysical Properties**. Oporto, Portugal. 31/08 - 04/09/2014.

   Poster: Integration of biogas in the natural gas grid: thermodynamic characterization of a biogas-like mixture. Roberto Hernández-Gómez, José J. Segovia, María C. Martín, Miguel A. Villamañán, Teresa E. Fernández-Vicente, Dolores del Campo, César R. Chamorro.

5. **19th Symposium on Thermophysical Properties**. Boulder, Colorado, USA. 21-26/06/2015.

   Poster: Experimental determination of (*p, ρ, T*) data for binary mixtures of methane and helium. R. Hernández-Gómez, D. Tuma, H. Kipphardt, M. A. Villamañán J. J. Segovia, M. C. Martín, C. R. Chamorro.

J. Chem. Thermodynamics 68 (2014) 253–259

Contents lists available at ScienceDirect

J. Chem. Thermodynamics

journal homepage: www.elsevier.com/locate/jct

Accurate thermodynamic characterization of a synthetic coal mine methane mixture

R. Hernández-Gómez [a], D. Tuma [b], M.A. Villamañán [a], M.E. Mondéjar [a], C.R. Chamorro [a,*]

[a] Grupo de Termodinámica y Calibración (TERMOCAL), Dpto. Ingeniería Energética y Fluidomecánica, Escuela de Ingenierías Industriales, Universidad de Valladolid, Paseo del Cauce, 59, E-47011-Valladolid, Spain
[b] BAM Bundesanstalt für Materialforschung und -prüfung, D-12200 Berlin, Germany

ARTICLE INFO

Article history:
Received 22 April 2013
Received in revised form 16 September 2013
Accepted 17 September 2013
Available online 27 September 2013

Keywords:
Coal mine methane
Density measurements
Single sinker densimeter
GERG-2008 equation of state

ABSTRACT

In the last few years, coal mine methane (CMM) has gained significance as a potential non-conventional gas fuel. The progressive depletion of common fossil fuels reserves and, on the other hand, the positive estimates of CMM resources as a by-product of mining promote this fuel gas as a promising alternative fuel. The increasing importance of its exploitation makes it necessary to check the capability of the present-day models and equations of state for natural gas to predict the thermophysical properties of gases with a considerably different composition, like CMM. In this work, accurate density measurements of a synthetic CMM mixture are reported in the temperature range from (250 to 400) K and pressures up to 15 MPa, as part of the research project EMRP ENG01 of the European Metrology Research Program for the characterization of non-conventional energy gases. Experimental data were compared with the densities calculated with the GERG-2008 equation of state. Relative deviations between experimental and estimated densities were within a 0.2% band at temperatures above 275 K, while data at 250 K as well as at 275 K and pressures above 10 MPa showed higher deviations.

1. Introduction

Coalbed methane (CBM) refers to all methane originated in coal seams by geological or biological processes. Depending on the production source of this fuel gas, it can be classified in several groups, each of them with specific reservoir characteristics, composition and extraction process. Thus, in order from highest to lowest methane concentration, we can identify virgin coalbed methane (VCBM), abandoned mine methane (AMM), coal mine methane (CMM) and ventilation air methane (VAM). CMM is obtained from working coal mines, either in advance of mining or from worked seams, by using drainage techniques. Although its composition depends significantly on the reservoir characteristics, it generally consists of a mixture of methane as the main compound (35% to 75% molar fraction) and higher alkanes, together with nitrogen, oxygen, carbon dioxide and, occasionally, water vapor [1].

Due to the rise of fuel prices in the last years caused by the advancing depletion of their reserves and increasing demand by the global economy, non-conventional and renewable fuels are gaining importance as an alternative to fossil fuels and also as a step to reduce the CO_2 emissions to the atmosphere. Among non-conventional fuels, coalbed methane arises as a potential energy resource in countries with an important coal production. As a by-product of mining, coalbed methane was traditionally used in local small-scale power production, but it can also contribute to the domestic and commercial gas supply.

The presence of CMM in coal mining is a challenge for working safety and from environmental reasons. On the one hand, the accumulation of the gas due to desorption from the distressed coal seam can affect the safety of the mine with an increase of the explosion risk. On the other hand, the uncontrolled release of this gas to the atmosphere can be even more harmful to the environment than CO_2 emissions, since the global warming potential (GWP) of methane is 25 times that of carbon dioxide [2]. Therefore, apart from the exploitation of a coal mining by-product, the controlled use of CMM reduces the overall greenhouse gases emissions and ensures safety in coal mines.

The significant difference in composition between CMM and natural gas, which manifests in a lower methane content and a corresponding higher content of carbon dioxide, nitrogen and other components of the first, makes it necessary to validate the performance of the existing equations of state for natural gases for gases with deviating compositions employing accurate experimental data of their thermophysical properties.

Experimental density data of different multi-component gas mixtures with common natural gas compositions have been previously measured by other authors. In 2007, Patil et al. [3] published experimental density data of a natural-gas-like mixture with a

* Corresponding author. Tel.: +34 983423756; fax: +34 983423363.
E-mail addresses: cescha@eis.uva.es, cescha@eii.uva.es (C.R. Chamorro).

0021-9614/$ - see front matter © 2013 Elsevier Ltd. All rights reserved.
http://dx.doi.org/10.1016/j.jct.2013.09.023

J. Chem. Thermodynamics 84 (2015) 60–66

Contents lists available at ScienceDirect

J. Chem. Thermodynamics

journal homepage: www.elsevier.com/locate/jct

Integration of biogas in the natural gas grid: Thermodynamic characterization of a biogas-like mixture

R. Hernández-Gómez [a], Teresa E. Fernández-Vicente [b], M.C. Martín González [a], M.E. Mondéjar [a], C.R. Chamorro [a,*]

[a] Grupo de Termodinámica y Calibración (TERMOCAL), Dpto. Ingeniería Energética y Fluidomecánica, Escuela de Ingenierías Industriales, Universidad de Valladolid, Paseo del Cauce, 59, E-47011 Valladolid, Spain
[b] Centro Español de Metrología (CEM), C/Alfar, 2, E-28760 Tres Cantos, Madrid, Spain

ARTICLE INFO

Article history:
Received 27 November 2014
Accepted 29 December 2014
Available online 6 January 2015

Keywords:
Biogas
Thermodynamic characterization
Density
Single sinker densimeter
GERG-2008

ABSTRACT

The composition of biogas may vary significantly due to the diversity of production sources, making it essential to have a detailed knowledge of their thermophysical properties in order to develop and validate methods for the estimation of density, heat capacity and calorific value of biogas and biomethane. In this work the thermodynamic behavior of a synthetic biogas-like mixture, composed of methane (50%), carbon dioxide (35%), nitrogen (10%) and carbon monoxide (5%), is studied through accurate (p,ρ,T) experimental data obtained by using a single sinker densimeter with magnetic suspension coupling. The mixture was prepared by the gravimetric method at the Spanish National Metrology Institute (Centro Español de Metrología, CEM) and the accurate density measurements have been performed in the temperature range from (275 to 400) K and pressures up to 20 MPa. This work is part of the research project 'Metrology for Biogas' supported by the European Metrology Research Program. Experimental data are compared with the densities calculated with the GERG-2008 equation of state. The deviation between experimental and estimated densities is within a ±0.2% band at all temperatures, except at the lower temperature, 275 K, and pressures from (6 to 15) MPa, which shows a higher deviation.

1. Introduction

The European Union has established that 20% of energy consumption should come from renewable sources by 2020, and that biofuels should provide at least 10% of transport petrol and diesel consumption by the same year [1]. This directive describes a framework for the promotion of energy from renewable sources, reducing CO2 emissions and establishes the need of integrating renewable energy in the existing transmission and distribution grids. A significant increase of the amount of biogas injected into natural gas networks is an urgent need to achieve this goal.

Due to the diversity of sources of biogas and other non-conventional energy gases, their composition may vary significantly. The significant difference in composition between biogas and natural gas manifests in a lower methane content (50 to 80%) and a corresponding higher content of carbon dioxide (20 to 50%), with small amounts of other components as nitrogen, carbon monoxide and hydrogen. The biogas matrix presents serious challenges concerning the applicability of the approaches used in the natural gas industry for measuring the moisture content and calculating gas properties, such as the density and calorific value. These problems are linked to the substantially higher carbon dioxide content of biogas.

Therefore it is essential to have a detailed knowledge of the thermophysical properties of biogas in order to solve technical and design problems during the transport and exploitation stages. The current models are based on binary mixture data and accurate experimental data on multicomponent mixtures are relatively scarce yet. A large number of very high accuracy experimental data over wide temperature and pressure ranges are needed to develop and validate methods for the estimation of density, heat capacity and calorific value of biogas and biomethane. Experimental density data of multicomponent natural-gas-like mixtures have been previously measured by other authors. In 2007, Patil *et al.* [2] published experimental density data of a natural-gas-like mixture with a methane mole fraction of 91%. In 2011, McLinden [3] presented density data of four natural-gas-like mixtures with similar compositions, which contained approximately 0.90 mol fraction methane and differed mainly in the content of nitrogen, carbon dioxide and high alkanes. In 2014, Hernández-Gómez *et al.* [4]

* Corresponding author. Tel.: +34 983423756; fax: +34 983423363.
E-mail address: cescha@eii.uva.es (C.R. Chamorro).

http://dx.doi.org/10.1016/j.jct.2014.12.028
0021-9614/

INTEGRATION OF BIO-METHANE IN THE NATURAL GAS GRID: THERMODYNAMIC CHARACTERIZATION OF NON-CONVENTIONAL ENERGY GASES

termocal Universidad de Valladolid
Grupo de Termodinámica y Calibración TERMOCAL
Escuela de Ingenierías Industriales. Universidad de Valladolid
Paseo del Cauce 59, 47011 Valladolid. Spain

Roberto Hernández-Gómez.
Supervisors: C.R. Chamorro and M.E. Mondéjar.

INTRODUCTION

The European Union has set as **priorities for 2020** a **20% contribution from renewable resources** to the total energy consumed and a **20% reduction of greenhouse gases emissions**.
The use of alternative energy gases as **bio-methane** and their blends with natural gas will allow a meaningful introduction of renewable and non-conventional fuels into the existing energy infrastructure and the reduction of carbon dioxide emissions.
Due to the **diversity of sources of non-conventional energy gases**, it is essential to have a detailed knowledge of their **thermophysical properties**.
This PhD project is intended to study the thermodynamic behavior of **multicomponent mixtures** through accurate (p,ρ,T) experimental data obtained by using a **single sinker densimeter with magnetic suspension coupling.**

SINGLE SINKER DENSIMETER WITH MAGNETIC COUPLING

This densimeter is based on the **Archimedes' principle**, by which the buoyancy force acting on a sinker immersed in a fluid is proportional to the density of that fluid. Thanks to the magnetic coupling, the sinker mass can be measured with an accurate balance avoiding any contact between the balance and the gas, allowing wide pressure and temperature working ranges.

Pressure range	<20 MPa
Temperature range	250 - 400 K
Expanded Uncertainty	(k=2)
Density	0.02-0.34%
Pressure	0.015%
Temperature	4 mK

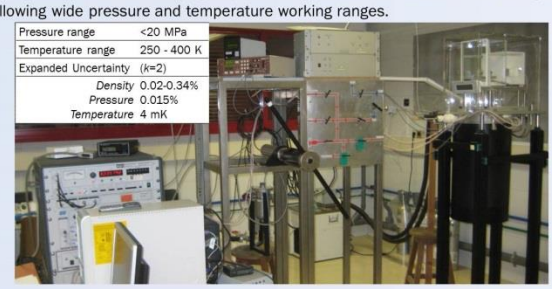

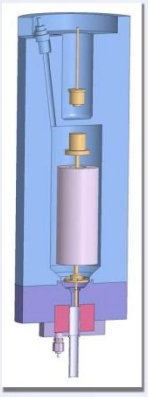

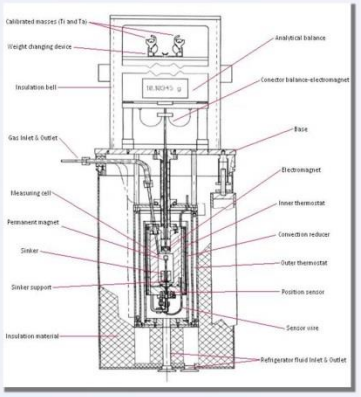

FIRST RESULTS – Coal Mine Methane

Materials

A synthetic **coal mine methane** (CMM) mixture of 10 components was prepared gravimetrically according to ISO 6142 at the Bundesanstalt für Materialforschung und -prüfung (BAM).

Component	Concentration (Mole fraction)
Oxygen	0.00503861
Nitrogen	0.16981633
Methane	0.64258731
Carbon dioxide	0.17352375
Ethane	0.00856491
Propane	0.00079081
i-butane	0.00010760
n-butane	0.00005800
i-pentane	0.00001728
n-pentane	0.00000757

Experimental procedure

Seven isotherms were measured at (250, 275, 300, 325, 350, 375 and 400) K and decreasing pressure steps of 1 MPa between 1 and 15 MPa.

Results

Experimental densities were compared with the densities calculated from the **GERG-2008 equation of state**. Relative deviations between experimental data and estimates were within a 0.2% band for temperatures above 275 K. However, data at 250 K and at 275 K and pressures above 10 MPa showed larger deviations which increased with pressure.

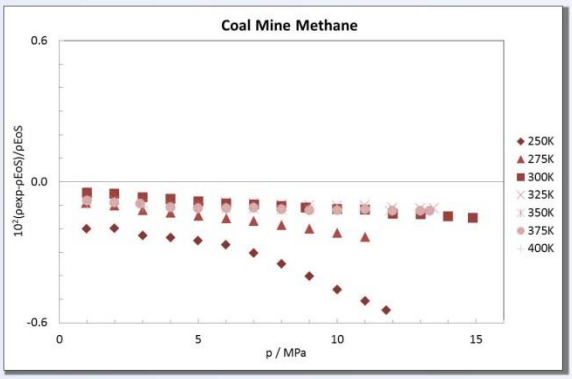

FUTURE WORK

Thanks to the collaboration with the Centro Español de Metrología (CEM) and the Bundesanstalt für Materialforschung und -prüfung (BAM), it is also planned to study other other energy gases mixtures such as biogas, bio-methane and even mixtures relates to carbon capture and sequestration processes.

ACKNOWLEDGMENTS

Support for this work came from the project ENE2009-14644-C02-01 of the Spanish Ministry of Science and Innovation, from the Junta de Castilla y León references GR 152 and Project VA391A12-1, and from the research project EMRP ENG01 of the European Metrology Research Program.

INTEGRACIÓN DE BIOMETANO EN LA RED DE GAS NATURAL: CARACTERIZACIÓN TERMODINÁMICA DE COMBUSTIBLES NO-CONVENCIONALES

termocal Universidad de Valladolid
Grupo de Termodinámica y Calibración TERMOCAL
Escuela de Ingenierías Industriales. Universidad de Valladolid
Paseo del Cauce 59, 47011 Valladolid. Spain

Roberto Hernández-Gómez.
Supervisores: C.R. Chamorro and M.E. Mondéjar.

INTRODUCCIÓN

La Unión Europea ha fijado como **prioridad para el año 2020** que el **20% del total de la energía consumida proceda de fuentes renovables** y, a su vez, **reducir en un 20% las emisiones de gases de efecto invernadero.**

El empleo de combustibles alternativos como el **biometano** y sus mezclas con gas natural permitirá una significativa introducción de combustibles no convencionales en las infraestructuras existentes actualmente, así como la reducción de las emisiones de CO_2.

Debido a la **diversidad de las fuentes de combustibles no-convencionales**, es necesario tener un conocimiento detallado de sus **propiedades termofísicas.**

Este proyecto de tesis profundiza en el estudio del comportamiento termodinámico de **mezclas multicomponentes** a través de precisos datos experimentales (p,ρ,T) obtenidos mediante un **densímetro de flotador sencillo con acoplamiento magnético.**

DENSÍMETRO DE FLOTADOR CON ACOPLAMIENTO MAGNÉTICO

El principio de medida de este densímetro se basa en el **principio de Arquímedes**, el cual indica que el empuje que actúa sobre un flotador inmerso en un fluido es proporcional a la densidad del fluido. Gracias al acoplamiento magnético, es posible medir la masa del flotador con una balanza de precisión sin que exista contacto entre la balanza y el gas. Esto permite realizar medidas en un amplio rango de presión y temperatura.

Pressure range	<20 MPa
Temperature range	250 - 400 K
Expanded Uncertainty	(k=2)
Density	0.02-0.34%
Pressure	0.015%
Temperature	4 mK

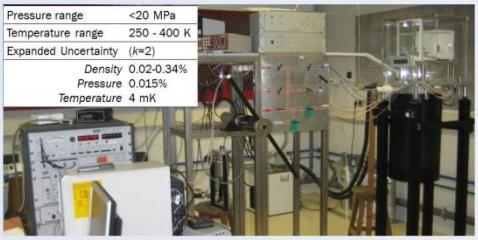

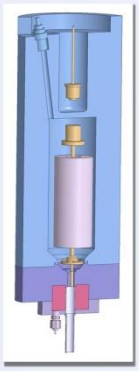

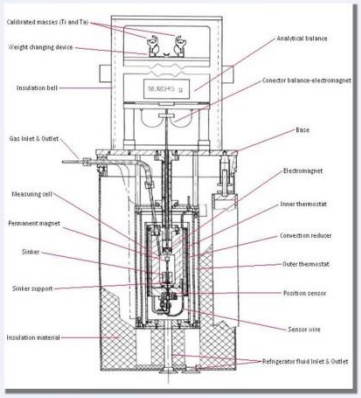

PRIMEROS RESULTADOS – Coal Mine Methane

Materiales

Mezcla sintética de ***coal mine methane*** (CMM) de 10 componentes preparada mediante métodos gravimétricos acordes a la norma ISO 6142 en el Bundesanstalt für Materialforschung und -prüfung (BAM).

Componente	Concentración (fracción molar)
Oxígeno	0.00503861
Nitrógeno	0.16981633
Metano	0.64258731
Dióxido de carbono	0.17352375
Etano	0.00856491
Propano	0.00079081
i-butano	0.00010760
n-butano	0.00005800
i-pentano	0.00001728
n-pentano	0.00000757

Procedimiento experimental

Se midieron 7 isotermas a (250, 275, 300, 325, 350, 375 and 400) K, disminuyendo la presión de 15 a 1 MPa en intervalos de 1 MPa.

Resultados

Los valores de densidad obtenidos experimentalmente fueron comparados con otros calculados con la ecuación de estado **GERG-2008**. Las desviaciones observadas entre los datos experimentales y los estimados fueron menores del 0.2% para temperaturas por encima de 275 K. Sin embargo, los datos obtenidos a 250 K y a 275 K para presiones superiores a 10 MPa muestran grandes desviaciones que aumentan con la presión.

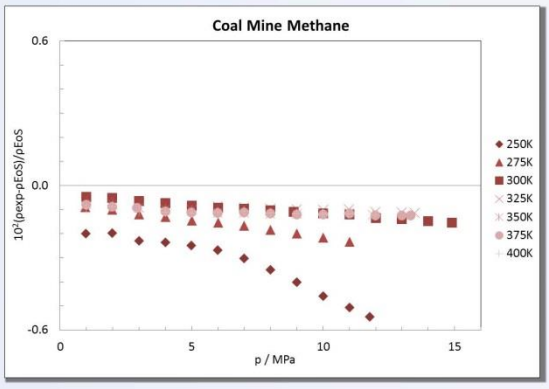

TRABAJO FUTURO

Gracias a la colaboración con el Centro Español de Metrología (CEM) y el Bundesanstalt für Materialforschung und -prüfung (BAM), iestá previsto estudiar otras mezclas combustibles como diferentes tipos de biogás, biometano e incluso mezclas relacionadas con los procesos de captura de CO_2.

AGRADECIMIENTOS

El apoyo para este trabajo provino del proyecto ENE2009-14644-C02-01 del Ministerio de Ciencia e Innovación español, de la Junta de Castilla y León referencias GR 152 y VA391A12-1, y del proyecto de investigación EMRP ENG01 del Programa de Investigación en Metrología de la Unión Europea .

INTEGRATION OF BIOGAS IN THE NATURAL GAS GRID
THERMODYNAMIC CHARACTERIZATION OF A BIOGAS LIKE MIXTURE

Roberto Hernández-Gómez[1], José J. Segovia[1], María C. Martín[1], Miguel A. Villamañán[1], Teresa E. Fernández-Vicente[2], Dolores del Campo[2], César R. Chamorro[1]
[1] Grupo de Termodinámica y Calibración TERMOCAL, Universidad de Valladolid, Spain
[2] Centro Español de Metrología, CEM. Tres Cantos, Madrid, Spain

INTRODUCTION

The European Union has established that 20% of energy consumption should come from renewable sources by 2020 [1]. A significant increase of the amount of **biogas injected into natural gas networks** is an urgent need to achieve this goal. Due to the diversity of sources of biogas and other non-conventional energy gases their composition may vary significantly, making that biogas matrix presents serious challenges concerning the applicability of approaches used in the natural gas industry. Therefore, it is essential to have a detailed **knowledge of the thermophysical properties of different biogas like mixtures** in order to solve technical and design problems during the transport and exploitation stages.
This work studies the thermodynamic behavior of a gravimetrically prepared biogas like mixture through accurate (p,ρ,T) experimental data obtained by using a single sinker densimeter with magnetic suspension coupling.

ACKNOWLEDGMENTS

Support for this work came from:
- Project ENE2013-47812-R of the Spanish Government.
- Project VA391A12-1 of the Junta de Castilla y León regional government.
- Project EMRP ENG54 of the European Metrology Research Program.

MIXTURE PREPARATION

Gas mixtures are **prepared gravimetrically** according to ISO 6142 [5] at the Spanish National Metrology Institute (CEM). Mixtures are prepared in 5 L aluminum alloy cylinders. The vacuum system with TM pump and heaters can reach vacuum down to 10^{-7} hPa. A mass comparator with 1 mg resolution and E2 class mass set is used.
Analytical Validation of gas mixtures is performed with an Agilent 6890 GC-TCD-FID gas chromatograph.


SINGLE SINKER DENSIMETER

This **densimeter** is based on the **Archimedes' principle**, by which the buoyancy force acting on a sinker immersed in a fluid is proportional to the density of that fluid. Thanks to the **magnetic coupling**, the sinker mass can be measured with an accurate balance avoiding any contact between the balance and the gas, allowing wide pressure and temperature working ranges [2, 3, 4].

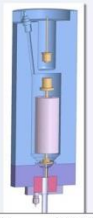


Pressure range	<20 MPa
Temperature range	250 - 400 K
Expanded Uncertainty (k=2)	
Density	0.02-0.34%
Pressure	0.015%
Temperature	4 mK

RESULTS

Gas mixture

A **synthetic biogas like mixture**, composed by methane, carbon dioxide, nitrogen and carbon monoxide, was prepared gravimetrically according to ISO 6142 at the Spanish National Metrology Institute (CEM)

Component	Concentration	Uncertainty
	10^{-2} mol/mol	10^{-2} mol/mol (k=2)
Methane	49.8141	0.0069
Carbon dioxide	35.2028	0.0022
Nitrogen	9.9916	0.0040
Carbon monoxide	4.9915	0.0050

Composition of the synthetic biogas like mixture

Experimental procedure

Six isotherms were measured at (275, 300, 325, 350, 375 and 400) K and decreasing pressure steps of 1 MPa between 1 and 20 MPa.

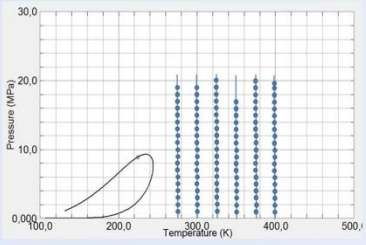

pT phase diagram showing the experimental points measured in this work and the calculated saturation curve for the biogas like mixture.

Density results

Experimental densities were compared with the densities calculated from the **GERG-2008 equation of state** [6]. Deviation between experimental and estimated densities is within a 0.2% band at all temperatures, except at 275 K and pressures from (5 to 15) MPa, which shows a higher deviation.

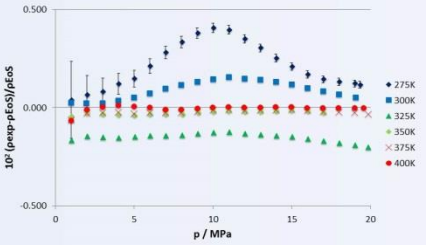

Relative deviations in density of experimental (p, ρ, T) data of the synthetic biogas, ρ_{exp} , from density values calculated from the GERG-2008 equation of state, ρ_{EoS} ,versus pressure. Error bars on the 275 K isotherm indicate the expanded uncertainty (k = 2) of the experimental data.

References

[1] COM (2010) 639, Energy 2020, a strategy for competitive, sustainable and secure energy.
[2] Klimeck J., Kleinrahm R., Wagner W., *J. Chemical Thermodynamics* 1998, 30, 1571-1588.
[3] W. Wagner, R. Kleinrahm, *Metrologia* 2004, 41, S24-S39.
[4] Mondéjar M.E., Segovia J.J., Chamorro C.R., *Measurement* 2011, 44, 1768-1780.
[5] ISO 6142: Preparation of calibration gas mixtures - Gravimetric method. *International Organisation for Standardization*, Geneva, 2012.
[6] Kunz O., Wagner W., *Journal of Chemical & Engineering Data* 2012, 57, 3032–3091.

Experimental determination of (p, ρ, T) data for binary mixtures of methane and helium

termocal Universidad de Valladolid

R. Hernández-Gómez[1], D. Tuma[2], H. Kipphardt[2], J.J. Segovia[1], M.A. Villamañán[1], M.C. Martín[1] and C.R. Chamorro[1]

[1] Grupo de Termodinámica y Calibración TERMOCAL, Universidad de Valladolid, Spain
[2] BAM Bundesanstalt für Materialforschung und -prüfung, Berlin, Germany

BAM Bundesanstalt für Materialforschung und -prüfung

INTRODUCTION

The **GERG-2008 and AGA8-DC92 equations of state** enable the calculation of thermal and caloric properties for natural gases and other related mixtures consisting of up to 21 pure components [1, 2]. Experimental characterization of the thermodynamic behavior of gas binary mixtures is of great importance because most of the binary systems were taken into account by using adjusted reducing functions for density and temperature. Only for those binary mixtures for which sufficient accurate experimental data were available, specific departure functions were developed. For the binary mixture methane-helium no departure function was developed so far.

This work studied the thermodynamic behavior of two gravimetrically prepared methane-helium binary mixtures through accurate (p, ρ, T) experimental data obtained by using a single-sinker densimeter with magnetic suspension coupling.

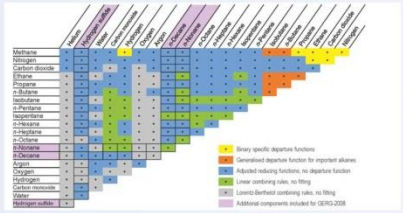

Figure 1. Overview of the 210 binary combinations that result from the 21 natural gas components considered for the development of the GERG-2008 equation of state. The diagram illustrates the different types of functions used for the description of the binary mixtures. The fields marked in yellow and orange show which of the two types of departure functions were used to fit the function to experimental data; in these cases, the parameters of the reducing functions were also fitted. The blue fields refer to binary mixtures where only the parameters of the reducing functions were fitted to experimental data. The green and gray fields indicate which combining rule the reducing functions (without any fitting) were used with. [1]

MIXTURES PREPARATION

Two **methane-helium binary mixtures** were prepared **gravimetrically** according to ISO 6142 [3] at the Federal Institute for Materials Research and Testing (BAM) in two stages. First, a methane-helium 50 % mixture was prepared by a consecutive introduction of helium (6.0, purity ≥ 99.9999 mol-%) and methane (5.5, purity ≥ 99.9995 mol-%) being determined using a Voland HCE 25 mechanical gas balance. Then, the intended mixtures were prepared in a similar way. A portion of the CH_4-He 50 % parent mixture introduced into the recipient cylinder was diluted by a properly measured amount of methane. Each mixture was finally homogenized and validated by gas chromatography against samples of similar composition.

Component	(0.95 CH_4 + 0.05 He)		(0.90 CH_4 + 0.10 He)	
	x_i Concentration	U (x_i) Uncertainty	x_i Concentration	U (x_i) Uncertainty
	10^{-2} mol/mol	10^{-2} mol/mol (k = 2)	10^{-2} mol/mol	10^{-2} mol/mol (k = 2)
Methane	95.001470	0.009236	89.993256	0.008336
Helium	4.998530	0.001365	10.006744	0.001702

Table 1. Composition of the CH_4/He binary mixtures.

SINGLE-SINKER DENSIMETER

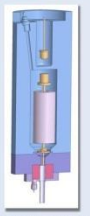

Figure 2. Schematic view of the measuring cell.

The **single-sinker densimeter with magnetic suspension coupling** is based on the **Archimedes' principle**, by which the buoyancy force acting on a sinker immersed in a fluid is proportional to the density of that fluid. The **magnetic coupling** allows to measure the sinker mass with an accurate balance avoiding any contact between the balance and the gas. It is one of the state-of-the-art methodologies for the measurement of the density of fluids over wide temperature and pressure ranges [4, 5, 6].

Pressure range	<20 MPa
Temperature range	250 – 400 K
Expanded uncertainty (k = 2)	
Density/ kg·m^{-3}	$2.31 \cdot 10^{-2} + 1.14 \cdot 10^{-4} \cdot \rho$
Pressure/ MPa	$75 \cdot 10^{-6} \cdot p + 3.52 \cdot 10^{-3}$
Temperature/ mK	4

Table 2. Operation range and estimated uncertainties of the single-sinker densimeter.

RESULTS

Experimental procedure

Seven isotherms were measured at (250, 275, 300, 325, 350, 375 and 400) K and decreasing pressure steps of 1 MPa between (1 and 20) MPa.

Density results

Experimental densities were compared with densities calculated from **GERG-2008** [1] and **AGA8-DC92** [2] **equations of state**. The uncertainty in density for typical natural gas compositions is 0.1 % for both equations.

Deviations between experimental and estimated densities are clearly higher from GERG-2008 than from AGA-DC92.

Values calculated from AGA8-DC92 deviate from experimental data by more than 0.1 % at high pressures and even exceed the 0.2 % limit at temperatures of 300 K and above for the (0.90 CH_4 + 0.10 He) mixture.

Deviations from GERG-2008 are within a 2 % band for the (0.95 CH_4 + 0.05 He) mixture and exceed the 3 % limit for the (0.90 CH_4 + 0.10 He) mixture. Deviations are higher at lower temperatures. Thus, the highest deviations are at 250 K and pressures between 17 and 19 MPa.

Mixture	(0.95 CH_4 + 0.05 He)		(0.90 CH_4 + 0.10 He)	
EoS	GERG-2008	AGA8-DC92	GERG-2008	AGA8-DC92
AAD	0.555	0.105	1.014	0.172
RMS	0.707	0.115	1.262	0.191
MaxD	−1.806	−0.168	−3.195	−0.296
$U(\rho)$ (k = 2)/ kg·m^{-3}	(0.024-0.046)		(0.023-0.043)	

Table 3. Statistical parameters of the deviations between experimental and estimated densities.

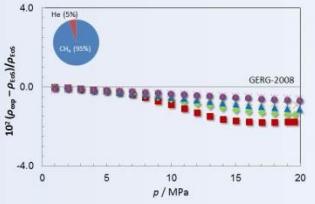

Figure 3. Relative deviations in density of experimental (p, ρ, T) data of the **(0.95 CH_4 + 0.05 He)** mixture ρ_{exp} from density values calculated from the **GERG-2008** ρ_{EoS} versus pressure.

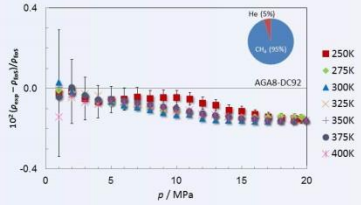

Figure 4. Relative deviations in density of experimental (p, ρ, T) data of the **(0.95 CH_4 + 0.05 He)** mixture ρ_{exp} from density values calculated from the **AGA8-DC92** ρ_{EoS} versus pressure.

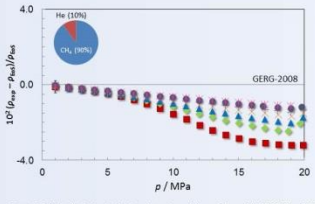

Figure 5. Relative deviations in density of experimental (p, ρ, T) data of the **(0.90 CH_4 + 0.10 He)** mixture ρ_{exp} from density values calculated from the **GERG-2008** ρ_{EoS} versus pressure.

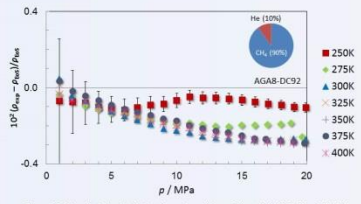

Figure 6. Relative deviations in density of experimental (p, ρ, T) data of the **(0.90 CH_4 + 0.10 He)** mixture ρ_{exp} from density values calculated from the **AGA8-DC92** ρ_{EoS} versus pressure.

ACKNOWLEDGMENTS

Support for this work came from:

- Gases energéticos: biogás y gas natural enriquecido con hidrógeno (ENE2013-47812-R) of the Spanish Government.
- Biogás renovable y procesos de captura del CO_2 de combustión asociados como base a la sostenibilidad energética ambiental: Investigación termodinámica experimental (VA391A12-1) of the Junta de Castilla y León Regional Government.
- Metrology for biogas (ENG54). European Metrology Research Program.

REFERENCES

[1] Kunz O., Wagner W., *J. Chem. Eng. Data* 2012, 57, 3032–3091.
[2] Starling K.E., Savidge J.L., *American Gas Association (AGA) Transmission Measurement Committee Report 8*, 2nd Ed., 1992.
[3] ISO 6142: Preparation of calibration gas mixtures – Gravimetric method. *International Organization for Standardization*, Geneva, 2012.
[4] Klimeck J., Kleinrahm R., Wagner W., *J. Chem. Thermodynamics* 1998, 30, 1571–1588.
[5] Wagner W., Kleinrahm R., *Metrologia* 2004, 41, S24–S39.
[6] Mondéjar M.E., Segovia J.J., Chamorro C.R., *Measurement* 2011, 44, 1768–1780.

Resumen en castellano

1. Introducción 261
2. Objetivos de la tesis 263
3. Metodología. El densímetro de flotador sencillo con sistema de acoplamiento de suspensión magnética 265
4. Incertidumbre de las medidas 273
5. Preparación de las mezclas estudiadas 275
6. Caracterización termodinámica de mezclas binarias de metano y helio 276
7. Caracterización termodinámica de una mezcla sintética de CMM (*coal mine methane*) ... 280
8. Caracterización termodinámica de una mezcla sintética de biogás 282
9. Conclusiones 284
10. Referencias 289

1. INTRODUCCIÓN

La Hoja de Ruta Energética de la Comisión Europea para el año 2050 [1] persigue lograr al menos una reducción del 80% en la emisión de gases de efecto invernadero respecto a los valores registrados en 2009, alcanzando niveles por debajo de los registrados en 1990 el para el año 2050. Todo ello manteniendo o incluso mejorando los niveles actuales de fiabilidad en el suministro de electricidad, la seguridad energética, el crecimiento económico y la prosperidad. Este objetivo, junto a lo establecido en la Directiva de Energías Renovables 2009/28/CE [2], cuyos objetivos especifican que el 20% del consumo de energía debería provenir de fuentes renovables para el año 2020, hace de la diversificación en el abastecimiento energético una apuesta clara para Europa. En este sentido, y entre otras iniciativas, la Unión Europea (UE) urge a aumentar significativamente la cantidad de combustibles alternativos empleados en el mix energético global. Además, la Hoja de Ruta Energética de la Comisión Europea para el año 2050 identifica el gas natural como combustible sustituto del carbón para la transformación del sistema energético a corto-medio plazo.

Según datos de 2012, en la Unión Europea de los 28 apenas se produce el 35 % del gas natural consumido, debiendo ser importado casi el 66 % [3].

La creciente dependencia en la UE del gas importado hace de la diversificación en el abastecimiento de este combustible un firme objetivo para los próximos años. De esta forma, debido a la diversidad de fuentes, materiales y residuos de los que proceden, combustibles gaseosos como el biogás o el gas de esquisto presentan grandes posibilidades para alcanzar el escenario deseado para el año 2050.

El biogás es una fuente de energía renovable producida a partir de la fermentación aeróbica de materia orgánica compuesto principalmente por metano (CH_4) y dióxido de carbono (CO_2). Su producción total en la UE en 2013 fue de 13.4 Mtoe, lo que representó un crecimiento del 10.2 % respecto al año anterior. Así mismo, se produjeron 52.3 TWh de electricidad a partir de la combustión de biogás en motores de cogeneración [4]. El volumen de producción previsto de biogás, según los planes de acción nacional de energías renovables de los países miembros para el año 2020, es de aproximadamente 280 Mtoe [5].

En cuanto al gas de esquisto, según la EIA, las reservas técnicamente recuperables identificadas a nivel mundial ascienden a $7299 \cdot 10^{12}$ m^3, siendo China, Argentina, Argelia,

EEUU y Canadá los países con mayores reservas estimadas [6]. Esta revelación ha obligado a Europa y muchos otros países a poner en marcha exploraciones y estudios para analizar la sostenibilidad y rentabilidad de proyectos de este tipo en su suelo. En Europa, el gas de esquisto está considerado como el combustible no-convencional con mayor potencial de desarrollo en comparación con otros combustibles fósiles no-convencionales: se calcula que los recursos de gas de esquisto técnicamente recuperables en la UE ascienden aproximadamente a $16 \cdot 10^{12}$ m^3.

Sin embargo, la diversa procedencia de estos combustibles alternativos y de la materia orgánica a partir de la cual se genera biogás hace que existan ciertas limitaciones técnicas, relacionadas especialmente con el almacenamiento y transporte, que deben resolverse antes de la completa introducción de estos combustibles en las redes existentes de gas natural. Además de la diversa procedencia, la aplicación final de los combustibles alternativos hace que pueda estar presentes en ellos una gran variedad de componentes en diferentes concentraciones. Por esta razón, es imprescindible contar con herramientas que permitan el cálculo de sus propiedades termodinámicas en un amplio rango de composición y condiciones de operación, tanto en las fases homogéneas de gas y líquido, como en las regiones supercríticas y estados de equilibrio líquido−vapor. Los equipos de medición y los modelos matemáticos actuales han sido desarrollados y evaluados únicamente para composiciones cercanas a la composición típica del gas natural, por lo que no satisfacen las necesidades de precisión para la correcta estimación de las propiedades termodinámicas de los nuevos combustibles alternativos. Esto se traduce en la necesidad de un mayor número de parámetros para simular el comportamiento de estos gases y estimar sus propiedades termodinámicas con la misma fiabilidad que el caso del gas natural. Por lo tanto, el conocimiento de estos parámetros es crucial para la correcta integración de los combustibles alternativos.

Nota: En el CD está disponible la versión completa de la tesis en castellano.

2. OBJETIVOS DE LA TESIS

La investigación desarrollada en este trabajo de tesis doctoral pretende contribuir al desarrollo e introducción de nuevos combustibles gaseosos de origen renovable en el mix energético europeo a través de la caracterización termodinámica de mezclas de los componentes principales de estos combustibles alternativos. Con los resultados obtenidos se espera contribuir al análisis y la mejora de las ecuaciones de estado de referencia con la finalidad de que la industria gasista pueda estimar de manera precisa y fiable las propiedades termofísicas clave de estos nuevos combustibles.

El presente trabajo de tesis doctoral ha contado además con el apoyo de varios proyectos de investigación. En el ámbito nacional:

- *Gases energéticos: biogás y gas natural enriquecido con hidrógeno* (ENE2013-47812-R). Financiado por el Ministerio de Economía y Competitividad de España en la modalidad de proyectos de I+D+i de la convocatoria 2013 del Programa Estatal de Investigación, Desarrollo e Innovación Orientada a los Retos de la Sociedad.
- *Biogás renovable y procesos de captura del CO_2 de combustión asociados como base a la sostenibilidad energética ambiental: Investigación termodinámica experimental* (VA391A12-1). Financiado por la Consejería de Educación de la Junta de Castilla y León dentro del Programa de Apoyo a Proyectos de Investigación.

En el ámbito internacional se ha contado con el apoyo de dos proyectos europeos de investigación financiados por la Asociación Europea de Institutos Nacionales de Metrología (EURAMET) y la UE. La Universidad de Valladolid (UVA) ha participado en estos proyectos a través del grupo de investigación TERMOCAL, donde se ha desarrollado este trabajo.

- EMRP ENG01 – *Characterization of non-conventional energy gases* [7].
- JRP ENG54 – *Metrology for Biogas* [8].

A continuación se detallan los principales objetivos de esta tesis doctoral.

1. Hacer una revisión de las tecnologías existentes para la determinación experimental de la densidad de gases en amplios rangos de presión y temperatura.

2. Poner a punto del densímetro de flotador sencillo con sistema de acoplamiento de suspensión magnética y realizar ensayos con gases de referencia para determinar su capacidad.

3. Estimar la incertidumbre total de las medidas de densidad con el equipo empleado, incluyendo las incertidumbres asociadas a las magnitudes involucradas en el proceso: temperatura, presión, densidad y composición del fluido.

4. Caracterizar termodinámicamente mezclas binarias de metano (CH_4) y helio (He) de distinta composición y estimar los coeficientes de interacción viriales a partir de los datos experimentales obtenidos.

5. Caracterizar termodinámicamente una mezcla sintética multicomponente simulando la composición de un combustible gaseosos no-convencional tipo CMM (*coal mine methane*).

6. Caracterizar termodinámicamente una mezcla sintética multicomponente simulando la composición de un biogás.

7. Analizar la adecuación de las ecuaciones de estado de referencia para el gas natural AGA8-DC92 y GERG-2008 para representar el comportamiento experimental registrado en las mezclas estudiadas.

8. Contribuir al desarrollo de nuevas ecuaciones de estado de referencia adecuadas a los combustibles gaseosos alternativos y la mezcla de éstos con gas natural mediante la aportación de datos (p, ρ, T) experimentales de gran precisión.

3. METODOLOGÍA. EL DENSÍMETRO DE FLOTADOR SENCILLO CON SISTEMA DE ACOPLAMIENTO DE SUSPENSIÓN MAGNÉTICA

El equipo utilizado en la caracterización termodinámica de las mezclas estudiadas es el densímetro de flotador sencillo con sistema de acoplamiento de suspensión magnética. A principios de la decada de 1990, Brachthäuser et al. [12] desarrollaron el primer densímetro de flotador sencillo, descrito en 1995 por Wagner et al. [13]. El método de medida se basa en el principio de Arquímedes, que consiste en medir la fuerza de empuje que experimenta un cuerpo (flotador) inmerso en el fluido. La fuerza de empuje es proporcional a la densidad del fluido y al volumen del flotador, por lo que conociendo el volumen del flotador se puede determinar la densidad del fluido mediante la ecuación 3.3.

$$\rho(T,p)=\frac{B}{g\cdot V_S(T,p)}=\frac{m_{S0}-m_{Sf}}{V_S(T,p)} \qquad \textbf{Ec. 3.3}$$

donde $\rho(T,p)$ es la densidad del fluido en kg·m^{-3} como función de su presión y temperatura; B es la fuerza de empuje expresada en N; g es la constante de aceleración de la gravedad en m·s^{-2}; $V_S(T,p)$ es el volumen del flotador en m^3 como función de la temperatura y la presión del fluido. La fuerza de empuje se determina midiendo la diferencia entre la masa real del flotador en el vacío m_{S0} y la masa aparente de éste cuando está inmerso en el fluido m_{Sf}, expresada en kg.

La parte central del densímetro de flotador sencillo utilizado en este trabajo fue fabricado por la empresa alemana '*Rubotherm Präzisionsmesstechnik GmbH*' y adquirido por la Universidad de Valladolid en 1996. Según las características técnicas del fabricante, opera en el rango de temperatura de (233 a 533) K y presiones de hasta 20 MPa. El equipo se completó con los sistemas de control y medida de temperatura y presión. La puesta en marcha y las pruebas iniciales fueron realizadas por Chamorro et al. [14] y posteriormente Mondéjar [15] realizó importantes modificaciones para mejorar la incertidumbre de medida de las tres magnitudes implicadas en el proceso: temperatura, presión y densidad.

El densímetro está formado por la celda de medida, una microbalanza analítica de precisión, el dispositivo de intercambio de masas, el sistema de acoplamiento de suspensión magnética, un sistema de control y medida de la temperatura, un sistema para el control de los procesos de llenado y vaciado de la celda y medida de la presión y un

sistema de vacío. Como líquido termostático se utiliza un aceite especial de transferencia de calor que es previamente termostatizado en un baño termostático comercial.

La Figura 3.3 representa un esquema del densímetro de flotador sencillo empleado para este trabajo y los principales elementos del densímetro de flotador sencillo.

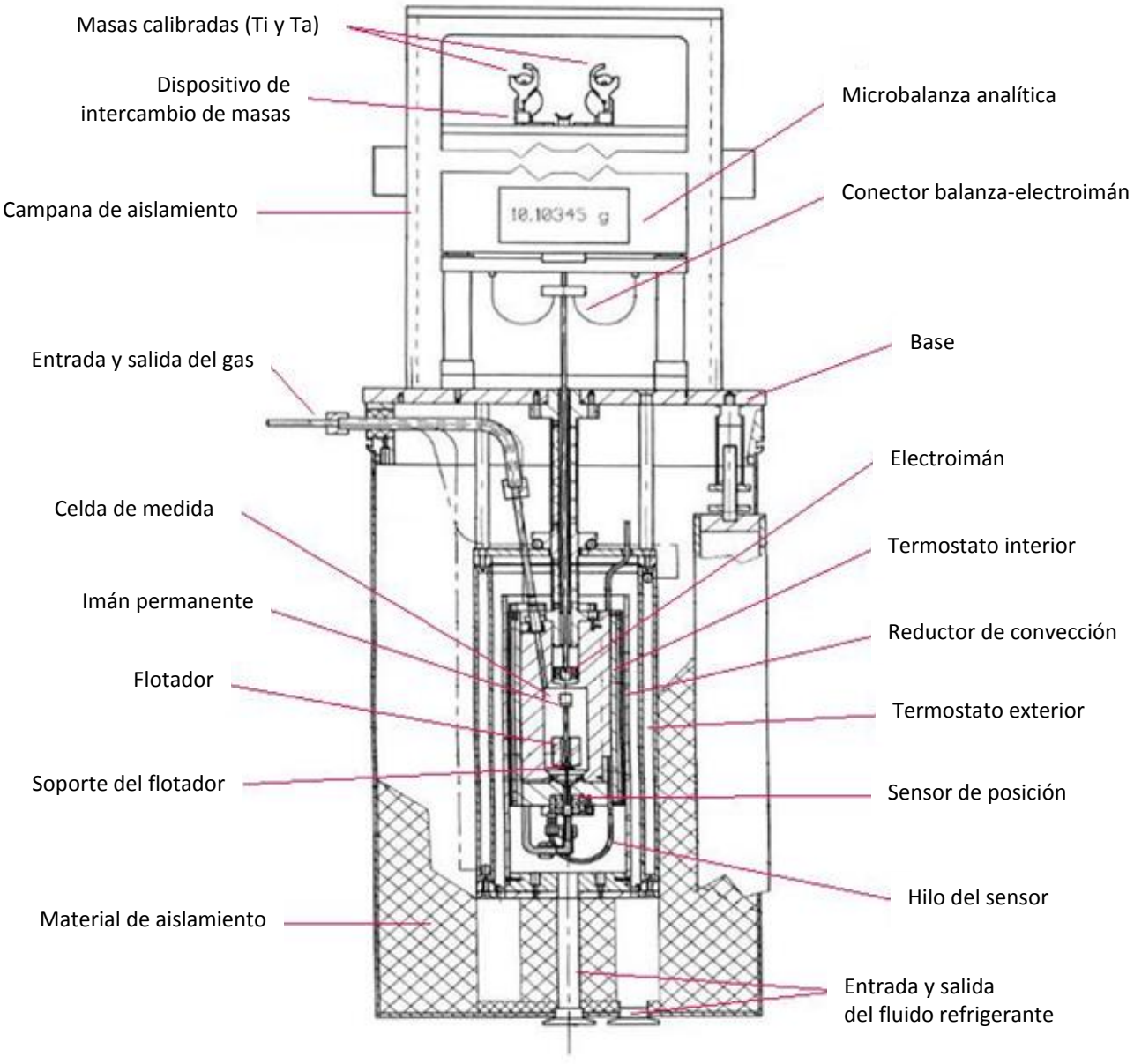

Figura 3.3. *Esquema del densímetro de flotador sencillo.*

La celda de medida

La celda de medida está dividida a su vez en dos espacios aislados estre sí: la carcasa de acoplamiento (superior) y la celda de medida propiamente dicha (inferior). La carcasa de acoplamiento aloja un electroimán físicamente conectado al gancho de la balanza mediante una fina varilla metálica. Por su parte, la celda de medida, situada debajo, contiene el flotador y un imán permamente del sistema de acoplamiento magnético, el cual está a su vez conectado al soporte del flotador. La celda está fabricada de una aleación de cobre, cromo y zirconio (CuCrZr) con la cual presenta un comportamiento magnético casi nulo y una alta resistencia mecánica. La celda de medida está aislada del exterior mediante una espuma de silicona de 250 $kg \cdot m^{-3}$ de densidad para un rango de trabajo de (213 a 473) K y una cubierta de polietileno (Armaflex) apropiada para temperaturas entre (203 y 383) K. El fluido que se desea medir se introduce y se evacúa de la celda mediante dos conducciones.

Microbalanza analítica de precisión

Las medidas de la masa aparente del flotador se llevan a cabo con una microbalanza analítica de precisión (Mettler Toledo AT261 DeltaRange) a través de un sistema de acoplamiento de suspensión magnética entre el enganche inferior de la balanza y el flotador en el interior de la celda de medida, de forma que no existe contanto físico entre ambos. Esto permite operar a presiones y temperaturas extremas en el interior de la celda sin que se vea afectado el funcionamiento de la balanza y proporcionando una alta precisión en las medidas. Aunque puede operar de modo manual, con el fin de automatizar el proceso, la balanza está conectada a un ordenador mediante un bus de datos, lo que permite trabajar completamente desde el programa de control y adquisición de datos, registrando en éste todas las medidas realizadas.

Dispositivo de intercambio de masas

La calibración de la balanza se realiza in situ de forma automática mediante un dispositivo de intercambio de masas previamente calibradas según las directrices para la calibración de instrumentos no automáticos de medida de masa desarrollados por Euramet [16]. Las masas están fabricadas de tántalo ($\rho \approx 16670\ kg \cdot m^{-3}$) y titanio ($\rho \approx 4507\ kg \cdot m^{-3}$) y ambas tienen un volumen de aproximadamente 4.9 cm^3 ($V_{Ta} \approx V_{Ti} \approx 4.9\ cm^3$). Para que la balanza

opere con mayor precisión en el rango justificado anteriormente es necesario que la diferencia de peso entre ambas sea próxima a la masa del flotador ($m_S \approx 60$ g). Las masas fueron suministradas por la empresa diseñadora del densímetro, *Rubotherm*, y tanto su masa como su volumen fueron calibrados en el Laboratorio de Masa del Centro Español de Metrología (CEM).

Sistema de acoplamiento de suspensión magnética

El principal componente del densímetro de flotador sencillo es el sistema de acoplamiento de suspensión magnética desarrollado por Lösch et al. [17], el cual transmite la fuerza de empuje que ejerce el fluido sobre el flotador en la celda de medida (presurizada y termostatizada) a la balanza de precisión a presión atmosférica sin que haya contacto entre ambos. El acoplamiento magnético se lleva a cabo a través de dos dispositivos. Por un lado se encuantre el electroimán, colgado de un enganche situado en la parte inferior de la balanza y aislado en carcasa de acoplamiento, y por otra parte el imán permanente, ensamblado al soporte del flotador en el interior de la celda de medida. Gracias a este sistema no se produce contacto directo entre el flotador inmerso en el fluido y la balanza, permitiendo así determinar la densidad de fluidos en un amplio rango de temperatura y presión.

Sistema de control y medida de la temperatura

La celda de medida se encuentra termostatizada a través de dos sistemas termostáticos independientes: uno exterior, con el que se realiza un “ajuste grueso” de la temperatura, y otro interior directamente en contacto con la celda de medida, con el que se realiza el “ajuste fino”. La combinación de ambos sistemas permite alcanzar la temperatura deseada en la celda de medida minimizando los gradientes térmicos en la celda. La temperatura en el interior de la celda de medida termostatizada se determina mediante dos sondas PRT-25 Minco S1059PJ5X6 (Minco 712 y Minco 713) colocadas una frente a la otra y a la mitad de la celda de medida. Las sondas se encuentran conectadas a un puente comparador de resistencias de corriente contínua (Automatic Systems Laboratory F700) a través de una caja de distribución multicanal (Automatic Systems Laboratory SB 148/01). Este puente mide el ratio de resistencia entre las sondas PRT-25 y un resistor externo estándar

calibrado y termostatizado a 36ºC (Tinsley 5685ª, 25Ω). Las calibraciones de las sondas utilizadas se realizaron por el propio laboratorio TERMOCAL, acreditado por ENAC.

Sistema de llenado, vaciado, control y medida de la presión

La presión en el interior de la celda se determina mediante dos transductores de presión. Para presiones entre (2 y 20) MPa se utiliza un Paroscientific 43KR-HHT-101, mientras que para el rango de presiones de (0 a 2) MPa se utiliza un Paroscientific 2300A-101. Ambos transductores están conectados a dos *Digiquartz® intelligent displays* (730 y 735, respectivamente) y al sistema de llenado. El transductor de presión para (0 - 2) MPa está separado del resto de la red mediante una válvula de accionamiento manual para evitar sobrepresiones en el dispositivo. Para establecer el valor final de la presión en el interior de la celda de medida, los valores registrados por ambos medidores de presión se corrigen mediante una función polinómica de grado cinco a partir de las constantes determinadas en el correspondiente certificado de calibración. Los medidores de presión fueron calibrados por el servicio de calibración de TERMOCAL.

Las conducciones de la red están fabricadas en acero inoxidable. Las líneas conectadas de la celda de medida a la línea de vacío tienen un diámetro externo de 1/4''. El cilindro que contiene el fluido de medida está conectado a la red mediante conducciones con un diámetro externo de 1/8''. El resto de conducciones tiene un diámetro externo de 1/16''. La red fue diseñada para operar a presiones de hasta 105 MPa. Todos los elementos fueron suministrados por HiP (*High Pressure Equipment Company*). La bomba manual empleada para incrementar la presión en la celda de medida (HiP Model 87-6-5; 5000 psi) está también fabricada en acero inoxidable.

Sistema de vacío

El sistema de vacío está conectado al sistema de llenado y vaciado, de forma que es posible evacuar las conducciones o la celda de medida de forma independiente. El vacío en el interior de la celda se genera mediante una bomba de vacío con rotor de dos etapas (Leybold TRIVAC D8B), capaz de crear un vacío de 0.5 Pa. Previamente a la bomba de vacío hay instaladas dos trampas para prevenir la transmisión de impurezas y vapores perniciosos que puedan contaminar la celda de vacío o la bomba. La primera trampa consiste en una trampa de zeolitas (Leybold FA 2-4) que impide la migración de agua o

moléculas de hidrocarburo desde la bomba de vacío a la celda de medida. La segunda trampa se trata de una trampa criogénica (Leybold TK 4-8) que proteje la bomba de vapores dañinos. Para medir la presión durante el proceso de generación de vacío en la celda de medida se utilizan dos sondas de vacío conectadas a a un vacuómetro (Thermovac TM22) que trabaja en el rango de presiones de $5 \cdot 10^{-4}$ Pa hasta presión atmosférica.

Procedimiento de medida

El proceso de toma de datos se lleva a cabo registrando la densidad del fluido en isotermas a (240, 250, 260, 275, 300, 325, 350, 375 y 400) K, descendiendo la presión automáticamente en pasos de 1 MPa desde 20 MPa hasta 1 MPa. Al final de cada isoterma se evacúa la celda de medida y se acciona el sistema de vacío para medir nuevamente la masa del flotador. En cada paso de presión se realizan 30 medidas (p, ρ, T).

La utilización del sistema de acoplamiento de suspensión magnética es sensible a desviaciones. La fuerza magnética transmitida entre el electroimán y el imán permanente del acoplamiento magnético puede verse influenciada por campos magnéticos externos e incluso por las propiedades magnéticas del flotador, la celda de medida o el mismo fluido de medida. A este efecto se le conoce con el nombre de "error de transmisión de fuerza" o FTE por sus siglas en inglés (*force transmision error*) y ha sido descrito en detalle por McLinden et al. [18]. En el densímetro de flotador sencillo el FTE puede separarse en dos términos: el error inducido por el equipo de medida y el inducido por el fluido. El FTE inducido por el aparato se refiere a la influencia que tienen los propios componentes del densímetro sobre el sistema de acoplamiento magnético. La medida de la masa del flotador en el vacío al finalizar cada isoterma anula cualquier influencia del FTE inducido por el aparato en las medidas de densidad, tal y como indica en su estudio McLinden et al. [18]. El FTE inducido por el comportamiento magnético del fluido o "efecto específico del fluido", depende de la susceptibilidad magnética del fluido χ_f, la diferencia de densidad entre el flotador y el fluido $(\rho_S - \rho_f)$ y la constante específica del aparato ε_ρ. A la vista del valor estimado para la constante específica del aparato (ε_ρ = 45.7 ppm) y teniendo en cuenta que el error de transmisión de fuerza debido al aparato influye en mayor medida al FTE total (excepto para fluidos fuertemente paramagnéticos) y que éste es anulado a través de la medida del vacío después de cada isoterma, no se ha considerado la corrección

del efecto específico del fluido en este trabajo. Además, ninguna de las mezclas medidas en este trabajo tiene comportamiento paramagnetico.

El procedimiento para la medida de la masa aparente del flotador se lleva a cabo combinando las diferentes posiciones del sistema de acoplamiento de suspensión magnética junto con el proceso de calibración de las masas. De esta forma, la medida de la masa del flotador, tanto en condiciones de presión m_{Sf} como en el vacío m_{S0}, se lleva a cabo de forma que se reduce al máximo la influencia del efecto de no-linealidad de la balanza.

El volumen del flotador $V_S(T, p)$ no es constante a lo largo del proceso de medida de la densidad, sino que varía influenciado por la presión y la temperatura del fluido de medida. Por lo tanto, el volumen del flotador debe ser determinado para cada punto de medida a partir de los datos obtenidos de presión, temperatura y del valor del volumen de calibración del flotador.

El proceso de medida de la densidad con el densímetro de flotador sencillo está totalmente automatizado. Los datos son recopilados en ficheros Excel, a partir de los cualesse realiza el correspondiente tratamiento de datos.

Mejoras realizadas en el equipo

En el marco de este trabajo se han acometido mejoras relacionadas con la estabilidad de la presión y la temperatura del proceso de medida con la adquisición de dos nuevos equipos. En primer lugar, se instaló un nuevo sistema de climatización (Daikin Inverter Room Air Conditioner model FTX50GV1B) en el laboratorio donde se encuentra el densímetro de flotador sencillo y todos los dispositivos auxiliares. La temperatura ambiente de la sala puede afectar al funcionamiento de los transductores de presión. Además, ésta se ve afectada por la temperatura del baño termostático. Por este motivo, la sala se encuentra permanentemente a una temperatura de (23 ± 2) ^{o}C

Como puede observarse en la Figura 3.23, la estabilidad de la temperatura ambiente en el laboratorio con el sistema de climatización anterior fue claramente menor que con el sistema instalado actualmente. Cabe señalar que la temperatura ambiente representada en la Figura 3.23 corresponde a la temperatura registrada por un termómetro instalado en el interior de la carcasa del transductor de presión de (0 - 2) MPa, por lo que los valores

mostrados no se corresponden con la temperatura real del laboratorio, aunque sí proporciona una idea de la variación de la misma durante la medida de una isoterma. La temperatura real del laboratorio no es registrada por el programa de adquisición de datos, pero sí puede ser consultada gracias a un termómetro independiente colocado en la sala. Otra mejora relacionada con la estabilidad de la temperatura en el interior de la celda ha sido la sustitución del criotermostato por un nuevo ultracriotermostato de circulación Julabo FP51-SL. El nuevo baño termostático fue instalado en octubre de 2015. Con él es posible obtener datos (p, ρ, T) a temperaturas desde 240 K (en lugar de 250 K).

4. INCERTIDUMBRE DE LAS MEDIDAS

A continuación se resume, el análisis de la incertidumbre de medida de las magnitudes implicadas en el proceso de determinación de la densidad a través de un densímetro de flotador sencillo con sistema de acoplamiento de suspensión magnética.

La incertidumbre expandida (k = 2) en la medida de la temperatura $U(T)$ se estimó en $3.87 \cdot 10^{-3}$ K.

La Incertidumbre en la medida de la presión depende del transductor de presión utilizado. Para el rango de presión de (2 - 20) MPa la incertidumbre expandida (k = 2) estimada ha sido $U(p) = 75 \cdot 10^{-6} \cdot p + 3.52 \cdot 10^{-3}$. Para el rango de presión de (0 - 2) MPa la incertidumbre expandida (k = 2) estimada ha sido $U(p) = 60 \cdot 10^{-6} \cdot p + 1.78 \cdot 10^{-4}$.

La incertidumbre expandida (k = 2) en la determinación de la densidad se ha estimado en $U(\rho) = 2.31 \cdot 10^{-2} \cdot \rho + 1.14 \cdot 10^{-4}$.

Según la GUM [19], para calcular la incertidumbre estándar total de las medidas (k = 1) $u_T(\rho)$, deben considerarse las incertidumbres típicas combinadas estimadas para la densidad, temperatura, presión y composición.

En el caso de la composición, su incertidumbre se puede estimar a partir de las incertidumbres de la composición de los componentes de la mezcla preparada por el método gravimétrico. Sin embargo, la composición dentro de la celda de medida puede verse alterada por diferentes razones, como la adsorción de las moléculas de gas en las paredes y el flotador o debido a una incorrecta homogeneización de la mezcla en las fases de llenado o evacuación. Estos efectos impredecibles suponen una fuente de incertidumbre adicional a la incertidumbre extraída de la composición gravimétrica de la mezcla. La densidad molar de una mezcla de vapor es constante para unos valores de temperatura, presión y composición dados, es decir, la densidad másica es proporcional a la masa molecular. Por lo tanto, la incertidumbre en densidad asociada a las incertidumbres en la composición es proporcional a la incertidumbre de la masa molecular M de la mezcla. La incertidumbre de la masa molecular asociada a los efectos impredecibles en el interior de la celda de medida puede ser estimada a partir de los resultados experimentales y utilizada para calcular la incertidumbre total de las medidas experimentales.

En vista de ello y con el fin de extraer las conclusiones oportunas, la incertidumbre total estándar $(k=1)$ $u_T(\rho)$ asociada a las medidas de densidad realizadas para este trabajo se ha calculado siguiendo dos métodos diferenciados.

El primero de ellos tiene en cuenta las contribuciones de la densidad, presión, temperatura y composición gravimétrica, tal y como indica en ecuación 4.13.

$$u_T(\rho)=\left[u(\rho)^2+\left(\left(\frac{\partial\rho}{\partial p}\right)_{T,x}u(p)\right)^2+\left(\left(\frac{\partial\rho}{\partial T}\right)_{p,x}u(T)\right)^2+\sum_i\left(\left(\frac{\partial\rho}{\partial x_i}\right)_{T,p,x_j\neq x_i}u(x_i)\right)^2\right]^{0.5} \quad \textbf{Ec. 4.13.}$$

donde p es la presión, T es la temperatura y x_i es la fracción molar de cada uno de los componentes de la mezcla.

El segundo método consiste en expresar la incertidumbre asociada a la composición como incertidumbre de la masa molecular, de forma que pueda incluirse la incertidumbre asociada a los efectos de adsorción o de falta de homogeneización. El valor de la incertidumbre total estándar $(k=1)$ $u_T(\rho)$ asociada a las medidas de densidad realizadas se calcula en este caso mediante la ecuación 4.14.

$$u_T(\rho)=\left[u(\rho)^2+\left(\left(\frac{\partial\rho}{\partial p}\right)_{T}u(p)\right)^2+\left(\left(\frac{\partial\rho}{\partial T}\right)_{p}u(T)\right)^2+\left(\left(\frac{\partial\rho}{\partial M}\right)_{p,T}\cdot u(M)\right)^2\right]^{0.5} \quad \textbf{Ec. 4.14.}$$

Las derivadas parciales pueden ser calculadas mediante la ecuación de estado GERG-2008 con el software REFPROP [20].

5. PREPARACIÓN DE LAS MEZCLAS ESTUDIADAS

Las mezclas estudiadas fueron preparadas expresamente para la medida de su densidad con un densímetro de flotador sencillo por dos laboratorios colaboradores con el grupo de investigación TERMOCAL: El Instituto Federal para la Investigación de Materiales y Ensayos (BAM, *Bundesanstalt für Materialforschung und –prüfung*) y el Centro Español de Metrología (CEM). En total se prepararon cinco mezclas, tres binarias y dos multicomponentes, de distinta naturaleza. En la Tabla 5.1 se detalla la composición de mezclas estudiadas y los laboratorios donde se prepararon siguiendo el método gravimétrico. Los parámetros críticos de cada mezcla fueron estimados con la ecuación de estado GERG-2008 [10] a través del software REFPROP [20].

Tabla 5.1. *Relación de mezclas estudiadas preparadas por el método gravimétrico.*

Mezcla	Componentes	Composición /mol-%	Laboratorio	Presión inicial	Volumen	Parámetros críticos
Metano + Helio (1)	CH_4 He	95.001470 4.998530	BAM	13.7 MPa	10 dm^3	T_c = 194.2 K p_c = 6.44 MPa
Metano + Helio (2)	CH_4 He	89.993256 10.006744	BAM	13.2 MPa	10 dm^3	T_c = 196.3 K p_c = 8.24 MPa
Metano + Helio (3)	CH_4 He	49.259240 50.740760	BAM	14.0 MPa	10 dm^3	-
CMM	CH_4 CO_2 N_2 C_2H_6 C_3H_8 *i*-C_4H_{10} *n*-C_4H_{10} *i*-C_5H_{12} *n*-C_5H_{12} O_2	64.207992 17.312271 17.031942 0.846613 0.078154 0.010716 0.005710 0.001723 0.000752 0.504128	BAM	4.9 MPa	10 dm^3	T_c = 207.1 K p_c = 6.86 MPa
Biogás	CH_4 CO_2 N_2 CO	49.8141 35.2028 9.9916 4.9915	CEM	10.0 MPa	5 dm^3	T_c = 224.8 K p_c = 8.9352 MPa

6. CARACTERIZACIÓN TERMODINÁMICA DE MEZCLAS BINARIAS DE METANO Y HELIO

Se realizaron medidas (*p, ρ, T*) con el densímetro de flotador sencillo con sistema de acoplamiento de suspensión magnética para tres mezclas de metano y helio, (0.95 CH_4 + 0.05 He), (0.90 CH_4 + 0.10 He) y (0.50 CH_4 + 0.50 He), a nueve temperaturas (240, 250, 260, 275, 300, 325, 350, 375 y 400) K. Dentro de cada isoterma se disminuyó la presión desde (20 hasta 1) MPa en pasos de 1 MPa.

Incertidumbre total de las medidas

A partir de los resultados de la densidad experimental se han estimado los valores de la incertidumbre total expandida (*k* = 2).

Tabla 6.1. *Resumen de las contribuciones a la incertidumbre total expandida (k = 2) de la medida de la densidad para las mezclas (0.95 CH_4 + 0.05 He), (0.90 CH_4 + 0.10 He) y (0.50 CH_4 + 0.50 He).*

Mezcla	Incertidumbre total expandida (*k* = 2)	Estimación en densidad	
		$kg \cdot m^{-3}$	%
(0.95 CH_4 + 0.05 He)	$U_{T1}(\rho)$ gravimétrica	(0.024 - 0.081)	(0.032 - 0.552)
	$U_{T2}(\rho)$ virial	(0.024 - 0.169)	(0.078 - 0.517)
(0.90 CH_4 + 0.10 He)	$U_{T1}(\rho)$ gravimétrica	(0.024 - 0.072)	(0.034 - 0.565)
	$U_{T2}(\rho)$ virial	(0.024 - 0.153)	(0.079 - 0.537)
(0.50 CH_4 + 0.50 He)	$U_{T1}(\rho)$ gravimétrica	(0.024 - 0.042)	(0.047 - 0.795)
	$U_{T2}(\rho)$ virial	(0.024 - 0.113)	(0.127 - 0.803)

Desviación relativa de los datos experimentales respecto de las ecuaciones de estado de referencia

Las desviaciones relativas de los datos experimentales respecto a los valores calculados mediante la ecuación GERG-2008 son claramente mayores que las estimadas con la AGA8-DC92. Para la mezcla (0.95 CH_4 + 0.05 He) la desviación de los datos experimentales respecto a la ecuación AGA8-DC92 tienen una desviación máxima del –0.2 %, mientras que las máximas desviaciones respecto a la GERG-2008 son del –2 %. Estas desviaciones son

mayores a altas presiones y bajas temperaturas. Las mayores desviaciones para esta mezcla fueron registradas en la isoterma de 240 K a presiones alrededor de 15 MPa. En contraste, las desviaciones respecto a la AGA8-DC92 son menores a bajas temperaturas.

Para la mezcla (0.90 CH_4 + 0.10 He), las desviaciones de la densidad experimental respecto a la AGA8-DC92 a altas presiones exceden el –0.2 % para temperaturas de 300 K y superiores. Las desviaciones respecto a la GERG-2008 superan el –3 %, siendo la mayor desviación registrada en la isoterma de 240 K a presiones cercanas a 17 MPa.

En la mezcla (0.50 CH_4 + 0.50 He), la desviación relativa de la densidad experimental respecto a la GERG-2008 alcanza valores máximos cercanos al –6.5 % a bajas temperaturas y altas presiones. En contraste, las desviaciones relativas respecto a la AGA8-DC92 presentan desviaciones máximas del 0.5 %. Estas desviaciones son negativas a altas temperaturas, mientras que a bajas temperaturas y altas presiones presentan desviaciones positivas.

A la vista de estos datos, puede afirmarse que la desviación relativa de la densidad experimental es mayor cuanto mayor sea la concentración de helio en la mezcla.

La alta desviación de los datos de densidad experimentales respecto a los calculados a través de la GERG-2008 es en cierta manera previsible. Formalmente, la ecuación de estado GERG-2008 es capaz de estimar las propiedades termodinámicas de mezclas arbitrarias consistentes en cualesquiera de los 21 componentes considerados en diferentes concentraciones y para un amplio rango de presión y temperatura. La incertidumbre de la ecuación de estado GERG-2008 para la fase gaseosa es del 0.1 % en densidad para un rango de temperaturas de (250 a 450) K y presiones hasta 35 MPa [10]. Sin embargo, hay identificados ciertos escenarios y mezclas para los que la ecuación GERG-2008 no es capaz de predecir satisfactoriamente el comportamiento termodinámico. Los modelos de mezcla desarrollados para la formulación de la GERG-2008 están basados en la energía libre de Helmholtz en su forma adimensional $a(\delta,\tau,\bar{x})$, la cual no es accesible mediante medidas experimentales, por lo que se divide en dos términos, una parte ideal y otra residual, dependiente de las variables reducidas de densidad δ y temperatura τ, así como de la composición $\bar{x}$. De esta forma, cuando los parámetros críticos de los componentes puros de una mezcla binaria son muy asimétricos, la mezcla muestra un comportamiento fuertemente alejado de la idealidad. Según las reivindicaciones de la ecuación de estado GERG-2008, cuando las temperaturas críticas de los componentes de una mezcla binaria difieren en más de 150 K, las incertidumbres en densidad pueden ser hasta del 1 %. Este es

el caso de la mezcla binaria de (CH_4 + He), cuyas temperaturas críticas de los componentes puros difieren en más de 185 K.

La moderada desviación de los datos experimentales con respecto a la AGA8-DC92 puede explicarse debido a que esta ecuación está desarrollada en términos del factor de compresibilidad y no depende de los parámetros críticos de los componentes puros, por lo que representa mejor que la GERG-2008 el comportamiento de las mezclas tan asimétricas con como las estudiadas.

Ajuste de los datos experimentales a la ecuación de estado del virial

A partir del ajuste de los datos experimentales obtenidos a la ecuación de estado del virial mediante una herramienta informática de regresión por ajuste de mínimos cuadrados desarrollada por Watson en el Laboratorio Nacional de Ingeniería de Glasgow [21] se han estimado los coeficientes de interacción viriales de segundo y tercer orden.

Tabla 6.9. *Coeficientes de interacción viriales de segundo orden estimados para las mezcla binarias de (CH_4 + He) e incertidumbres expandidas (k = 2).*

Isoterma	240 K	250 K	260 K	275 K	300 K	325 K	350 K	375 K	400 K
				(0.95 CH_4 + 0.05 He)					
T_{media}/K	240.047	249.996	260.005	275.002	299.958	324.955	349.938	374.924	399.997
B_{12}/ $cm^3 \cdot mol^{-1}$	21.43	21.44	22.60	23.06	22.01	21.29	20.66	19.56	15.35
$U(B_{12})$/ $cm^3 \cdot mol^{-1}$	0.84	0.85	0.85	0.85	1.72	1.72	1.72	1.66	1.68
B_{12} GERG/ $cm^3 \cdot mol^{-1}$	21.72	17.13	17.27	16.30	15.18	14.49	13.89	13.57	12.97
				(0.90 CH_4 + 0.10 He)					
T_{media}/K	240.045	250.005	260.013	274.994	299.951	324.958	349.939	374.923	400.006
B_{12}/ $cm^3 \cdot mol^{-1}$	20.26	22.12	22.86	23.19	24.77	23.46	21.53	22.31	23.10
$U(B_{12})$/ $cm^3 \cdot mol^{-1}$	0.88	0.87	0.87	0.87	1.74	1.73	1.73	1.67	1.67
B_{12} GERG/ $cm^3 \cdot mol^{-1}$	15.91	15.56	15.23	14.51	13.98	13.21	12.73	12.77	12.63

	(0.50 CH_4 + 0.50 He)								
T_{media}/K	240.032	249.998	259.991	275.007	299.922	324.970	349.914	374.906	399.990
B_{12}/ $cm^3 \cdot mol^{-1}$	22.58	22.00	23.38	23.99	24.03	23.80	22.32	23.58	23.68
$U(B_{12})$/ $cm^3 \cdot mol^{-1}$	1.09	1.02	0.95	0.98	1.77	1.77	1.79	1.77	1.75
B_{12} GERG/ $cm^3 \cdot mol^{-1}$	6.95	7.39	7.82	8.44	9.38	10.24	11.03	11.86	12.60

La incertidumbre expandida $U(B_{12})$ *ha sido calculada acorde a la GUM* [19] *a partir de las incertidumbres de los coeficientes de interacción de las sustancias puras* [22] *y la incertidumbre de la composición gravimétrica.*

Los resultados obtenidos en este trabajo están en sintonía con los valores de B_{12} reportados por Bignell et al. [23] para el sistema (CH_4 + He) a temperaturas entre (290 y 310) K.

Tabla 6.10. *Coeficientes de interacción viriales de tercer orden estimados para las mezclas binarias de (CH_4 + He).*

T/K	240	250	260	275	300	325	350	375	400
C_{112}/ $cm^6 \cdot mol^{-2}$	1983	1551	1610	1760	2105	2934	3920	4430	4713
C_{122}/ $cm^6 \cdot mol^{-2}$	1688	2833	2020	1510	1631	1167	1508	197	-97
$U(C_{ijk})$/ $cm^6 \cdot mol^{-2}$	183	183	183	185	179	178	566	708	714

No se han encontrado datos con los que comparar los resultados obtenidos para los coeficientes de interacción viriales de tercer orden estimados.

7. CARACTERIZACIÓN TERMODINÁMICA DE UNA MEZCLA SINTÉTICA DE CMM (COAL MINE METHANE)

Las siglas CMM (coal mine methane) se corresponden con el gas metano en capa de carbón proveniente de minas activas. Se trata por tanto de una fuente de producción de gas no-convencional. Las medidas de densidad se realizaron en el rango de temperaturas de (250 a 400) K y presiones hasta 15 MPa. En total se registraron siete isotermas a las temperaturas de (250, 275, 300, 325, 350, 375 y 400) K y presiones de (1 a 15 MPa) en intervalos de 1 MPa.

Incertidumbre total de las medidas

La incertidumbre expandida total $U_{T1}(\rho)$ (k = 2) de las medidas de densidad, calculada mediante la ecuación 4.13 está comprendida entre (0.027 y 0.400) kg·m^{-3}; expresado en porcentaje se estima entre (0.148 y 0.388) %. La incertidumbre total expandida teniendo en consideración el ajuste virial y calculada mediante la ecuación 4.14 $U_{T2}(\rho)$ está entre (0.028 y 0.425) kg·m^{-3} o (0.205 y 0.540) %.

Desviación relativa de los datos experimentales respecto de las ecuaciones de estado de referencia

Respecto a la ecuación de estado GERG-2008, los resultados experimentales presentan una desviación relativa en densidad inferior al 0.2 % en las isotermas entre (300 y 400) K. El mismo comportamiento puede apreciarse en la isoterma de 275 K a presiones por debajo de los 10 MPa. En cambio, los datos experimentales obtenidos en la isoterma de 250 K y a 275 K para presiones superiores a 10 MPa muestran desviaciones negativas que se incrementan según aumenta la presión. Las desviaciones observadas respecto a la ecuación de estado AGA8-DC92 son muy similares a las obtenidas a través de la GERG-2008, incluso ligeramente menores.

Para mezclas gaseosas con un contenido de dióxido de carbono superior al 14 % se han identificado desviaciones sistemáticas superiores al 0.3 % [19] con la ecuación de estado GERG-2008. Los resultados obtenidos muestran que apenas el 7 % de los datos presentan desviaciones superiores al 0.3 % y todos ellos fueron registrados en la isoterma a 250 K.

Por tanto, los resultados obtenidos se ajustan a lo estimado según los análisis previos de la ecuación de estado GERG-2008.

Ajuste de los datos experimentales a la ecuación del virial

Las desviaciones de los valores obtenidos para los coeficientes del virial de segundo y tercer orden de la mezcla a partir de los datos experimentales y los calculados mediante la ecuación de estado GERG-2008 son muy pequeñas aunque sutilmente mayores que las incertidumbres estimadas para la mayoría de temperaturas.

8. CARACTERIZACIÓN TERMODINÁMICA DE UNA MEZCLA SINTÉTICA DE BIOGÁS

Se registraron seis isotermas para este estudio a las temperaturas de (275, 300, 325, 350, 375 and 400) K. Cada isoterma fue medida desde una presión de 20 MPa hasta 1 MPa en pasos de 1 MPa.

Incertidumbre total de las medidas

La incertidumbre total expandida $U_{T1}(\rho)$ (k = 2) de las medidas de densidad, calculada a partir la ecuación 4.13 está comprendida entre (0.025 y 0.259) kg·m^{-3}; expresado en porcentaje se estima entre (0.043 y 0.465) %. La incertidumbre total expandida teniendo en consideración la expansión virial y calculada a partir de la ecuación 4.14 $U_{T2}(\rho)$ está entre (0.026 y 0.448) kg·m^{-3} o (0.124 y 0.315) %.

Desviación relativa de los datos experimentales respecto de las ecuaciones de estado de referencia

La desviación relativa de los datos experimentales respecto a los calculados con la ecuación de estado GERG-2008 está dentro del rango ±0.2 %. Únicamente el rango de presión de (6 a 15) MPa a la temperatura de 275 K está fuera de estos límites. La isoterma de 275 K muestra a 10 MPa una cresta en la cual la mayor desviación entre la densidad experimental y la calculada con la ecuación GERG-2008 es de 0.41 %. Al igual que para la mezcla de CMM al presentar un contenido de CO_2 mayor del 0.14, las reivindicaciones de la ecuación GERG-2008 reconocen desviaciones sistemáticas superiores al 0.3 %. El 60 % de los resultados obtenidos están dentro de la incertidumbre estimada para la GERG-2008 y solo presenta desviaciones mayores de 0.3 % a 275 K y presiones mayores de 10 MPa. Por lo tanto, el comportamiento registrado en las medidas está de acuerdo con la incertidumbre definida para la ecuación de estado GERG-2008.

En el caso de la ecuación de estado AGA8-DC92, la desviación de los datos de densidad experimental respecto a los estimados es mucho mayor que la obtenida al comparar los datos con la ecuación de estado GERG-2008, especialmente a altas presiones y bajas temperaturas. La máxima desviación registrada es de –4.5 % y fue registrada en la isoterma de 275 K a una presión de 16 MPa.

Ajuste de los datos experimentales a la ecuación del virial

Las desviaciones de los valores obtenidos a partir de los datos experimentales y los calculados mediante la ecuación de estado GERG-2008 son muy pequeñas en el caso del segundo coeficiente del virial, aunque sutilmente mayores que las incertidumbres estimadas para la mayoría de temperaturas. Las diferencias con el tercer coeficiente del virial son en cambio sustancialmente mayores que las incertidumbres estimadas.

9. CONCLUSIONES

Los resultados obtenidos en esta tesis doctoral a partir de la caracterización termodinámica de mezclas gaseosas relacionadas con combustibles gaseosos alternativos, como el biogás o gases no-convencionales, contribuyen al conocimiento de las propiedades termodinámicas de este tipo de fluidos y a su futura y completa introducción en el mix energético global. A continuación se detallan las principales contribuciones científicas de este trabajo.

Análisis de alternativas a los combustibles fósiles tradicionales

Tras presentar la situación actual de producción y consumo de gas natural y las alternativas existentes para disminuir la actual dependencia energética de los combustibles fósiles tradicionales, se han analizado las necesidades técnicas para la introducción de combustibles gaseosos alternativos y el papel de la termodinámica en este reto.

La generación y aprovechamiento de biometano es una de las alternativas más prometedoras, sin embargo, para su completa introducción es necesario superar ciertas barreras políticas y técnicas. En este último ámbito, se hace necesaria la adaptación de ciertas tecnologías y modelos matemáticos desarrollados inicialmente para el gas natural, como las ecuaciones de estado.

Revisión de las tecnologías existentes para la determinación experimental de la densidad de gases en amplios rangos de presión y temperatura

La densidad es una de las propiedades más importantes para el desarrollo de ecuaciones de estado de referencia. Por ello, se han revisado brevemente las tecnologías existentes para su determinación, identificando las más adecuadas para la obtención de datos termodinámicos de alta precisión en amplios rangos de presión y temperatura con una incertidumbre total en densidad aceptable para el desarrollo de nuevas ecuaciones de estado, así como para la evaluación de las ya existentes.

El densímetro de flotador con sistema acoplamiento magnético, de uno o dos flotadores, continúa siendo la técnica que proporciona los resultados de mayor precisión en amplios rangos de presión y temperatura.

Puesta a punto y mejora del densímetro de flotador sencillo con sistema de acoplamiento de suspensión magnética

Utilizando nitrógeno como fluido de referencia, se ha realizado la puesta a punto y se ha validado el funcionamiento del densímetro de flotador sencillo con sistema de acoplamiento magnético del laboratorio del grupo TERMOCAL de la UVA. Además, se han identificado y ejecutado mejoras en el equipo relacionadas con la estabilidad de la temperatura y la presión en el interior de la celda de medida. Así, se ha instalado en el laboratorio un nuevo sistema de climatización, el cual mejora la estabilidad de los transductores de presión, y un nuevo baño termostático que permite realizar medidas de densidad en un rango más amplio de temperaturas con mayor estabilidad. Por último, se han realizado mejoras en las plantillas de Microsoft Excel® empleadas en el tratamiento de los datos experimentales, pudiéndose obtener de forma automática y sencilla los valores de desviación relativa de la densidad respecto a las ecuaciones de estado de referencia, la incertidumbre asociada a las medidas, representaciones gráficas de los datos, coeficientes del virial, etc. Todo ello en un formato adecuado para su presentación.

Estimación de la incertidumbre de las medidas de densidad

Se ha realizado un exhaustivo análisis de las incertidumbres de las magnitudes asociadas a la determinación de la densidad: temperatura, presión, densidad y composición de la mezcla. Posteriormente, se ha estimado la incertidumbre total expandida de las medidas a través de dos métodos diferenciados. El primero de ellos tiene en cuenta únicamente la incertidumbre de la composición derivada de la preparación de la mezcla por el método gravimétrico. El segundo método pretende incluir además la posible variación de la composición en el interior de la celda de medida debido a efectos impredecibles. Esta variación en la composición se relaciona con el valor de la masa molecular de la mezcla en el interior de la celda de medida estimado mediante el ajuste de los datos experimentales a la ecuación de estado del virial. El cálculo de la incertidumbre total teniendo en cuenta la variación de la composición en el interior de la celda es apropiado si se tienen dudas sobre

la estratificación u homogeneización de la mezcla o se sospecha que pueda producirse la adsorción de alguno de los componentes de la mezcla en el interior de la celda de medida.

Los resultados obtenidos muestran unos valores de incertidumbre total calculados con ambos métodos muy similares, con lo que se puede concluir que la variación de la composición de la mezcla en el interior de la celda de medida puede ser despreciada. Además, los resultados obtenidos en la masa molecular de la mezcla mediante el ajuste de la ecuación del virial son compatibles con los valores calculados a partir de la composición gravimétrica.

Caracterización termodinámica de mezclas binarias de metano (CH_4) y helio (He) de distinta composición

Dentro de las consideraciones para mejorar la ecuación de estado GERG-2008 está el desarrollo de funciones residuales generalizadas para diferentes mezclas binarias, entre las que se incluyen mezclas binarias que contengan helio. Considerando el continuo incremento en la demanda de helio y la falta de datos experimentales de mezclas que contengan helio se ha abordado la caracterización termodinámica de mezclas binarias de metano y helio de distinta composición. La tesis aporta 522 datos (*p, ρ, T*) experimentales de alta precisión de tres mezclas binarias de (CH_4 + He) con (5, 10 y 50 mol-% He), a nueve temperaturas distintas entre (240 y 400) K y hasta 20 MPa de presión, así como una estimación de los coeficientes de interacción viriales de segundo B_{12} y tercer orden C_{112} y C_{122}. Estos resultados son útiles para la mejora en el futuro de la ecuación de estado GERG-2008.

Caracterización termodinámica de una mezcla sintética de CMM (*coal mine methane*)

En el marco de los objetivos del proyecto europeo "*Characterization of non-conventional energy gases*" se ha llevado a cabo la caracterización termodinámica de una mezcla sintética multicomponente de un gas no-convencional tipo CMM (*coal mine methane*) con diez componentes y una concentración de metano del 64 mol-%. La mezcla fue preparada en el Instituto Federal para la Investigación de Materiales y Ensayos (BAM) en Berlín, Alemania. En esta tesis se presentan 90 datos de densidad determinados

experimentalmente para la mezcla de CMM en un rango de temperatura de (250 a 400) K y presiones hasta 15 MPa, junto con una estimación de los coeficientes viriales de la mezcla de segundo y tercer orden.

Caracterización termodinámica de una mezcla sintética de biogás

Dentro de los objetivos de la primera fase del proyecto europeo "*Metrology for Biogas*" se ha realizado la caracterización termodinámica de una mezcla sintética de cuatro componentes simulando un tipo de biogás con una concentración de 50 mol-% de metano. La mezcla fue elaborada por el Centro Español de Metrología (CEM) en Madrid. En la tesis se recopilan 116 datos (*p, ρ, T*) en el rango de temperatura de (275 a 400) K y presiones hasta 20 MPa, junto con la estimación de los coeficientes viriales de la mezcla de segundo y tercer orden.

Evaluación de las ecuaciones de estado de referencia del gas natural para representar el comportamiento experimental registrado en las mezclas estudiadas

Las ecuaciones de estado de referencia para el gas natural son la GERG-2008 y, previamente, la AGA8-DC92. Los datos experimentales de densidad obtenidos en las mezclas estudiadas han sido comparados con los valores estimados a través de ambas ecuaciones de estado en las mismas condiciones de presión y temperatura.

Respecto a las mezclas de (CH_4 + He), las desviaciones relativas de los datos experimentales respecto a los valores calculados mediante la ecuación GERG-2008 son elevadas, especialmente a bajas temperaturas (240, 250 y 260 K) y presiones por encima de 10 MPa. Estas desviaciones pueden llegar a ser superiores al 6 % para la mezcla con 50 mol-% He a presiones superiores a 16 MPa para 240 K, 18 MPa para 250 K y 19 MPa para 260 K. Esto puede deberse a que los componentes de la mezcla presentan una gran diferencia en el valor de sus temperaturas críticas. Por otra parte, las composiciones de las mezclas estudiadas están considerablemente alejadas de la proporción en que estos elementos se encuentran en el gas natural de cualquier procedencia, lo cual queda fuera del rango de aplicación para el cual está diseñada la ecuación de estado GERG-2008.

En las mezclas sintéticas de CMM y biogás, las desviaciones respecto de la GERG-2008 fueron menores del 0.2 % para temperaturas mayores a 275 K. En los datos registrados a menores temperaturas y presiones por encima de 10 MPa se observan mayores desviaciones (hasta del 0.55 % para el CMM y 0.41 % para el biogás), debidas probablemente al alto contenido en dióxido de carbono de las mezclas.

La identificación y cuantificación de estas desviaciones contribuirá al desarrollo de versiones mejoradas de las ecuaciones de estado orientadas a la estimación de las propiedades termodinámicas de los combustibles alternativos y mezclas de éstos con gas natural.

10. REFERENCIAS

[1] European Climate Foundation, "Roadmap 2050," 2010. [Online]. Available: http://www.roadmap2050.eu/. [Accessed: 04-Mar-2015].

[2] "DIRECTIVE 2009/28/EC OF THE EUROPEAN PARLIAMENT AND OF THE COUNCIL of 23 April 2009 on the promotion of the use of energy from renewable sources and amending and subsequently repealing Directives 2001/77/EC and 2003/30/EC." [Online]. Available: http://eur-lex.europa.eu/legal-content/EN/ALL/?uri=CELEX:32009L0028. [Accessed: 04-Mar-2015].

[3] European Comission, "EU Energy. Statistical Pocketbook," 2014.

[4] EurObserv'ER, "Biogas Barometer 2013," 2013.

[5] Ministerio de Industria Turismo y Comercio. Gobierno de España, "Plan de acción nacional de energías renovables de españa (paner) 2011 - 2020," pp. 2011–2020, 2011.

[6] U.S. Energy Information Administration (EIA), "Shale gas and tight oil are commercially produced in just four countries," 2015. [Online]. Available: http://www.eia.gov/todayinenergy/detail.cfm?id=19991. [Accessed: 05-Mar-2015].

[7] "Characterization of energy gases: EMRP ENG01 N 912/2009/EC (2010-2013)," European Metrology Research Programme.

[8] "JRP Summary Report for ENG54 Biogas 'Metrology for biogas.'" [Online]. Available: http://www.euramet.org/fileadmin/docs/EMRP/JRP/JRP_Summaries_2013/Energy_JRPs/ENG54_Publishable_JRP_Summary.pdf. [Accessed: 05-May-2014].

[9] M. E. Mondéjar, C. R. Chamorro, and R. Span, "Contribution to the development and introduction of renewable gaseous fuels through the thermodynamic characterization of mixtures of their components by using an optimized single sinker densimeter whit magnetic suspension coupling (Phd thesis)," Valladolid, 2012.

[10] O. Kunz and W. Wagner, "The GERG-2008 Wide-Range Equation of State for Natural Gases and Other Mixtures: An Expansion of GERG-2004," *J. Chem. Eng. Data*, 2012.

[11] K. E. Starling and J. L. Savidge, "Compressibility factors of natural gas and other related hydrocarbon gases - AGA Transmission Measurement Committee Report 8," 1992.

[12] K. Brachthäuser, R. Kleinrahm, H. W. Lösch, and W. Wagner, "Entwicklung eines neuen Dichtemeßverfahrens und Aufbau einer Hochtemperatur-Hochdruck-Dichtemeßanlage," 1993.

[13] W. Wagner, K. Brachthäuser, R. Kleinrahm, and H. W. Lösch, "A new, accurate single-sinker densitometer for temperatures from 233 to 523 K at pressures up to 30 MPa," *Int. J. Thermophys.*, vol. 16, no. 2, pp. 399–411, 1995.

[14] C. R. Chamorro, J. J. Segovia, M. C. Martín, M. A. Villamañán, J. F. Estela-Uribe, and

J. P. M. Trusler, “Measurement of the (pressure, density, temperature) relation of two (methane+nitrogen) gas mixtures at temperatures between 240 and 400K and pressures up to 20MPa using an accurate single-sinker densimeter,” *J. Chem. Thermodyn.*, vol. 38, no. 7, pp. 916–922, Jul. 2006.

[15] M. E. Mondéjar, J. J. Segovia, and C. R. Chamorro, “Improvement of the measurement uncertainty of a high accuracy single sinker densimeter via setup modifications based on a state point uncertainty analysis,” *Measurement*, vol. 44, no. 9, pp. 1768–1780, 2011.

[16] E. (European A. of N. M. Institutes), “Guidelines on the calibration of Non-Automatic Weighing Instruments,” vol. cg-18 / v., 2007.

[17] H. W. Losch, R. Kleinrahm, and W. Wagner, “New Magnetic Suspension Weighers for Gravimetric Measurements In-Process Engineering,” *Chemie Ing. Tech.*, vol. 66, no. 8, pp. 1055–1058, Aug. 1994.

[18] M. O. McLinden, R. Kleinrahm, and W. Wagner, “Force transmission errors in magnetic suspension densimeters,” *Int. J. Thermophys.*, vol. 28, no. 2, pp. 429–448, 2007.

[19] I. E. C. BIPM IFCC, ISO, IUPAC, IUPAP and OIML, “Guide to the Expression of Uncertainty in Measurement,” *Guid. to Expr. Uncertain. Meas.*, 1995.

[20] “Lemmon, E.W., Huber, M.L., McLinden, M.O. NIST Standard Reference Database 23: Reference Fluid Thermodynamic and Transport Properties-REFPROP, Version 9.1, National Institute of Standards and Technology, Standard Reference Data Program, Gaithersburg, 2013.” .

[21] J. T. R. Watson and National Engineering Laboratory-FPT Division, “‘A generalised fitting package for the least squares analysis of data’.” East Kilbride, Glasgow G75 0QU, Scotland., 1991.

[22] J. H. Dymond and E. B. Smith, *The Virial Coefficients of Pure Gases and Mixtures. A Critical Compilation*. 1980.

[23] C. M. Bignell and P. J. Dunlop, “Second virial coefficients for fluoromethanes and their binary mixtures with helium and argon,” *J. Chem. Eng. Data*, vol. 38, no. 1, pp. 139–140, Jan. 1993.